

ACS SYMPOSIUM SERIES 245

# Size Exclusion Chromatography

## Methodology and Characterization of Polymers and Related Materials

Theodore Provder, EDITOR  
*Glidden Coatings and Resins*

Based on a symposium sponsored by  
the Division of Organic Coatings  
and Plastics Chemistry  
at the 185th Meeting  
of the American Chemical Society,  
Seattle, Washington,  
March 20-25, 1983



American Chemical Society, Washington, D.C. 1984



### Library of Congress Cataloging in Publication Data

Size exclusion chromatography.

(ACS symposium series, ISSN 0097 6156; 245)

"Based on a symposium sponsored by the Division of Organic Coatings and Plastics Chemistry at the 185th Meeting of the American Chemical Society, Seattle, Washington, March 20-25, 1983."

Includes bibliographies and indexes.

1. Gel permeation chromatography-- Congresses.
2. Polymers and polymerization-- Analysis-- Congresses.

I. Provder, Theodore, 1939-- II. American Chemical Society. Division of Organic Coatings and Plastics Chemistry. III. Series.

QD272.C444S6 1984 547.7'046 83 27515  
ISBN 0 8412 0826 3

Copyright © 1984

American Chemical Society

All Rights Reserved. The appearance of the code at the bottom of the first page of each chapter in this volume indicates the copyright owner's consent that reprographic copies of the chapter may be made for personal or internal use or for the personal or internal use of specific clients. This consent is given on the condition, however, that the copier pay the stated per copy fee through the Copyright Clearance Center, Inc. for copying beyond that permitted by Sections 107 or 108 of the U.S. Copyright Law. This consent does not extend to copying or transmission by any means—graphic or electronic—for any other purpose, such as for general distribution, for advertising or promotional purposes, for creating a new collective work, for resale, or for information storage and retrieval systems. The copying fee for each chapter is indicated in the code at the bottom of the first page of the chapter.

The citation of trade names and/or names of manufacturers in this publication is not to be construed as an endorsement or as approval by ACS of the commercial products or services referenced herein; nor should the mere reference herein to any drawing, specification, chemical process, or other data be regarded as a license or as a conveyance of any right or permission, to the holder, reader, or any other person or corporation, to manufacture, reproduce, use, or sell any patented invention or copyrighted work that may in any way be related thereto. Registered names, trademarks, etc., used in this publication, even without specific indication thereof, are not to be considered unprotected by law.

PRINTED IN THE UNITED STATES OF AMERICA

**American Chemical  
Society Library**

**1155 16th St. N. W.**

In Size Exclusion Chromatography; Brandon, T.;  
ACS Symposium Series; American Chemical Society: Washington, DC, 1984.

# ACS Symposium Series

**M. Joan Comstock, *Series Editor***

## *Advisory Board*

**Robert Baker**  
U.S. Geological Survey

**Martin L. Gorbaty**  
Exxon Research and Engineering Co.

**Herbert D. Kaesz**  
University of California— Los Angeles

**Rudolph J. Marcus**  
Office of Naval Research

**Marvin Margoshes**  
Technicon Instruments Corporation

**Donald E. Moreland**  
USDA, Agricultural Research Service

**W. H. Norton**  
J. T. Baker Chemical Company

**Robert Ory**  
USDA, Southern Regional  
Research Center

**Geoffrey D. Parfitt**  
Carnegie Mellon University

**Theodore Provder**  
Glidden Coatings and Resins

**James C. Randall**  
Phillips Petroleum Company

**Charles N. Satterfield**  
Massachusetts Institute of Technology

**Dennis Schuetzle**  
Ford Motor Company  
Research Laboratory

**Davis L. Temple, Jr.**  
Mead Johnson

**Charles S. Tuesday**  
General Motors Research Laboratory

**C. Grant Willson**  
IBM Research Department

## FOREWORD

The ACS SYMPOSIUM SERIES was founded in 1974 to provide a medium for publishing symposia quickly in book form. The format of the Series parallels that of the continuing ADVANCES IN CHEMISTRY SERIES except that in order to save time the papers are not typeset but are reproduced as they are submitted by the authors in camera-ready form. Papers are reviewed under the supervision of the Editors with the assistance of the Series Advisory Board and are selected to maintain the integrity of the symposia; however, verbatim reproductions of previously published papers are not accepted. Both reviews and reports of research are acceptable since symposia may embrace both types of presentation.

# PREFACE

**T**HE FIELD OF SIZE EXCLUSION CHROMATOGRAPHY (SEC) continues to grow in scope and in depth. Since the last American Chemical Society symposium on this subject in 1979, about 300 papers have been published annually. The continuing interest in the field is a result of (1) improved column technology, (2) availability of improved and varied in-line detectors, and (3) improved data treatment procedures and methods facilitated by the microcomputer explosion of the last 5 years.

This volume deals with the methodology involved in the practice of SEC from both a theoretical and a pragmatic perspective along with the application of this methodology to the characterization of polymers and related materials. The three sections reflect the major efforts in the field over the last 3 years.

In the first section, the mechanisms involved in size exclusion chromatography are discussed; this is an area where additional understanding and clarification still are needed. Data treatment with respect to statistical reliability of the data along with corrections for instrumental broadening is still a valid concern. Instrumental advances in the automation of multiple detectors and the development of a pressure-programmed, controlled-flow supercritical fluid chromatograph are presented.

In the second section, improved column technology is emphasized. The effects of operational variables on the performance of the chromatographic system are considered. Some of the operational variable concerns are shear degradation of high molecular weight polymers, the use of mixed solvent systems, and the optimization of resolution for analysis of oligomers and small molecules.

In the third section, the emphasis is on the application of SEC methodology for the characterization of polymers. The use of continuous in-line low-angle laser light-scattering detection is illustrated for the high-temperature SEC analysis of polyethylene and of linear and branched block copolymers. The development of a continuous in-line viscosity detector and its application as an absolute molecular weight detector is described. The application of SEC for cross-linked network analysis by studying thermoset resin cure kinetics and cross-linked network morphology is of special interest.

This book has brought together papers that represent current activity in the field of SEC. It is hoped that this book will spur further activity in the field.

Special thanks are given to the authors for their effective oral and written communication and to the reviewers for their critiques and constructive comments.

THEODORF PROVIDER  
Glidden Coatings and Resins  
Strongsville, Ohio

December 1983

# Mathematical Modeling of Particle Chromatography

D. C. FRANCIS and A. J. MCHUGH

Department of Chemical Engineering, University of Illinois, Urbana, IL 61801

A discussion is given of the mathematical modelling of the separation mechanisms associated with the packed column chromatography of particulate systems. Primary emphasis is on the derivation of models for the HDC and pore partitioning processes which occur with porous packing systems. Comparison is made of predictions for the separation factor - particle size behavior for a purely flow-through model, published earlier, and models developed herein to account for simultaneous pore partitioning effects. Comparison to literature data indicates that accounting for pore partitioning leads to a more accurate fit. The results of these calculations indicate the need for further experimental studies to characterize the model parameters associated with the possible separation mechanisms.

A large and important class of colloids are the polymer latexes which consist of charged (by ionogenic surface groups and/or adsorbed species) generally spherical particles with diameters ranging from tens of nanometers to microns. The role of particle size analysis in characterizing such systems, for both fundamental studies and technological applications, is equivalent in scope to that of molecular weight analysis in characterizing bulk polymers. Reviews of the various techniques and important areas of application of particle size analysis can be found in several references (e.g. (1,2)).

In the past, analyses of submicron particles have been limited to time-consuming techniques, such as electron microscopy, or, to methods such as light scattering, which require a fairly narrow size distribution for accuracy. Recently, reports of a number of studies of a new method have been published in which modifications

0097-6156/84/0245-0003\$06.50/0  
© 1984 American Chemical Society

of the chromatographic techniques used in polymer molecular weight analysis have been employed to determine particle size and particle size distribution of suspensions (see reference (3) for a brief overview). These papers stem from experimental studies (4,5) which demonstrated that stabilized, dilute suspensions of latex particles fractionate by size when pumped through beds of porous or nonporous packing. There is now a clear indication that the development of such techniques for sizing submicron particles will have much the same impact on the science and technology of colloidal systems as liquid size exclusion chromatography analysis has had on the field of bulk polymers.

The purpose of this paper is to present a brief overview and description of a modelling approach we are taking which is aimed at developing a quantitative understanding of the mechanisms and separation capabilities of particle column chromatography. The main emphasis has been on the application of fundamental treatments of the convected motion and porous phase partitioning behavior of charged Brownian particles to the development of a mechanistic rate theory which can account for the unique size and electrochemical dependent separation behavior exhibited by such systems.

#### Background Description and Review of Separation Mechanisms

The experimental methods reported for particle chromatography have employed glass or stainless steel columns packed with nonporous copolymer or glass beads, porous gel matrices, or various GPC porous glass materials. Most studies have analyzed polymer latex solute particles suspended in stabilized aqueous media with the common mode of signal detection being light scattering. Small's work (4) with various nonporous packing systems demonstrated that for a range of eluant ionic strengths, larger latex particles elute from the column ahead of smaller ones and that the primary factors affecting the elution time were eluant ionic strength, packing diameter, and flow rate. The fractionation process occurs solely in the mobile phase and results from the fact that the latex particles are preferentially excluded from the slower moving solvent streamlines nearest the packing surfaces and thus obtain average velocities in excess of the solvent and these velocities increase with solute size. The name Hydrodynamic Chromatography or HDC has therefore been used to describe the process.

A number of publications (6-10) have demonstrated that the size separation mechanism in HDC can be described by the parallel capillary model for the bed interstices. The relevant expression for the separation factor,  $R_F$ , (ratio of eluant tracer to particle mean residence times) is given by,

$$R_F = \langle v_p \rangle / \langle v_m \rangle \quad (1)$$



where the particle and marker average velocities through the bed,  $\langle v_p \rangle$  and  $\langle v_m \rangle$ , are given by

$$\langle v_p \rangle = \frac{\int_0^{R_o - R_p} v_p(r) \exp \frac{-\phi(r)}{kT} r dr}{\int_0^{R_o - R_p} \exp \frac{-\phi(r)}{kT} r dr} \quad (2)$$

and (8)

$$\langle v_m \rangle = \frac{\int_0^{R_o} v_o \left(1 - \frac{r^2}{R_o^2}\right) \exp \left[ \frac{-2e\psi_{01}}{kT} \exp(-\kappa a) \right] r dr}{\int_0^{R_o} \exp \left[ \frac{-2e\psi_{01}}{kT} \exp(-\kappa a) \right] r dr} \quad (3)$$

In these equations,  $R_o$  represents the equivalent capillary radius (given by the bed hydraulic radius (7)),  $R_p$  is the particle radius,  $v_o$  is the eluant maximum velocity in the capillary tube,  $\psi_{01}$  is the packing surface potential,  $e$  is the protonic charge,  $\kappa$  is the inverse Debye double layer thickness,  $a$  is the distance of approach of the solute and wall,  $k$  is the Boltzmann constant, and  $T$  is the temperature. The expression for  $v_p(r)$  in Equation 2 contains a correction for the hydrodynamic wall effect, and the total potential energy of interaction,  $\phi$ , contains terms for the double layer and Born repulsion, and van der Waals attraction (8). The expression in Equation 3 is the limiting form appropriate for an ionic marker species (8).

Fits (in some cases zero free parameter (8,12)) of Equations 1 to 3 to experimental data have shown excellent agreement with the model (8-10,12) including an explanation of the ionic strength role of surfactants (10), universal calibration behavior (8,10), and the possibility of separating equi-sized particles of differing chemistry at high ionic strength conditions (3). The model therefore offers an excellent quantitative vehicle for describing the HDC mechanism. Of particular note is that the need for specification of the potential energy effects,  $\phi$ , and hydrodynamic effects,  $v_p(r)$ , requires specification of a flow geometry. In this respect, modelling of particle chromatography is in some sense more restrictive in its assumptions than the pseudo-continuum rate theories which have been developed for macromolecular size exclusion chromatography (26-28).

The work of Krebs and Wunderlich (5) has been followed by a number of studies (3,13,15-20), demonstrating that particle size fractionation will also occur with a porous matrix. In this case,

in addition to the purely hydrodynamic effects, the possibility exists for added fractionation due to steric exclusion from the matrix pores, similar to the macromolecular size exclusion mechanism (21). However, to our knowledge only one paper (13) has given a quantitative model for a separation mechanism for porous HDC. Calculations were based on a modified form of the hydrodynamic model developed to describe the separation mechanism of size exclusion chromatography (22-24). In this model the bed is assumed to consist of a fraction,  $\phi_i$ , of capillaries of radius  $R_o$  in a parallel array with a fraction,  $\phi_p$ , of flow-through capillaries whose radius equals that of the packing pores. The expression which results for the separation factor is (13)

$$\frac{1}{R_F} = \frac{\phi_P}{R_{F,p}} + \frac{\phi_i}{R_{F,i}} \quad (4)$$

where  $R_{F,p}$  and  $R_{F,i}$  are respectively, the separation factors for the porous matrix capillaries, and the interstitial capillaries, given in each case by an expression in the form of Equations 1 to 3 (the upper limit radius  $R_o$  in this case refers to either the porous matrix capillary radius or the interstitial capillary radius).

Figure 1 shows the fit obtained using Equation 4 with the appropriate expressions for the potential energy and wall effect parameters and corrections for the micelle phase (13). The data were obtained with a large pore diameter (2.5  $\mu\text{m}$ ) Fractosil packing. One sees that the separation factor increases over that for HDC despite the fact that larger packing size, in this case 90  $\mu\text{m}$ , should lead to a reduction (4,8). This represents an influence of the small pores in the separation behavior. Although the model calculations can reasonably well describe the trend of the data, the fit is not as convincing as the HDC model for nonporous systems (despite the fact that the interstitial capillary radius and Hamaker constants have been slightly adjusted (13)). On the other hand, model calculations varying parameters, show clearly that the smaller diameter capillaries, representative of the porous matrix, do play a controlling role in the separation factor behavior.

The presence of the pores adds two parameters - the pore volume fraction and the pore radius. The predicted  $R_F$  increases as the pore radius decreases suggesting a preference for small pore packings. However, for a small pore radius of 1.0  $\mu\text{m}$  a single value of the separation factor corresponds to two values of the particle diameter (13). Such double-valued behavior is of course undesirable in an analytic technique.

An obvious shortcoming of these calculations is that no account is taken of the possibility of size exclusion phase partitioning of the particle-pore system.

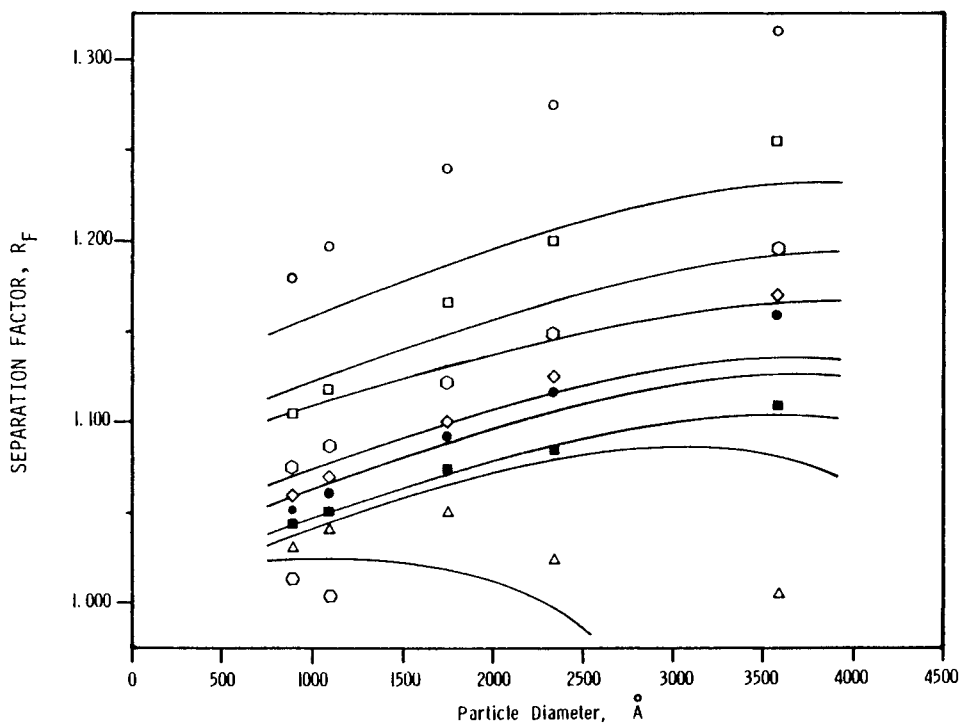


Figure 1. Comparison between capillary HDC model calculations (-) and experimental data. (Reproduced with permission from Ref. 13. Copyright 1980, Plenum Publishing Corporation.) Total ionic strengths:

○ = 0.00022M	□ = 0.00055M	◐ = 0.00129M
◇ = 0.00515M	● = 0.0101M	■ = 0.0210M
△ = 0.035M	◑ = 0.105M	

### Pore Partitioning HDC

The basis for Equations 2 and 4 has been a more or less ad hoc comparison to the relations for the mean residence time rigorously derived by Brenner and Gaydos (25) for particle transport through small capillaries. In order to compare mechanistic models for porous and nonporous chromatographic systems, a fundamental basis for deriving separation factor expressions is needed since in general both the HDC and pore-partitioning processes have to be accounted for. A rigorous starting point for deriving a particle chromatography rate theory would be the pseudo-continuum or volume averaging process which has been used for classical chromatography (see for example discussions in references (26 - 28)). In our approach, we are taking the view that the details of the bed geometry are needed in order to evaluate important hydrodynamic wall and electrostatic interaction effects. However, in order to arrive at a workable set of equations which can be tested against experiment, a number of simplifications are necessary. For example in HDC, use of the parallel capillary bed model in effect means the volume averaging process is simplified to an area-average of the transport equations across the bank of tubes representing the bed. Employing a steady state assumption for the radial concentration gradient leads directly to the applicable expression (see reference (25) Equation 4.22 and arguments preceding) for the interstitial pore flow (29).

$$\frac{\partial C_m}{\partial t} + \langle v_p \rangle \frac{\partial C_m}{\partial z} = \bar{D}^* \frac{\partial^2 C_m}{\partial z^2} \quad (5)$$

In Equation 5,  $C_m$  represents the average or bulk concentration of solute particles in the mobile phase,  $\langle v_p \rangle$  is the average solute particle velocity given in Equation 2 and  $\bar{D}^*$  is the phenomenological dispersion coefficient given in (25). Neglecting the dispersion effect in Equation 5 leads, by means of the moment analysis (25) directly to the HDC expression given in Equations 1 to 3.

In the case of porous HDC, as indicated, one needs to account for both HDC, pore partitioning, and hindered diffusion processes. A model should also have as asymptotes the mean residence time behavior given by Equations 1 to 3 for a nonporous system and Equation 4 for a purely flow-through porous system. Rate equation analyses for classical size exclusion chromatography have been based on treating the porous matrix as a homogeneous, spherical medium within which radial diffusion of the macromolecular solute takes place (e.g. (28,30,31)) or if mobile phase lateral dispersion is considered important, a two dimensional channel has been used as a model for the bed (32). In either case, however, no treatment of the effects to be expected with charged Brownian solute particles has been presented. As a

first approach to this problem we have carried out a simplified analysis of the rate theory equation to be expected for a porous system in which only partitioning occurs. The bed geometry is assumed to consist of a series of parallel capillaries with attached, cylindrical pores as shown in Figure 2.

The starting point is the convective-diffusion equation suitably modified to account for wall effects and potential field effects (25).

$$\frac{\partial P}{\partial t} + \nabla \cdot [P \nabla_p - \underline{D} \cdot \nabla P - \underline{P} \cdot \nabla \phi] = 0 \quad (6)$$

In Equation 6, the diffusivity and mobility are second rank tensors whose positional dependence is a consequence of the hydrodynamic wall effect and  $P$  represents the probability that the Brownian particle, initially at some fixed point, will be at some position in space  $\underline{R}$  at a later time  $t$ . At low concentrations,  $P$  is replaced by the number concentration,  $C$  (25). Conceptually the approach followed is similar to that developed by Brenner and Gaydos (25), however, one needs to include an expression for the flux of particles at the wall due to exchange with the pores. Upon averaging over the interstitial tube cross section of Figure 2, one arrives at the following expression (29) for the area averaged rate equation for the mobile phase transport.

$$\frac{\partial C_m}{\partial t} + \langle v_p \rangle \frac{\partial C_m}{\partial z} = \bar{D}_m \frac{\partial^2 C_m}{\partial z^2} - \frac{(1-\phi_1)\bar{D}_s}{\ell\phi_1} \left( \frac{\partial C_s}{\partial x} \right)_x = 0 \quad (7)$$

In Equation 7, solute concentrations are area averaged with the subscripts referring to the mobile or stationary phase,  $\ell$  is the length of the dead end pores, and the diffusivities  $\bar{D}_m$  and  $\bar{D}_s$  refer to the appropriately averaged values as defined in (25) to account for hydrodynamic wall effects and potential energy profiles between the packing and solute particles. Since in the present analysis these will either be neglected or treated as constants, rewriting their form in detail is not necessary. Similarly for the stationary pore phase, one has for the simplified one dimensional case,

$$\frac{\partial C_s}{\partial t} = \bar{D}_s \frac{\partial^2 C_s}{\partial x^2} \quad (8)$$

Initial conditions and boundary conditions complete the model description:

$$C_s = C_m = 0, \text{ for all } z \text{ at } t = 0 \quad (9a)$$

$$C_m \text{ is bounded as } z \rightarrow \infty \quad (9b)$$

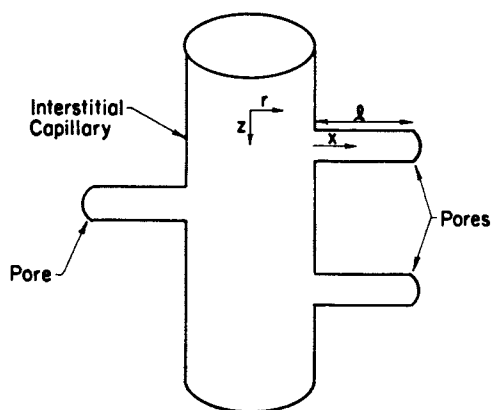


Figure 2. Schematic illustration of capillary-cylindrical pore model for porous-partitioning HDC system.

$$\int_0^{\infty} [\phi_1 C_m + \phi_p C_s] dz = M \quad (9c)$$

$$\bar{D}_s \left( \frac{\partial C_s}{\partial x} \right)_{x=l} = 0 \quad (9d)$$

$$C_s = KC_m \quad (9e)$$

where  $M$  is the mass of solute particles injected per unit column area and  $K$  is the equilibrium partition coefficient (33,34).

Equation 9e expresses the assumption of local equilibrium of the partitioning process at the stationary phase - mobile phase interface.

Equating chemical potentials for the particle concentrations in the mobile and stationary phases leads directly to the expression for  $K$  in terms of the potential energy,  $\phi$ , the particle radius,  $R_p$ , and the pore radius  $R$  (29,33-35).

$$K = \frac{\int_0^{R-R_p} R_p \exp(-\phi/kT) r dr}{\int_0^R r dr} \quad (10)$$

Evaluation of  $K$  is possible using the forms for sphere-plane interactions (11) (a simplification necessitated by the otherwise complicated forms needed to account for pore wall curvature (35)).

The solution of Equations 7 and 8 evaluated at the column exit yields the chromatogram. Since these equations cannot be solved analytically, statistical moments were obtained using the method of Laplace transforms (29).

The first moment is the mean retention time  $\theta$ :

$$\theta = [1 + K\sigma] (L/\langle v_p \rangle) \quad (11)$$

where  $L$  is the column length, and  $\sigma = \frac{1-\phi_1}{\phi_1}$ .

The second moment is the standard deviation,  $\mu_2$ ,

$$\mu_2 = 2/3 [K\sigma\ell^2 / \bar{D}_s] (L/\langle v_p \rangle) \quad (12)$$

In these expressions, it has been assumed that the mobile phase diffusivity will be negligible (29).

Equation 11 when manipulated according to the definitions of  $R_F$  yields an expression for the separation factor:

$$\frac{1}{R_F} = \frac{1}{R_{F,1}} \left[ \frac{1 + K\sigma}{1 + K_m \sigma} \right] \quad (13)$$

where  $K_m$  is the partition coefficient for the marker species, and  $R_{F,i}$  is the separation factor in the interstitial capillaries as given by equations 1 to 3.

In the limit of total exclusion of both the marker and the particles from the pores ( $K = K_m = 0$ ), the separation factor equals the separation factor in the interstitial capillaries. This is not true if the particles but not the marker ions are excluded ( $K = 0, K_m \neq 0$ ). Also, in the limit of zero pore volume, the separation factor equals the separation factor in the interstices.

Interaction Energy Expressions. Previous papers (8,10,12,13) have used exact sphere-plane interaction energy expressions to approximate the sphere-cylinder interaction. In this work, these exact expressions were replaced with recently published approximate expressions. For the double layer repulsion, this avoided the inconvenience and inaccuracy of using tabular values (8) while for the van der Waals attraction, using the approximate solution simplified the programming task.

The previously mentioned expressions were originally derived by Bell et al. (36) to calculate the double layer repulsion. These expressions are valid for  $\kappa R_p > 5$  where  $\kappa$  is the inverse Debye length. For  $\kappa R_p < 5$ , tabular values (8) were used.

For our work, expressions of Ohshima et. al. (37) obtained from an approximate form of the Poisson-Boltzmann equation were used. These analytical expressions agree with the exact solution for  $\kappa R_p \geq 1$ . (All of our calculations meet this criterion.) The relation between the surface potential and the surface charge density is (37)

$$I = 2 \sinh (Y_s/2) \left\{ 1 + \frac{2}{A \cosh^2 (Y_s/4)} + \frac{8 \ln [\cosh (Y_s/4)]}{A^2 \sinh^2 (Y_s/2)} \right\}^{1/2} \quad (14)$$

where  $A = \kappa R_p$ ,  $I$  is the dimensionless surface charge density, and  $Y_s$  is the dimensionless surface potential defined in (37).

The double layer interaction energy is given in terms of the eluant dielectric constant  $\epsilon$  by (37).

$$\phi_{DL} = \epsilon \left( \frac{kT}{e} \right)^2 R_p [4 \tanh (Y_{pk}/4)] Y_2 \exp (-\kappa a) \quad (15)$$

$$\text{where } Y_2 = 8 \tanh (Y_s/4) \left[ \frac{1}{1 + \left\{ 1 - \frac{2A+1}{(A+1)^2} \tanh^2 \left( \frac{Y_s}{4} \right) \right\}^{1/2}} \right] \quad (15b)$$

$a$  is the distance of approach between the particle and wall surfaces, and  $Y_{pk}$  is the dimensionless packing potential.



Expressions used for the van der Waals energy were originally developed by Clayfield and Lumb (38) for the van der Waals attraction between a sphere and a flat plate. These complex expressions have a discontinuity in the first derivative at the transition between the region of small separations, for which the retardation effect is negligible, and the region of large separations for which retardation must be considered. In this work, an approximate expression developed by Gregory (39) was used:

$$\phi_{vw} = -\frac{A_H}{6a} \left( \frac{1}{1 + 14a/\lambda} \right) \quad (16)$$

where  $\phi_{vw}$  is the interaction energy between a sphere and a flat plate,  $A_H$  is the Hamaker constant, and  $\lambda$  is the wavelength of the dispersion interaction, given in reference (8). This expression is valid for  $\phi_{vw}/A_H < 0.1$ . For values greater than 0.1, the van der Waals attraction is so small that any error will be insignificant.

The effects of experimental parameters on the predicted separation factor for the partition model are shown in Figures 3 to 6. As was seen with the parallel capillary model, the separation factor increases with particle diameter, increases with decreasing ionic strength, becomes more sensitive to the Hamaker constant as the ionic strength increases, increases with decreasing pore radius, and increases with decreasing packing size. In contrast to the parallel capillary model, the partition model predicts that the separation factor at low ionic strengths does not approach a constant value as the particle diameter increases.

Separation factors predicted by the partition model are compared with the experimental data from reference (13) in Figure 7. The partition model predicts the magnitude of the separation factor better than the parallel capillary model (see Figure 1), however the parallel capillary model predicts the shape of the curves better. This suggests that neither model alone is sufficient to account for the separation.

### Combination of Models

The previous calculations indicate that both flow-through pore capillaries and partitioning may contribute to porous HDC separation. To investigate this possibility, the column can be modelled as banks containing large capillaries, small capillaries, and large capillaries with attached cylindrical pores as illustrated in Figure 8. In the model sketched, || refers to the portion of the bed cross-section which consists of a parallel array of large diameter flow-through interstitial capillaries, denoted  $l$ , and small diameter flow through capillaries,  $s$ , which correspond to the portion of the porous phase which is

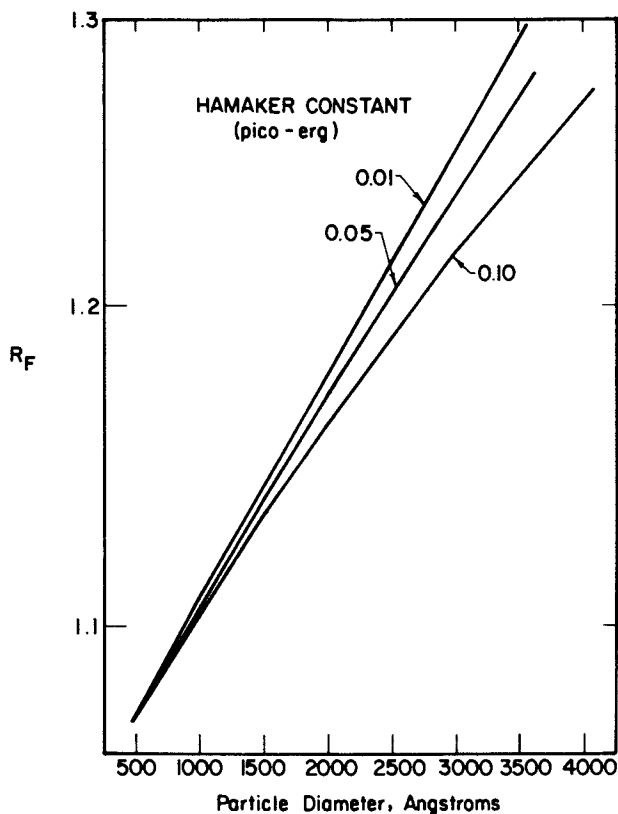


Figure 3. Separation factor-particle diameter behavior computed from the pore-partitioning model showing the effect of the Hamaker constant at a low eluant ionic strength (0.001 M). Other parameters are  $\Phi_p = 0.60$ , interstitial capillary radius =  $16 \mu\text{m}$ , pore radius =  $1.25 \mu\text{m}$ , cylinder (packing) surface potential 30 mV, particle surface charge density =  $1.5 \times 10^4 \text{ stc/cm}^2$ ,  $\epsilon = 74.3$ , and  $T = 300 \text{ }^\circ\text{K}$ .

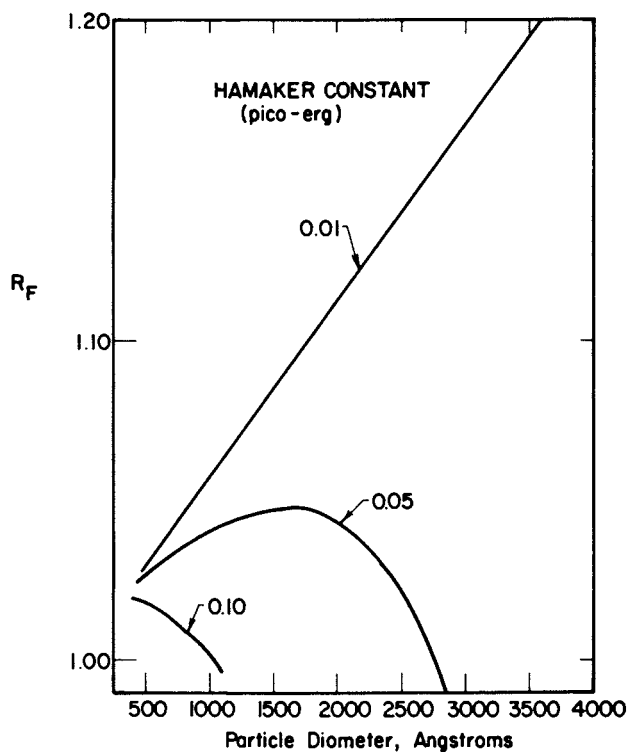


Figure 4. Separation factor-particle diameter behavior computed from the pore partitioning model showing the effect of the Hamaker constant at high ionic strength, 0.1 M. Other model parameters have same values as Figure 3.

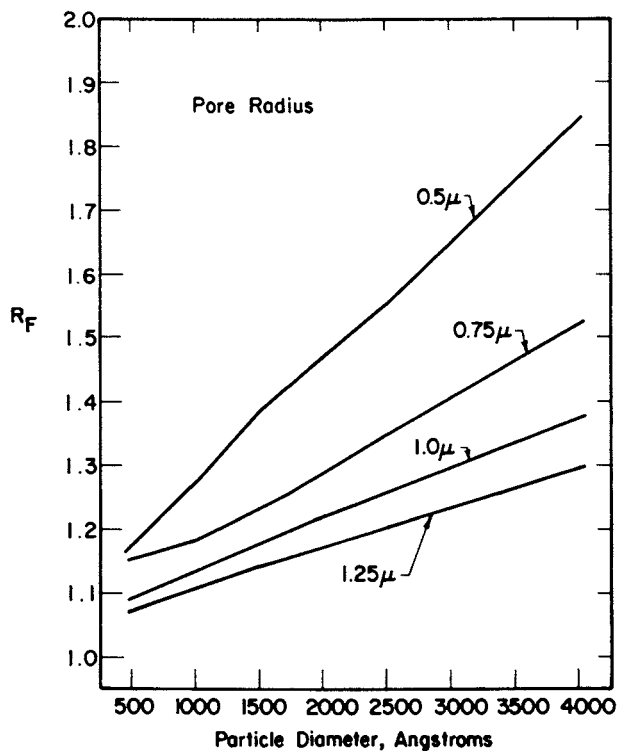


Figure 5. Separation factor-particle diameter behavior as a function of the pore radius for the pore-partitioning model. Hamaker constant = 0.05 pico-erg; all other parameters are the same as in Figure 3.

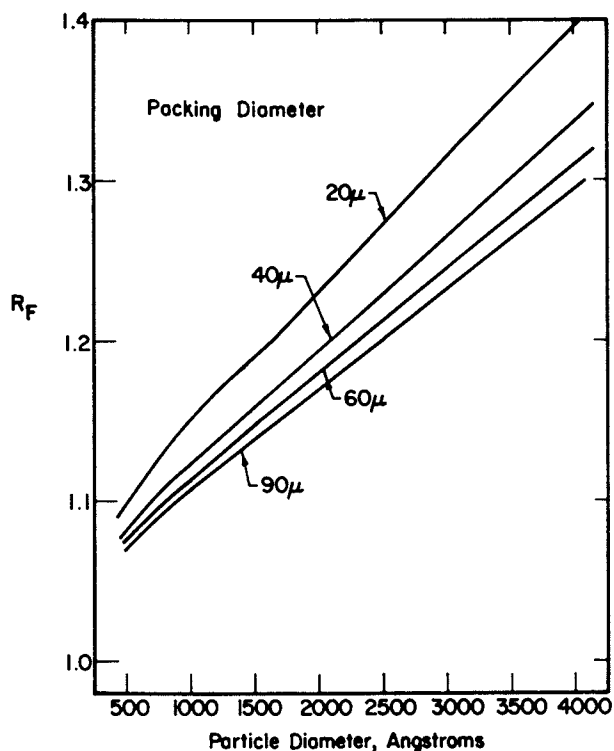


Figure 6. Separation factor-particle diameter behavior as a function of packing diameter for the pore-partitioning model. Parameters are the same as in Figure 3 with the exception of the interstitial capillary radius which was computed from the bed hydraulic radius (Equation 11 (7), with void fraction = 0.358).

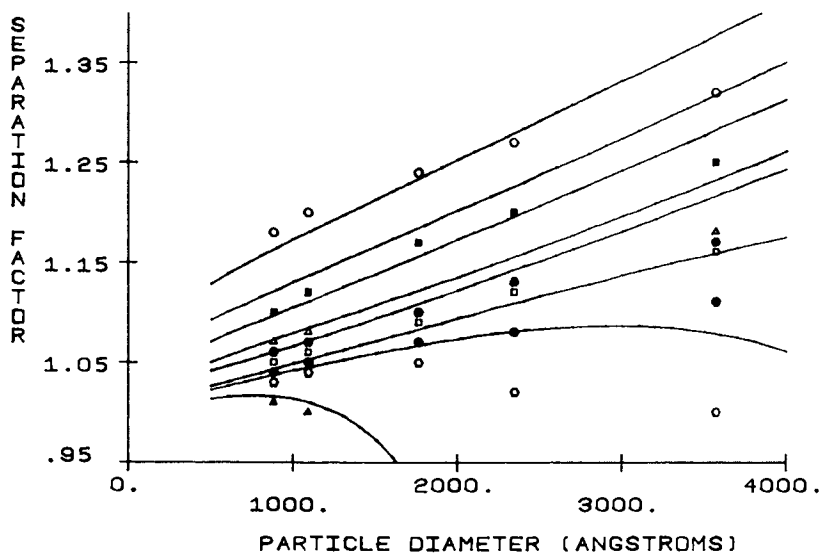


Figure 7. Comparison between  $R_F$  - particle size data of Figure 1 and the pore partitioning model. Parameters for model are the same as in Figure 3. Total ionic strengths:

Total ionic strengths:

- |              |              |              |
|--------------|--------------|--------------|
| ○ = 0.00022M | ■ = 0.00055M | △ = 0.00129M |
| ● = 0.00515M | □ = 0.0101M  | ● = 0.0210M  |
| ○ = 0.035M   | ▲ = 0.105M   |              |

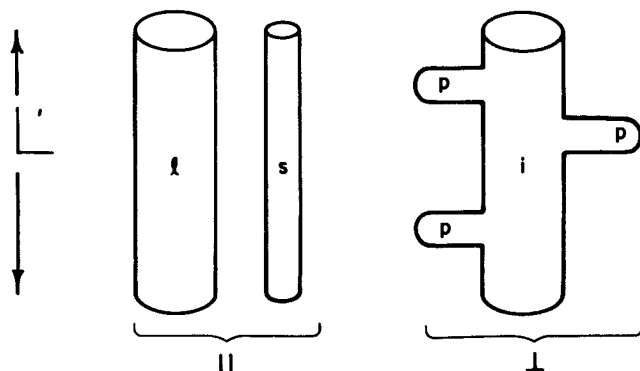


Figure 8. Schematic illustration of bed cross section for the combination model. See text for explanation of nomenclature.

flow-through. The portion of the cross section associated with the partitioning process is denoted  $l$ , and consists of large, flow-through interstitial capillaries,  $i$ , to which are attached stagnant pore volume cylinders,  $p$ , with which particles partition during passage through the  $i$  tubes. Derivation of the separation factor for this model follows the development given earlier for a purely flow-through system (13). The particle elution volume is given by

$$V_{R,P} = Q_F \langle t \rangle \quad (17)$$

where  $Q_F$  is the eluant flow rate, and  $\langle t \rangle$  is the mean residence time. Since the average residence time is the sum of the times the particle spends in each capillary,

$$\langle t \rangle = n_l \langle t \rangle_l + n_s \langle t \rangle_s + n_l \langle t \rangle_l \quad (18)$$

where  $n_j$  is the total number of capillaries of type  $j$  the particle samples, and  $\langle t \rangle_j$  is the average retention time in a capillary of type  $j$ .

Since the probability that a particle will sample a capillary of type  $j$  is given by

$$p_j = N_j q_j / Q_F \quad (19)$$

where  $N_j$  is the number of capillaries of type  $j$  in a bank, and  $q_j$  is the flow rate in a capillary of type  $j$ , then the total number of capillaries of type  $j$  a particle samples is

$$n_j = n p_j = n N_j q_j / Q_F \quad (20)$$

where  $n$  is the number of banks. The average marker velocity in a capillary of type  $j$  is given by

$$\langle v_m \rangle_j = q_j / a_j \quad (21)$$

where  $a_j$  is the cross-sectional area of the capillary and the average time for a particle in a given capillary is

$$\langle t \rangle_j = \frac{L'}{\langle v_p \rangle_j} \quad (22)$$

Combining Equations 17 to 22 yields

$$\frac{1}{R_F} = \frac{V_l}{V_m} \frac{1}{R_{F,l}} + \frac{V_s}{V_m} \frac{1}{R_{F,s}} + \frac{V_i}{V_m} \frac{1}{R_{F,i}} \frac{\langle v_m \rangle_i}{\langle v_m \rangle_l} \quad (23)$$

where  $V_j$  is the volume of all capillaries of type  $j$ , and  $R_{F,j}$  is the separation factor in a capillary of type  $j$ .

The expression for the mean particle retention time (Equation 11) may be written for the marker and manipulated to yield

$$\frac{\langle v_m \rangle_l}{\langle v_m \rangle_i} = \frac{1}{1 + K_m \sigma} \quad (24)$$

Substituting Equations 13 and 24 into Equation 23 yields

$$\frac{1}{R_F} = \frac{V_l}{V_m} \frac{1}{R_{F,l}} + \frac{V_s}{V_m} \frac{1}{R_{F,s}} + \frac{V_i}{V_m} \frac{1}{R_{F,i}} [1 + K\sigma] \quad (25)$$

Since  $R_{F,l}$  simply refers to the HDC separation factor associated with the interstitial capillaries (i and l of Figure 9), to be consistent with the nomenclature of Equation 4 we shall now refer to it as  $R_{F,i}$ . Likewise  $R_{F,s}$  refers to the hydrodynamic flow-through pores of Figure 8 and in the nomenclature of Equation 4 this becomes  $R_{F,p}$ . Making these changes in Equation 25 and rearranging gives the final result.

$$\frac{1}{R_F} = \frac{\phi_i}{R_{F,i}} + \frac{(1 - \psi)(1 - \phi_i)}{R_{F,p}} + \frac{\psi(1 - \phi_i)K}{R_{F,i}} \quad (26)$$

In Equation 26, the term  $\phi_i$  is as originally defined (i.e., volume fraction of the total void volume associated with the interstitial void space),  $\psi$  represents the fraction of the porous phase with which the particles interact by pure partitioning, and  $\Psi$  represents the fraction of the interstitial void volume associated with the partitioning process (l phase of Figure 9). The definition of  $\phi_i$  is based on the total void volume associated with the marker species, which in general will not be the same as the true void volume due to electrostatic repulsion and partitioning of the marker. On the other hand,  $V_p$  is the experimentally accessible quantity and the problem formalism explicitly corrects for the latter effects through expressions of the type given by Equations 3 and 24.

It is useful to check the asymptotic behavior of this expression. For nonporous packing,  $\phi_i = 1$ , and Equation 26 becomes

$$\frac{1}{R_F} = \frac{1}{R_{F,i}} \quad (27)$$

which is the expression for nonporous HDC.

For porous packing with all flow-through pores,  $\psi = 0$ ,  $\Psi = 0$ , and Equation 26 becomes

$$\frac{1}{R_F} = \frac{\phi_i}{R_{F,i}} + \frac{(1 - \phi_i)}{R_{F,p}} \quad (28)$$



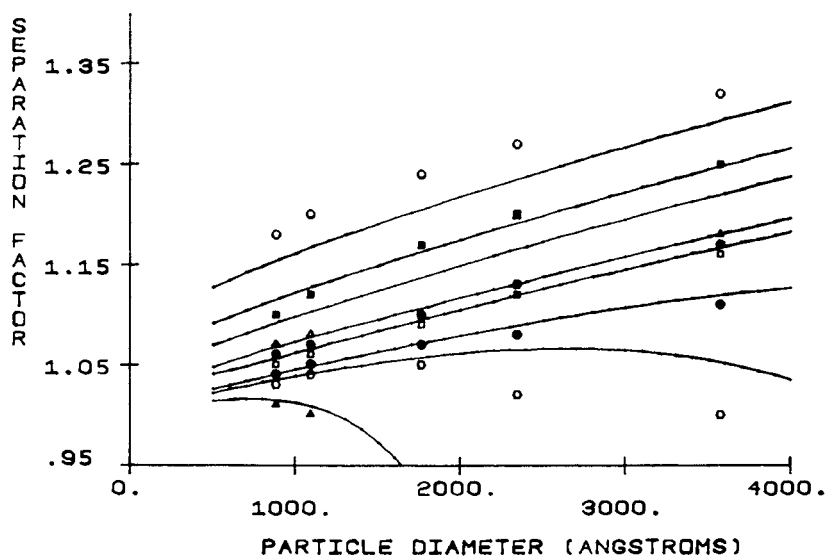


Figure 9. Comparison between the data of Figure 1 and the combination model for  $\psi = \Psi = 0.5$ . All other parameters are the same as in Figure 3. Ionic strengths are the same as in Figure 8.

and since for this case,  $\phi_p = 1 - \phi_1$  the above is the expression for the parallel capillary model of porous HDC given by Equation 4.

For a system which consists of a porous matrix which is purely partitioning, all of the interstitial capillaries will have connected pores,  $\Psi = 1$ , and all of the pores will partition particles,  $\psi = 1$ , thus Equation 26 becomes

$$\frac{1}{R_F} = \frac{\phi_1}{R_{F,1}} (1 + K\sigma) \quad (29)$$

which is the expression for the partition model with  $K_m = 1$  given in Equation 13.

Figure 9 shows the data fit obtained by use of Equation 26 with  $\psi = \Psi = 0.5$ . These results illustrate that by including all three mechanisms (HDC in small and large capillaries, and particle partitioning) an improved fit results. At this point, it must be emphasized that although  $\psi$  and  $\Psi$  are computational parameters with arbitrarily chosen values, they represent physically meaningful quantities with regard to the separation process.

Further work is needed to relate all of the parameters to experimentally accessible quantities.

#### Literature Cited

- (1) Collins, E. A.; Davidson, J. A.; Daniels, C. A. J. Paint Technol. 1975, 47, 604.
- (2) Kavanaugh, M.; Leckie, J. O., Eds.; "Particulates in Water: Characterization, Fate, Effects, and Removal"; ADVANCES IN CHEMISTRY SERIES, American Chemical Society: Washington, D. C., 1980.
- (3) McHugh, A. J.; Nagy, D. J.; Silebi, C. A. in "Size Exclusion Chromatography (GPC)"; Provder, T., Ed.; ACS SYMPOSIUM SERIES No. 138, American Chemical Society: Washington, D.C., 1980; pp. 1-25.
- (4) Small, H. J. Colloid Interface Sci., 1974, 48, 147.
- (5) Krebs, K. F.; Wunderlich, W. Angew. Makromol. Chem., 1971, 20, 203.
- (6) Stoitsits, R. F.; Poehlein, G. W.; Vanderhoff, J. W. J. Colloid Interface Sci. 1976, 6, 237.
- (7) McHugh, A. J.; Silebi, C. A.; Poehlein, G. W.; Vanderhoff, J. W. "Colloid Interface Science"; Vol. IV, Academic: New York, 1976, p. 549.
- (8) Silebi, C. A.; McHugh, A. J. AIChE J. 1978, 24, 204.
- (9) Prieve, D. C.; Hoysan, P. M. J. Colloid Interface Sci. 1978, 64, 201.
- (10) Nagy, D. J.; Silebi, C. A.; McHugh, A. J. J. Colloid Interface Sci. 1981, 79, 264.
- (11) Silebi, C. A.; McHugh, A. J. J. Appl. Polym. Sci. 1979, 23, 1699.

- (12) Silebi, C. A.; McHugh, A. J. in "Emulsions, Latices, and Dispersions"; Becher, P.; Yudenfreund, M. N., Eds.; Marcel Dekker: New York, 1978; pp. 155-174.
- (13) Nagy, D. J.; Silebi, C. A.; McHugh, A. J. in "Polymer Colloids II"; Fitch, R. M., Ed.; Plenum: New York, 1980; pp. 121-137.
- (14) Nagy, D. J.; Silebi, C. A.; McHugh, A. J. J. Appl. Polym. 1981, 26, 1555.
- (15) Gaylor, V. F.; James, H. L. Preprints, Pittsburgh Conference on Analytical Chemistry, Cleveland, March 1975.
- (16) Coll, H.; Fague, G. R. J. Colloid Interface Sci. 1980, 76, 116.
- (17) Singh, S.; Hamielic, A. E. J. Appl. Polym. Sci. 1978, 22, 577.
- (18) Nagy, D. J.; Silebi, C. A.; McHugh, A. J. J. Appl. Polym. Sci. 1981, 26, 1567.
- (19) Johnston, J. E.; Cowherd, C. L.; MacRury, T. B. in Size Exclusion Chromatography (GPC)", T. Provder, Ed., ACS SYMPOSIUM SERIES, No. 183, American Chemical Society; Washington, D.C., 1980, pp. 27-45.
- (20) Husain, A.; Hamielec, A. E.; Vlachopoulos, J. *ibid*, pp. 47-75.
- (21) Yau, W. W.; Kirkland, J. J.; Bly, D. D. "Modern Size-Exclusion Liquid Chromatography"; Wiley: New York; 1979.
- (22) DiMarzio, E. A.; Guttman, C. M.; Macromolecules, 1970, 3, 131.
- (23) Guttman, C. M.; DiMarzio, E. A.; Macromolecules, 1970, 3, 681.
- (24) Verhoff, H. F.; Sylvester, N. D.; Macromol. Sci-Chem., 1970, A4, 979.
- (25) Brenner, H.; Gaydos, L. J.; J. Colloid Interface Sci., 1977 58, 312.
- (26) Lee, H. L.; Lightfoot, E. N.; Reis, J. F. G.; Waissbluth, M. D. in "Recent Developments in Separation Science"; Li, N. N.; Ed. CRC Press: Cleveland; 1977, pp. 1-69.
- (27) Novak, J.; Janak, J.; Wicar, S.; in Jour. of Chromatogr., 3, "Liquid Column Chromatography", Deyl, Z.; Macek, K.; Janak, J.; Eds. Elsevier: New York; 1975; pp. 25-43.
- (28) Horn, F. J. M. AIChE J., 1971, 17, 613.
- (29) Francis, D. C., M. S. Thesis, University of Illinois, 1983.
- (30) Hermans, J. J., J. Polym. Sci., 1968, A-2, 6, 1217.
- (31) Reis, J.F.G.; Lightfoot, E. N.; Noble, P. T.; Chang, A. S. Sep. Sci. Techn., 1979, 14, 367.
- (32) Ouano, A. C.; Barker, J. A. Sep. Sci., 1973, 8, 673.
- (33) Giddings, J. C.; Kucera, E.; Russell, C. P.; Myers, M. N. J. Phys. Chem., 1968, 72, 4397.
- (34) Giddings, J. C. in "Treatise Anal. Chem.", 2nd ed., P. Elving, Ed., 1982, 1, (5).
- (35) Smith, F. G.; Deen, W. M. J. Colloid Interface Sci., 1980, 78, 444.

- (36) Bell, G. M.; Levine, S.; McCartney, L. N. J. Colloid Interface Sci., 1970, 33, 335.
- (37) Ohshima, H.; Healy, T. W.; White, L. R. J. Colloid Interface Sci., 1982, 90, (1), 17.
- (38) Clayfield, E. J.; Lumb, E. C. Disc. Faraday Soc., 1966, 42, 285.
- (39) Gregory, J. J. Colloid Interface Sci., 1981, 83, (1), 138.

RECEIVED September 12, 1983

# Computer Model for Gel Permeation Chromatography of Polymers

DONG HYUN KIM<sup>1</sup> and A. F. JOHNSON<sup>2</sup>

Department of Chemical Engineering, University of Waterloo, Waterloo, Ontario, Canada, N2L 3G1

A novel dynamic mass-balance model has been developed to describe the fractionation of polymers by gel permeation chromatography. The model embodies several dimensionless parameter groups which are particularly convenient to use in order to predict the performance of the chromatograph under a wide variety of conditions. It is shown that the molecular separation processes are readily explained in terms of the accessible void volume fraction in the gel column packing material and the broadening effect by a dimensionless parameter ( $\alpha$ ) which is a function of column length, particle radius of the column packing, eluant flow rate and the effective diffusivity of the polymer molecules in the gel. Good agreement has been observed between the model predictions and experimental results. The model predictions are compared with other published data.

Since the technique was introduced (1) in 1964, gel permeation chromatography (GPC), or size exclusion chromatography (SEC), has played an increasingly important role for the characterisation of polymers. The theory and practice of this chromatographic method have been extensively reported and a comprehensive text has recently been published on modern size exclusion chromatography (2).

One of the least well understood aspects of the whole field is the precise physical nature of the process whereby polymer chains of a different size are separated by passage through a gel column. On a qualitative level adequate explanations of the phenomenon exist but it has proved to be a more difficult task to formulate and solve anything other than the simplest of mathematical models of the chromatographic process.

Broadly, there are two classes of model which have found application (2): The plate theory is based on an oversimplified

<sup>1</sup>Current address: Korea Advanced Institute of Science and Technology, Seoul, Korea

<sup>2</sup>Current address: School of Polymer Science, University of Bradford, Bradford, BD7 1DP, England

view of the chromatographic process and has been widely described and used especially as an aid to the interpretation of gas chromatographic phenomena. The appeal of the plate theory is its simplicity but, as will be seen later, in many aspects it is far from adequate when used to describe some experimentally observed phenomena in gel permeation chromatography. The alternative modelling approach, the rate theory, appears to have grown out of the van Deemter equation (3) and takes into account axial dispersion phenomena and mass transfer between the bulk flow and the column packing material. A limitation of the van Deemter equation is that it does not take into account intra-particulate diffusion. However, an extension of this approach through the use of Fick's Law, has made it possible to formulate the differential equations which describe solute mass balance in a very small column section.

There have been relatively few applications of the rate theory to GPC, presumably because of the apparent complexity of this approach. One of the most widely quoted interpretations of the rate theory to GPC is that of Ouano and Baker (4). These authors have attempted to take advantage of the undoubted potential of the rate theory approach in constructing a model. They identified the key parameters in their model as the flow rate of the eluant, gel particle size, diffusion coefficient in the stationary and mobile phases and the partition coefficient for solute between phases. Although there is little doubt that the important parameters have been correctly identified, it is not immediately apparent how they are inter-related and hence how their coupled effect can be interpreted. A critical account of the various attempts which have been made to model the GPC process will be given elsewhere.

In the model described in this work every effort has been made to ensure that it embodies physically meaningful parameters. It is inevitable, however, that some simplistic idealizations of the physical processes involved in GPC must be made in order to arrive at a system of equations which lends itself to mathematical solution. The parameters considered are, the axial dispersion, interstitial volume fraction, flow rate, gel particle size, column length, intra-particle diffusivity, accessible pore volume fraction and mass transfer between the bulk solution and the gel particles. A coherent inter-relationship has been established between each of these parameters through a few, readily handled, dimensionless parameters.

Amongst the assumptions we have made in developing the model are the following: that Fick's law is applicable to the diffusion processes, the gel particles are isotropic and behave as hard spheres, the flow rate is uniform throughout the bed, the dispersion in the column can be approximated by the use of an axial dispersion coefficient and that polymer molecules have an independent existence (i.e. very dilute solution conditions exist within the column). Our approach borrows extensively many of the concepts which have been developed to interpret the behaviour of packed bed tubular reactors (5).

### Model Development

The proposed model can be developed by consideration of three important steps in the chromatographic process:

- (i) Dispersion and/or backmixing.
- (ii) Mass transfer between the gel and the mobile phase.
- (iii) Diffusion of the solute within the gel structure.

These are illustrated in Figure 1. The importance of these phenomena can be best shown by a general description of the gel permeation separation process.

The introduction of the polymer sample solution to the chromatographic column can be regarded as a sharp concentration pulse and is usually commonly represented mathematically as a Dirac delta function. Although this is an adequate description of the concentration pulse, it does not adequately represent the polydispersity which might exist in the polymer. In all modelling studies the polymer sample (e.g. monodisperse polystyrene standards), have been considered to be truly monodisperse although it is known that they do have a Poisson distribution of molecular sizes (6). As the sample is eluted through the packed column it is fractionated according to molecular size by the difference in the accessible pore volume of the gel. The chromatogram will be 'broadened' by a combination of factors such as diffusion within the gel particles, dispersion in the mobile phase and solute transfer between the gel and the eluant. The observed chromatogram is, in effect, the sum of many overlapping peaks.

The gel particles making up the column packing are commonly spherical in shape and have diameters in the range of  $5-50 \times 10^{-6}$  m. In order to facilitate modelling it is assumed that in any given column the particles are all of equal size and that each particle has an equal pore-size distribution. It is generally accepted that, when column packing particles have a diameter which is a factor of at least 20 less than that of the column, plug flow with some superimposed dispersion can be assumed in the column.

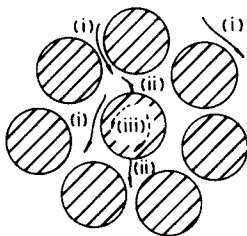


Figure 1. Three different mechanisms for fractionation:  
(i) Dispersion; (ii) Mass transfer between gel and mobile phase; (iii) Diffusion within the gel structure.

On the above basis the mobile phase material balance equation can be written as:

$$D_{ax} \frac{\partial^2 c^*}{\partial x^2} - u \frac{\partial c^*}{\partial x} - \frac{3 D_e}{R_0} \left( \frac{1 - \epsilon}{\epsilon} \right) \left( \frac{\partial c_s^*}{\partial r^*} \right)_{R_0} = \frac{\partial c^*}{\partial t} \quad (1)$$

where  $D_{ax}$  is the axial diffusion coefficient,  $D_e$  the effective diffusivity coefficient for the solute in the gel,  $c^*$  is the solute concentration in the mobile phase,  $c_s^*$  solute concentration within the gel,  $R_0$  the radius of the gel particle,  $x$  and  $r^*$  represent distance variables along the column and within the particle respectively and  $\epsilon$  is the interstitial volume fraction.

The stationary phase material balance equation is:

$$\frac{D_e}{\epsilon_p} \left( \frac{\partial^2 c_s^*}{\partial r^{*2}} + \frac{2}{r^2} \frac{\partial c_s^*}{\partial r^*} \right) = \frac{\partial c_s^*}{\partial t} \quad (2)$$

Here  $\epsilon_p$  is the accessible pore volume fraction of the gel which is a function of the pore size distribution as well as the size of a polymer molecule. The value of  $\epsilon_p$  is given by Equation 3:

$$\epsilon_p = \int_{\bar{r}}^{\infty} K_{SEC}(\bar{r}, \eta) \phi(\eta) d\eta / \int_{\bar{r}}^{\infty} \phi(\eta) d\eta \quad (3)$$

where  $K_{SEC}$  is the solute distribution coefficient,  $\bar{r}$  the equivalent hard-sphere radius,  $\eta$  the pore radius and  $\phi$  is the pore size distribution.

The initial and boundary conditions are:

$$C^*(x, 0) = C_s^*(r^*, 0) = 0 \quad (4)$$

$$K_f (C^* - C_s^*) = \frac{D_e}{\epsilon_p} \left( \frac{\partial C_s^*}{\partial r^*} \right) \quad (\text{for all } x, r^* \leq R_0) \quad (5)$$

$$C_{in}^*(t) = C^*(0^+, t) - \frac{D_{ax}}{u} \frac{\partial c^*}{\partial x} \Big|_{x=0^+} \quad (6)$$

$$\frac{\partial c^*}{\partial x} \Big|_{x=L^-} = 0 \quad (7)$$

Equations 6 and 7 are the well known Danckwerts boundary conditions (7). In Equation 5,  $K_f$  is the mass transfer coefficient around the gel, and  $C_{in}^*(t)$  the inlet solute concentration which is a function of analysis time.

The above equations can be most conveniently handled in their dimensionless forms.



$$\frac{1}{Pe} \frac{\partial^2 c}{\partial z^2} - \frac{\partial c}{\partial z} - 3\alpha \left( \frac{1-\epsilon}{\epsilon} \right) \left( \frac{\partial c_s}{\partial r} \right)_{r=1} = \frac{\partial c}{\partial \theta} \quad (1a)$$

$$\frac{\alpha}{\epsilon_p} \left( \frac{\partial^2 c_s}{\partial r^2} + \frac{2}{r} \frac{\partial c_s}{\partial r} \right) = \frac{\partial c_s}{\partial \theta} \quad (2a)$$

$$\text{where } \alpha = \frac{L D_e}{u R_o^2}, \quad z = \frac{x}{L}, \quad \theta = \frac{ut}{L}, \quad Pe = \frac{Lu}{D_{ax}}, \quad r = \frac{r^*}{R_o} \quad (3a)$$

$$c = \frac{C}{C_o}, \quad c_s = \frac{C_s}{C_o}$$

The equivalent dimensionless initial and boundary conditions are:

$$c(z, 0) = c_s(r, 0) = 0 \quad (4a)$$

$$\gamma (c - c_s) = \left( \frac{\partial c_s}{\partial r} \right) \text{ at } r = 1, \text{ all } z \quad (5a)$$

$$c_{in}(\tau) = c(0^+, \tau) - \frac{1}{Pe} \frac{\partial c}{\partial z} \Big|_{z=0^+} \quad (6a)$$

$$\frac{1}{Pe} \cdot \frac{\partial c}{\partial z} \Big|_{z=1^-} = 0 \quad (7a)$$

$$\text{where } c_{in} = \frac{C_{in}^*}{C_o}, \quad \gamma = K_f \frac{R_o \epsilon_p}{D_e}$$

Equations 1a - 7a do not have an analytical solution in a closed form in the time domain and of necessity have to be handled in the Laplace domain.

The Laplace domain solution is:

$$\frac{\bar{c}(z, s)}{\bar{c}_{in}(s)} = 2 \exp\left\{ \frac{Pe \cdot z}{2} \right\} \frac{\sinh\left[ \frac{Pe}{2} \beta (1-z) \right] + \beta \cosh\left[ \frac{Pe}{2} \beta (1-z) \right]}{(1+\beta^2) \sinh\left( \frac{Pe}{2} \cdot \beta \right) + \cosh\left( \frac{Pe}{2} \cdot \beta \right)} \quad (8)$$

$$\text{where } \beta = \sqrt{1 + \frac{4}{Pe} h(s)} \quad (9)$$

$$\text{and } h(s) = 3\alpha \left( \frac{1-\epsilon}{\epsilon} \right) \cdot \gamma \cdot \left[ \frac{\sqrt{\frac{s \cdot \epsilon_p}{\alpha}} \coth \sqrt{\frac{s \cdot \epsilon_p}{\alpha}} - 1}{\sqrt{\frac{s \cdot \epsilon_p}{\alpha}} \coth \sqrt{\frac{s \cdot \epsilon_p}{\alpha}} - 1 + \gamma} \right] \quad (10)$$

Here  $s$  is the Laplace variable and  $\bar{c}_{in}(s)$  the Laplace transform of the input. When  $\bar{c}_{in}(t)$  can be approximated by a Dirac delta function,  $\bar{c}_{in}(s) = 1$  and the right hand side of Equation 8 is the Laplace transform of the solute concentration at any  $z$ .

The solutions of Equations 8-10 were obtained with an IBM 370 computer using an improved version of the Filon method (8).

The leading moments at the exit ( $z=1$ ) were used to obtain the mean, variance and skewness of the peaks and these can be calculated from the relation:

$$M_n = \int_0^{\infty} \theta^n c(1, \theta) d\theta = \lim_{s \rightarrow 0} (-1)^n \frac{d^n}{ds^n} \bar{c}(1, s) \quad (11)$$

The first moment  $M_1$  provides the mean dimensionless elution time:

$$M_1 = \delta_1 - 1 + \frac{1 - \epsilon}{\epsilon} \cdot \epsilon_p \quad (12)$$

The second moment is:

$$M_2 = \left( \frac{2}{Pe} \right)^2 \delta_1^2 \left( \frac{Pe^2}{4} + \frac{Pe}{2} - \frac{1}{2} + \frac{1}{2} \exp(-Pe) \right) + \delta_2 \quad (13)$$

$$\text{where } \delta_2 = \frac{2}{3} \alpha \left( \frac{1 - \epsilon}{\epsilon} \right) \left( \frac{\epsilon_p}{\alpha} \right)^2 \left( \frac{1}{5} + \frac{1}{\gamma} \right) \quad (14)$$

and the third moment is:

$$M_3 = \left( \frac{2}{Pe} \right)^3 \delta_1^3 \left( -3 + \frac{3}{4} Pe + \frac{3}{4} Pe^2 + 3 \exp(-Pe) + \frac{Pe^3}{8} + \frac{9}{4} Pe \exp(-Pe) \right) + 3\delta_1 \delta_2 \left( \frac{2}{Pe} \right)^2 \left( \frac{Pe^2}{4} + \frac{Pe}{2} - \frac{1}{2} + \frac{1}{2} \exp(-Pe) \right) + \delta_3 \quad (15)$$

$$\text{where } \delta_3 = \frac{2}{3} \alpha \left( \frac{1 - \epsilon}{\epsilon} \right) \left( \frac{\epsilon_p}{\alpha} \right)^3 \left( \frac{6}{105} + \frac{2}{5\gamma} + \frac{1}{\gamma^2} \right) \quad (16)$$

The central moments may be obtained from Equation 17:

$$\mu_n = \int_0^{\infty} (\theta - M_1)^n c(1, \theta) d\theta \quad (17)$$

The second central moment which provides the variance of the distribution has the form:

$$\mu_2 = \left( \frac{2}{Pe} \right)^2 \delta_1^2 \left( \frac{Pe}{2} - \frac{1}{2} + \frac{1}{2} \exp(-Pe) \right) + \delta_2 \quad (18)$$

The third central moment is:

$$\begin{aligned} \mu_3 = 3 \left(\frac{2}{Pe}\right)^3 \delta_1^3 \left(\frac{Pe}{2} - 2 + \left(\frac{Pe}{2} + 1\right) \exp(-Pe)\right) + 3\delta_1 \delta_2 \\ \left(\frac{2}{Pe}\right)^2 \left(\frac{Pe}{2} - \frac{1}{2} + \frac{1}{2} \exp(-Pe)\right) + \delta_3 \end{aligned} \quad (19)$$

The peak skew is given by:

$$\mu_s = \frac{\mu_3}{\mu_2^{3/2}} \quad (20)$$

From the general plate theory (2) it is known that:

$$L \cdot \frac{\sigma^2}{V_R^2} = H \quad (21)$$

where H is the individual plate height,  $\sigma^2$  the variance and  $V_R$  the mean retention volume. Therefore it follows that:

$$\begin{aligned} H &= L \left(\frac{\mu_2}{M_1^2}\right) \\ &= L \left(\frac{2}{Pe}\right)^2 \left(\frac{Pe}{2} - \frac{1}{2} + \frac{1}{2} \exp(-Pe)\right) + \frac{\delta_2}{\delta_1} \end{aligned} \quad (22)$$

Column efficiency is most simply related to L/H.

### Model Input Parameters

In solving the model the quality of the result depends greatly on the accurate estimation of many parameters. It is not always easy to estimate the parameter required by the proposed model, hence some attention will be given to the methods we have adopted in obtaining them.

(i) Accessible Pore Volume Fraction,  $\epsilon_p$ . One of the primary factors in the effective separation of polymer molecules according to size is the accessible volume of the gel pores which is a function of the solute size as can be clearly seen from Equation 3.

Both  $K_{SEC}$  and the pore size distribution have been measured experimentally for hard-sphere column packing materials (9), but for soft gel packing materials there does not seem to be any reliable information presumably because the accepted method of pore structure characterisation in porous materials, mercury porosimetry, cannot be used. However,  $\epsilon_p$  can be measured for gels without great difficulty from the column calibration curve (as is manifest from Equation 12) provided the calibration is made on the basis of the peak mean position, i.e. the first moment of the peak

rather than the usual peak maximum. Obviously for perfectly symmetrical peaks the mean and the maximum coincide. In this work we have adopted the latter route to  $\epsilon_p$ .

(ii) Effective Diffusivity,  $D_e$ . Effective diffusivity in porous structures is relatively well understood for gases but much less well understood for liquids and is virtually unknown for polymer solute molecules (10). In attempting to arrive at a meaningful estimate for  $D_e$  we have adopted the following simple model (11) (Equation 24) which has frequently been used for gas phase effective diffusivity.

$$D_e = \frac{D_m \epsilon_p K_r}{\tau} \quad (24)$$

In this equation  $D_m$  is the diffusivity of the polymer solute in the bulk solution which may be estimated (12) from Equation 25:

$$D_m = \frac{RT}{6\pi\mu_o N_o} \left( \frac{10\pi N_o}{3K} \right)^{1/3} \left( \frac{\bar{M}_v}{M_v} \right)^{-(1+a)/3} \quad (25)$$

where  $R$  is the gas constant,  $T$  the absolute temperature,  $\mu_o$  the solvent viscosity  $K$  and  $a$  are the constants of the Mark-Houwink-Sakura equation and  $\bar{M}_v$  the viscosity average molecular weight. In Equation 24,  $K_r$  is the fractional reduction in the diffusivity within the gel pores which may be attributed to the friction effects of the solute with the 'walls' of the pores and it, in turn, may be obtained (11) through the use of Equation 26.

$$K_r = (1 - 2.104 \lambda + 2.09 \lambda^3 - 0.95 \lambda^5) \quad (26)$$

$$\text{where } \lambda = \frac{\bar{r}}{\bar{\eta}} \quad (27)$$

The value of  $\bar{\eta}$  was estimated using the simple approximation:

$$\bar{\eta} = (\bar{r} + \eta_{\max})/2 \quad (28)$$

The  $\eta_{\max}$  can be obtained from the GPC calibration curve by estimating the maximum molecular size of the solute which can penetrate the pores of the gel.

To be more rigorous  $K_r$  should be obtained from Equation 29:

$$K_r = \int_r^{\infty} (1 - 2.104\lambda + 2.09\lambda^3 - 0.95\lambda^5) \phi(\eta) \cdot d\eta / \int_{\bar{r}}^{\infty} \phi(\eta) d\eta \quad (29)$$

but since the use of this equation requires a value for the pore size distribution in the gel it cannot be readily used. As far as we are aware there are no experimental data available for pore size distributions in soft gels.

In Equation 24,  $\tau$  is the tortuosity, a term well established for gas diffusion into porous materials (10). It is unfortunate, but necessary to introduce  $\tau$  into our model. The value of  $\tau$  cannot be obtained a-priori and must be obtained experimentally since it is an almost impossible task to describe the complicated pore geometry in a gel. Given idealised perfect pore geometry it has been possible to estimate  $\tau$  for gas diffusion processes. In our work, of necessity  $\tau$  becomes an adjustable parameter to help achieve better agreement between the model predictions and experimental results. Since  $\tau$  is unmeasurable our only concern has been to use reasonable values in our simulations.

It will be seen later that it is very important to use a 'good' value for  $D_e$  in order to obtain agreement between the model predictions and experimental chromatograms. The parameter  $D_e$  is not only responsible for the fractionation of the polymer but also in determining the extent of broadening.

(iii) Mass Transfer Coefficient,  $K_f$ . Under the normal operating conditions for a chromatograph, particularly for the more recent high performance instruments, the Reynolds number, ( $Re_p$ ) is very low ( $\sim 0.001 - 0.5$ ). Numerous correlations have been proposed for  $K_f$  for situations where  $Re_p$  is relatively large (13), but for GPC only one appears to be suitable (14) for the estimation of  $K_f$  (Equation 30).

$$\epsilon j_D = 1.09 Re_p^{-2/3} \quad 0.0016 < Re_p < 55 \quad (30)$$

where  $j_D$  is the mass transfer Colburn j factor ( $\frac{K_f}{G} \rho Sc^{2/3}$ )  $G$  being the mass velocity of fluid,  $\rho$  is the fluid density and  $Sc$  the Schmidt number.

The value of  $K_f$  estimated in this way is far greater than the magnitude of  $D_e$  and for this reason plays a negligible role in the overall broadening effect as will be seen later. As already mentioned, the van Deemter model is also inadequate under most operating conditions of chromatographs as it only takes into account external (the gel particles) mass transfer and neglects the internal diffusion of the solute through the gel structure.

(iv) Axial Dispersion,  $D_{ax}$ . There are ample descriptions of the axial dispersion phenomenon in the field of packed bed reactors (15). The axial dispersion coefficient embodies all the factors which contribute to broadening from inter-particulate movement of solution. In this work  $D_{ax}$  can be related to terms of interest through Equation 31 since

$$\epsilon Pe_p = 0.011 Re_p^{0.48} + 0.20 \quad (31)$$

$$Pe_p = \frac{2\bar{u}R_0}{D_{ax}} \quad (32)$$

It is apparent from Equation 31 that when  $Re_p$  is very low, then  $Pe_p$  has an essentially constant value.

Experimental

A Waters Associates GPC (Model ALC/GPC 301) was used for experimental measurements. The instrument was fitted with a 100  $\mu$ l injection loop, a UV detector and a single  $10^3$  A Styragel column. The column specifications are:

Catalogue No. 26913 (Waters Associates)  
 Particle size 37-75  $\mu$   
 Plate count 350  
 Column ID 7.8 mm  
 Column length 61 cm

The following polystyrene standards (Pressure Chemical Co.) were used:

Sample	$\bar{M}_n$	$\bar{M}_w/\bar{M}_n$
A	1,800,000	1.28
B	390,000	1.09
C	51,000	1.05
D	37,500	1.05
E	17,500	1.05
F	9,000	1.05
G	4,000	1.10
H	2,100	1.15
Toluene	92	1.0

All measurements were carried out in THF at ambient temperature with sample concentrations of 0.1 wt. %. Normally a flow rate of 1.25 ml  $\text{min}^{-1}$  was used but with sample F further measurements were made at a flow rate of 2.21 ml  $\text{min}^{-1}$ .

Results and Discussions

The quality of the mathematical model can only be judged by its ability to predict the likely experimental results over a wide range of conditions. The goodness of the agreement between the predictions of our proposed model and experimental observations is very much dependent on the key parameters in the model being clearly defined and well understood as mentioned previously. One of the difficulties we have encountered in attempting to compare the model behaviour and experimental GPC traces has been in obtaining reliable estimates of  $P_e$  and  $D_e$ .

Calibration Curve. Figure 2 shows the calibration curve obtained for the single column. It is similar in character to others which have been reported.

This curve was used to calculate  $\epsilon_p$  from Equation 12 (which in turn required the calculations of  $\epsilon$  which will be described in the next section). It is important to note that the accessible pore volume varies for different solutes. If  $K_{SEC}$  and  $\phi$  (M) were explicitly available then Equation 3 could be used to obtain  $\epsilon_p$ .

The Case of Total Exclusion. One would expect for very fine particles that in the case of polymer samples which are totally excluded from the particle pores that the observed chromatogram would be symmetrical as the Pe should be very high ( $\sim 10,000$ ). Figure 3 shows the experimentally observed result for a polymer sample of molecular weight  $\sim 2,000,000$ . An identical result was obtained with a sample of molecular weight  $\sim 390,000$ . It can be seen that the curve is much as expected showing only slight skewing. Since the two samples gave indistinguishable results we conclude that the very slight skewing which can be detected stems from the fact that the column did not behave precisely according to the assumptions we have made in this work where perfect symmetry would be expected. Obviously this kind of minor discrepancy cannot be readily quantified as so many factors could be used by way of explanation for the effect and these might well have to be changed from column to column.

Figure 3 also illustrates that good agreement between the model prediction and experimental observation was obtained when  $Pe = 1130$ . The value for Pe was low on the basis of the correlation equation, Equation 31, which predicts a value of  $\sim 5000$ . Perhaps the discrepancy in Pe values is not too surprising in view of the large scatter of the data from which Equation 31 was obtained.

The total exclusion chromatogram provides the means to obtain the  $\epsilon$  values and this was found to be 0.423. It is interesting to compare this value with that reported (4) for the interstitial volume of randomly packed rigid spheres which is 0.364. We assume that our value deviates from the hard sphere value primarily because of the inefficient packing of particles in the case of the column used in this work varied substantially in size (35 - 75  $\mu$ ).

### Chromatographic Curves

(i) Symmetrical peaks - symmetrical chromatograms (within experimental error) were obtained with polymer samples of low molecular weight ( $< 9000$ ). Our model predicts this symmetry as will become apparent when the importance of the dimensionless group  $\alpha$  in the model is discussed below. It will be seen that as  $\alpha$  increases then the resulting peak should approach perfect symmetry. For all low molecular weight samples, it is evident from Equation 25 that  $D_m$  must be relatively large and in consequence  $D_e$  must also be

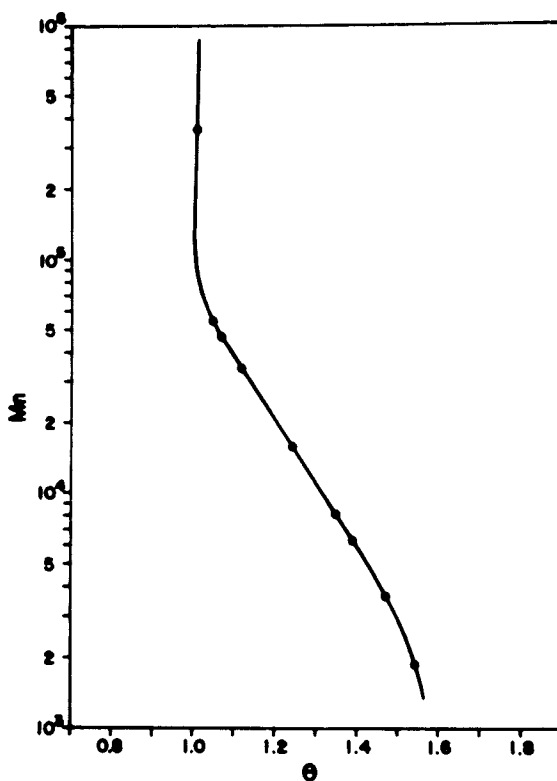


Figure 2. Calibration curve: this curve was obtained by using the mean of the chromatographic peak of each polystyrene standard.



large (Equation 24) which increases  $\alpha$ . The model readily fits any symmetrical chromatogram as can be seen in the typical example shown in Figure 4. In fitting the symmetrical chromatograms the calculated  $Pe$  (1130) was used throughout but some changes were made to  $\tau$  in order to achieve better fits. The  $\tau$  values are normally in the range 2-10 for hard spheres with gas phase systems (10). In this work values in the range 8-12 were adopted which we feel are reasonable for this convenient 'general purpose' adjustable parameter.

The computer model is capable of dealing with any eluant flow rate but it has only been possible to test the capacity of the model over a very small range of flow rates because of the danger of damaging a column when conducting experiments at high flow rates. Figure 4 also shows the good agreement which was obtained between experiment and calculation when the flow rate is approximately doubled. Increasing the flow rate broadens the peak and shifts the peak maximum in the manner anticipated (16).

(ii) Skewed peaks - for polymer of molecular weight 37,000 the chromatographic peak was distinctly skewed. The model proposed was also capable of fitting such curves as can be seen from Figure 5. To fit such curves the same  $Pe$  was used but the  $\tau$  was adjusted as before to achieve good fit between the model predictions and the experimental value.

On the basis of these preliminary experimental results we are confident the proposed model is capable of explaining many of the experimentally observed features of size exclusion chromatograms. It is perhaps appropriate to comment further on the physical importance of the major parameters of interest in the model.

The value of  $K_f R_0 \epsilon_p / D_e$  (or  $\gamma$ ) will, in our experience be large and on the order of several hundred. When Equations 13 and 15 are considered in the light of this information they can be simplified and  $\gamma$  plays no part in the overall broadening effect. This was readily apparent from the computer simulations.

The influence of  $Pe$  on the computed chromatogram can be seen in Figure 6. When the  $Pe > 10,000$  its influence on peak broadening is relatively insignificant. However, at low values it plays a significant role in determining peak shapes. In the experimental work reported here the column used was very short and hence  $Pe$  was also low and therefore influenced the peak shapes in the simulations. When  $Re_p$  is small then  $Pe_p$  becomes constant (see Equation 31) and hence  $Pe$  is proportional to column length. If longer column lengths are adopted than those used in this work (as will normally be the case) then  $Pe$  rapidly approaches a value where its effect on broadening becomes negligible.

Following the above rationalisation it becomes apparent that  $\alpha$  is the only significant dimensionless group in our model. Its influence is vividly demonstrated in Figure 7 which shows that by altering  $\alpha$  alone it is possible to cover all known peak shapes.

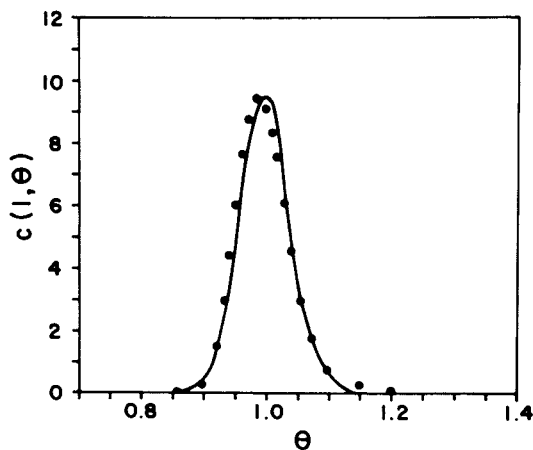


Figure 3. Model fitting of chromatogram of totally excluded standard polymer;  $\bar{M}_n = 1,800,000$ ,  $u = 0.103 \text{ cm sec}^{-1}$ ,  $Pe = 1130$ ,  $\epsilon = 0.423$ ,  $\circ$  = experimental data, — computed curve.

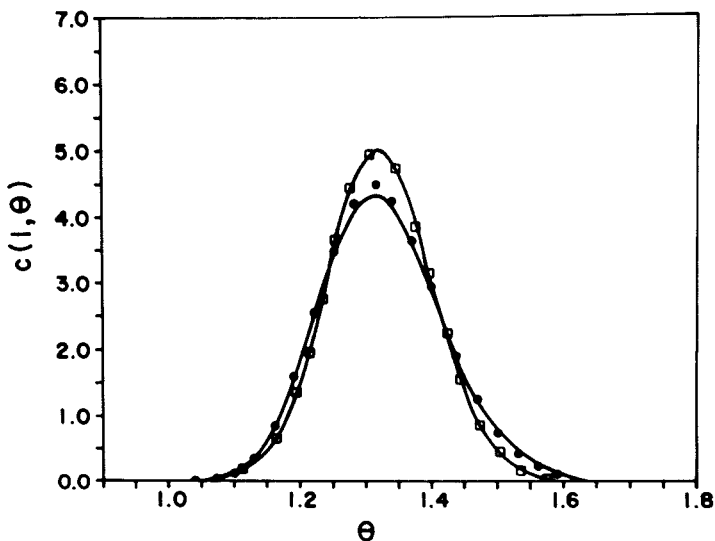


Figure 4. Model fitting of chromatograms which are approximately symmetrical;  $\bar{M}_n = 9,000$ ,  $Pe = 1130$ ,  $\epsilon = 0.423$ ,  $\epsilon_p = 0.224$ ,  $D_e = 3.79 \times 10^{-8} \text{ cm}^2 \text{ sec}^{-1}$ . Experimental data:  $u = 0.103 \text{ cm sec}^{-1}$  ( $\circ$ ),  $u = 0.182 \text{ cm sec}^{-1}$  ( $\square$ ), — computed curves with  $\tau = 12$ .

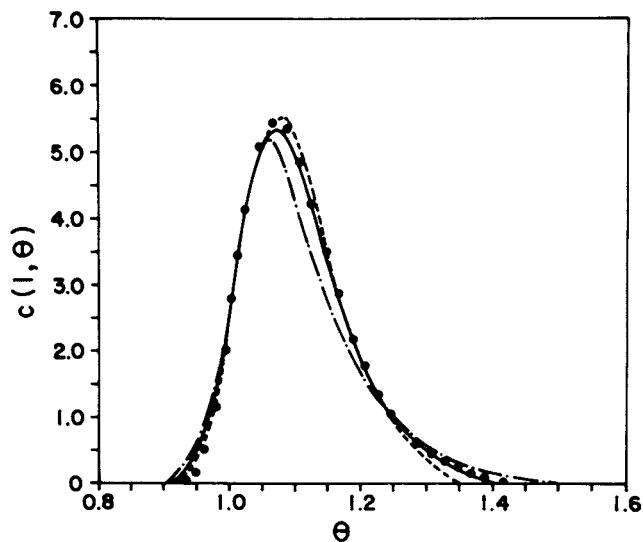


Figure 5. Model fittings of skewed chromatograms;  $\bar{M}_n = 37,000$ ,  $Pe = 1130$ ,  $\epsilon = 0.423$ ,  $\epsilon_p = 0.077$ ,  $D_e = 2.55 \times 10^{-9} \text{ cm}^2 \text{ sec}^{-1}$  ( $\tau = 8$ ),  $u = 0.103 \text{ cm sec}^{-1}$ . Experimental data: ( ), — computed curves. The computed curves with  $\tau = 6$  (----) and  $\tau = 12$  (- . - . -).

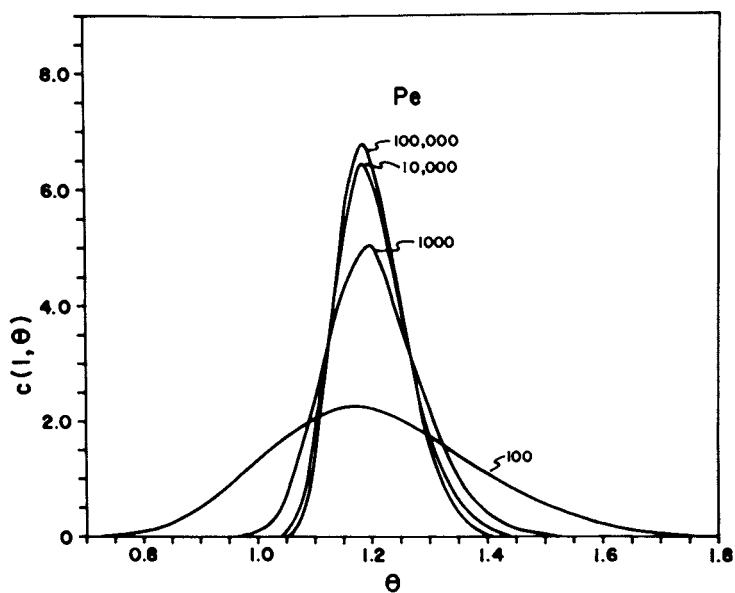


Figure 6. Effect of  $Pe$  values on model predictions. In each case  $\alpha = 1.0$ ,  $\epsilon_p = 0.15$ ,  $\gamma = 400$ ,  $\epsilon = 0.423$ .

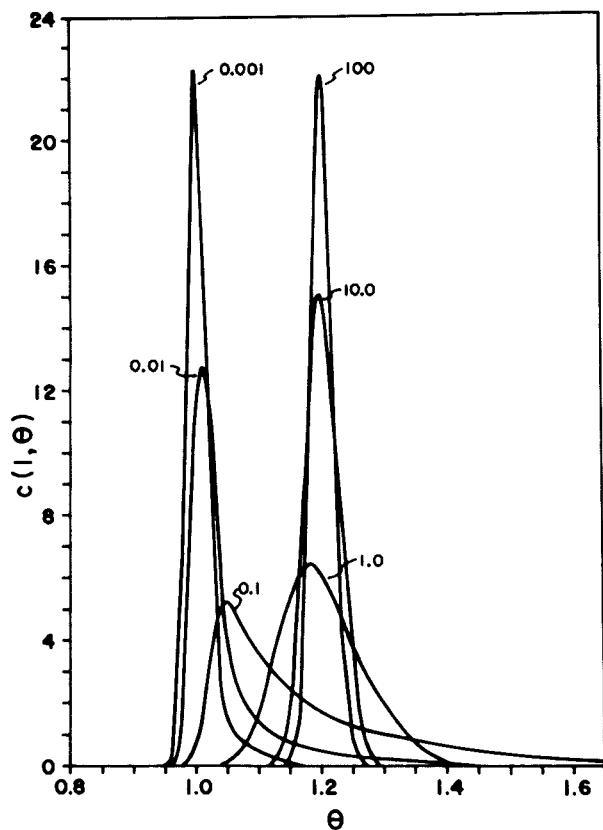


Figure 7. Effect of  $\alpha$  values on model predictions. In each case  $Pe = 10,000$ ,  $\epsilon_p = 0.15$ ,  $\gamma = 400$ ,  $\epsilon = 0.423$ .

When  $\alpha$  is large ( $> 100$ ) then the peak is symmetrical with a mean value of 1.20. In the extreme as  $\alpha \rightarrow \infty$  then the simulated peak approaches the input function which in our model simulation is a Dirac delta function at  $\theta = 1.2$ . In the real situation it should approach the true MWD of the polymer being analysed. As  $\alpha$  decreases the simulated peak is first broadened and then skewed. It is apparent that the peak maximum shifts in a manner expected. As  $\alpha \rightarrow 0$  the peak becomes similar to that expected for total exclusion. There is an apparent anomaly evident from Figure 7. The simulated peaks appear to have very different means, particularly where  $\alpha$  is small, yet one would expect from Equation 12 for the mean to be invariate with  $\alpha$ . In fact, at low  $\alpha$  values there are always extremely long tails at towards high  $\theta$  which cannot be adequately shown pictorially. The mean does, in fact, remain constant and it is only when  $\alpha = 0.0$  that the peak mean abruptly shifts to 1.0, i.e. there is a discontinuity of the mean as a function of  $\alpha$  at zero. This can be verified by the manipulation of Equations 8-11.

It is evident from Figure 7 that as  $\alpha$  increases the resolution as well as the symmetry is enhanced which explains the trend with modern columns towards fine gel particles. The parameter  $\alpha$  is such that it leads to the conclusion that when achieving the same resolving power it is possible to decrease the total analysis time by reducing the particle size, the time of analysis being proportional to  $1/R_0^2$ . This prediction is substantiated by published work (see Figure 5) (17). In going from particle sizes of 120  $\mu\text{m}$  to 6  $\mu\text{m}$  it has been shown that the total analysis time is reduced from 250 min to 37.5 sec which conforms exactly to the proportionality factor suggested (17). By increasing  $u$  one would expect poorer chromatograph performance which can be seen from Figure 5. The performance of the GPC should also increase in direct proportion to column length. The resolving power should increase with increasing  $D_e$  (i.e. decreasing molecular weight). Each of the other predictions conform to well established observations.

The proposed model can be readily related to the plate theory. The number of theoretical plates can be deduced from the moment expressions and when  $Pe$  and the  $K_f$  are large then Equation 33 follows from Equation 23.

$$\frac{1}{N} = \frac{2}{Pe} + \frac{2}{15} \frac{\left(\frac{1-\epsilon}{\epsilon}\right) \frac{\epsilon_p^2}{\alpha}}{\left(1 + \frac{1-\epsilon}{\epsilon} \epsilon_p\right)^2} \quad (34)$$

It is evident that  $\alpha$  also plays an important role in this equation. For a given  $\epsilon_p$  and  $Pe$  as  $\alpha$  increases then  $N$  also increases. This can be best demonstrated by varying the flow rate. Several experimental studies have been reported (18-19) with flow rates being changed over the range  $\sim 0-8$  ml/min. There is an interesting contradiction in these reports on the way in

which  $N$  varies at low flow rates. In one case (18) when using gel particles of 5  $\mu\text{m}$  and 10  $\mu\text{m}$  a maximum is observed in  $N$  at  $\sim 1\text{--}3$  ml/min which suggests that there is an optimum operating flow rate for GPC with these packing materials. In the same publication when 20  $\mu\text{m}$  particles were used  $N$  increased continuously down to very low flow rates, behaviour similar to that observed by other workers (19) with 10  $\mu\text{m}$  particles. The van Deemter model was invoked to explain the observed maximum in  $N$ . However, this model only takes into account the external mass transfer effect and does not consider  $D_e$ . Our model suggests that the correct relationship between  $N$  and flow rate does not contain a maximum (see Figure 4). At most one might expect, at extremely high  $\alpha$  values a plateau at very low flow rates ( $0.1$  ml  $\text{min}^{-1}$ ) and therefore the previously inexplicable experimental observations are the correct ones according to our model. The experimentally observed maximum may result from agglomeration effects with particles less than 20  $\mu\text{m}$  in size or other experimental anomalies. Clearly, additional experimental studies are desirable in order to clarify the behaviour of  $N$  with flow rate.

A further interesting feature of plate count predictions from the model is that  $N$  values can be compared with those quoted by column manufacturers for their products. In this work the quoted  $N$  value was 350 and that calculated was 280 at 1.25 ml/min when using polystyrene standard  $\bar{M}_n = 9000$ , i.e. one which gives a symmetrical curve. In making such comparisons one must bear in mind that the plate theory assumes that  $N$  is independent of polymer molecular weight which is not the case with our model. When a standard of  $\bar{M}_n = 37,000$  was used the calculated  $N$  was 160.

It has been suggested (20) that  $N$  varies with  $1/R_0$ . Clearly, this does not conform to our model prediction of  $N$  being proportional to  $1/R_0^2$ . We feel that this discrepancy stems entirely from the limited range of  $R_0$  values which were used in the experimental work. Had a wide range been used the parabolic nature of the relationship would probably have been seen.

On the basis of the above discussion we feel that our simple dimensionless parameter approach has a generality which has advantages over previously described models (2).

There are many facets of this study which we feel merit further investigation. In particular it is necessary to consider an extension of the proposed model, which in its present form is confined to the performance of a simple column, to cover the behaviour of any set of columns since it is column sets which are normally used. In addition, it is important to consider the input to the model which should be truly representative of polymers with a molecular weight distribution and not merely a concentration pulse of perfectly monodisperse polymer. In relation to this latter suggestion it would be significant if it were possible to link this model to the very real problem of deconvolution, i.e. the removal of instrumental and column broadening from the observed chromatogram to produce the true molecular weight distri-

bution of the input sample. Although we have given some preliminary consideration to this point, it is not immediately apparent as to how the problem can be resolved mathematically.

### Summary

Despite the assumptions and simplifications we have made in arriving at a model we feel that the physical basis we have adopted is sufficiently realistic to give good predictions, certainly as far as our present experimental results enable us to make tests. The numerical solution of the model equations we have used presented no difficulties using a fast computer ( $\sim 5$  secs per solution).

We feel that one of the attractions of the approach we have adopted is that very few parameters are required to control the model. We have proposed that the use of a particularly important dimensionless parameter  $\alpha$  which plays a significant role not only in predicting our own experimental observations but also in explaining the results of others. Indeed, several anomalies in the literature have come to light as a result of comparing our predictions with published information.

It is apparent that the plate theory cannot possibly explain skewed chromatograms. We suggest that the major reason for this limitation is that it is not correct to assume that an equilibrium is achieved between the solute in the mobile and stationary phase during analysis.

### Acknowledgments

The authors wish to express their gratitude to their respective Institutions for leave of absence and to the Department of Chemical Engineering, University of Waterloo for its generosity in providing the support and facilities which has made this work possible. We also appreciate the assistance given by Mr. A. Burczyk with GPC measurements and Mr. S. Lee for the drawing of the figures.

### Glossary

$\alpha$	$L \cdot D_e / u \cdot R_0^2$ dimensionless number
$a$	Mark-Houwink-Sakurada constant
$D_{ax}$	Axial diffusion coefficient
$D_e$	Effective diffusivity coefficient of the solute in the gel
$D_m$	Diffusivity of the solute in solution
$c = c^* / C_0$	Dimensionless concentration
$c_0^*$	Initial concentration of solute in eluant
$c^*$	Solute concentration in the mobile phase
$c_{s1}^* \Rightarrow c_{s1}^* / C_0$	Dimensionless concentration within gel
$c_{s2}^*$	Solute concentration within the gel
$c_{in}^*(t)$	Inlet solute concentration which is a function of time

$\epsilon$	Interstitial volume fraction
$\epsilon_p$	Accessible pore volume fraction of gel
G	Mass velocity of fluid
H	Plate height
$J_D = K_f \cdot \rho \cdot Sc^{2/3} / G$	Colburn mass transfer j factor
K	Mark-Houwink-Sakurada constant
$K_f$	Mass transfer coefficient around gel
$K_r$	Fractional reduction in diffusivity within gel pores resulting from frictional effects
$K_{SEC}$	Solute distribution coefficient
$\mu_0$	Solvent viscosity
$\mu_n$	nth central moment
$\mu_s$	Peak skewness
$M_n$	nth leading moment
$\bar{M}_v$	Viscosity average molecular weight
N	Number of theoretical plates
$Pe = L \cdot u / D_{ax}$	Dimensionless number
$Pe_p = 2uR_0 / D_{ax}$	Dimensionless number
R	Gas constant
$R_0$	Radius of gel particle
$Re_p$	Reynolds Number
$\bar{r} = r^* / R$	Dimensionless radius
$\bar{r}$	Equivalent hard sphere radius
$r^*$	Distance within gel particle
s	Laplace variable
Sc	Schmidt Number
$\sigma^2$	Variance
T	Absolute temperature
$\tau$	Tortuosity
$\bar{\eta}$	Pore radius
$\eta$	Mean pore radius
$\phi$	Pore size distribution
$\rho$	Density
$\theta = u \cdot t / L$	Dimensionless number
$V_R$	Mean retention volume
X	Distance along column
$z = X / L$	Dimensionless distance

### Literature Cited

1. Moore, J. C.; *J. Polym. Sci.*, PtA, 1964, 2, 835.
2. Yau, W. W.; Kirkland, J. J. and Bly, D. D.; 'Modern Size Exclusion Chromatography, Wiley-Interscience, N.Y., 1979.
3. van Deemter, J. J.; Zuiderweg, F. J.; Klinkenberg, A. *Chem. Eng. Sci.*, 1956, 5, 271.
4. Ouano, A. C.; Barker, J. A. *Sep. Sci.*, 1973, 8, 673.  
Ouano, A. C. *Adv. Chrom.*, 1977, 15, 233.
5. Wen, C. Y.; Fan, L. T.; 'Models for Flow Systems and Chemical Reactors', Chemical Processing and Engineering, Vol. 3, L. F. Albright; R. N. Maddox; J. J. McKetta; Dekker Inc: NY, 1975.



6. Szwarc, M.; 'Carbanions, Living Polymers and Electron Transfer Processes', Interscience, 1968.
7. Danckwerts, P. V.; Chem. Eng. Sci., 1953, 2, 1.
8. Kim, D.H. and Chang, K. S. (to be published).
9. de Vries, A. J.; LePage, M.; Beau, R.; Guillemin, C. L., Anal. Chem., 1967, 39, 935.
10. Satterfield, C. N.; Sherwood, T. K.; 'The Role of Diffusion in Catalysis', Addison-Wesley, London, 1963.
11. Satterfield, C. N.; Colton, C. K.; Pitcher, W. H.(Jr.); A.I.Ch.E. Journal, 1973, 19(3), 628.
12. Rudin, A.; Johnston, H. K.; J. Polym. Sci., PtB, 1971, 9, 55.
13. Wakao, N.; Funazukuri, T.; Chem. Eng. Sci., 1978, 33, 1375.
14. Wilson, E. J.; Geankopolis, J.; Ind. Eng. Chem. Fund., 1966, 5, 9.
15. Chung, S. F.; Wen, C. Y.; A.I.Ch.E. Journal, 1968, 14, 857.
16. van Kreveland, M. E.; van den Hoed, N.; J. Chromatogr. 1978, 149, 71.
17. Otacka, E. P.; Acc. Chem. Res., 1973, 6, 348.
18. Vivilecchia, R. V.; Lightbody, B. G.; Thimot, N. Z.; Quinn, H. M.; J. Chromatogr. Sci., 1977, 15, 424.
19. Mori, S.; J. Appl. Polym. Sci., 1977, 21, 1921.
20. Dawkins, J. V.; Stone, T.; Yeadon, G.; Polymer, 1977, 18, 1179.

RECEIVED September 1, 1983

# Pressure-Programmed Controlled-Flow Supercritical Fluid Chromatograph

E. W. ALBAUGH and D. BORST

Gulf Research & Development Company, Pittsburgh, PA 15230

P. TALARICO

Waters Associates, Milford, MA 01757

Supercritical fluid chromatography is a form of chromatography in which the system is held near the critical temperature of the mobile phase and pressure utilized to effect solvency and hence migration. The advantages of this technique have been shown to be increased mass transfer and the migration of high molecular compounds. Most of the instruments designed for this technique have not attempted to control the flow as pressure is programmed. In this paper, an instrument is described in which the inlet liquid flow is held constant and the pressure regulated by a pneumatically activated flow control valve at the exit of the column. This approach permits the use of a wide pressure program with a controlled flow and the use of several conventional liquid chromatographic detectors. Separations of model systems including normal aliphatic hydrocarbons, polynuclear aromatics and polymers with molecular weights ranging up to one million are reported.

Supercritical fluid chromatography is a form of chromatography in which the temperature is held near the critical temperature of the mobile phase and pressure utilized to effect solvency and hence migration. The advantages of this technique have been shown to be increased mass transfer and the migration of high molecular weight compounds.<sup>(1,2,3,4)</sup> Since this work was reported, high performance liquid chromatography has made rapid advancement and overshadowed much of the early appeal of supercritical fluid chromatography.<sup>(5)</sup> However, in the area of wide molecular weight-range samples, supercritical fluid chromatography with pressure programming appears to have advantages.<sup>(4)</sup> Jentoft has demonstrated the potential of this technique and described the design of a pressure programmed instrument.<sup>(6)</sup> In this instrument the system pressure

0097-6156/84/0245-0047\$06.00/0  
© 1984 American Chemical Society

Society Library

1155 16th St. N. W.

Washington, D. C. 20036

In Size Exclusion Chromatography; Provier, T.;

ACS Symposium Series; American Chemical Society: Washington, DC, 1984.

was controlled by programming the inlet pressure, but the flow was not controlled. Bartman, in an instrument designed for use with carbon dioxide, has used a flow meter and a motor driven expansion valve at the column exit to regulate pressure and gas flow. (7) The current state of the field has been reviewed by Randal, (8) Gere, (9) and Peadar. (10)

In this paper, an instrument is described in which the inlet liquid flow rate is held constant and the pressure regulated by a pneumatically actuated flow control valve at the exit of the column. This approach permits the use of a wide-range pressure program with a controlled flow. Also, by selecting mobile phases that are liquids at ambient laboratory conditions, several types of conventional liquid chromatographic detectors may be utilized.

### EXPERIMENTAL

A schematic diagram of the instrument is shown in Figure 1. The liquid mobile phase flows from the reservoir, through a heated chamber for degassing, and a 10  $\mu$  filter to a syringe pump (Ruska, Cat. No. 1441 with a Boston Ratiotrol variable speed motor control). A safety relief line leads from the pump through a 207 bar rupture disc in the reservoir. A line from the pump also runs to a pneumatic pressure transmitter (Moore Model No. 1735) which provides the process (pressure) signal for a controller (pressure) (Moore, Nullmatic Controller, Model 50). From the pump the solvent flows to shut-off valves A and B (High-Pressure Equipment Co. Model 15-12 AFI-316). With B closed and A open, the solvent flows through the sample valve (Chromatronix Model HPSV, with 25  $\mu$ l loop) and into the column oven. The sample valve is enclosed in an oven with a maximum temperature of 200°C which is maintained by a temperature controller (West Guardsman, Jr.). When B is open and A is closed, the solvent flows through the preheater and into the oven. The preheater consists of 2 ft of 1/8 in. stainless steel tubing wound around a Chromalox heater and coated with 2 in. of insulation. The temperature is maintained 10°C above the column oven temperature.

Inside the column oven, the solvent flows through 0.75 m of 0.009 in. I.D. conditioning coil, through a low dead-volume tee containing a thermocouple to monitor solvent temperature, and then to the column. The column oven, with a 425°C maximum temperature, is heated by two 2-kilowatt wire wound heaters which are controlled with a Gulton Model 2GB Controller which provides either isothermal or programmed temperature control.

After leaving the oven, the mobile phase flows through 1 m of 0.009 in. capillary tubing which is immersed in a heat exchanger to return the solvent to ambient temperature. A control valve, (Research Control Valve, Precision Products, Tulsa, Oklahoma, Type 78S with a P-9 trim) with a low dead-volume head as shown in Figure 2, is placed after the heat exchanger. This valve is positioned by the controller (pressure). The set point of the

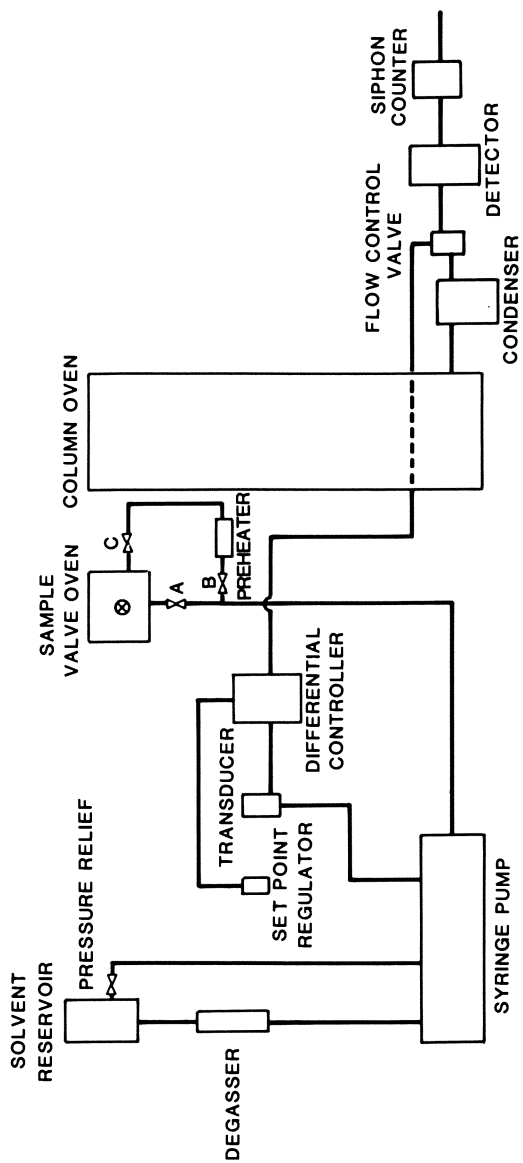


Figure 1. Supercritical fluid chromatograph.

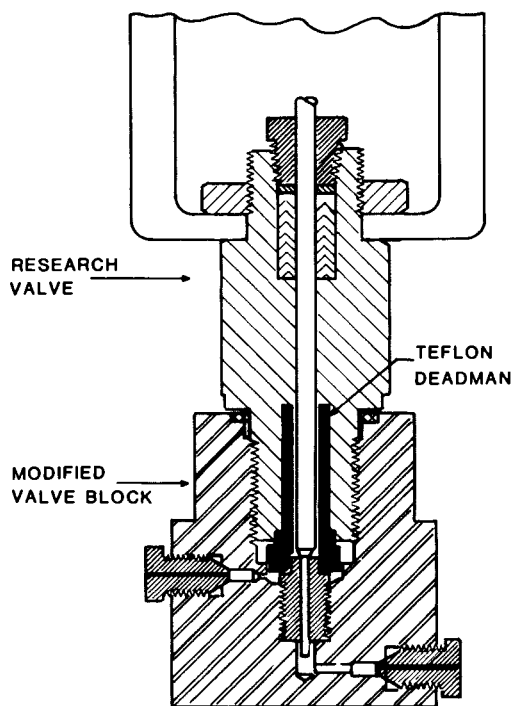


Figure 2. Modified research valve.

controller (pressure) is positioned by a variable speed motor which is regulated by a GKHT-2 motor controller (G. K. Keller Corp.). For isobaric operation, the set point is driven to the desired position and the drive deactivated. The controller then maintains the selected pressure. For pressure programming, the motor speed is selected to drive the set point at the desired rate. In operation, the flow rate is first set by the pump control and then the pressure adjusted. A siphon counter (Waters Associates, Model C908) is placed at the end of the system to measure volumetric flow.

The solvent system used here consisted of cyclohexane and 5% ethanol. This mobile phase will dissolve many petroleum fractions, produce a stable base line, and is compatible under ambient laboratory conditions with many common liquid chromatographic detectors. The system was operated at 10°C above the critical temperature of cyclohexane (280°C).

The stationary phase utilized was 75-100 mesh Porosil C packed into four, 4-ft lengths of 1/4 in. O.D. stainless steel tubing fitted with 10  $\mu$  snubber, swagelock 1/4 in. to 1/16 in. unions.

The minimum pressure in this system at 1 ml/min. flow rate and 280°C is 20.6 bar. The maximum operating pressure of the instrument is 206.8 bar. As the pressure is increased, the flow rate is constant from 20.6 to 48.2 bar and the base line is excellent. In the region from approximately 48.2-55.2 bar the flow rate slows slightly and the base line rises with an ultraviolet detector. This change is reproducible and believed due to a phase change in the solvent system. From approximately 55.2 to 206.8 bar the flow rate is again constant and the base line excellent. Depending upon the pressure program rate, a short period of compression is initially required, and then the flow stabilizes.

### RESULTS AND DISCUSSION

The separation of a mixture of aromatic compounds (benzene, naphthalene, anthracene, chrysenes, and benz(a)pyrene) at 31 bar is shown in Figure 3. This chromatogram was obtained with a Perkin Elmer Model 250 ultraviolet detector with the high-pressure cell placed after the cooling heat exchanger and before the flow control valve. A similar chromatogram is obtained with an Isco Model UA4 with a 10 mm micro cell placed after the flow control valve.

The effect of pressure (measured at the pump) on this separation can be seen in Figure 3 and Table I. As the pressure is increased, the retention volume of benzene and naphthalene continually increase, while the retention volume of anthracene, chrysene, and benz(a)pyrene first increase, go through a maximum, and then decrease. The maximum separation occurs at 38.5 bar while the minimum satisfactory separation volume (shortest analysis

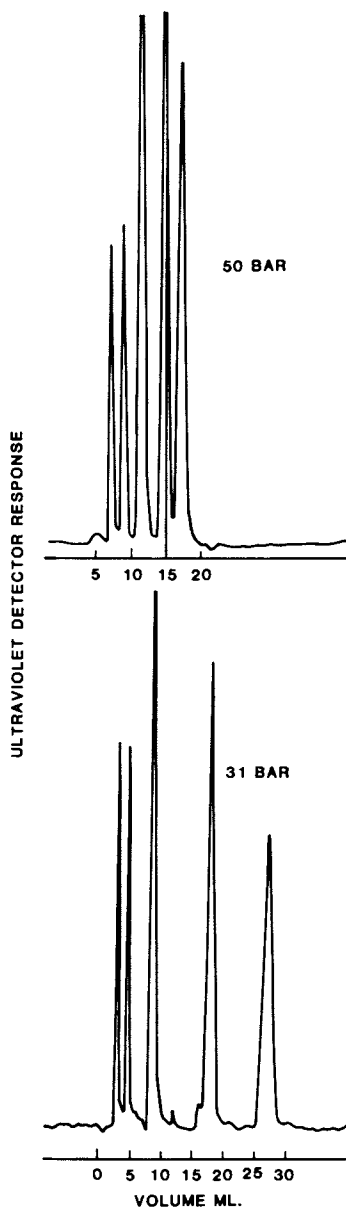


Figure 3. Separation of benzene, naphthalene, anthracene, chrysene, and benz( $\alpha$ )pyrene at 50 and 31 bar.

time) occurs at 50 bar. At 51.7 bar, the higher molecular weight materials are not resolved.

Table I. EFFECT OF PRESSURE ON SEPARATION OF POLYNUCLEAR AROMATIC COMPOUNDS

Compound Pressure, bar	Elution Volume, ml					
	31	40	44.1	46.5	50	51.7
Benzene	2.5	5	6.0	6.5	8.0	8.0
Naphthalene	4.0	8	8.5	9.0	10.0	10.0
Anthracene	8.5	13.5	15.0	13.0	13.0	10-13
Chrysene	18.0	26.0	24.5	16.5	17	10-13
Benz(a)Pyrene	27.5	35.5	32.0	18.0	18.5	10-13

The separation of a somewhat higher molecular weight material is shown in Figure 4. Here, a polystyrene with an average molecular weight of 600 has been separated into eleven components at 50 bar. The effect of pressure programming is also shown. The program was started at 46 bar at a rate of 0.34 bar per min. As the pressure increases, the elution volumes of the various compounds decrease and the peak widths become more narrow in a manner similar to that for temperature programming in gas chromatography and solvent programming in liquid chromatography. At 65.5 bar the sample elutes essentially as one peak.

To demonstrate the behavior of high molecular weight compounds in this system, a series of polystyrene standards were analyzed. The highest molecular weight material (average molecular weight of 1,800,000) is shown in Figure 5. A pressure program rate of 0.69 bar per minute was used. A small amount of material elutes at approximately 75.8 bar, but the major portion of the sample elutes between 89.6 bar and 134.4 bar. A sample was taken from the 117.2 bar region and analyzed by conventional exclusion chromatography. It was found to have a molecular weight in the range of 1,000,000. Thus, these high molecular compounds survive the column and are resolved at pressures below 2000 psi. The other lower molecular weight polystyrene standards eluted at correspondingly lower pressures.

A series of normal hydrocarbons were analyzed using the same chromatographic system and the Pye LCM II flame ionization detector. In Figure 6 is shown the separation of a mixture of  $C_{16}$ ,  $C_{32}$ ,  $C_{40}$  and  $C_{44}$  normal hydrocarbons. With the high molecular weight capability shown for the polystyrenes, this system should also handle the higher molecular weight saturated hydrocarbons that are beyond the range of gas chromatography.

Several polynuclear compounds containing both aromatic and alkyl functions were chromatographed. The higher the molecular weight of the compound, the greater was the elution volume, indicating that separation was not occurring according to the number of aromatic rings.



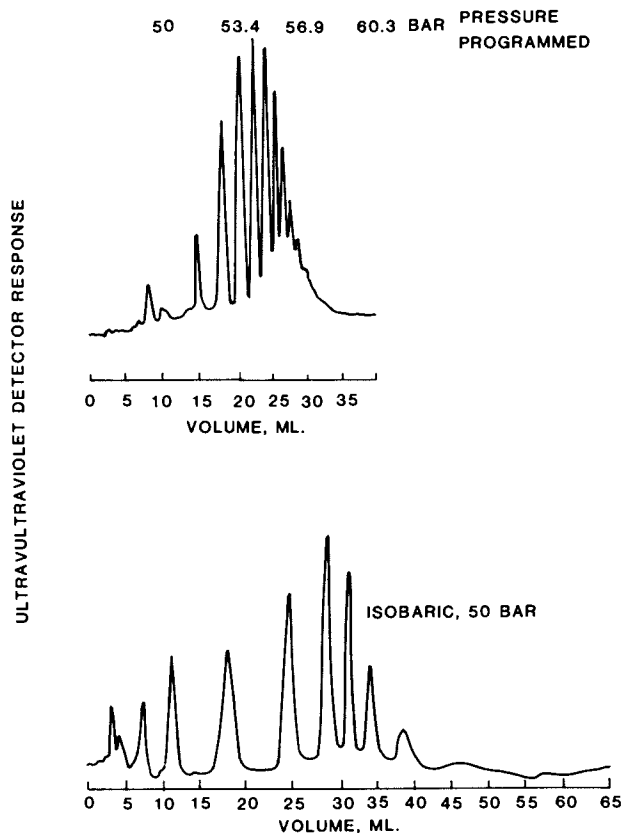


Figure 4. Separation of low molecular polystyrene by pressure programming.

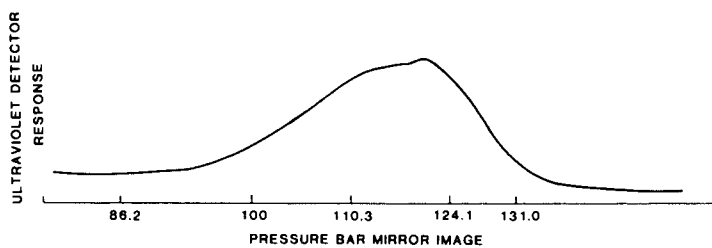


Figure 5. Pressure separation of 1,800,000 molecular weight polystyrene by pressure programming.

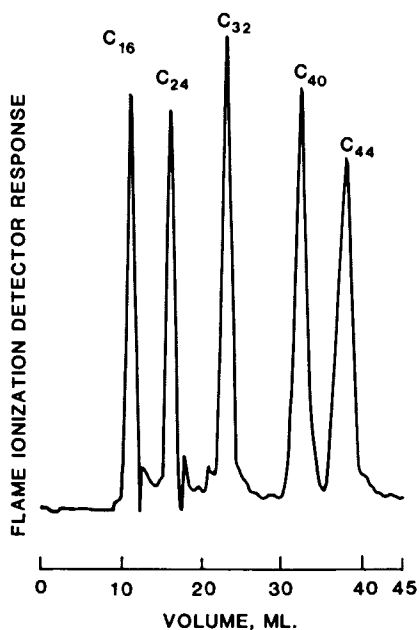


Figure 6. Separation of  $C_{16}$ ,  $C_{24}$ ,  $C_{32}$ ,  $C_{40}$ , and  $C_{44}$  normal hydrocarbons at 48.3 bar mirror.

In the area of polar compounds, phenol, resorcinol, and benzoic acid were chromatographed. Phenol gives a nearly symmetrical peak with essentially no tailing. Resorcinol is separated from phenol but shows some tailing. Benzoic acid falls in the same elution region as resorcinol, but tails to a much greater extent.

In one application, styrene still bottoms were chromatographed. Here styrene and the individual lower molecular weight oligomers were separated, and as the pressure was increased, the higher molecular weight polystyrene eluted.

The instrument described here has been found to be essentially trouble-free. Pressure settings and control are reproducible, requiring only the positioning of a switch. One of the attractive attributes of supercritical fluid chromatography is the short time required for the column to reach equilibrium when conditions are changed. After operating at 172.4 bar, for example, the instrument can be rapidly depressurized to 20.7 bar and the system, including the columns, equilibrated within a few minutes. The column conditioning problems often found in high-pressure liquid chromatography-solvent programming were not experienced here. The reproducibility of elution volumes is comparable to isocratic high pressure liquid chromatography.

#### LITERATURE CITED

1. Giddings, J. C., Myers, M. N., and King, J. W., J. Chromatogr. Sci., 7, 276(1969).
2. Giddings, J. C., Science, 162, 7(1968).
3. Su, S. T., Rynders, G. W. A., Anal. Chem. Act., 38 31(1967).
4. Gouw, T. H., Jentoft, R. E., J. Chromatogr., 68, 303(1972).
5. Doran, T., Soc. Analyt. Chem., 117, May 1974.
6. Jentoft, R. E., Gouw, T. H., J. Chromatogr. Sci., 8, 138(1970).
7. Bartman, D., Berichte der Bunsen--Gesellschaft Bd. 76, NY 3/4, 336(1972).
8. Randal, L. G., Separation Science and Technology, 17(1) 1(1982).
9. Gere, D. R., Board, R., McManigill, Anal. Chem., 54, 736(1982).
10. Peaden, P. A., Lee, M. L., J. Liq. Chromatogr. 5(2), 179(1982).

RECEIVED October 13, 1983

# Automated Data Analysis System for a Gel Permeation Chromatograph with Multiple Detectors

M. E. KOEHLER, A. F. KAH, T. F. NIEMANN, C. KUO, and T. PROVDER

Glidden Coatings and Resins, Division of SCM Corporation, Strongsville, OH 44136

A Waters Model 150C ALC/GPC was interfaced to a minicomputer system by means of a microcomputer for automated data collection and analysis. Programs were developed for conventional molecular weight distribution analysis of the data and for liquid chromatographic quantitative composition analysis of oligomeric materials. Capability has been provided to utilize non-standard detectors such as a continuous viscometer detector and spectroscopic detectors for compositional analysis. The automation of the instrument has resulted in greater manpower efficiency and improved record keeping.

Efficient use of a modern high performance gel permeation chromatography (HPGPC) instrument requires computer aided analysis in order to take full advantage of both the quality and the quantity of information the instrument is capable of providing. Commercial data analysis packages for this purpose are, for the most part, simplistic and inflexible. This is particularly true when multiple or non-standard detectors are required. This work describes an automated data analysis system used in conjunction with a Waters Associates Model 150C ALC/GPC to read operational parameters from the instrument, to collect data from multiple detectors, and transmit the data to a minicomputer system for storage, analysis, reporting and plotting.

## Data Acquisition System

Automated data analysis for the chromatograph is achieved by interfacing the instrument and detectors to a microcomputer for data acquisition. The microcomputer is connected to the Intelink

0097-6156/84/0245-0057\$06.00/0

© 1984 American Chemical Society

interface of the instrument so that the operational parameters for each sample analysis can be transferred to the minicomputer. The microcomputer is responsible for all real-time activities involved in data collection. At the completion of the experiment, data are transferred via a serial line to the minicomputer for storage and analysis. Report generation and plotting may be done at any time after the completion of the experiment. The minicomputer system uses a Digital PDP 11/44 processor running the RSX 11-M operating system. Programming for communications and data analysis on the minicomputer is done in FORTRAN-77. The microcomputer uses an 8080A processor and is composed primarily of standard Pro-Log circuit cards. Programming for the microcomputer is done in assembly language and cross assembled on the minicomputer. Details of the mini-microcomputer system and its organization have been reported elsewhere (1,2,3).

#### Automated Instrument Analysis Process

There are four stages in an automated instrument analysis. In the first stage, the instrument operator initiates the experiment by means of dialog programs on the minicomputer. Examples of the dialogs for the HPGPC operation are shown in Figures 1-4.

Dialog 15, shown in Figure 1, is used for sample definition. This includes identification of the location of the sample in the automatic injector, the column set in use, the data collection rate, the detectors to be used, the operators initials and the sample identification. This definition file may be modified and displayed on the terminal, or printed. The file is updated during operation to show the current status of the samples. Before initiating an analysis, the instrument must be programmed for automatic operation and the samples placed in the appropriate positions of the injector. Dialog 16, shown in Figure 2, starts operation of the microcomputer. Intelink communication with the instrument is established and the parameters for the first sample are taken from the sample definition file on the minicomputer and are transmitted to the microcomputer. The microcomputer turns on a ready status light at the instrument to signal to the operator to begin automatic operation of the instrument.

The second stage is data acquisition. This stage is entered when the operator starts the instrument. The instrument makes the first injection and signals the microcomputer via Intelink. After a delay proportional to the void volume of the column set, data are collected on a time basis (constant flow rate assumed) at the predetermined rate from each of the detectors selected, up to a maximum of three simultaneous detectors. When the sample run is complete, the instrument again signals the microcomputer which places the instrument in a hold state while it reads the operational parameters from the instrument for that sample and

```

DIA 15
Instrument No. 34 - HPGPC Sample Definition
Options:
    C - Create new file
    A - Add sample data to old file
    D - Delete sample from file
    E - Edit sample data
    T - Type file on terminal
    P - Print file on printer
    X - Exit

Option...T
Pos  Job  Err  Inj  Tot  Col  Flow  DATA  RI  UV  IR  VI  Dpp      Sample ID
No    No    No    Inj  Set  ml/m  pt/m
  1   6797  0    1    1    3    1.0   30    1  0  0  0   AFK   5872, PHOSPHATE MOI
OK
>DIA 15C
Instrument No. 34 - HPGPC Sample Definition

Initials... AFK
Column Set... 3
Default Values:
Detectors (RI, UV, IR, VI)<RI>...
Flow Rate (ml/min)... 1
Data Collection Rate (pts/min)<60>... 30
Number of samples (1 - 16)<1>... 2

Position  1      Job No.  6803
Sample ID... TEST SAMPLE # 1
Customer... KUD

Position  2      Job No.  6804
Sample ID... TEST SAMPLE # 2
Customer... KUD

OK
>

```

Figure 1. Sample definition dialog for automated instrument operation.

```

DIA 16
INSTRUMENT NO. 34 - HPGPC
STARTING HPGPC SAMPLE ANALYSIS

OK
>

```

Figure 2. Dialog for initiation of automated instrument operation.

```
DIA 17

Instrument No. 34 - HPGPC Column Set Definition

Options:

    A - Add new column set
    D - Delete column set from file
    E - Edit column set data
    P - Print file on printer
    X - Exit

Option...A

DEFINE NEW HPGPC COLUMN SET

Column Set No.    4

Void Volume (ml)... 3
Total Volume (ml)... 8
Description... TEST COLUMN SET

OK
>DIA 17E

Instrument No. 34 - HPGPC Column Set Definition

Edit GPC Column Set

Column set... 4
Void volume (ml) < 3.0>... 3.2
Total volume (ml) < 8.0>...
Description <TEST COLUMN SET>
...

OK
>DIA 17D

Instrument No. 34 - HPGPC Column Set Definition

Delete GPC Column Set From File

Column set... 4

Column Set    4
TEST COLUMN SET

Delete this column set? Y

OK
>
```

Figure 3. Dialog for column set definition.

```
>DIA 18

Instrument No. 34 - HPGPC Calibration Curve Definition

Options:

    A - Add new calibration curve
    D - Delete calibration curve from file
    E - Edit calibration curve data
    P - Print file on printer
    X - Exit

Option...A

DEFINE NEW HPGPC CALIBRATION CURVE

Calibration Curve No. 12

Column Set... 1
Detector (RI, UV, IR, VI)... IR
Flow rate (ml/min)... 1
Solvent... THF
Temperature... 40
Polymer... POLYSTYRENE

Coefficients for Chain Length Calibration Curve:

    0
    1
    2
    3
    4
    5
    6
    7

Coefficients for Molecular Weight Calibration Curve:

    0  42.46
    1  -1.827
    2   .0356
    3  -.00183
    4
    5
    6
    7

OK
>DIA 18D

Instrument No. 34 - HPGPC Calibration Curve Definition

Delete HPGPC Calibration Curve

Curve No... 12

Curve 12 Column Set 1 Detector 3 22-OCT-82

Delete this calibration curve? Y

OK
>
```

Figure 4. Dialog for definition of calibration curves.



combines this information with the raw data and sample definition information in memory.

The third stage is data transmission during which the microcomputer transmits the entire data set for the sample to the minicomputer. The data is stored on disk until the operator initiates the fourth stage, data reduction. If multiple samples and injections have been programmed, the minicomputer sends to the microcomputer the information in the sample definition file for the next sample, and operation continues without further operator intervention.

Calibration is performed by using narrow molecular weight distribution polystyrene standards. A polynomial up to sixth order is fit to the  $\log_{10}$ (molecular weight) vs retention volume data for the standards using conventional polynomial regression methods, and the coefficients of the best fit polynomial (usually fourth order or less) are used to define the calibration curve. Dialogs 17 and 18, shown in Figures 3 and 4, are used by the operator to define column sets and calibration curves. This information is stored in files on the minicomputer until modified or deleted by the operator and is used by the data analysis programs.

An example of operator interaction with the primary analysis program, GPC, is shown in Figure 5. The job number assigned by the computer during sample definition is entered along with the detector selected for analysis. The operator then selects the baseline and the limits for data analysis by entering the times of the desired points. The plots desired and the disposition of the report file are chosen. The most recent calibration curve on file for the column set is used by default but others may be selected at the operator's option.

Integration of the data for the calculation of molecular weight distribution averages is performed in time-volume space using Simpson's Rule (assuming constant flow rate). Molecular weight averages are calculated using the equation

$$\bar{M}_j = \frac{\int_{M_H}^{M_L} M^{j-1}(V)F(V)dV}{\int_{M_H}^{M_L} M^{j-2}(V)F(V)dV} \quad (1)$$

where  $j = 1, 2, 3,$  and  $4$  correspond to the  $N, W, Z$  and  $Z+1$  averages, respectively;  $M(V)$  represents the molecular weight calibration curve as a function of retention volume and  $F(V)$  is the normalized chromatogram height as a function of retention volume. The weight differential molecular weight distribution,  $f_w(\log_{10}M)$ , is calculated according to the method of Pickett et al. (5) using the equation

$$f_w(\log_{10} M) = F(V) \cdot \frac{1}{2.303 (d\log_{10} M(V)/dV)} \quad (2)$$

where  $d\log_{10} M(V)/dV$  is the slope of the molecular weight calibration curve. An example of the weight differential molecular weight distribution plot is shown in Figure 8 along with the weight cumulative molecular weight distribution. The position of the molecular weight averages,  $\bar{M}_n$ ,  $\bar{M}_w$ ,  $\bar{M}_z$ ,  $\bar{M}_{z+1}$  and  $\bar{M}_{z+2}$  on the  $\log_{10} M$  axis also are indicated in Figure 8. Examples of the plots and report generated by the program are shown in Figures 6-9. The report shown in Figure 9 is composed of four sections: molecular weight distribution statistics, sample information, raw chromatogram statistics and column set information. The variance, skewness and kurtosis statistics which involve moments about the mean are calculated from equations relating moments about the mean to moments about the origin (6). Customized plot presentations and coplotting of data from multiple samples can be generated when required.

Other analysis methods dependent on multiple detectors can be implemented using this automated system. Two methods under development are the use of a continuous viscometer detector with a refractive index detector to yield absolute molecular weight and branching, utilizing the universal calibration curve concept (4), and the use of a UV or IR detector with the refractive index detector to measure compositional distribution as a function of molecular weight.

Oligomer analysis is performed by a separate program OLIG by a method analogous to conventional liquid chromatograph peak analysis. This program utilizes the Digital Equipment Corporation scientific subroutine PEAK. Since the subroutine operates on progressively broadening peaks, the data is analyzed in reverse order, that is, from long to short retention times. The operator can select a baseline, or let the program select and adjust the baseline automatically. Response factors may be calculated at the operator's discretion, or concentrations can be calculated from known response factors on an area basis. The operator interaction with OLIG and samples of the report and plot from this program are shown in Figures 10-12.

### Conclusions

Benefits have been realized from the automation of the Waters Model 150C ALC/GPC in several areas. First, a significant amount of time has been saved by performing automated data collection with automatic injection during night operation while unattended. Secondly, record keeping is more complete and accurate. This has

&gt;RUN \$GPC

```

JOB NUMBER, RUN NUMBER <1>                9034
SAMPLE 9165; 1306-12-B PMMA
Detector: RI, UV, or IR <RI>             RI
CURVE 10, 13-AUG-82 - CHANGE ?           N
PLOTS: RAW, VOLUME, MOLWT, CHAIN         RVH
BASELINE IN MINUTES
      START < 23.93 >                     36
      STOP  < 79.87 >                     75
DATA LIMITS IN MINUTES
      START < 36.00 >                     40
      STOP  < 75.00 >                     63
OUTPUT FILE (PRINT, SAVE) < DELETE >     P
      FILE HPGPC.LST CREATED
      PLOT FILES PRODUCED:
          RAWDAT
          RVOL
          MOLWT

```

Figure 5. Operator interaction with program GPC.

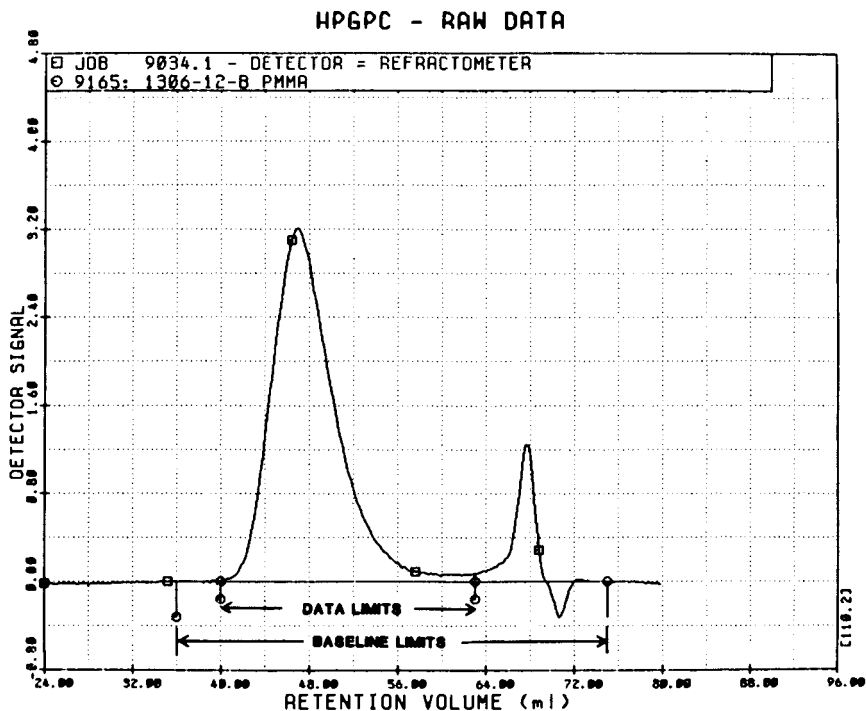


Figure 6. Raw HPGPC data with operator selected baseline.

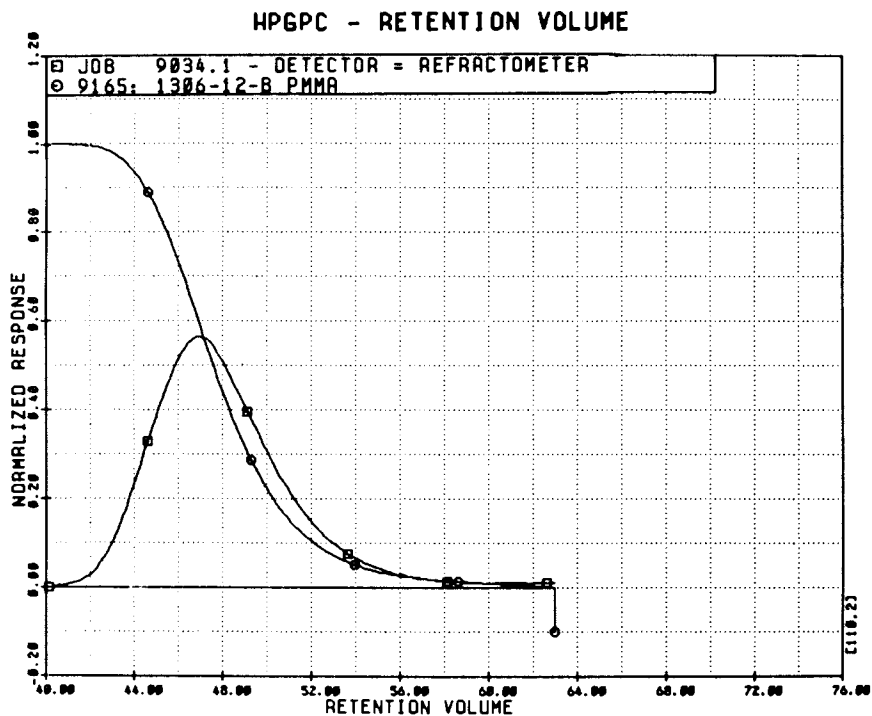


Figure 7. Baseline corrected normalized retention volume data over the region to be analyzed.

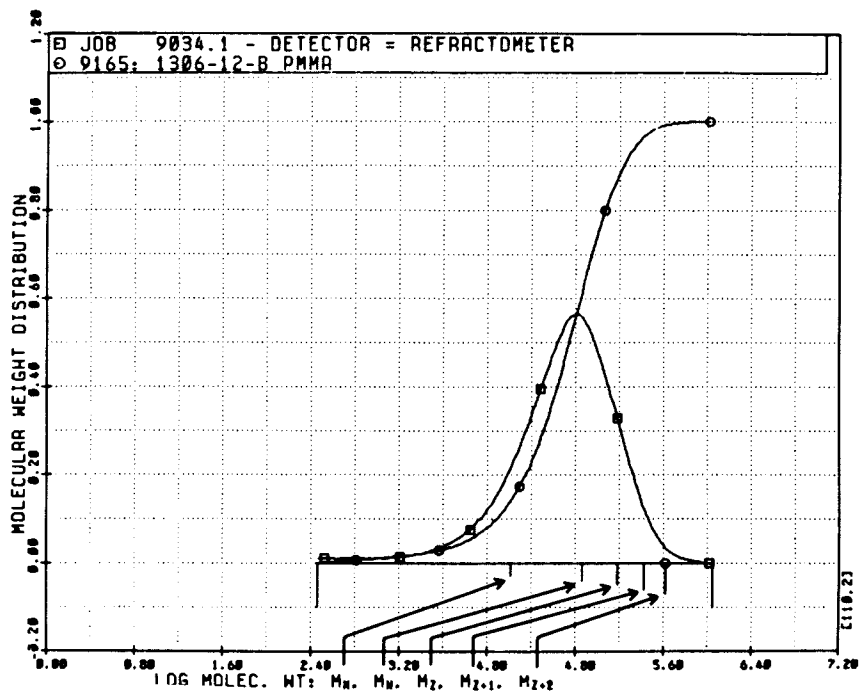


Figure 8. Weight differential and integral molecular weight distribution plots.

```

JOB 9034.1 HPGPC - REFRACTIVE INDEX DETECTOR -----
          9165: 1306-12-B PMMA

MOLECULAR WEIGHT DISTRIBUTION -----
          MEAN      VARIANCE    SKEWNESS    KURTOSIS
NUMBER AVERAGE      0.163E+05    0.929E+09    0.461E+01    0.409E+02
WEIGHT AVERAGE      0.732E+05    0.568E+10    0.302E+01    0.166E+02
Z AVERAGE            0.151E+06    0.173E+11    0.237E+01    0.819E+01
Z+1 AVERAGE          0.266E+06
Z+2 AVERAGE          0.416E+06
LOW MOLECULAR WEIGHT                                0.291E+03
HIGH MOLECULAR WEIGHT                                0.110E+07
POLYDISPERSITY, MEAN WT/MEAN NUMBER                 4.4906
PEAK MOLECULAR WEIGHT                                0.633E+05
SLOPE OF CALIBRATION CURVE 10 AT PEAK              -0.153389

** NO COEFFICIENTS FOR CHAIN LENGTH IN CALIBRATION CURVE 10

SAMPLE INFORMATION -----
          REQUESTED BY GARY CARLSON                SAMPLE VOLUME, UL                200
          INSTRUMENT NUMBER      34                BASELINE TIME, LOW                36.00
          OPERATOR                AFK                BASELINE TIME, HIGH                75.00
          RUN DATE                11-OCT-82          BASELINE SLOPE                    -0.000952
          RUN TIME                22:53:37          DATA TIME, LOW                    40.00
          SENSITIVITY             0032          DATA TIME, HIGH                   63.00
          SCALE FACTOR            32                NUMBER OF DATA POINTS            690

RAW CHROMATOGRAM STATISTICS -----
          MEAN VOLUME             48.08                PEAK TIME                          47.00
          VARIANCE                10.6909             PEAK VOLUME                         47.00
          SKEWNESS                1.1792             PEAK HEIGHT                         3.2058
          KURTOSIS                2.4579             MOMENT 3 ABOUT MEAN                41.2097
          AREA                    21.2442             MOMENT 4 ABOUT MEAN                625.1477

COLUMN SET -----
          Waters u-Styrigel, 6-col, 1000000-100000-10000-1000-500-100

          COLUMN SET NUMBER      3                CALIBRATION -----
          FLOW RATE, ML/MIN      1.0
          COLUMN TEMPERATURE     50C                CURVE NUMBER                       10
          SOLVENT                THF                CALIB. DATE                        13-AUG-82
          VOID VOLUME            34.0                CALIB. TEMP.                       50.0
          TOTAL VOLUME           75.0                CALIB. POLYMER:                    PS 4th order

```

Figure 9. Sample report from program GPC.

```

RUN $OLIG
Job end run numbers ?    10758,1
9344: RESIMENE
Enter editing limits in minutes ( ^Z for full range of data )
  Lower limit < 10.52 > 21
  Upper limit < 44.97 > 31
Enter baseline limits in minutes ( ^Z for computed baseline )
  Lower limit < 21.00 > 20
  Upper limit < 31.00 > 37
Dens, Base, Gate, Diff, Reset < 3, 8, 2, 2, R > 1,18,,,N

9344: RESIMENE

```

PEAK	Z	TIME	AREA	START	END	HEIGHT	START	END	WIDTH	AREA	DENS
1	25.33	20.43	21.73	25.53	98.	251.	248.	248.	0.200	261.47	2.
2	26.10	13.67	25.53	26.57	248.	298.	234.	234.	0.367	174.93	2.
3	27.27	21.86	26.57	28.07	234.	405.	160.	160.	0.467	279.74	2.
4	29.45	44.04	28.07	30.95	160.	648.	106.	106.	0.583	563.65	2.

```

Print the file ? (No/Yes/Plot/Edit/Save/Response factors)    S
Files created: OLIG.T1,T2 and OLIG.LST
>

```

Figure 10. Operator interaction with program OLIG.

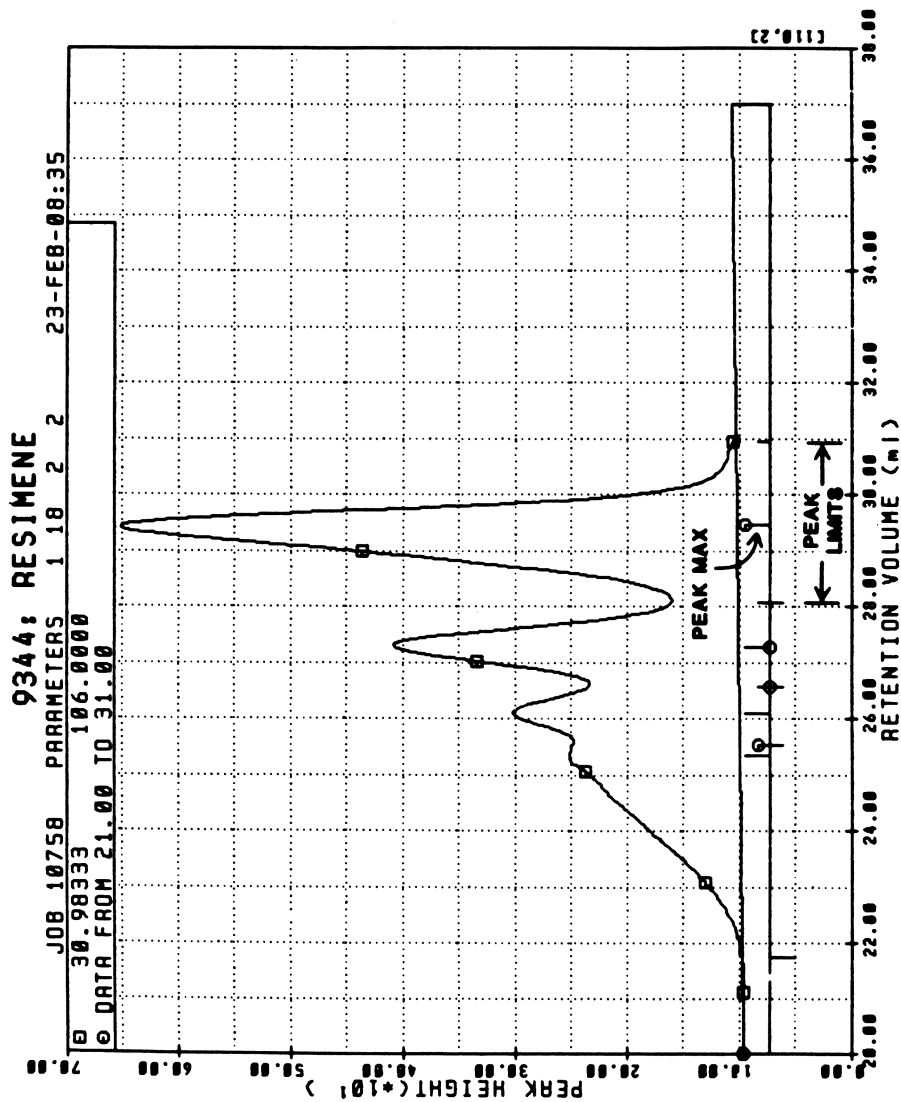


Figure 11. Plot from program OLIG showing baseline selection and peak locations.



JOB 10758.J HPGPC - REFRACTIVE INDEX DETECTOR -----09-MAR-09:49

9344: RESIMENF

#	PEAK		---TIME---		-----HEIGHT-----			HALF- WIDTH	AREA	PT DENS
	TIME	% AREA	START	END	START	PEAK	END			
1	25.33	20.43	21.73	25.53	98.	251.	248.	0.200	261.47	2.
2	26.10	13.67	25.53	26.57	248.	298.	234.	0.367	174.93	2.
3	27.27	21.86	26.57	28.07	234.	405.	160.	0.467	279.74	2.
4	29.45	44.04	28.07	30.95	160.	648.	106.	0.583	563.65	2.

SAMPLE INFORMATION

REQUESTED BY SWAFFORD		SAMPLE VOLUME, UL	100
INSTRUMENT NUMBER	34	DATA TIME, LOW	21.00
OPERATOR	AFK	DATA TIME, HIGH	31.00
RUN DATE	22-FEB-83	BASELINE TIME, LOW	20.00
RUN TIME	13:04:47	BASELINE TIME, HIGH	37.00
NUMBER OF DATA POINTS	600	BASELINE SLOPE	0.625000

COLUMN SET

VARIAN MICROPAC TSK - 2000 H, 3000 H

		TUNING PARAMETERS	
COLUMN SET NUMBER	1	ORIGINAL POINT DENSITY	1
FLOW RATE, ML/MIN	1.0	BASELINE TEST	18
VOID VOLUME	15.0	GATE FACTOR	2
TOTAL VOLUME	35.0	MINIMUM DIFFERENCE	2
COLUMN TEMPERATURE	50C	POINT DENSITY NOT RESET	

Figure 12. Sample report from program OLIG.

simplified accurate reproduction of experimental results and has helped discern subtle or long term variability in the operating characteristics of the instrument. Finally it has facilitated the development of experimental methodology for non-standard detectors.

#### Literature Cited

1. Niemann, T. F.; Koehler, M. E.; Provder, T. "Microcomputers used as Laboratory Instrument Controllers and Intelligent Interfaces to a Minicomputer Timesharing System" in "Personal Computers in Chemistry"; Lykos, P., Ed.; John Wiley and Sons: New York, 1981; pp. 85-91.
2. Kah, A. F.; Koehler, M. E.; Niemann, T. F.; Provder, T.; Eley, R. R. "An Automated Ferranti-Shirley Viscometer" in "Computer Applications in Applied Polymer Science"; Provder, T., Ed.; ACS SYMPOSIUM SERIES No. 197, American Chemical Society: Washington, D.C., 1982; pp.223-241.
3. Kah, A. F.; Koehler, M. E.; Grentzer, T. H.; Niemann, T. F.; Provder, T. "An Automated Thermal Analysis System for Reaction Kinetics" in "Computer Applications in Applied Polymer Science"; Provder, T., Ed.; ACS SYMPOSIUM SERIES No. 197, American Chemical Society: Washington, D.C., 1982; pp. 197-311.
4. Malihi, F. B.; Kuo, C.; Koehler, M. E.; Provder, T.; Kah, A. F. "Development and Application of a Continuous GPC Viscosity Detector for the Characterization of Absolute Molecular Weight Distribution of Polymers", this volume.
5. Pickett, H. E.; Cantow, M. J. R.; Johnson, J. F. Appl. Polym. Sci. 1966, 10, 917.
6. Aitken, A. C. "Statistical Mathematics"; Oliver and Boyd: London, 1962; Chap. 2.

RECEIVED October 4, 1983

# Comparison of Size Exclusion Chromatography Calibration Techniques

## Using Narrow and Broad Molecular Weight Distribution Standards

THOMAS V. ALFREDSON, LORI TALLMAN, and WILLIAM J. PERRY

Varian Instrument Group, Walnut Creek, CA 94598

Size exclusion chromatography (SEC) polymer elution profiles yield information regarding the molecular size distributions of polydisperse macromolecules. Polymer molecular weight distribution (MWD) represents an intrinsic property which provides direct correlation with many end-use physical properties and a universal criterion for polymer characterization (1). In order to convert elution profiles or chromatograms into MWD information proper calibration methods are required. SEC molecular weight calibration techniques represent experimental approaches for transformation of polymer elution profiles into MWD information and are dependent upon instrumentation, columns, and the polymer/solvent system under study.

SEC calibration methods can be generally categorized into techniques which employ a series of narrow MWD standards and those which employ one (or more) broad MWD standards (2). Calibration techniques which utilize polydisperse, broad MWD standards have been found to be particularly useful when narrow MWD standards are not available or universal calibration methodology is impractical as for example with most water-soluble polymers or polymer/solvent/temperature combinations for which appropriate Mark-Houwink constants are not known or readily available.

Methods of molecular weight calibration using polydisperse standards are of two fundamental types. Techniques which utilize a polydisperse standard with known molecular weight distribution (referred to as integral methods) and those which make use of one or more broad MWD standards for which any pair of  $\bar{M}_n$ ,  $\bar{M}_w$  or  $\bar{M}_v$  values are known and assume a linear molecular weight calibration curve (referred to as linear methods). Methodologies have also been developed for SEC calibration which employ a polydisperse standard and use the universal molecular weight calibration curve obtained with a series of narrow MWD polystyrene standards (3) or use a polydisperse standard to calculate effective Mark-Houwink constants for utilization of universal calibration approaches (4).

Integral methods of SEC calibration which make use of a well

0097-6156/84/0245-0073\$06.75/0

© 1984 American Chemical Society

characterized, broad MWD standard, such as the method developed by Cantow et al. (5), correlate molecular weights and elution volumes by successively super-imposing the cumulative molecular weight distribution and the integrated, normalized SEC chromatogram. Historically, the well-characterized molecular weight distribution of a polydisperse standard was experimentally obtained by column fractionation in which the molecular weight of each fraction was determined by conventional methods such as light scattering and osmometry. Weis and Cohn-Ginsberg (6) developed an alternative procedure based upon theoretical polymer molecular weight distribution shape and known average molecular weight values in order to yield the required molecular weight distribution information necessary for use of the polydisperse standard in calibration. Characterization of organic-soluble polymers by Swartz et al. (7) and water-soluble polymers by Abdel-Alim and Hamielec (8) has been accomplished using this approach to SEC calibration. In general, the information required of a polydisperse standard by integral calibration methods is not readily available or can be time consuming to generate. Prediction of molecular weight distribution shape also is not always straightforward. Thus the utility of integral methods using polydisperse standards for calibration has been limited compared to linear methods using polydisperse standards.

Linear calibration methods employing a broad MWD standard with a known pair of  $\bar{M}_n$ ,  $\bar{M}_w$  or  $\bar{M}_v$  values and assume a linear molecular weight calibration curve are based upon a method originally developed by Frank et al. (9) which relied upon known  $\bar{M}_n$  and  $\bar{M}_w$  values of a single broad MWD standard and utilized a graphical approximation method to obtain a working calibration curve. Balke, Hamielec, LeClair and Pearce (10) developed a much improved refinement to this technique by replacing the graphical approximation method with a computer program using a Rosenbrock search routine to determine a linear calibration curve. Such an iterative, two variable search routine was employed to develop a calibration curve which can be expressed as follows:

$$V_e = C_1 - C_2 \log_{10} (M) \quad (1)$$

where

$V_e$  = elution volume

$M$  = molecular weight

$C_1$  and  $C_2$  = constants to be found by computer search program.

Using a search routine, a computer program can calculate the constants  $C_1$  and  $C_2$  from definitions of the moments of the distribution:

$$\bar{M}_w = \sum_i W_i M_i \quad (2)$$

$$\bar{M}_n = \frac{1}{\sum_i (W_i/M_i)} \quad (3)$$

where

$W_i$  = weight fraction

$M_i$  = molecular weight

Substituting the expression for  $M$  listed in eqn (1) into eqns (2) and (3) it is easily shown that:

$$\bar{M}_w = \sum_i W_i 10(C_1 - V_i/C_2) \quad (4)$$

$$\bar{M}_n = \frac{1}{\sum_i W_i / 10(C_1 - V_i/C_2)} \quad (5)$$

The Rosenbrock search routine in the computer program employed by Balke and Hamielec was found to converge to the correct optimum values of  $C_1$  and  $C_2$  within approximately 200 iterations.

Loy (11) has published a procedure based upon the method of Balke and Hamielec which uses a more efficient iterative, single-variable search algorithm which relies upon the fact that the dispersity ( $\bar{M}_w/\bar{M}_n$ ) is a function of  $C_2$  only. The computer program incorporating this much faster algorithm converges to the optimum  $C_2$  within 36 iterations.

Pollock et al. (12) have also exploited the fact that polydispersity index is a function of  $C_2$  only in a study utilizing a Monte-Carlo simulation technique to compare error propagation in the method of Balke and Hamielec to a revised method (GPCV2) proposed by Yau et al. (13) which incorporated correction for axial dispersion.

Malawer and Montana (14) have developed an efficient iterative, sequential single variable search algorithm which relies upon a polydisperse standard with known  $\bar{M}_n$  and  $\bar{M}_w$  values. A direct graphical proof of the algorithm was presented.

A reliable and very rapid search algorithm in the computer program for use in linear calibration methods is highly desirable when data processing is performed with a microcomputer for automated, on-line calibration and MWD calculations. A fast search algorithm requiring few iterations ensures that convergence will be achieved within a few minutes even on an inexpensive, small personal computer. With this goal in mind, a proprietary iterative, two-variable search algorithm has recently been developed in our laboratory and incorporated into a user-interactive computer program for SEC polymer characterization (15). The highly efficient search algorithm is used in a linear calibration method based upon that of Balke and Hamielec which employs a single, broad MWD standard with known  $\bar{M}_n$  and  $\bar{M}_w$  values. The

calibration curve in this method can be described as follows:

$$\log 10 (M) = C_0 + C_1 V_e \quad (6)$$

where

M = molecular weight

$V_e$  = elution volume

$C_0, C_1$  = constants to be found by search algorithm

The search algorithm employs a successive approximation and accelerated convergence technique on the independent variable in eqn (6), then approximates the dependent variable from the simultaneous solution of the equations for  $\bar{M}_n$  and  $\bar{M}_w$  moments of the polydisperse standard distribution. Convergence to within 0.1% of true  $\bar{M}_n$  and  $\bar{M}_w$  values of a broad MWD standard is usually achieved in six to nine iterations.

SEC calibration methods which employ a series of narrow MWD standards are based upon a peak position method and traditionally have been the most widely practiced calibration procedures. The peak position method simply correlates the peak elution volume of each standard to its nominal molecular weight or size value. A curve fitting procedure (usually a least squares regression) is used to obtain a working calibration curve. The serious limitation of polymer chemical types for which a series of narrow MWD standards covering a wide molecular weight range can be obtained led to the development of experimental approaches which could be applied to polymer chemical types other than that of the narrow MWD standards employed in calibration.

The Q-factor approximation method (16) was an early attempt at extending the application of the peak position method to polymers of different chemical types than the calibration standards.

The Q-factor approach is based upon the weight-to-size ratios (Q-factors) of the calibration standard and the polymer to be analyzed. The Q-factors are employed to transform the calibration curve for the chemical type of the standards (e.g. polystyrene) into a calibration curve for the chemical type of polymer under study. The inherent assumption in such a calibration approach is that the weight-to-size ratio is not a function of molecular weight but a constant. The assumption is valid for some polymer types (e.g. polyvinylchloride) but not for many polymer types. Hence the Q-factor method is generally referred to as an approximation technique.

A direct consequence of the development of hydrodynamic volume theory in SEC has been the universal calibration method as introduced by Benoit (17). Universal calibration methodology is based upon the fact that retention in SEC can be described as a function of the hydrodynamic volume of polymer molecules.

Usually the function  $[(\eta) \cdot M]$  (intrinsic viscosity times molecular weight) is used to represent hydrodynamic volume which is plotted versus elution volume. For such a plot the calibration curves of many polymers fall on the same line irrespective of polymer chemical type. Universal calibration methodology usually requires knowledge of Mark-Houwink constants for the polymer/temperature/solvent system under study.

The purpose of this study was to evaluate the linear calibration technique employing a single polydisperse standard and the search algorithm described above for non-aqueous and aqueous SEC. Comparison of this calibration technique to peak position, universal calibration, and Q-factor approximation techniques which make use of a series of narrow MWD polystyrene standards was also carried out.

Experimental Techniques. Chromatography was performed on a Varian model 5060 HPLC equipped with a RI-3 refractive index detector. A Vista Plus Gel Permeation Chromatography (GPC) data system was used consisting of a Vista 401 chromatography data system serially connected to an Apple II microcomputer. The Vista 401 performs data acquisition and allows data storage and automations capability while all SEC data processing is performed on the Apple II by means of user-interactive GPC software for automated, on-line calibration and polymer analysis.

Non-Aqueous SEC Experiments. Non-aqueous SEC separations were carried out at ambient temperatures using two Varian MicroPak TSK GMH6 columns in series (7.5mm i.d. x 30cm each). This column is a mixed bed column containing pore sizes from 250 Å to  $10^7$  Å blended to ensure linearity of the molecular weight calibration curve. The mobile phase employed tetrahydrofuran at a flow rate of 1 ml/min. Sample injection volumes were 50  $\mu$ l using a Rheodyne 7126 manual loop injector.

Samples of narrow MWD polystyrene standards were obtained from Toyo Soda Mfg. Co., Ltd. (Tokyo, Japan) of the following molecular weights:

<u>Designation</u>	<u>MW</u>	<u><math>(\bar{M}_w/\bar{M}_n)</math></u>	<u>Designation</u>	<u>MW</u>	<u><math>(\bar{M}_w/\bar{M}_n)</math></u>
A-500	$5 \times 10^2$	1.15	F-10	$1.07 \times 10^5$	1.01
A-1000	$1 \times 10^3$	1.15	F-20	$1.86 \times 10^5$	1.07
A-2500	$2.8 \times 10^3$	1.05	F-40	$4.22 \times 10^5$	1.05
A-5000	$6.2 \times 10^3$	1.04	F-80	$7.75 \times 10^5$	1.01
F-1	$1.02 \times 10^4$	1.02	F-126	$1.26 \times 10^6$	1.05
F-2	$1.67 \times 10^4$	1.02	F-240	$2.42 \times 10^6$	1.09
F-4	$4.28 \times 10^4$	1.01			

A polydisperse polystyrene standard was obtained from Dow Chemical Co. (Midland, Michigan). This material was designated Dow 1683 polystyrene standard and has been well characterized with reported values as follows (18):

$\bar{M}_n = 100,000$   
 $\bar{M}_w = 250,000$   
 Polydispersity Index = 2.5

Dow 1683 polystyrene standard was utilized as a broad MWD standard in the linear calibration method due to its distribution symmetry and particular lack of significant tail at the low end of its MWD.

NBS 706 broad distribution polystyrene, NBS 705 narrow distribution polystyrene, and NBS 1478 narrow distribution polystyrene reference materials were used as samples in the evaluation of the proposed linear calibration method in this study. These reference materials have the following reported values:

<u>NBS Standard Reference Material</u>	<u><math>\bar{M}_w^{**}</math></u>	<u><math>\bar{M}_n</math></u>	<u><math>(\bar{M}_w/\bar{M}_n)</math></u>	<u>Concentration injected (%W/V)</u>
NBS 706 broad polystyrene	257,800	122,700	2.1	0.15%
NBS 705 narrow polystyrene	179,300	170,900	1.05	0.15%
NBS 1478 narrow polystyrene	37,400	35,800	1.05	0.20%

\*\* Measured by light scattering

Polystyrene Mark-Houwink constants of  $K=1.6 \times 10^{-4}$  dg/l and  $a = 0.706$  were employed (19).

Polyvinyl chloride (PVC) broad MWD standard obtained from Polysciences Inc. (Warrington, Penn.) was employed in the linear calibration method in a study of calculated molecular weight accuracy as a function of calibration methodology. The PVC polydisperse standard (lot #5-0069) had reported values of  $\bar{M}_w = 83,500$  and  $\bar{M}_n = 37,100$ . In this study the accuracy of results using the linear calibration method was compared to the accuracy of results using a Q-factor approximation method and universal calibration methodology employing a series of narrow MWD polystyrene standards. A PVC polymer with  $\bar{M}_w = 152,000$  (measured by light scattering) was used as the sample in the study of accuracy of calculated molecular weight as a function of calibration method. A concentration of 0.15% was injected for each PVC material. PVC Mark-Houwink constants of  $K=1.63 \times 10^{-4}$  dg/l and  $a=0.766$  were employed (20).

Aqueous SEC Experiments. Aqueous SEC separations were carried out at ambient temperature using two column sets of MicroPak TSK PW Type gel which were investigated for linearity of molecular weight calibration curve using polyethylene glycol (PEG) and polyethylene oxide (PEO) narrow MWD standards. Columns were matched in pore volume as closely as possible to promote linearity of the molecular weight calibration curve. Column set A consisted



of MicroPak TSK 3000PW + 4000PW + 5000PW + 6000PW (7.5mm i.d. x 30cm each) columns in series. Column set B consisted of MicroPak 3000PW + 3000PW + 6000PW + 6000PW (7.5mm i.d. x 30cm each) columns in series. Mobile phase for analysis of PEG and PEO standards was 50mM sodium sulfate at a flow rate of 1 ml/min. Injection volume was 100 $\mu$ l.

Samples of narrow MWD PEG standards were obtained from Fluka Chemical Co., (Hauppauge, NY) of the following molecular weights:

<u>Designation</u>	<u>MW</u>	<u>Designation</u>	<u>MW</u>
PEG 400	$4 \times 10^2 \pm 5\%$	PEG 4000	$4 \times 10^3 \pm 12\%$
PEG 600	$6 \times 10^2 \pm 5\%$	PEG 6000	$6 \times 10^3 \pm 12\%$
PEG 1540	$1.54 \times 10^3 \pm 9\%$	PEG 10K	$1 \times 10^4 \pm 15\%$
PEG 2000	$2 \times 10^3 \pm 8\%$		

Samples of narrow MWD PEO standards were obtained from Toyo Soda Mfg. Co. Ltd (Tokyo, Japan) of the following molecular weights:

<u>Designation</u>	<u>MW</u>	<u>(<math>\bar{M}_w/\bar{M}_n</math>)</u>	<u>Designation</u>	<u>MW</u>	<u>(<math>\bar{M}_w/\bar{M}_n</math>)</u>
SE-2	$2.5 \times 10^4$	1.14	SE-30	$2.8 \times 10^5$	1.05
SE-5	$4.0 \times 10^4$	1.03	SE-70	$6.6 \times 10^5$	1.10
SE-8	$7.3 \times 10^4$	1.02	SE-150	$1.2 \times 10^6$	1.12
SE-15	$1.5 \times 10^5$	1.04			

Sample concentrations were 0.3% w/v and 0.15% w/v respectively for the PEG and PEO standards. To aid dissolution of the PEO standards, 0.5% ethanol was added to the aqueous solutions.

Dextrans were employed to evaluate the linear calibration method for utility in aqueous SEC. The dextrans were obtained from Pharmacia Chemical Co. (Upsala, Sweden) of the following molecular weights:

<u>Designation</u>	<u><math>\bar{M}_w</math></u>	<u><math>\bar{M}_n</math></u>	<u>(<math>\bar{M}_w/\bar{M}_n</math>)</u>	<u>Comments</u>
Dextran T-70	64,200	44,000	1.46	—
Dextran T-40	39,900	26,200	1.52	T-40 used as sample for evaluation
Dextran Blend	52,050	32,850	1.58	Blend (1 part T-70 and 1 part T-40) used as polydisperse calibration standard.

The blend of T-70 and T-40 dextran materials was utilized as a polydisperse calibration standard for the linear calibration method and the T-40 dextran standard was used as a sample for evaluation. Concentrations of 0.15% W/V were injected for each dextran material chromatographed.

## Results and Discussion

Non-Aqueous SEC Evaluation. The SEC calibration report for a peak position method using a series of narrow MWD polystyrene standards is shown in Table I. As can be seen, a linear fit produces a high correlation to the data ( $r=0.9997$ ). Figure 1 displays the molecular weight calibration plot of elution volume versus log molecular weight for the series of polystyrene standards.

Table I. Calibration Report for a Series of Narrow MWD PS Standards

Curve Type		Least-Squares Curve Fit To Data				
		Correlation Coefficient	A	B	C	D
Y=A+B(X)		.9997	11.1495	-.4046		
Y = Log (Mol. Weight)						
X = Elution Volume (mls)						
Actual Elution Vol.	Actual Log (Mol. Wt.)	Actual Mol. Wt.	Calculated Log (Mol. Wt.)	Calculated Mol. Wt.	% Difference	
11.7	6.4609	2890000	6.4156	2604020	-9.9	
12.46	6.1004	1260000	6.1081	1282768	1.81	
12.92	5.8893	775000	5.922	835665	7.83	
13.6	5.6253	422000	5.6469	443511	5.1	
14.51	5.2695	186000	5.2787	189984	2.14	
15.1	5.0204	107000	5.04	109649	2.48	
16.17	4.6314	42800	4.6071	40465	5.46	
17.15	4.2227	16700	4.2106	16240	-2.76	
17.74	4.0086	10200	3.9719	9373	-8.11	
18.13	3.7924	6200	3.8141	6517	5.12	
19	3.4472	2800	3.4621	2898	3.49	

Table II shows the report from the linear calibration method employing the Dow 1683 broad MWD polystyrene standard. As can be seen in the report, the elution volume profile of the polydisperse standard contained 122 area/time slices upon which calibration calculations were based. The correlation coefficient listed in this report is an index of degree of fit of the calibration curve based upon the difference between calculated and true values of molecular weight averages of the standard. A plot of the linear calibration method molecular weight calibration curve is displayed in Figure 2. A comparison of molecular weight calibration curve plots for calibration using a peak position method with a series of narrow MWD standards (Figure 1) and a linear calibration method with a polydisperse standard (Figure 2) reveals that both calibration curves cover approximately the same elution volumes. This is not surprising due to the fact that both methodologies use standards which cover similar molecular weight ranges - about 3000 to  $2 \times 10^6$ . As can be seen by comparing Table I and II, the curve coefficients are very similar with almost identical slopes.

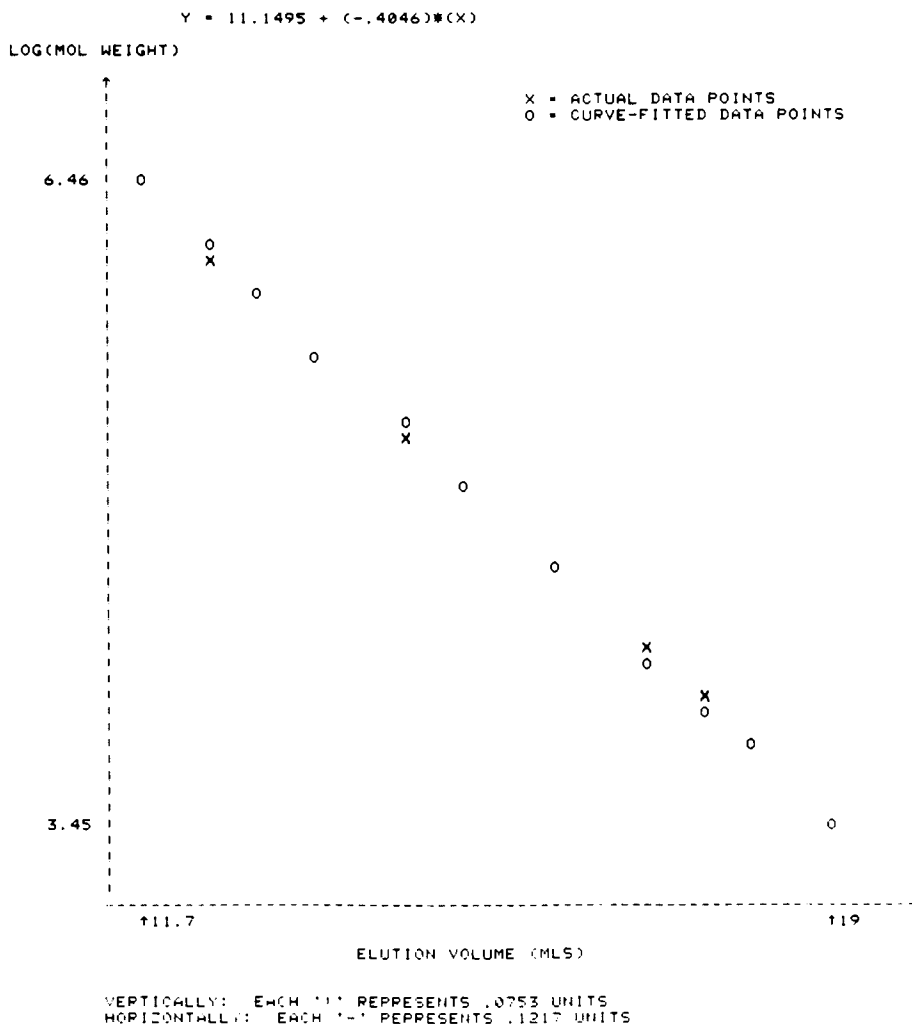


Figure 1. Calibration curve for a series of narrow MWD PS standards. Linear least squares fit for log (MW) versus elution volume.



Table II. Calibration Report for Polydisperse PS Standard

Curve Type	Correlation Coefficient	A	B	C	D
Y=A+B(X)	1.0005	11.0744	-.3988		
Y = Log (Mol. weight)					
X = Elution Volume (mls)					
		Calculated		Actual	
Number - average molecular weight:		100091		100000	
Weight - average molecular weight:		250227		250000	
Number of slices: 122		Slice width: 3 seconds/slice			

NBS 706 broad polystyrene, NBS 705 narrow polystyrene, and NBS 1478 polystyrene reference materials were used as samples for investigation of molecular weight accuracy as a function of calibration method. A peak position method using a series of narrow MWD polystyrene standards was compared to a linear calibration method utilizing a single broad MWD standard (Dow 1683 polystyrene standard). SEC peak processing parameters used for calculation of MWD values were held constant. Molecular weight averages were calculated for each NBS reference material by means of each calibration method. Table III lists the results of this study. Overall no significant difference in accuracy of calculated  $\bar{M}_w$  and  $\bar{M}_n$  values can be discerned on the basis of calibration methodology.

Table III. Molecular Weight Accuracy as a Function of Calibration Technique

	NBS 705 Narrow PS Reference STD			
	$\bar{M}_w$	% Difference	$\bar{M}_n$	% Difference
Reported value	179,300	—	179,900	—
Peak Position Method	173,509	- 3.2%	146,174	- 14.5%
Linear Method Using Polydisperse Std.	177,433	- 1.0%	150,246	- 12.1%
	NBS 706 Broad PS Reference STD			
	$\bar{M}_w$	% Difference	$\bar{M}_n$	% Difference
Reported Value	257,800	—	122,700	—
Peak Position Method	276,055	+ 7.1%	123,345	+ 0.5%
Linear Method Using Polydisperse Std.	279,574	+ 8.4%	127,870	+ 4.2%
	NBS 1478 PS Reference STD			
	$\bar{M}_w$	% Difference	$\bar{M}_n$	% Difference
Reported Value	37,400	—	35,800	—
Peak Position Method	35,716	- 4.5%	33,487	- 6.5%
Linear Method Using Polydisperse Std.	37,389	< 0.1%	35,121	- 1.9%

The NBS 706 broad polystyrene reference material is very similar in molecular weight and dispersity to the Dow 1683 polystyrene standard used for calibration. The NBS 705 narrow polystyrene material is lower in molecular weight and much narrower in dispersity than the Dow 1683 polystyrene standard and the NBS 1478 polystyrene reference material is significantly lower in molecular weight and dispersity. However, all three reference materials elute within the calibrated elution volume range of the molecular weight calibration curve generated by the linear calibration method utilizing the Dow 1683 polystyrene standard. SEC chromatograms of the Dow 1683 polystyrene standard and the NBS polystyrene reference materials are shown in Figure 3.

In a similar study by Yau et al. (21) which compared molecular weight accuracy as a function of a peak position calibration method and a linear polydisperse standard method using polystyrene standards, it was found that the peak position method using a series of narrow MWD standards gave more accurate results for narrow polydispersity samples and the linear calibration method gave more accurate results on samples of polydispersity similar to the polydisperse standard used for calibration. Based upon the results of the present study, it appears that accuracy is not a function of polydispersity of the sample when a linear, polydisperse standard method is used for calibration provided that the samples being analyzed elute within the calibrated elution volume range of the polydisperse standard and axial dispersion is minimized by use of high efficiency SEC columns. Axial dispersion for the non-aqueous SEC experiments was measured and found to be  $< 5\%$  over the molecular weight range of interest. Since dispersion was found to be minimal, no corrections to calculated molecular weight values were made.

Polyvinyl chloride polymers were utilized in a separate study to evaluate calculated molecular weight accuracy as a function of a universal calibration method, a Q-factor approximation method, and a linear calibration method employing a polydisperse standard. Table IV displays the calibration report generated from a linear calibration method using a broad MWD PVC calibration standard. At a slice rate of 3 second/slice, 130 slices were used in the calibration calculations to define the elution volume profile of the polydisperse PVC standard. Table V lists the calibration report obtained from use of a series of narrow MWD polystyrene standards utilizing universal calibration methodology. A comparison of calibration curves generated with a series of narrow MWD polystyrene standards utilized in a universal calibration method (Table V) and a linear polydisperse standard calibration method (Table IV) shows that the calibration curve coefficients are very similar.

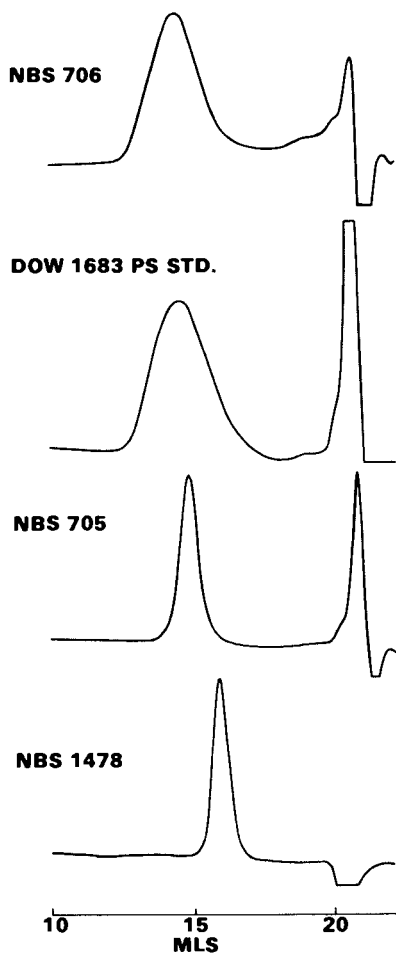


Figure 3. Chromatograms of NBS 706, Dow 1683, NBS 705, and NBS 1478 standard polystyrene reference materials. Detector: Refractive Index.

Table IV. Calibration Report for Polydisperse PVC Standard

<u>Curve Type</u>	<u>Correlation Coefficient</u>	<u>A</u>	<u>B</u>	<u>C</u>	<u>D</u>
Y=A+B(X)	.9996	11.3079	-.4252		
Y = Log (Mol. Weight)					
X = Elution volume (mls)					
			<u>Calculated</u>		<u>Actual</u>
Number - Average Molecular Weight:			37068		37100
Weight - Average Molecular Weight:			83430		83500
Number of Slices: 130			Slice Width: 3		seconds/slice

Table V. Universal Calibration Method Report for PVC

<u>Least-Squares Curve Fit To Data</u>					
<u>Curve Type</u>	<u>Correlation Coefficient</u>	<u>A</u>	<u>B</u>	<u>C</u>	<u>D</u>
Y=A+B(X)	.9997	10.7639	-.39		
Y= Log (Mol. Weight)					
X= Elution Volume (mls)					
<u>Actual Elution Vol.</u>	<u>Actual Log (Mol. Wt.)</u>	<u>Actual Mol. Wt.</u>	<u>Calculated Log (Mol. Wt.)</u>	<u>Calculated Mol. Wt.</u>	<u>% Difference</u>
11.7	6.2441	1754284	6.2005	1586657	- 9.56
12.46	5.8966	788134	5.9041	801785	1.73
12.92	5.6931	493287	5.7246	530448	7.53
13.6	5.4386	274536	5.4594	288019	4.91
14.51	5.0956	124624	5.1045	127201	2.07
15.1	4.8641	73131	4.8744	74881	2.39
16.17	4.4805	30234	4.457	28644	- 5.26
17.15	4.0865	12204	4.0748	11880	- 2.66
17.74	3.8801	7588	3.8447	6993	- 7.84
18.13	3.6717	4696	3.6926	4927	4.92
19	3.3389	2182	3.3532	2256	3.37

Table VI lists the results of this study of calculated molecular weight accuracy as a function of calibration method with the PVC polymers. A PVC polymer sample was analyzed and molecular weight averages were calculated by means of each calibration method. All SEC peak processing parameters used for calculation of MWD values were held constant. As shown in Table VI, the universal calibration method provided a somewhat more accurate  $M_w$  value than the Q-factor approximation method or the linear, polydisperse standard method.



Table VI. Molecular Weight Accuracy As A Function of Calibration Technique for PVC Polymer Sample

	$\bar{M}_w$	% Difference	$\bar{M}_n$
Reported Value	152,000*		
Q-Factor Approx. Method**	136,093	-10.5%	58,718
Universal Calibration Method	146,876	- 3.4%	67,318
Linear Method Using Poly-disperse Std.	166,024	+ 9.2%	65,662

\* Determined by light scattering

\*\*  $Q_{pvc} = 25$ 

Universal calibration methodology has been successfully applied to PVC and many other chemical types of polymers (22). However, availability of Mark-Houwink constants can limit the utility of universal calibration. In these cases, the use of a linear, polydisperse standard calibration method is a viable alternative for generation of a molecular weight calibration curve.

Aqueous SEC Evaluation. A comparison of SEC calibration reports from peak position methods using a series of PEG and PEO narrow MWD standards is shown in Table VII for the two MicroPak TSK Type

Table VII. Comparison of Calibration Reports Using A Series of Narrow MWD Polyethylene Oxide Standards for MicroPak TSK PW Column Sets

Column Set A:	Column Set B:
3000PW + 4000PW + 5000PW + 6000PW	3000PW + 3000PW + 6000PW + 6000PW
Standard Type: Narrow Standards	Narrow Standards
Calibration Basis: Molecular Weight	Molecular Weight
Curve Type: $Y = A + B (X)$	$Y = A + B (X)$
Correlation Coefficient: 0.995	0.996
Curve Coefficients: A = 10.9739 B = -.2135	A = 13.1186 B = -.267

PW gel column sets investigated for linearity. A least squares polynomial curvefitting procedure was employed to determine a first order polynomial fit to the data. The column set consisting of MicroPak TSK 6000PW + 6000PW + 3000PW + 3000PW (7.5 mm i.d. x 30 cm each) had a slightly higher correlation coefficient ( $r = 0.996$ ). Figure 4 displays the plots of elution volume versus log molecular weight for each column sets molecular weight calibration curve. Although column set A (3000PW + 4000PW + 5000PW + 6000PW) provided slightly higher resolution (i.e. lower slope), column set B (3000PW + 3000PW + 6000PW + 6000PW) was chosen for subsequent experiments on the basis of higher correlation to a linear fit of the data.

Dextran polymers were used to evaluate the utility of the linear, polydisperse calibration method for water-soluble polymer characterization. A blend of T-40 and T-70 dextran standards was used as a polydisperse calibration standard. Table VIII displays the report from the linear calibration method using this standard. Nine iterations of the search algorithm were required for convergence to the true  $\bar{M}_w$  and  $\bar{M}_n$  values of the standard. As can be seen in the report, the elution volume profile of the standard contained 72 area/time slices upon which calibration calculations were based. The slice width was set at 10 seconds/slice. Figure 5 shows a plot of the calibration curve generated from the linear calibration method utilizing the dextran standard,

Table VIII. Calibration Report For Polydisperse Dextran Standard

<u>Curve Type</u>	<u>Correlation Coefficient</u>	<u>A</u>	<u>B</u>	<u>C</u>	<u>D</u>
Y = A+B(X)	.9995	9.0638	- .1399		
Y= Log (Mol. Weight)					
X= Elution Volume (mls)					
			<u>Calculated</u>		<u>Actual</u>
Number - Average Molecular Weight:			32805		32850
Weight - Average Molecular Weight:			51999		52050
Number of Slices: 72			Slice Width:10 seconds/slice		

A T-40 dextran standard material was used as a sample for evaluation of calculated molecular weight accuracy using the linear calibration method. Results of this study are shown in Table IX. Errors of 5.3% in  $\bar{M}_w$  and 14.8% in  $\bar{M}_n$  were found. Hamielec and Omorodion (23) have investigated the use of dextrans standards in a linear calibration method using two broad standards. Comparison of the calibration curve generated with this method and a calibration curve generated by use of  $M_{TMS}$  vs peak elution volume for a series of dextran standards showed excellent agreement. Figure 6 displays the chromatograms of the dextran standard and T-40 dextran sample.

## Column Set A

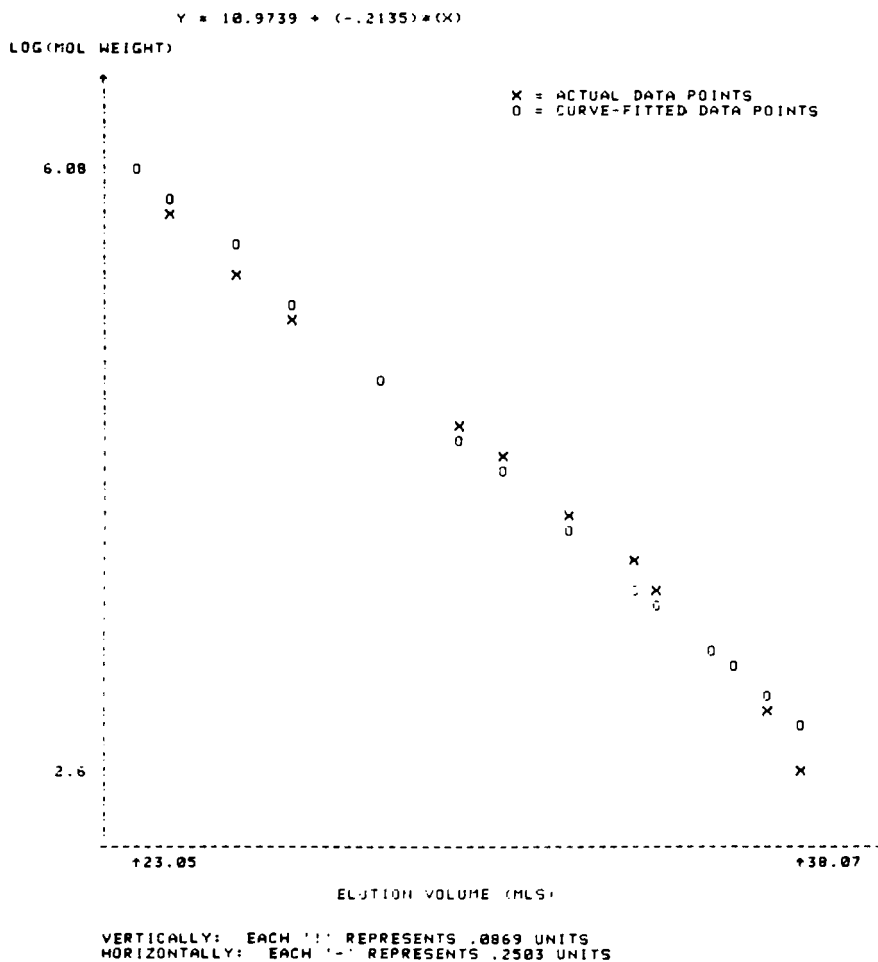


Figure 4A. Calibration curves using a series of narrow MWD polyethylene oxide standards for MicroPak TSK PW column sets. Linear least squares fit for log (MW) vs. elution volume. Column set A: MicroPak TSK 3000PW + 4000PW + 5000PW + 6000PW.

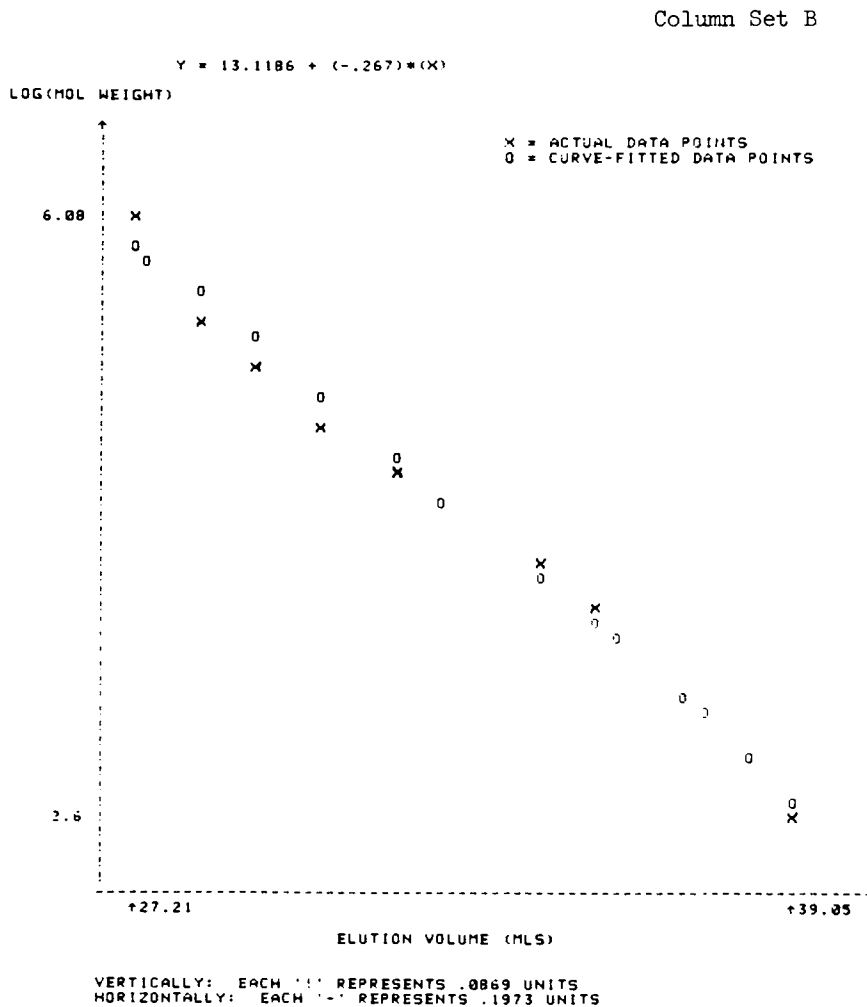


Figure 4B. Calibration curves using a series of narrow MWD polyethylene oxide standards for MicroPak TSK PW column sets. Linear least squares fit for log (MW) vs. elution volume. Column set B: MicroPak TSK 3000PW + 3000PW + 6000PW + 6000PW.

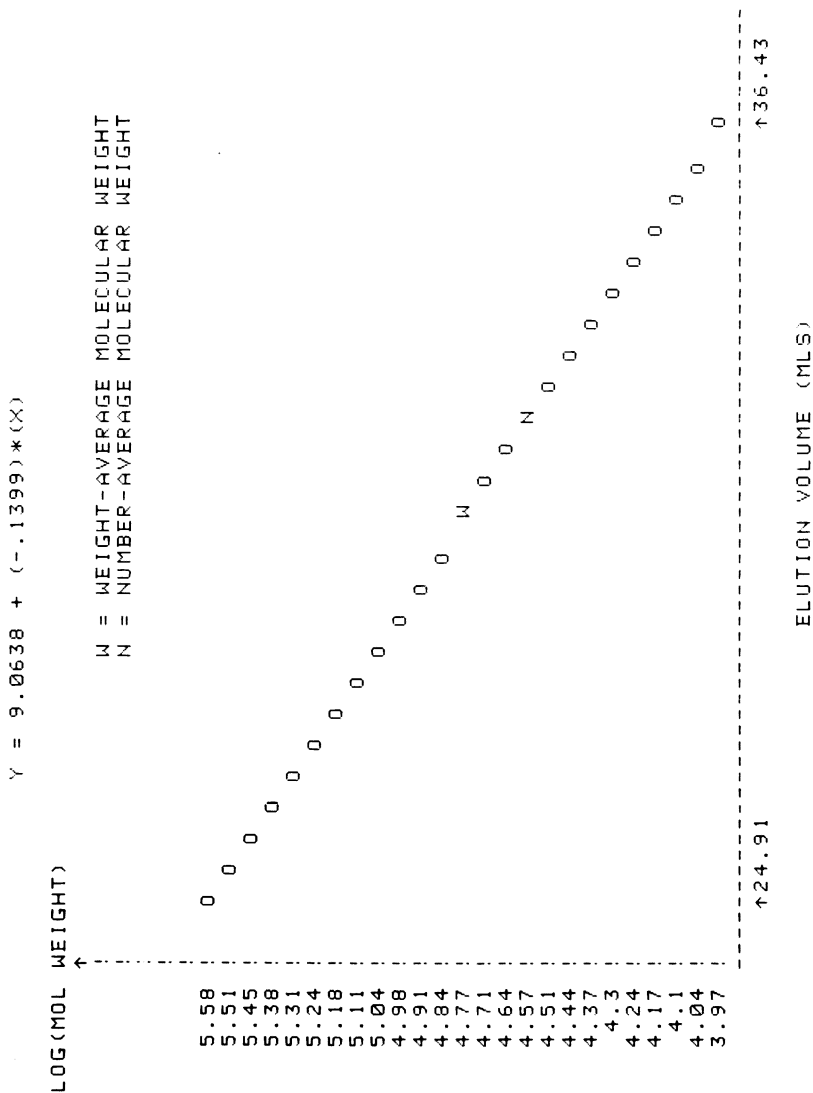


Figure 5. Calibration curve for polydisperse dextran standard using a linear method. Plot of log (MW) vs. elution volume. Horizontally, each - represents 0.48 units.

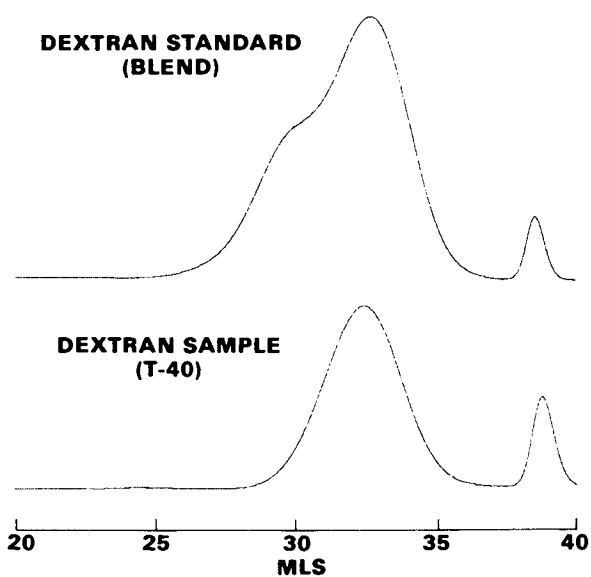


Figure 6. Chromatograms of polydisperse dextran calibration standard and dextran T-40 sample. Detector: refractive index.

Table IX. Molecular Weight Accuracy of the Linear Calibration Method for Dextran

	$\bar{M}_w$	$\bar{M}_n$
Reported Value	39,900	26,200
Linear Method Using a Poly-disperse Std.	37,799	30,091
% Difference	-5.3%	+14.8%

Due to the fact that application of universal calibration is not always practical in aqueous SEC, a linear calibration method using a single polydisperse standard has a high degree of viability for characterization of water-soluble polymers. Although few water-soluble polymers with characterized MWD moments are commercially available, in many instances an in-house polydisperse standard can be generated by measuring  $\bar{M}_n$  and  $\bar{M}_w$  of one lot of polymer of the same chemical type as that under study.

Optimization of Linear Calibration Methodology. The accuracy of linear calibration methods for utilization of polydisperse calibration standards depends upon (1) how well the column set approximates true linearity over the molecular weight calibration range and (2) the extent to which instrumental band broadening affects the elution volume profile of the polydisperse standard.

Linearity of the SEC column set can be achieved by use of commercially available mixed bed columns that have been optimized for linearity. Alternatively, the linearity of a SEC column set can be optimized by coupling columns of different pore sizes but equal pore volumes (24).

Instrumental band broadening or axial dispersion can cause calibration errors when employing polydisperse standards. Correction of the polydisperse standard calibration data for instrumental band broadening will minimize the effect on molecular weight analyses of polymer samples. However, as previously demonstrated in this report, when low dispersion SEC columns are employed instrumental band broadening is minimized and the effect on use of linear calibration methodology is negligible.

Conclusion. A linear calibration method based upon that of Balke and Hamielec and incorporating a very efficient two variable search algorithm was evaluated from the standpoint of calculated molecular weight accuracy in both non-aqueous and aqueous SEC. A comparison to calculated molecular weight accuracy with peak position, universal calibration, and Q-factor approximation methods using a series of narrow MWD standards was performed. From these studies the following conclusions have been drawn:

1. The linear calibration method provides an equivalent molecular weight calibration curve to a peak position method of calibration using a series of polystyrene standards.

2. Based upon studies with the NBS standard reference materials, the linear calibration method appears to give equivalent accuracy compared to a peak position method irrespective of sample dispersity provided that the sample elute over the elution volume range covered by the polydisperse standard and low dispersion SEC column are utilized.
3. In comparing the linear calibration method to a universal calibration method for PVC polymers, the universal calibration method appeared to be slightly more accurate suggesting that universal calibration methodology be applied whenever possible. In cases where universal calibration can not be utilized, the linear calibration method provides a viable alternative.
4. The linear calibration method has utility for characterization of water-soluble polymers due to the constraints imposed in aqueous SEC towards universal calibration methodology. A cursory evaluation of the linear calibration method for aqueous SEC indicates the method can be used with a high degree of accuracy to calculate molecular weight distribution values.

#### Acknowledgments

The authors would like to kindly thank Denise Thomas for preparation of the manuscript.

#### Literature Cited

1. E.A. Collins, J. Bares, and F.W. Billmeyer, Experiments in Polymer Science, John Wiley and Sons Inc., New York, 1973, p. 312.
2. W.W. Yau, J.J. Kirland, and D.D. Bly, Modern Size-Exclusion Liquid Chromatography, John Wiley and Sons, New York, 1979 Chapter 9.
3. Provder, T., Woodbrey, J.C., and Clark J.H., Separation Sciences, 1971, 6, p. 101.
4. Hamielec, A.E., and Omorodion, S.N.E., Size Exclusion Chromatography (GPC), ACS SYMPOSIUM SERIES, No. 138, 1980, Chapter 9.
5. Cantow, M.J.R., Porter R.S. and Johnson, J.F., Journal of Polymer Science: Part A-1, 5, 1967, pp 1391-1394.
6. Weiss, A.R., and Cohn-Ginsberg, E., J. Polymer Science, Part A-2, 8, 1970, p 148.
7. Swartz, T.D., Bly D.D. and Edwards, A.S.M., J. Applied Polymer Science, 16, 1972, p. 3353.
8. Abdel-Alim, A.H. and Hamielec, A.E., J. Applied Polymer Science, 18, 1974, p. 297.
9. Frank, F.C., Ward, I.M., Williams, T., Wills, H.H., J. Polymer Science, Part A-2, 6, 1969, pp 1357-1369.
10. Balke, S.T., Hamielec, A.E., LeClair, B.P., and Pearce, S.L., Ind. Eng. Chem. Prod. Res. Develop., 8, 1969, pp 54-57.



11. Loy, B.R., J. Polymer Science: Polymer Chem. Ed., 14, 1976, p 2321.
12. Pollock, M. MacGregor, J.F. and Hamielec, A.E., J. Liquid Chrom., 2, 1979, pp 895-917.
13. Yau, W.W., Stoklosa, H.J., and Bly D.D., J. Applied Polymer Science, 21, 1977, pp 1911-1920.
14. Malawer, E.G., and Montana, A.J., J. Polymer Science: Polymer Physics, 18, 1980, pp 2303-2305.
15. Alfredson, T.V., Perry W.J., and Tallman, L., Automated GPC Data Handling for Molecular Weight Calculations of Polymers, paper presented at 1982 Pittsburgh Conference and Exposition on Analytical Chemistry and Applied Spectroscopy, March 1982, Atlantic City, NJ.
16. Cazes, J., J. Chem. Educ., 43, p A567-A625, 1966.
17. Grubistic, Z., Rempp, R. and Benoit, H., J. Polym. Science Part B, 5, p 753, 1967.
18. Alfredson, T.V., personal communication from Edwin R. North, Analytical Laboratories, Polymer Analysis Group, Dow Chemical USA, Midland, Michigan
19. Provder, T. and Rosen E.M., Separation Science, 5, 1970, p 437.
20. Freeman, M., and Manning, P.B., Journal of Polymer Science, Part A-2, Polymer Physics, 1964, p 2017.
21. Yau, W.W., Stocklosa, H.J. and Bly D.D., J. Applied Polymer Science, 21, 1977, p 1911.
22. Ambler, M.R., J. Polymer Science: Polymer Chem. Ed., 11, 1973, p 191.
23. Hamielec, A.E. and Omorodion, S.N.E., Size Exclusion Chromatography (GPC), ACS SYMPOSIUM SERIES, No. 138, Chapter 9, p. 193.
24. Yau, W.W., Ginnard, C.R. and Kirland, J.J., J. Chromatogr., 149, p 465, 1978.

RECEIVED October 4, 1983

## Size Exclusion Chromatography of Polyethylenes Reliability of Data

L. A. UTRACKI and M. M. DUMOULIN

National Research Council Canada, Industrial Materials Research Institute, 75 Boulevard de Mortagne, Montréal, Québec, Canada, J4B 6Y4

A reliable procedure for determination of molecular parameters: number, weight and z-averages of the molecular weight ( $M_i$ ,  $i = n, w$  and  $z$  respectively) for polyethylenes, PE, by means of Size Exclusion Chromatography, SEC, has been developed. The Waters Sci. Ltd. GPC/LC Model 150C was used at 135°C with trichlorobenzene, TCB, as a solvent. The standard samples as well as commercial stabilized and not stabilized PE-resins were evaluated. The effects of: sampling, method of solution preparation, addition of antioxidant(s), thermal and shear degradation were studied. The adopted procedure allows reproducible determination of  $M_n$  and  $M_w$ , with a random error of  $\pm 4\%$  and  $M_z$ , with  $\pm 9\%$ , within 2 to 72 hrs from the initial moment of preparation of solutions.

While separation of ions according to size had already been observed by Ungerer in 1925 the first application of the principle to polymers occurred 19 years later (1). Between 1960 and 1962, Vaughan and Moore (2) independently developed methods for preparation of crosslinked polystyrene gel beads. The latter author is also credited with design of the analytical SEC as we know it today. Modern equipment (3, 4) operates at higher pressure, which combined with the higher temperature required for analysis of most polyolefins, results in a drastic shortening of column life time. Tempered alkali borosilicate glasses, leached with acids to produce uniform pore size, may eventually provide a solution (5-14). Unfortunately, they exhibit two disadvantages: low efficiency and solute adsorption.

Polyethylenes, PE, have been characterized by SEC since the mid-sixties and frequent problems with polystyrene gel columns have been reported (6). The low density PE, LDPE, because of complexity of the molecular weight and branching distributions,

0097-6156/84/0245-0097\$06.00/0

Published 1984, American Chemical Society

enjoyed more attention (3,15-23) than the simpler, and historically newer, high density, HDPE (24, 25). The results on the ultra high molecular weight, UHMWPE, have been published only recently (26, 27).

In this first report on SEC of PE, we want to comment on reproducibility of the measurements. This has been discussed by Nakajima (24) and others (28). In both cases seven PE samples were dissolved in 1,2,4-trichlorobenzene, TCB, and tested at 130°C using 4 or 5 polystyrene-gel columns. The standard deviations:  $\sigma_n = 6.43$  and 3.4 to 5.6%, as well as  $\sigma_w = 7.43$  and 3.4 to 4.4 were reported in these publications, respectively (subscript n and w refers to number and weight averages). The maximum spread of values  $\Delta_n = 17.4$  and  $\Delta_w = 25\%$  was observed. The authors (28) reported significant time changes in column separation properties. Standard deviations in low temperature SEC:  $\sigma_n = 4$ ,  $\sigma_w = 5\%$ , were reported (29, 30).

### Experimental

A Waters Sci. Ltd, GPC/LC Model 150C with Waters Model 130 Data Module was used. The instrument was operated at 135°C with TCB as a solvent (HPLC grade from Fisher Sci., filtered through 0.5  $\mu\text{m}$  filter with silicagel). Four and five  $\mu$ -Styragel (Waters Sci. Inc.) columns with pore sizes: (500),  $10^3$ ,  $10^4$ ,  $10^5$ ,  $10^6$  Å (from pump to detector) were calibrated using 21 narrow MWD polystyrene samples supplied by Pressure Chemicals and Waters Sci. (peak molecular weight  $M_p = 826$  to  $1.987 \times 10^6$  and polydispersity ratio  $M_w/M_n = 1.02$  to 1.21). The columns were calibrated (31) at 135°C using 0.06% of polymer (three standards per solution) in TCB. The calibration was checked once a week.

For calibration, the solutions were prepared overnight at ambient temperature without agitation, filtration or addition of antioxidants (a mild agitation and filtration resulted in an increase of retention time, RT, by 0.40 min, equivalent to a reduction of molecular weight by 26%). The calibration curve for the four columns Figure 1 was non-linear; addition of the fifth, 500 Å column, Figure 2 linearized the dependence:

$$\log M_p = 11.655222 - 0.170919 \text{ RT}, \quad 30 \leq \text{RT} \leq 55 \quad (1)$$

with the standard error of estimate  $\sigma = 0.043816$  and the correlation coefficient  $r^2 = 0.99914$ . During the calibration, as well as during the testing, the same conditions, listed in Table I, were used. Neither spinning nor filtering operational options were used.

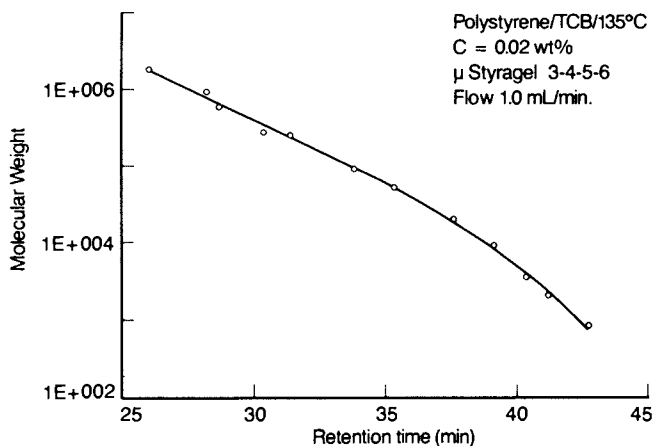


Figure 1. Calibration curve for four  $\mu$ -styrigel columns (PS in TCB at 135 °C).

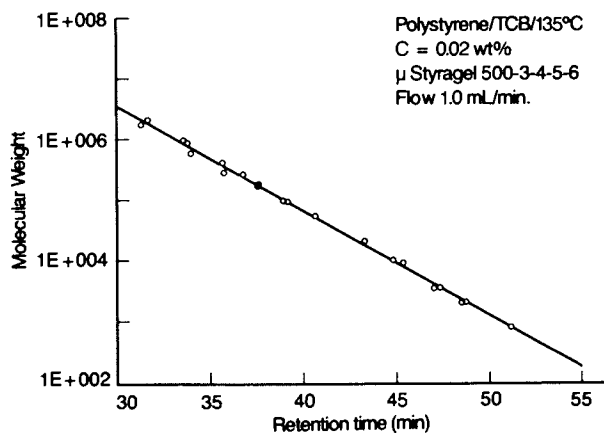


Figure 2. Calibration curve for five  $\mu$ -styrigel columns (PS in TCB at 135 °C).



**TABLE III: THE CHARACTERISTICS OF THE COMMERCIAL PE RESINS**

N°	RESIN	DENSITY $\rho$ (Kg/L)	MELT INDEX MI(g/10min)	ZERO SHEAR VISCOSITY $\eta_0$ (Pa.s) $\times 10^{-3}$ 190°C	$M_w \times 10^{-3}$	$M_z/M_n$
1	HDPE	0.955	14	1.4	125	11
2	MDPE	0.941	0.25	74.5	325	32
3	LDPE	0.924	0.80	29.0	155	8.5
4	LLDPE	0.920	1.1	8.9	212	6.3

Most of the initial work was done using the "as received" HDPE resin. The effects of its degradation during processing and testing on the molecular weight parameters were also studied; in the text the following code for these samples will be used: V - as received, G - mixed at 210°C for 15 min on a roll mill and granulated, M-in addition to G molded at 170°C in 8 min, C and CC-in addition to M sheared for 0.5 and 1.5 hrs at 190°C and frequency  $\omega = 0.1$  (rads/s).

### Results

First, a 50 ml solution was prepared of the sample V without (V-0) and with (V-A) antioxidants. The solution was poured into 12 sampling bottles and injected immediately and then every 2 hrs for 72 hrs. The variation of  $M_i$ 's with time for these samples is shown in Figures 4 and 5, respectively.

The results were fitted to the exponential relation:

$$M_i = M_{0,i} \exp\{-b_i t\} \quad (2)$$

where  $i = n, w$  and  $z$  for number, weight and  $z$ -average molecular weight,  $b_i$  is the degradation kinetics constant and  $t$  is the degradation time. The parameters of eq. (2) along with the:  $r^2$ -correlation coefficient squared,  $M_i$ -average value of the molecular weight,  $\sigma_i$ -standard error of the estimate and the  $\Delta_i$ -maximum spread, are listed in Table IV. The polydispersity ratios:  $M_w/M_n$  or  $M_z/M_n$  did not show any time dependence. For this reason only their average values as well as  $\sigma_i$  and  $\Delta_i$  are listed.

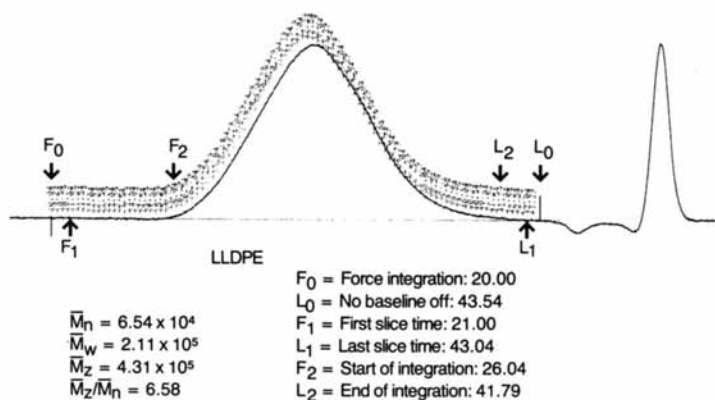


Figure 3. Example of chromatogram with the indicated location of the computational parameters.

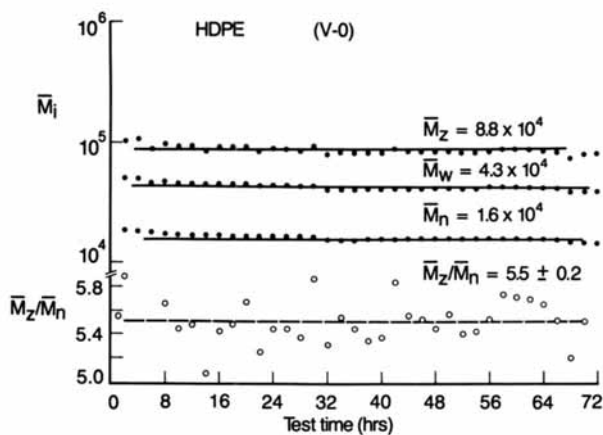


Figure 4. Molecular weight averages vs. residence time at 135 °C; HDPE without antioxidant.

**TABLE IV: STATISTICS OF SEC MEASUREMENTS OF HDPE  
WITHOUT (I) AND WITH (II) ANTIOXIDANT**

PARAMETER	$M_{0,i}$	$b_i$	$r$	$M_i$	$\pm\sigma_i(\%)$	$\Delta_i(\%)$
I without antioxidants (V-0)						
1. $M_n$	17,510	39.32	0.7484	16,055	5.99	28.0
2. $M_w$	46,845	101.27	0.6304	43,098	6.15	31.1
3. $M_z$	95,321	181.44	0.4429	88,312	6.70	39.4
4. $M_w/M_n$	-----	-----	-----	2.68	1.49	5.4
5. $M_z/M_n$	-----	-----	-----	5.50	3.45	17.8
II with antioxidants (V-A)						
1. $M_n$	36,777	34.06	0.2480	35,483	3.89	16.3
2. $M_w$	122,934	-56.37	0.0685	125,076	3.48	18.7
3. $M_z$	391,302	-806.41	0.1659	421,945	9.48	47.5
4. $M_w/M_n$	-----	-----	-----	3.53	4.25	14.6
5. $M_z/M_n$	-----	-----	-----	11.91	9.99	41.6

Next, seven randomly selected pellets of the resin V were dissolved in seven bottles and injected after 6 hrs at 135°C. The solutions contained the two antioxidants. The statistics are shown in Table V.

**TABLE V: EFFECT OF PE SAMPLING ON SEC DATA**

PARAMETER	$M_i$	$\pm\sigma(\%)$	$\Delta\%$
$M_n$	33,135	6.88	21
$M_w$	130,527	7.46	25
$M_z$	452,356	15.79	56
$M_w/M_n$	3.57	5.55	--
$M_z/M_n$	12.51	14.10	--



Similarly, the processed samples (V through to CC) were each dissolved and injected after 2 to 17 hrs at 135°C. The average values of molecular parameters are given in Table VI. These solutions contained the two antioxidants. The standard deviations varied from the minimum values of 1.72, 1.51 and 2.25 for  $M_n$ ,  $M_w$  and  $M_z$  of sample C, respectively to the maximum values of 5.99, 6.15 and 6.70 recorded for sample V.

**TABLE VI: EFFECT OF PROCESSING OF PE**

HDPE CODE	$t_{190}(\text{min})$	$M_n$	$M_w$	$M_z$	$M_z/M_n$
V	0	35,962	122,252	397,110	10.99
G	25.64	40,216	130,913	393,728	9.81
M	30.10	37,718	124,380	383,230	10.18
C	60.10	38,009	123,922	357,619	9.41
CC	120.10	36,458	119,602	337,851	9.28

To check on the general applicability of the method the remaining MDPE, LDPE and LLDPE were tested using the same experimental procedure. The results are shown in "Figures 6 to 8", respectively.

### Discussion

As seen in Table IV the  $M_n$ ,  $M_w$  and  $M_z$  for the stabilized solutions of the HDPE sample are larger than those for the unstabilized ones by a factor of 2.2, 2.9 and 4.8 respectively. Assuming that this variation is due to thermal degradation during the dissolution and testing one can calculate the activation energy  $E_a = 62.5$  (kcal/mole). This value compares well with  $E_a = 52.6$  to  $66.1$  determined (32) at  $T = 375$  to  $436$  (°C) for HDPE of molecular weight of 16 to 23 thousand, respectively. The initial results, and those collected after prolonged storage in the injection chamber, were not consistent with those collected within the "stable period":  $4 \leq t \leq 68$  hrs. This fact was further demonstrated in another series of measurements where the samples were injected for 230 hrs. The initial values of  $M_i$  widely scattered, whereas those for  $t > 68$  hrs systematically increased with time (this increase is responsible for the negative values of  $b_w$  and  $b_z$  in Table IV). Apparently, dissolving HDPE sample at 165°C for the period of 1.5 hrs is not sufficient. Only after an additional 2.5 hrs in the injection chamber at 135°C is the

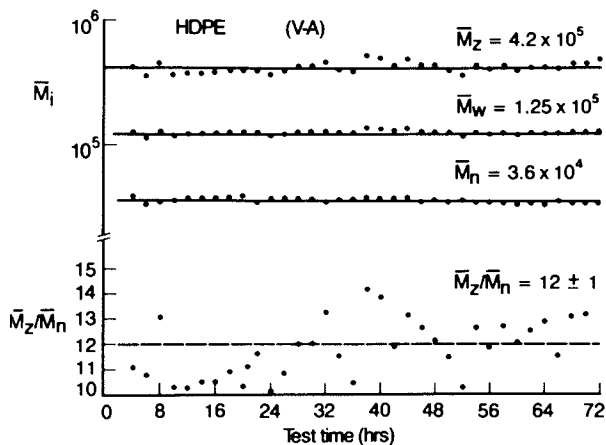


Figure 5. Molecular weight averages vs. residence time at  $135^\circ\text{C}$ ; HDPE with antioxidants.

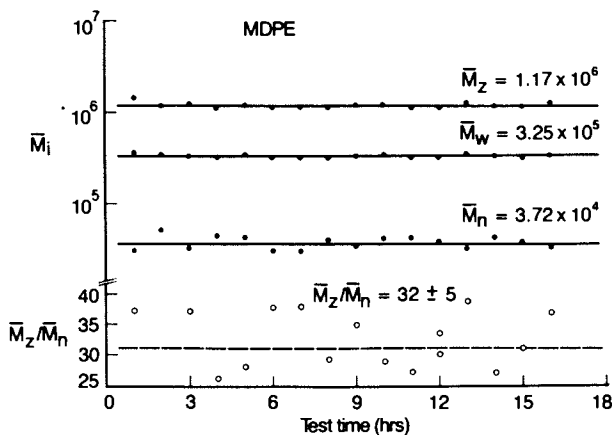


Figure 6. Molecular weight averages vs. residence time at  $135^\circ\text{C}$ ; MDPE with antioxidants.

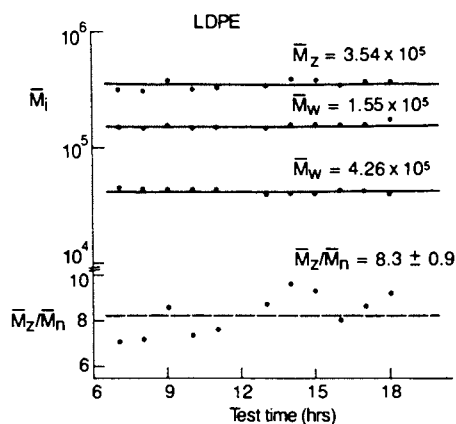


Figure 7. Molecular weight averages vs. residence time at 135 °C; LDPE with antioxidants.

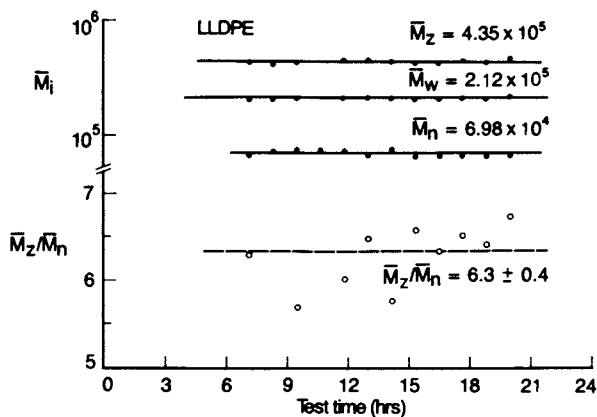


Figure 8. Molecular weight averages vs. residence time at 135 °C; LLDPE with antioxidants.

dissolution process completed and the stable, reproducible values of  $M_i$ 's are obtained. On the other hand, prolonged heating of the sample in the presence of antioxidants leads to gradual increase of  $M_i$ 's for times  $t_c \geq t \geq 32$  hrs. The value of  $t_c$  was observed to vary from one resin to another. It is worth noting that  $r^2$  for  $M_i$  in V-A series is very low, indicating a random variation. The standard deviations of these data ( $0 \leq t \leq 72$ ) are  $\sigma_n = \sigma_w = 4\%$  and  $\sigma_z = 9\%$ , which compare quite well with the previously quoted literature results.

It has been reported (33) that MWD of HDPE can be described by the log-normal distribution function (34):

$$p(x) = [\sigma(2\pi)^{1/2}]^{-1} \exp \{-t^2/2\} \quad (3)$$

$$t = (x - \bar{x})/\sigma$$

where  $x = \log M$ ,  $\bar{x}$  is the mean value of  $x$  and  $\sigma$  is the standard deviation. Defining the normal equivalent deviate as a proportion of  $p(x)$  which exceeds the integral:

$$p(s) = (2\pi)^{-1/2} \int_{-\infty}^s \exp \{-t^2/2\} dt \quad (4)$$

one can conveniently plot the probability function as  $p$  vs. probit, where probit is taken as  $(s+5)$ .

The V-A data follow Equation 3 quite well, with  $x = \log M_n$ ,  $M_n = 41,527 \pm 878$  and  $\sigma = 1.585 \pm 0.005$ . On the other hand, the V-0 data cannot be represented by this function. One can postulate that PE in TCB undergoes a random scission similar to that observed for polymer melts at much higher temperatures. In Figure 9 the integral distribution curves of samples HDPE (V-0) and (V-A), both taken after 10 hrs of dissolution, are shown in the form of log-normal distribution plot:  $M$  vs. probits. Two facts are apparent: (1) the molecular weights of sample V-A (broken line) are systematically higher than those of V-0 (points); (2) when the V-A distribution curve is displaced vertically to coincide with that of V-0 in the region of low molecular weight, it is quite apparent that the degradation preferentially affected the molecules with  $M > 10^5$ , while below this value  $M_{V-A} = KM_{V-0}$ , with  $K$  being a constant,  $K \approx 2.2$ . For  $M > 10^5$   $K$  increases with molecular weight approximately as:  $K = 2.2 + 2.1 \log M$ .

The above analysis should not be construed as authors' opinion that molecular weight distribution, MWD, of PE's should follow log-normal probability. The method of analysis is general and does not require that Equation 3 be obeyed; if it does,  $\log M$  vs. probit is a straight line, which simply makes the

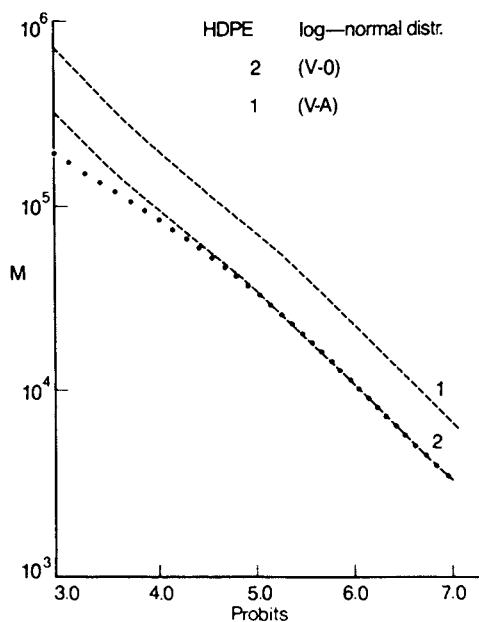


Figure 9. Log-normal distribution of HDPE molecular weight after 1.5 h at 165 °C and 10 h at 135 °C; 1 (upper line) - HDPE with antioxidant; circles - HDPE without antioxidant; 2 (lower line) upper broken line has been displaced vertically by a factor of 2.2 to coincide with the low molecular weight data of unstabilized sample.

work a little easier. We found that the plot is useful in interpreting the data even in the case of multimodal distributions.

The commercial resins are seldom a result of a single polymerization; in order to meet the specifications they are blended. The results of Table V show that the variability of  $M_1$ 's in this series is larger than that in Table IV; in the first case the results refer to average values for seven different pellets of HDPE-V dissolved separately, in the second to a variability of data of the same solution. The statistical analysis of the first set of data indicates that there is about 9% pellet-to-pellet variability in  $M_w$ .

In Table VI the results of SEC-testing of the processed samples are shown. The  $t_{190}$  represents the equivalent degradation time at 190°C calculated from the actual times and temperatures reported in the table; in the calculation, a simple Arrhenian function was assumed, with the activation energy  $\Delta E_a = 11.9$  (kcal/mole) obtained during the previous work (35). In Figure 10 the  $M_1$ 's dependence on  $t_{190}$  is shown. The results are most encouraging. It can be seen that even prolonged heating of the resin, under processing conditions, does not lead to a significant alteration of its  $M_1$ 's. The onset of degradation becomes apparent only for sample CC; here  $M_z$  is 17.5% lower than that of sample V. Since standard deviation of the measurements is  $\pm 9.5\%$  the drop in  $M_z$  reflects the true degradation. This is more clearly visible on Figure 10, where the polydispersity parameter,  $M_z/M_n$ , decreases systematically from a value of about 11 to 9.3. The initially more rapid decrease of this parameter is most likely due to the easy access of oxygen during this stage of the process - a factor neglected in calculating  $t_{190}$ .

Finally, a few words on the general reliability of the developed method of the measurements. The method, as shown in Figures 4 and 6 to 8 works quite well for all PE's of a normal, commercial range of  $M_1$ 's. We observed a need for longer dissolution time of HDPE than that of LDPE or LLDPE of equivalent molecular weight. The adopted dissolution time is 1.5 hrs at 165°C and 2.5 hrs at 135°C. With the weekly recalibration procedure the long term repeatability of data during the two years period was found to be random, and within the range of the reported standard deviations. Some initial work on SEC of the UHMWPE has been conducted; it was found that the above conditions were grossly inadequate.

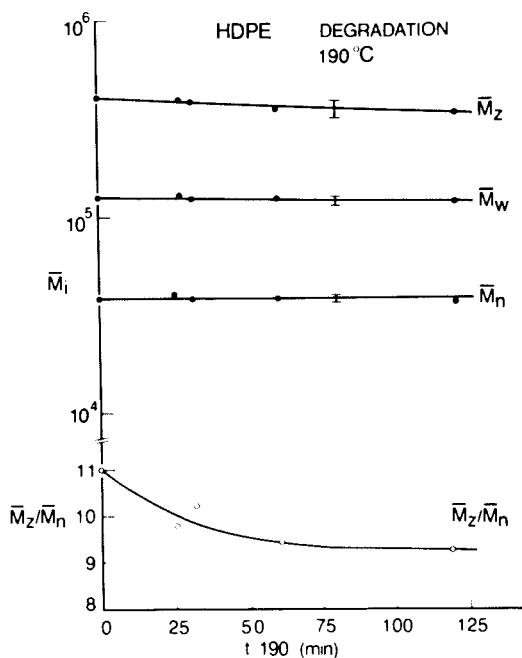


Figure 10. Molecular weight parameters of HDPE vs. the processing time at 190 °C; see text.

Acknowledgments

The authors would like to thank Mr. J. Dufour for his careful work in collecting the SEC data.

Literature Cited

1. J. Claesson and S. Claesson, Arkiv. Kemi, 19A, 1 (1944).
2. J.C. Moore, J. Polymer Sci., A2 835 (1964).
3. E.E. Drott and R.A. Mendelson, J. Polymer Sci., Part A-2, 8, 1361, 1373 (1970).
4. Polymer Laboratories "PLgel GPC columns" technical buletin 5/82.
5. W. Haller, Nature, 206, 693 (1965).
6. J.H. Ross and M.E. Casto, J. Polymer Sci., Part C, 21, 143 (1968).
7. A. Titterton, Ind. Polym., May 1-2, 1973 pg. 83-88.
8. A.R. Cooper, J. Polymer Sci., Polymer Phys. Ed., 12, 1969 (1974).
9. L. Westerman, Chromatog. Sci., 13, 257 (1980).
10. M. Kubin, J. Appl. Polymer Sci., 27, 2933, 2955 (1982).
11. B.W. Hatt, Develop. Chromatogr., 1, 157 (1978).
12. J.V. Dawkins and G. Yeadon, Develop. Polym. Charact., 1, 71 (1978).
13. J.V. Dawkins, Pure Appl. Chem., 51, 1473 (1979).
14. R.A. Ellis, Pigm. Res. Techn., Sept. 1979, pg. 10-21.
15. Z. Grubisic, P. Rempp and H. Benoit, J. Polymer Sci., B5, 753 (1967).
16. B.H. Zimm and W.H. Stockmayer, J. Chem. Phys., 17, 1301 (1949).
17. J.A. Cote and M. Shida, J. Polymer Sci., Part A-2, 9, 421 (1971).
18. J.A. Miltz and A. Ram, Polymer, 12, 685 (1971); A. Ram and J. Miltz, J. Polymer Sci., 15, 2639 (1971).
19. G.R. Williams and A. Cervenka, Eur. Polymer J., 8, 1009 (1972).
20. S. Nakano and Y. Goto, J. Appl. Polymer Sci., 19 2655 (1975); ibid., 20, 3313 (1976).
21. L. Wild, R. Ranganath and A. Barlow, J. Appl. Polymer Sci., 21, 3319, 3331 (1977).
22. L. Lecacheux, J. Lescq and C. Quivoron, ACS Polymer Prepr., 23(2) 126 (1982).
23. A. Hamielec, Pure Appl. Chem., 54, 293 (1982).
24. N. Nakajima, J. Appl. Polymer Sci., 15, 3089 (1971); idid. 16, 2417 (1972).
25. J.V. Dawkins and J.W. Maddok, Eur. Polymer J., 7, 1537 (1971).
26. A. Barlow and T. Ryle, Plastics Eng., August 1977, pg. 41-43.



27. Polymer Laboratories, technical information 5/82.
28. G. Samay and L. Fuzes, J. Polymer Sci., Polymer Symp., 68, 185 (1980).
29. J.H. Duerksen and A. Hamielec, ACS Symp. on Analytical GPC, Chicago, Sept. 1967.
30. J.P. Busnel, Polymer, 23, 137 (1982).
31. A.E. Hamielec and A.C. Ouano, J. Liq.Chromatography, 1, 111 (1978).
32. H.H.G. Jellinek, J. Polymer Sci., 4, 13 (1949).
33. H. Wesslun, Makromol. Chem., 20, 111 (1956).
34. W.D. Lansing and E.O. Kraemer, J. Am. Chem. Soc., 57, 1369 (1935).
35. L.A. Utracki and J. Lara, Proceedings of the Int'l Workshop on Extensional Flows, Mülhouse - La Bresse, France, 24-28 January 1983.

RECEIVED September 12, 1983

# Gel Permeation Chromatography

## Correction Procedure for Imperfect Resolution

B. A. ADESANYA, H. C. YEN, and D. C. TIMM

University of Nebraska, Lincoln, NE 68588-0126

N. C. PLASS

Brunswick Corporation, Lincoln, NE 68504

In part I, Timm and Rachow (1) describe an algorithm for interpretation of chromatograms for imperfect resolution. The instrument was one of low plate counts, and yet population density distributions consistent with theoretical, kinetic models were achieved (2,3). Research, using high plate count columns, shows that convergent distributions are achieved and that results are not a function of instrument resolution. Linear polystyrene resins had a polydispersity in the interval  $1.5 < \overline{M}_w/\overline{M}_n < 2.0$ . Data analysis includes mass fractions of unreacted monomers and species of similar molecular weight.

A second algorithm is described for analysis of resins of narrow, molecular distributions  $\overline{M}_w/\overline{M}_n \approx 1.0$ . Experimental testing incorporates polystyrene initiated with n-butyl lithium and a linear, step-growth epoxy comprised of nadic methyl anhydride and phenyl glycidyl ether. Kinetic distributions are described by a Poisson molar distribution. The accuracy of experimental population density distributions for macromolecular species is observed to be limited by the precision of the average molecular weights determination by light scattering and by vapor pressure osmometry. The algorithm may be constrained to fit a Poisson molar distribution. Experimental error is more pronounced for higher molecular weight resins, which require greater precision in assignments of molecular weights.

### Calibration

The algorithm calibration sequence is pictorially shown in Figure 1. Chromatograms for monomers plus polymers of narrow, molecular distribution are experimentally observed, normalized to a unit mass and labeled  $S_{ij}$ . The index  $i$  identifies equally-spaced, elution volume increments from time of sample injection; the index  $j$  defines the standard number. For each polymeric standard, the molecular weight of species eluting in the volume interval  $VE_i$  is assumed to be a semilogarithmic function of elution volume

NOTE: This is Part II in a series.

0097-6156/84/0245-0113\$06.00/0

© 1984 American Chemical Society

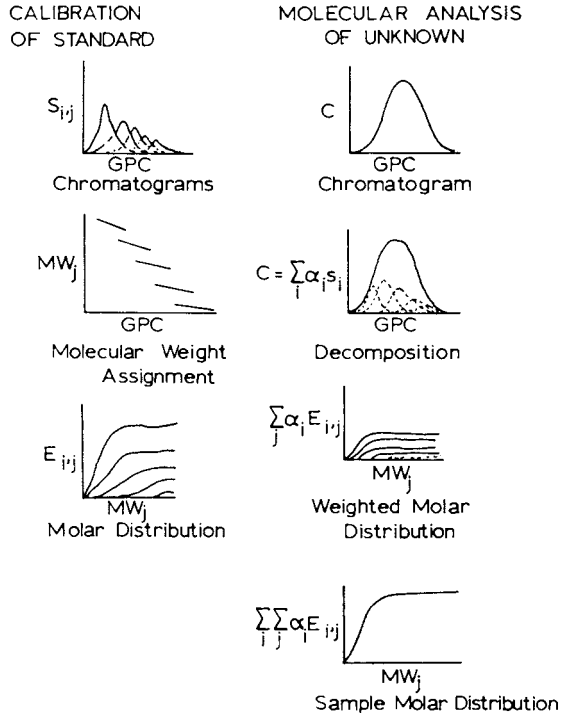


Figure 1. Schematic for GPC calibration and sample analysis.

$$\ln MW_{ij} = A_j + B_j(VE_i) \quad (1)$$

Analysis of resins described by Poisson distributions shows the validity of this constraint for standards. A cumulative, molar distribution of macromolecules is determined from the normalized chromatogram  $S_{ij}$  and Relationship 1:

$$E_{nj} = \sum_{i=1}^n S_{ij}/MW_{ij} \quad (2)$$

Degree of polymerization is  $n$ . Molar distributions are interpolated to specific degrees of polymerization.

In evaluation of the parameters  $A_j$  and  $B_j$ , Timm and Ratchow (1) utilized number and weight average molecular weights coupled with the observed, normalized chromatogram for that standard. Specifically,

$$PD_j = \frac{\sum_i (S_{ij} \exp(B_j VE_i))}{\sum_i (S_{ij} \exp(-B_j VE_i))} \quad (3)$$

A Newton/Raphson iteration yields the value for  $B_j$ . An average molecular weight yields the value of  $A_j$ . In reference to Figure 1, the calibration sequence is now completed. Block data storage incorporates  $S_{ij}$  and  $E_{nj}$ .

#### Population Density Distributions

Figures 2 and 3 present typical results obtained from a low plate count column and a high plate count column. The graphs present the calculated molar concentrations of macromolecular species as a function of their degree of polymerization. The straight lines are the theoretical, kinetic distributions. Inasmuch as convergent solutions are obtained, the algorithm is effective for correction for imperfect resolution.

The polystyrene data were collected from a steady state, continuous, well-mixed reactor. The initiator was *n*-butyllithium for data of Figure 2 and was azobisisobutylnitrile for data of Figure 3. Toluene was used as a solvent. The former polymerization yields an exponential population density distribution (2),  $\bar{M}_w/\bar{M}_n = 1.5$ ; the latter yields a molar distribution defined as the product of degree of polymerization and an exponential (3),  $\bar{M}_w/\bar{M}_n = 2.0$ . Standards utilized in calibration of both instruments were polystyrene supplied by Pressure Chemical Company.

#### Poisson Distribution

For a polymerization comprised of propagation kinetics only, a Poisson molar distribution exists for a batch polymerization initially seeded with a polymeric species  $A_1(0)$ . Rate of propagation is defined by

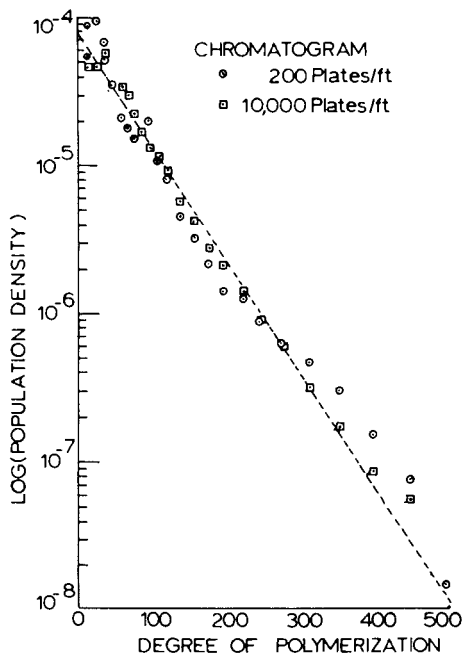


Figure 2. Frequency distributions for polystyrene initiated with n-BuLi.

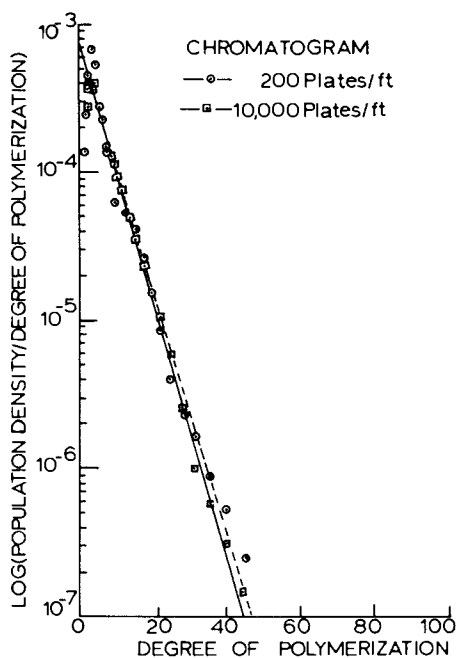
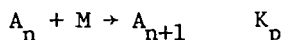


Figure 3. Frequency distributions for polystyrene initiated with AIBN.



The molar concentration of a polymeric molecule of degree of polymerization  $n$  is expressed as

$$\frac{dA_n(t)}{K_p M(t) dt} = \frac{dA_n(t)}{d\tau} = A_{n-1}(t) - A_n(t)$$

Seeding yields a null initial condition except for

$$A_1(0) \neq 0$$

Integration yields a Poisson, molar frequency distribution

$$A_n(\tau) = A_1(\tau) \tau^{n-1} \exp(\tau)/(n-1)! \quad (4)$$

The weight distribution is

$$W_n(\tau) = M_o n A_n(\tau) \quad (5)$$

The molecular weight of the repeat unit is  $M_o$ . The number average and weight average degrees of polymerization are

$$\overline{DP}_n = \frac{\overline{M}_n}{M_o} = \frac{\sum_{k=0}^{\infty} k^1 A_k(\tau)}{\sum_{k=0}^{\infty} k^0 A_k(\tau)} = 1 + \tau \quad (6)$$

$$\overline{DP}_w = \frac{\overline{M}_w}{M_o} = \frac{\sum_{k=0}^{\infty} k^2 A_k(\tau)}{\sum_{k=0}^{\infty} k A_k(\tau)} = 1 + \tau + \frac{\tau}{1+\tau} \quad (7)$$

Hence, polydispersity is

$$PD = \frac{\overline{DP}_w}{\overline{DP}_n} = 1 + \frac{\tau}{(1 + \tau)^2} \geq 1.0 \quad (8)$$

To experimentally control the average molecular weight for such polymerizations, the initial concentration of seeds  $A_1(0)$  relative to monomer  $M(0)$  is manipulated. The lower this ratio, the higher will be the ultimate average molecular weight, which, in turn, increases the value of  $\tau$ , the integral conversion of monomer. Chain-growth polymerizations of styrene, initiated with *n*-butyllithium approximate such a kinetic mechanism (4). The step-growth polymerization of the following epoxy resins will also yield a Poisson, molar, frequency distribution.

Catalyst	Basic tertiary amine
Seed	Benzoic acid
Monomers	Phenyl glycidyl ether Nadic methyl anhydride

The reactive hydrogen site supplied by the organic acid controls the number of polymer molecules; the basic catalyst effectively results in the alternate addition of oxirane/anhydride monomers, forming ester linkages at the reactive hydrogen site (5).

The algorithm utilizes block data sets for  $S_{ij}$  of actually observed chromatograms and regenerates an unknown sample's chromatogram  $C_i$  by

$$C_i = \sum_j \alpha_j S_{ij} + \epsilon_i \quad (9)$$

The weight fraction for each standard is  $\alpha_j$  and the error in the fit is  $\epsilon_j$ . Sufficient standards must be run so as to reconstruct the chromatogram  $C_i$ . Experience suggests that about fifteen are normally adequate for broadly distributed resins, i.e.

$$\frac{M_w}{M_n} \geq 1.5.$$

When a polymer of narrow distribution is subjected to analysis, its chromatogram may fall between those for two adjacent standards. A least squares fit then yields a weighted bimodal distribution. If the chromatogram for the unknown coincides with that for a standard, the calculated distribution will be that of the standard (see Figure 1). The former results in broadening of the numerical results; the latter is desirable, but unlikely. Experience has, therefore, resulted in the development of a subroutine for such analyses. Adesanya (6) selected the observed chromatogram to be  $S_{ij}$  and initially explored average molecular weights to evaluate the parameter  $\tau$  of the Poisson distribution, Equations 6 and 7. Normally reported values yield a degree of uncertainty in its numerical value assignment which becomes more significant as molecular weight increases. Thus, the constraint of Equation 3 was modified, particularly for higher molecular weight standards.

Poisson distributions exhibit a maximum near  $\tau = j-1$  (7). The chromatogram's maximum, coupled with an overall calibration (the logarithm of the average molecular weight vs eluent volume at the chromatogram peak), was utilized to assign the value for  $\tau$  for the unknown. The weight average molecular weight was utilized. Relationships 4 and 5 were then utilized to evaluate the theoretical, kinetic, weight distribution and correlated as a function of degree of polymerization  $n$ .

The area of the chromatogram for the unknown sample can also be utilized to generate a weight fraction distribution, but as a function of eluent volume,  $i$  (see Figure 4). At a constant mass fraction, the two distributions are equal and can be utilized to generate a calibration curve to check the validity of the semi-logarithmic calibration constraint, Equation 1. Figure 5 pre-



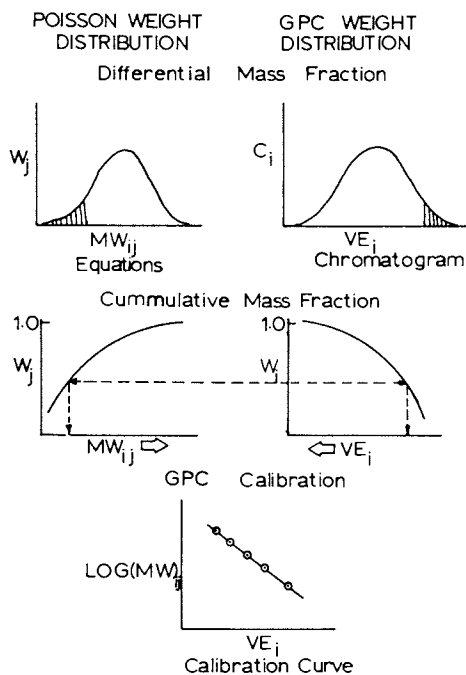


Figure 4. Schematic for GPC calibration subject to Poisson constraints.

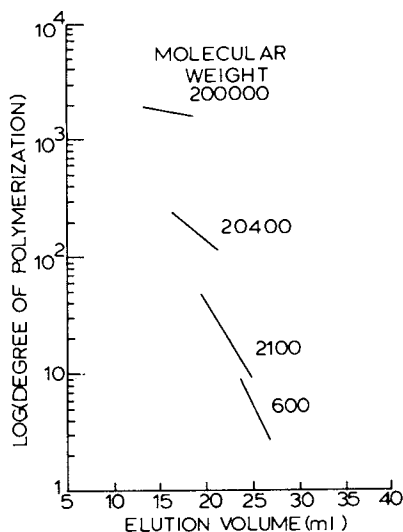


Figure 5. Individual standard's calibration curve subject to Poisson constraints.

sents results for four polystyrenes. A semilogarithmic relation is generated. Therefore, Equation 1 is a valid relationship for evaluation of the cumulative, molar distribution during calibration.

As the molecular weight of the material increases, the polydispersity of that material must approach 1. Specifically, for the 200,000 molecular weight sample, light scattering and vapor pressure osmometry yields a polydispersity value near 1.06. If the material is distributed according to a Poisson distribution, the polydispersity will be 1.0005. Normal errors reported in measurements of average molecular weights preclude this accuracy. However, if one believes an average molecular weight is correct and forces the second average to be consistent (Equation 6 or 7), the calibration procedure described by Timm and Rachow, Equation 3, will yield a Poisson molecular frequency distribution. If both experimentally observed molecular weights are utilized, the calculated distribution is normally a broader distribution than is the Poisson distribution.

### Monomer Analysis

Yen (8) and Tien (9) utilized vapor pressure osmometry and light scattering for molecular weight analysis of linear, epoxy resins. These have subsequently been extensively utilized by our research group as calibration standards in the analysis of thermoset, epoxy resins (10). To obtain better estimates, chromatography was utilized to correct observations for monomer contamination. The algorithm was modified such that the originally observed chromatogram  $C_i$  was expressed in terms of standards  $S_{ij}$  by:

$$C_i = \sum_{j=1}^{m1} \alpha_j S_{ij} + \sum_{j=m1}^{m2} G_{ij} + \sum_{j=m2}^N \alpha_j S_{ij} + \epsilon_i$$

The first summation incorporates a block data set for observed monomeric standards; the second is a null buffer; the third are polymeric standards. Testing through the addition of monomers to polymer standards verified that the decomposition concept is again valid. Accuracy within the chromatogram is the error-determining step. Table I presents analysis of material after blending known quantities.

The polymerizations were designed such that formulation, coupled to stoichiometry, would control the ultimate molecular weight. Table II presents theoretical, kinetic, average molecular weights, as well as those initially determined. Low molecular weight measurements were acceptable, but high molecular weights were in serious error, due to monomer contamination. The observed number average molecular weight can be expressed by

$$\bar{M}_n \text{ observed} = \frac{\sum \text{gram(monomer)} + \sum \text{gram(polymer)}}{\sum \text{moles(monomer)} + \sum \text{moles(polymer)}} \quad (10)$$

Table I: Decomposition of Epoxy Resin Plus Monomer, Mass Fractions

Matl	$\overline{MW}_n$	Monomer only		Resin plus Monomer		Resin plus Monomer		PGE
		true	observed	true	observed	true	observed	
BDMA	135	0.08	0.053	.023	.028	.024	.025	
PGE	150	0.30	0.317	.029	.020	.121	.119	
NMA	178	0.56	0.554	.174	.166	.074	.085	
ROH	130	0.06	0.076	.016	.022	.016	.010	
Polymer	500	0.00	0.000	.758	.764	.765	.760	
Total		1.00	1.000	1.000	1.000	1.000	1.000	

Table II: Epoxy Average Molecular Weights Due to Monomeric Contamination

Kinetic*	$\overline{MW}_n$		$\overline{MW}_w$		$\overline{PD}$
	observed**	corrected	observed***	corrected	
$\overline{MW}_n$					
330	470	490	495	500	1.02
490	650	710	1090	1100	1.54
1400	1000	1730	1630	1850	1.07
6560	2050	7600	7770	8200	1.08
328000	2250	----	21600	25700	----

\*Grams monomer/mole initiator; \*\*Vapor pressure osmometry;

\*\*\*Light scattering

Chromatography analysis yields the mass of monomeric species and polymer in the cured resin, from which the moles of monomer are readily calculated. This relationship, coupled with the observed molecular weight, can be utilized to determine the moles of polymer. Hence, the corrected number average molecular weight is

$$\bar{M}_n \text{ correct} = \frac{\sum \text{gram}(\text{polymer})}{\sum \text{moles}(\text{polymer})} \quad (11)$$

Column 2 of Table II presents these results. Columns 4&5 represents corrected weight average molecular weights. For the highest molecular weight standard, the moles of monomer compared to polymer in Equation 9 are such that the correction procedure failed. However, this sample could be cleaned of monomer by fractionation techniques without serious danger of removing significant quantities of oligomers. Alternately, an analysis based solely on chromatography will yield a definitive description of the macromolecular content.

### Discussion

The algorithm accurately determines the monomeric and polymeric fractions plus population density distributions of macromolecules within an unknown sample, from which mass distributions and moments may be calculated. The modified algorithm is shown to accurately evaluate resins for which  $1.0 \leq \bar{M}_w/\bar{M}_n \leq 2.0$ , subject to assignments of average molecular weights. Resins with polydispersity greater than 2.0 may also be evaluated, yielding expected, theoretical distributions (10). The data of Table II show that at high concentrations of initiator ROH, some species do not initiate the polymerization process. Similarly at low initiator concentrations, the achieved molecular weight is less, perhaps due to other sources of polymerization sites in the resin, one of which could be moisture.

The chromatograph is interfaced with a Digital LSI-11 microprocessor. Calibration, though requiring observations of chromatograms for monomeric and polymeric standards, can be efficiently achieved. Research over several years shows that styragel/microstyragel columns are very stable under continuous utilization.

A substantial asset of the algorithm is its flexibility, allowing for simultaneous, analytical analysis of monomeric and polymeric species, both in terms of average molecular weights and population density distributions of constitutive molecules. The technique is being extended to the analysis of extracts of quality cured thermoset resins. Simultaneous analysis by chromatography and by dynamic mechanical spectroscopy shows that oligomeric fractions' average molecular weights by chromatography closely correlate with crosslink average molecular weight determined by spectroscopy (11). Resins are of constant chemical composition, but are subjected to molecular variance through controlled cure

cycles. The technique has also successfully determined theoretical, kinetic distributions of constitutive molecules for a variety of thermoplastic resins, using a broad spectrum of polymerization mechanisms.

#### Acknowledgments

Financial and technical support from the Engineering Research Center and from Brunswick Corporation are appreciated.

#### Literature Cited

1. Timm, D.C.; Rachow, J.W. J. Polym. Sci. 1975, 13, 1401.
2. Timm, D.C.; Kubicek, L.F. Chem Engr. Sci. 1974, 29, 2145.
3. Scamehorn, J.F.; Timm, D.C. J. Polym. Sci. 1975, 13, 1241.
4. Hsieh, H.L. J. Polym. Sci. 1965, A3 153, 163, 173, 181, 191.
5. Chen, C.P.; Timm, D.C.; Ho, V. Proc. First Int'l Conf. on Reactive Processing of Polymers 1980, II, 4.
6. Adesanya, B.A., M.S. Thesis, University of Nebraska, Lincoln, NE, 1978.
7. Weast, R.C.; Selby, S.M., Ed. CRC Handbook of Tables for Mathematics CRD Press: Cleveland, 1975, 952.
8. Yen, H.C., M.S. Thesis, University Nebraska, Lincoln, NE,
9. Tien, C.S., M.S. Thesis, University Nebraska, Lincoln, NE, 1980.
10. Ayorinde, A.J.; Lee, C.H.; Timm, D.C.; Humphrey, W.D., submitted to ACS Symposium Series (1983).
11. Timm, D.C.; Ayorinde, A.J.; Huber, F.K.; Lee, C.H.; submitted to Int'l Rubber Conf. '84, 4-8 Sept., '84, Moscow.

RECEIVED September 12, 1983

# Size Exclusion Chromatography Molecular Weight Separation and Column Dispersion

## Simultaneous Calibration with Characterized Polymer Standards

RONG-SHI CHENG and SHU-QIN BO

Changchun Institute of Applied Chemistry, Academia Sinica, Changchun, Jilin, People's Republic of China

With the aid of the theoretical relationship between the calibration relation of a SEC column for the monodisperse polymer species under ideal working conditions and the effective relations between the molecular weight and the elution volume for characterized polymer samples, a computational procedure for simultaneous calibration of molecular weight separation and column dispersion is proposed. From the experimental chromatograms of narrow MWD polystyrene standards and broad MWD 1,2-polybutadiene fractions the spreading factors of a SEC column was deduced by the proposed method. The variation of the spreading factor with the elution volume is independent upon the polymer sample used.

A number of computer searching methods for estimating the molecular weight calibration curve of SEC with characterized polydisperse polymer standards had been proposed (1-9). Recently it has been shown that the calibration curve for a SEC column and the calculated effective relation or experimental relation between the molecular weight and the elution volume for a sample are quite different (10,11) and it is possible to estimate the molecular weight calibration curve and the spreading factor simultaneously by coupling SEC with LALLS (12). In this paper, a simple digital searching method is proposed for calibrating the molecular weight separation and column dispersion of a SEC column simultaneously with characterized polymer samples.

### Theory

The molecular weight calibration function  $M(V_R)$  of a SEC column may be defined as the relationship between the molecular weights of the monodisperse polymer species and their retention volume  $V_R$  under ideal working condition, i.e. in the absence of instrumental spreading effect. It is unique for a given column and the true weight and number average molecular weight of any polydis-

0097-6156/84/0245-0125\$06.00/0  
© 1984 American Chemical Society

perse polymer sample may be calculated by definition as

$$\langle M \rangle_w = \int W(V_R) M(V_R) dV_R \quad (1)$$

$$\langle M \rangle_n = 1 / \int (W(V_R) / M(V_R)) dV_R \quad (2)$$

where  $W(V_R)$  is the true chromatogram of the sample. In a real SEC column, the experimental chromatogram  $F(V)$  of a sample is broadened by the instrumental spreading effect and the molecular weights calculated by Equation 1 and 2 using  $F(V)$  instead of  $W(V_R)$  differ from the true values. We may define an effective relation between the molecular weight and elution volume  $M^*(V)$  so that the true average molecular weights also satisfy the following relations:

$$\langle M \rangle_w = \int F(V) M^*(V) dV \quad (3)$$

$$\langle M \rangle_n = 1 / \int (F(V) / M^*(V)) dV \quad (4)$$

The effective relation  $M^*(V)$  is not unique to a given SEC column but varies with samples and also differs from the calibration relation  $M(V_R)$ .

For a linear SEC column, the monodisperse calibration relation and the effective relations may be represented by

$$M(V_R) : \quad \ln M = A_m - B_m V_R \quad (5)$$

$$M^*(V) : \quad \ln M = A_m^* - B_m^* V \quad (6)$$

respectively. By using the results of the moment analysis of Tung's integral equation of instrumental spreading (13), the effective relation of a polydisperse sample may be written as (10,11)

$$M^*(V) : \quad \ln M = (A_m - (1 - \xi) B_m \bar{V}) - \xi B_m V \quad (7)$$

where  $\bar{V}$  is the mean elution volume of  $F(V)$  and  $\xi$  is a parameter defined as

$$\xi^2 = (\sigma_f^2 - \langle \sigma_0^2 \rangle) / \sigma_f^2 \quad (8)$$

in which  $\sigma_f^2$  is the variance of  $F(V)$  and  $\langle \sigma_0^2 \rangle$  is the average spreading factor of the polydisperse sample exerted on the column as expressed by

$$\langle \sigma_0^2 \rangle = \int W(V_R) \sigma_0^2(V_R) dV_R$$

The spreading factor  $\sigma_0^2$  is the variance of the chromatograms of the monodisperse polymer species, i.e. of the instrumental spreading function  $G(V, V_R)$ . If  $\sigma_0^2$  varies linearly with the retention volume of the monodisperse polymer, then  $\langle \sigma_0^2 \rangle$  is numerically equal to the interpolated value  $\sigma_0^2(\bar{V})$  of the function  $\sigma_0^2(V_R)$  for the polydisperse sample at its mean elution volume.

It can be seen from Equation 5 and 7 that the effective rela-

tion  $M^*(V)$  of a sample crosses with the unique calibration relation of the column at the mean elution volume  $\bar{V}$  of that sample. After the effective relations of several samples have been deduced, the molecular weight of each sample at its crosspoint may be calculated by Equation 6 and the line connecting all the crosspoints is just the calibration relation  $M(V_R)$  of the column. The calibration relation may be linear or otherwise nonlinear. For the latter case the coordinates of the crosspoints may be fitted by a polynomial and then Equation 5 should be regarded as the tangent line of the polynomial which varies with the mean elution volume of the sample.

Comparing the coefficients of Equation 6 with that of Equation 7, we get

$$A_m^* = A_m - (1 - \xi) B_m \bar{V} \quad (9)$$

$$B_m^* = \xi B_m \quad (10)$$

The parameter  $\xi$  of a sample could be deduced from the slope or intercept of the effective relation and the calibration relation or its tangent and thereafter the spreading factor  $\langle \sigma_{\xi}^2 \rangle$  could be determined from  $\xi$  by Equation 8.

With the procedure outlined above, simple programs of programmable calculator (TI 59) and microprocessor (Z80) for finding  $M(V_R)$  and  $\sigma_{\xi}^2(V_R)$  were written. The mean elution volume and total variance of the experimental chromatograms of well characterized polymer samples are first calculated according to

$$\bar{V} = \sum H_i V_i / \sum H_i \quad (11)$$

$$\sigma_T^2 = \sum H_i V_i^2 / \sum H_i - \bar{V}^2 \quad (12)$$

where  $H_i$  is the height of the chromatogram at elution volume  $V_i$ .

Next the coefficients of the effective relation of each sample with known weight and number average molecular weight are evaluated by iteration. Combining Equation 3, 4 and 6, the average molecular weights and inhomogeneity index may be expressed as

$$\langle M \rangle_w = \text{Exp}(A_m^*) \sum H_i \text{Exp}(-B_m^* V_i) / \sum H_i \quad (13)$$

$$\langle M \rangle_n = \text{Exp}(A_m^*) \sum H_i / \sum H_i \text{Exp}(B_m^* V_i) \quad (14)$$

$$\begin{aligned} D &= \langle M \rangle_w / \langle M \rangle_n \\ &= (\sum H_i \text{Exp}(B_m^* V_i)) (\sum H_i \text{Exp}(-B_m^* V_i)) / (\sum H_i)^2 \end{aligned} \quad (15)$$

Putting

$$f(B_m^*) = (\sum H_i \text{Exp}(B_m^* V_i)) (\sum H_i \text{Exp}(-B_m^* V_i)) - D (\sum H_i)^2 \quad (16)$$

and taking the first derivative



$$f'(B_m^*) = (\sum H_i V_i \text{Exp}(B_m^* V_i)) (\sum H_i \text{Exp}(-B_m^* V_i)) - (\sum H_i \text{Exp}(B_m^* V_i)) (\sum H_i V_i \text{Exp}(-B_m^* V_i)) \quad (17)$$

the coefficient  $B_m^*$  could be evaluated by the Newtonian iteration formula

$$B_m^*(k+1) = B_m^*(k) - f(B_m^*)/f'(B_m^*) \quad (18)$$

with the known inhomogeneity index and the experimental chromatogram of the sample using

$$\epsilon \geq B_m^*(k+1) - B_m^*(k) \quad (19)$$

as the objective function. Coefficients  $A_m^*$  are then evaluated by substituting  $B_m^*$  into Equation 13 or 14.

The third step of computation is to find  $M(V_R)$  by linear regression or polynomial fitting after the crosspoint coordinates of all of the samples have been evaluated.

The fourth step is to estimate the parameter  $\xi$  and the spreading factor by Equation 9, 10 and 8, taking  $\sigma_0^2(V)$  as an approximation of function  $\sigma_0^2(V_R)$ .

### Experimental

Six commercial narrow MWD polystyrene standards (Applied Research Laboratories Limited, England) and five broad MWD 1,2-polybutadiene fractions were used to calibrate an ARL 950 GPC instrument with silica bead packed columns. The ARL polystyrene standards were also used to calibrate a number of home-made SEC column units packed with silica beads or styrene-divinylbenzene copolymer beads. The average molecular weights of these samples are listed in Table I. Tetrahydrofuran or toluene was used as eluents for these columns.

Table I. The Average Molecular Weight and SEC Data of Polystyrene and 1,2-Polybutadiene

Polymer	$\langle M \rangle_w 10^{-5}$	$\langle M \rangle_n 10^{-5}$	$\bar{V}$	$\sigma_1^2$	
Polystyrene	A1	0.04	0.037	166.4	17.8
	A2	0.10	0.093	157.9	18.5
	A3	0.204	0.198	151.5	17.9
	A4	1.1	1.09	140.4	15.8
	A5	3.9	3.85	132.2	17.0
	A6	28.6	24.7	115.0	42.5
Polybutadiene	S1A	2.33	1.60	133.9	46.4
	S1	6.46	3.10	127.3	79.2
	S2	10.7	6.41	120.4	61.0
	S3	13.4	8.69	117.9	55.5
	S4	21.2	15.1	114.8	47.3

Results and Discussion

The mean elution volume and total variance calculated from the experimental chromatograms of polystyrene and 1,2-polybutadiene on the ARL 950 GPC instrument are also listed in Table I. The coefficients of the effective relation, coordinates of the cross-point, parameter  $\xi$  and spreading factor were computed by the scheme outlined above. The results obtained are listed in Table II and III. The effective relations and calibration

Table II. The Calculated Coefficients of the Effective Relation

Polymer		$A_m^*$	$B_m^*$	$M^*(\bar{V})10^{-5}$
Polystyrene	A1	19.19	0.0657	0.038
	A2	19.42	0.0649	0.096
	A3	16.08	0.0407	0.201
	A4	14.98	0.0241	1.10
	A5	16.51	0.0276	3.88
	A6	21.61	0.0593	26.6
Polybutadiene	S1A	24.29	0.0906	1.92
	S1	25.53	0.0984	4.49
	S2	24.76	0.0925	8.30
	S3	24.41	0.0892	10.8
	S4	24.18	0.0853	17.8

Table III. The Calculated Results of the Parameter  $\xi$  and the Spreading Factor

Polymer		$\xi$		$\sigma_0^2$	
		S	I	S	I
Polystyrene	A1	0.500	0.505	13.4	13.3
	A2	0.494	0.489	14.0	14.1
	A3	0.310	0.300	16.2	16.3
	A4	0.183	0.185	15.3	15.3
	A5	0.210	0.233	16.3	16.2
	A6	0.450	0.444	33.9	34.1
Polybutadiene	S1A	0.816	0.814	15.4	15.5
	S1	0.886	0.893	17.0	16.1
	S2	0.833	0.829	18.6	19.1
	S3	0.804	0.799	19.6	20.1
	S4	0.769	0.775	19.3	18.9

S: from slope, I: from intercept.

relation for polystyrene and 1,2-polybutadiene are shown in Figure 1 and 2 respectively. The coefficients of the calibration relation obtained by linear regression are  $A_m = 30.30$ ,  $27.05$  and  $B_m = 0.1316$ ,  $0.1110$  for polystyrene and 1,2-polybutadiene respectively. The variation of spreading factor with elution volume derived from polystyrene and 1,2-polybutadiene are coincident and in accord with that obtained by the method of coupling GPC with LALIS for the same column (12) as shown in Figure 3.

The uncertainty of the calculated spreading factor  $\Delta(\sigma_0^2)$  depends upon the accuracy of the inhomogeneity index of the sample and that of the total variance of experimental chromatogram. It may be expressed as

$$\Delta(\sigma_0^2) = (\partial\sigma_0^2 / \partial\sigma_T^2)\Delta(\sigma_T^2) - (\partial\sigma_0^2 / \partial D)\Delta D. \quad (20)$$

If the experimental chromatogram is Gaussian, the spreading factor could be represented by

$$\sigma_0^2 = \sigma_T^2 - \ln D / B_m^2 \quad (21)$$

Substituting its partial derivatives into Equation 20 we have

$$\Delta(\sigma_0^2) = \Delta(\sigma_T^2) - (1 / B_m^2) (\Delta D / D) \quad (22)$$

Thus the absolute error of the calculated spreading factor depends upon the absolute uncertainty of total variance, the slope of the calibration curve and the relative uncertainty of the inhomogeneity index  $\Delta D/D$  of the sample. Equation 22 was verified by arbitrarily changing the inhomogeneity index of polystyrene standards, recalculating the spreading factor with the same computing program and plotting the deviation  $\Delta(\sigma_0^2)$  versus  $\Delta D/D$  as shown in Figure 4. Therefore, if the standard sample was well characterized, the error of the calculated spreading factor is mainly caused by the uncertainty of the total variance. It is shown in Figure 3 that the spreading factor derived from polystyrene sample A6 is much larger than others'. It is probably caused by the larger total variance due to the greater extent of adsorption of high molecular weight polystyrene on the porous silica gel.

It is interesting to examine the effect of the molecular weight of polymer and the role of the packing material on the spreading factor. The ARL polystyrene standards were used to determine the spreading factor of a number of SEC units packed with styrene-divinylbenzene copolymer gel (SDG) or silica gel (SG) beads using tetrahydrofuran or toluene as eluent by the present method. The data cannot be compared directly because the volumes of the siphon tubes and columns of these SEC units are different. But if the relative value of spreading factor i.e. the ratio of the spreading factor of the standards to that with lowest molecular weight (A1) is considered, some interesting features could be realized as shown in Figure 5 in which the relative spreading factor is plotted as a function of molecular weight. The molecular weight dependency of the spreading factor, in other words the restricted diffusion of the macromolecule in the pore is much pronounced for styrene-divinylbenzene copolymer gel.

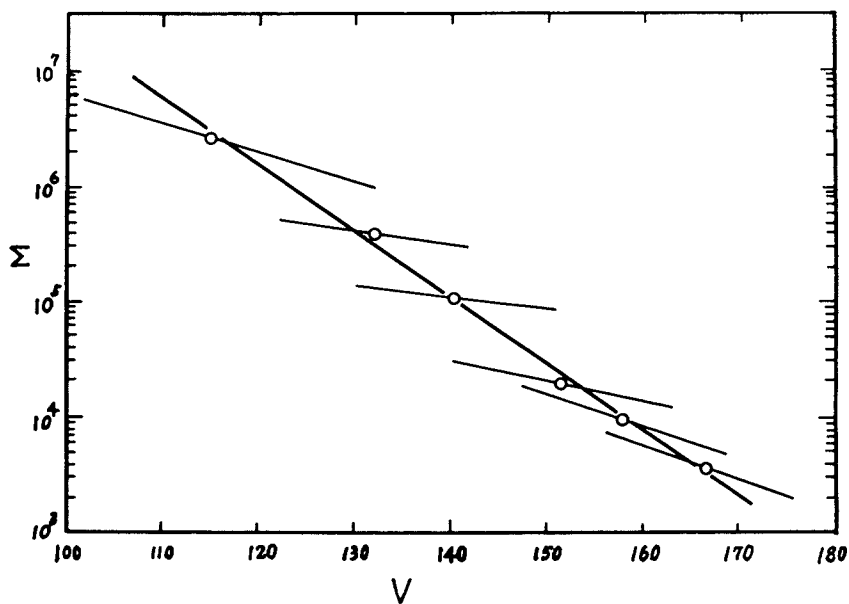


Figure 1. The calibration relation  $M(V_R)$  and effective relations  $M^*(V)$  of narrow MWD polystyrene standards.

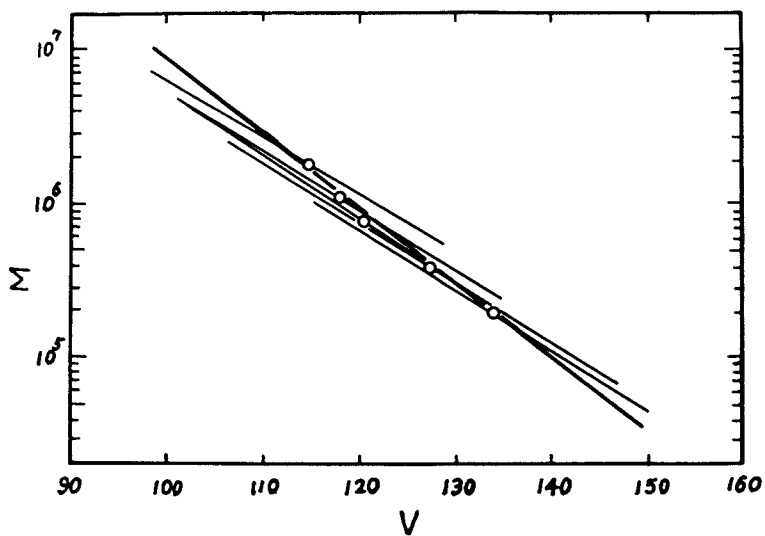


Figure 2. The calibration relation  $M(V_R)$  and effective relations  $M^*(V)$  of broad MWD 1,2-polybutadiene fractions.

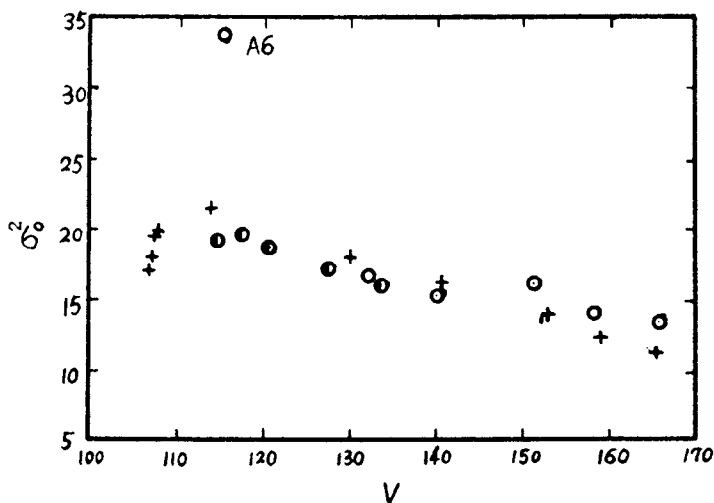


Figure 3. Variation of the spreading factor with the elution volume. Key:  $\circ$ , PS;  $\bullet$ , PB,  $+$ , GPC-LALLS, PS.

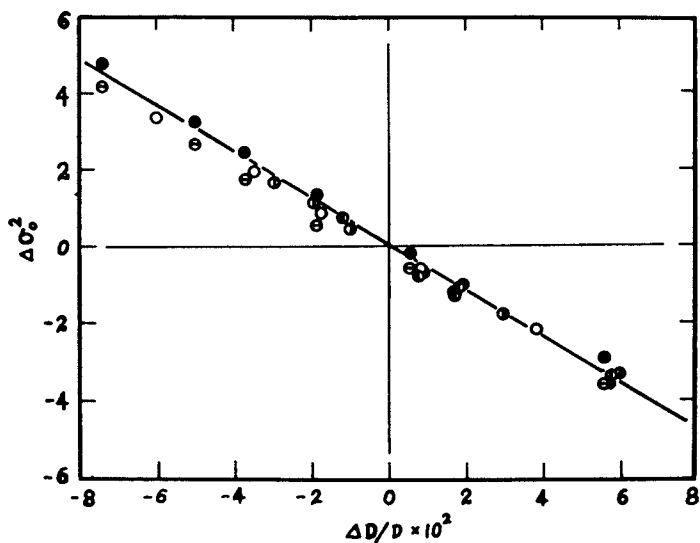


Figure 4. Dependency of the uncertainty of spreading factor on the relative error of inhomogeneity index. Key:  $\circ$ , A1;  $\bullet$ , A2;  $\circ$ , A3;  $\circ$ , A4;  $\circ$ , A5; and  $\bullet$ , A6.

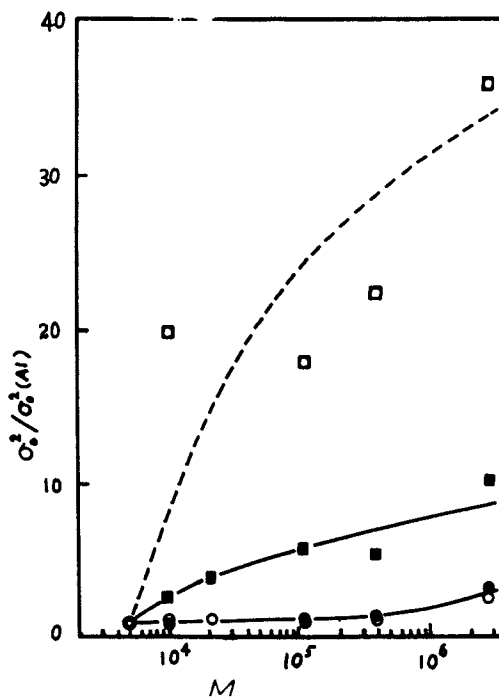


Figure 5. Variation of relative spreading factor with the molecular weight of polystyrene standards. Key:  $\circ$   $\bullet$  SG, SEC unit 1 and 2;  $\square$   $\blacksquare$  SDG, SEC unit 3 and 4.

It is believed that the surface structure of the porous packing material plays an important role. The presence of the free chain ends of styrene-divinylbenzene copolymer may prevent the movement of the macromolecules in the pore.

#### Literature Cited

1. Balke, S. T.; Hamielec, A. E.; Leclair, B. P.; Pearce, S. L. Ind. Eng. Chem., Prod. Res. Dev. 1969, 8, 54.
2. Cardenas, J. N.; O'Driscoll, K. F. J. Polym. Sci., Polym. Lett. Ed. 1975, 13, 657.
3. Loy, B. R. J. Polym. Sci., Polym. Chem. Ed. 1976, 14, 2321.
4. Szewczyk, P. Polymer, 1976, 17, 90.
5. McCrackin, F. L. J. Appl. Polym. Sci. 1977, 21, 191.
6. Yau, W. W.; Stoklosa, H. J.; Bly, D. D. J. Appl. Polym. Sci. 1977, 21, 1911.
7. Vrijbergen, R. R.; Soeteman, A. A.; Smit, L. A. M. J. Appl. Polym. Sci. 1978, 22, 1267.
8. Chaplin, R. P.; Ching, W. J. J. Macromol. Sci., Chem. 1980, A14, 257.
9. Malawer, E. G. J. Polym. Sci., Polym. Phys. Ed. 1980, 18, 2303.
10. Cheng, R. S. Proceedings of China-U. S. Bilateral Symposium on Polymer Chemistry and Physics 1979, p.43 ; Gaofenzi Tongxun 1981, 123.
11. Cheng, R. S. J. Liq. Chromatogr. , in press.
12. He, Z. D.; Zhang, X. C.; Cheng, R. S. J. Liq. Chromatogr. 1982, 5, 1209.
13. Tung, L. H. J. Appl. Polym. Sci. 1966, 10, 375.

RECEIVED September 12, 1983

## Evaluation of Fűzes Statistical Methods For Testing Identity of Size Exclusion Chromatography Molecular Weight Distributions of Polymers

SADAO MORI

Department of Industrial Chemistry, Faculty of Engineering, Mie University, Tsu,  
Mie 514, Japan

The sequential U test proposed by L. Fűzes could differentiate two polymers whose molecular weight averages are identical within the experimental errors. Parallel measurements of SEC chromatograms of the two polymers were performed in series and the distinguished points (DPs), which are defined as the elution volumes at 10, 30, 50, 70, and 90 % of the each integral chromatogram, were calculated. By the statistical treatments of the DP values, identity of molecular weight distributions (MWDs) of the two polymers was established with more than four pairs of parallel measurements, and the disagreement of MWDs with two to four pairs of runs. However, this statistical treatment could not detect small differences in shapes of the both chromatograms.

Polymer samples of same species can be confirmed in their identity by the agreement with the respective values of both the molecular weight average and the molecular weight distribution (MWD). These values are to be measured by size exclusion chromatography (SEC). In the determination of SEC, we often experience the conflicts that polymer samples having the identical molecular weight averages, within the experimental errors, show different SEC chromatograms or vice versa. It is very important to know if the observed differences between MWDs or between the molecular weight averages are due to real deviations or to experimental errors. The identity of molecular weight averages can be tested by the t-test by determining these values repeatedly and by knowing the standard deviation. However, another statistical treatment must be required in the case of MWDs in order to judge the difference to be due to the experimental variations or the real MWD.

Recently, L. Fűzes reported the method of "distinguished points (DPs)" for comparing the SEC chromatograms of two or more polymer samples (1). The sequential U and t tests were suggested in order

0097-6156/84/0245-0135\$06.00/0  
© 1984 American Chemical Society



to indicate the significant deviation or the agreement of the DP values of SEC chromatograms of two polymer samples. In this report, the validity of this statistical method was tested by using several polystyrene mixtures of known broad and narrow MWDs. Whether the difference in the two MWDs of polystyrenes having the similar molecular weight can be regarded as significant or not was tested using several pairs of test samples, one is polystyrene NBS 706 and the other the mixture of polystyrene NBS 706 and another polystyrene having different molecular weights than NBS 706.

### Calculation

Basic parameters for the comparison of two polymers, A and B, are

$$h_o = -h_1' = -\frac{2\sigma^2}{\delta} \ln \left( \frac{1 - 0.5\alpha}{\beta} \right) \quad (1)$$

and

$$h_1 = -h_o' = \frac{2\sigma^2}{\delta} \ln \left( \frac{1 - \beta}{0.5\alpha} \right) \quad (2)$$

where  $\alpha$  is the error of type I,  $\beta$  the error of type II,  $\delta$  the least difference of the elution volume in this case one wants to detect,  $\sigma$  the standard deviation of the DP values which are the elution volumes at 10, 30, 50, 70, and 90 % of the integral curves of the chromatograms in the order of increasing elution volume.

The term  $\Delta T_{ij}$  is defined as

$$\Delta T_{ij} = T_{Aij} - T_{Bij} \quad (3)$$

where  $T_{Aij}$  and  $T_{Bij}$  are the DP values of each chromatogram, the index  $i$  defines the number of parallel measurements (1, 2, -----,  $n$ ), and the index  $j$  identifies the per cent of the integral curve of each chromatogram (10, 30, 50, 70, and 90 %). After every parallel run of polymers A and B, compute  $\Delta T_{ij}$  for each  $i$  and  $j$  and summarize the  $\Delta T_{ij}$  values for  $i$  in the case of each  $j$

$$\sum_{i=1}^n \Delta T_{ij} \quad (4)$$

and plot this value at each  $n$ . The broken lines on Figure 2 are defined as  $T_1 (= h_1 + S_n)$ ,  $T_o (= h_o + S_n)$ ,  $T_1' (= h_1' - S_n)$ , and  $T_o' (= h_o' - S_n)$  in the order from the top to the bottom, where  $S = \delta/2$  and  $n$  is the number of parallel measurements.

### Experimental

SEC measurements were performed on a Jasco TRIROTAR high-performance liquid chromatograph with a Model SE-11 differential refractometer. Two Shodex A80M high-performance SEC columns (50 cm x 8 mm i.d.) packed with a mixture of polystyrene gels of nominal exclusion limits of  $10^5$ ,  $10^6$ ,  $10^7$ , and about  $10^8$  molecular weights as polystyrene were used and thermostated at 25 °C in an air oven, Model TU-100. The data were evaluated automatically by using a Sord micro-computer Model 220 to which the out-put of the detector was connected via an A/D converter.

Tetrahydrofuran was used as the mobile phase. The flow rate of the pump dial was adjusted to 1.0 mL/min and sample concentration was 0.2 % (w/v). A 0.25-mL loop was used to inject these sample solutions. Sample polymers were standard polystyrene NBS 706 ( $\bar{M}_w = 2.71 \times 10^5$ ,  $\bar{M}_n = 1.30 \times 10^5$  measured at our laboratory), commercial polystyrene ESBRITE ( $\bar{M}_w = 2.26 \times 10^5$ ,  $\bar{M}_n = 1.08 \times 10^5$ ) and two narrow MWD polystyrenes, PS 411000 and PS 200000 (molecular weights are 411,000 and 200,000, respectively).

### Results and Discussion

First, we estimated the parameters  $\alpha$  to be 0.01 and  $\beta$  to be 0.05. For the estimation of the standard deviation of the DP values, twenty chromatograms of NBS 706 polystyrene were measured and elution volumes at the distinguished per cent points of the integral curve of each chromatogram were calculated. Then, the value  $\sigma$  was obtained to be 0.042 mL. The value  $\delta$  was estimated to be 0.1 mL, which corresponds to 0.3 % of the elution volume at the center of the calibration curve of this SEC system and 5 % difference of molecular weight.

The sequential U test was performed by using several pairs of polymer samples. First example is shown in Figure 1. The sample mixture is a combination of NBS 706 (98.5 %) and PS 200000 (1.5 %). Two normalized chromatograms, NBS 706 (A) and the mixture (B), are nearly the same and molecular weight averages (the mean from three determinations) calculated are almost identical. The results of the sequential U test is shown in Figure 2. After the fourth pair of runs, all the values of  $\Sigma \Delta T_{ij}$  were found to be located in the area A = B, and it could be stated with a risk of 5 % that the two polymer samples had the same MWDs. Normalized chromatogram of a similar mixture of NBS 706 (97 %) and PS 200000 (3 %) is shown with that of NBS 706 in Figure 3 and the sequential U test is shown in Figure 4. In this example, the value of  $\Sigma \Delta T_{ij}$  at  $j = 10$  % exceeded the critical value after the fifth pair of parallel measurements. It could be stated with a risk of 5 % that the MWD of the mixture was not the same to that of NBS 706 though they had the almost identical molecular weight averages. Since the

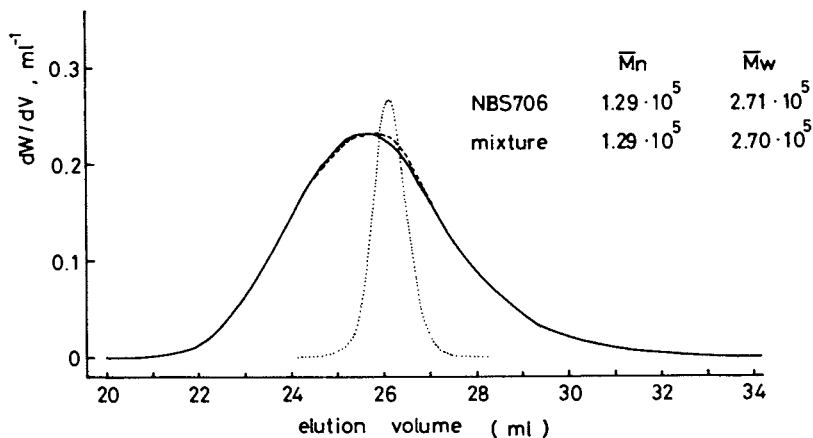


Figure 1. Normalized SEC chromatograms of NBS 706 (—), PS 200000 (.....), and the mixture of NBS 706 (98.5 %) and PS 200000 (1.5 %) (----).

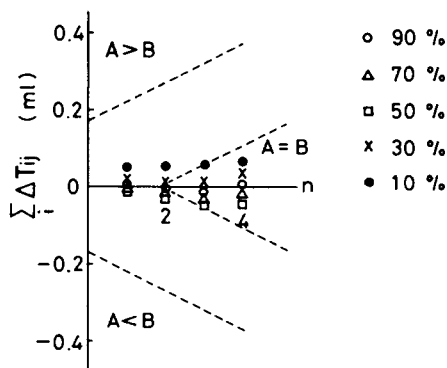


Figure 2. Sequential U test for (A) NBS 706 and (B) the mixture of NBS 706 (98.5 %) and PS 200000 (1.5 %).

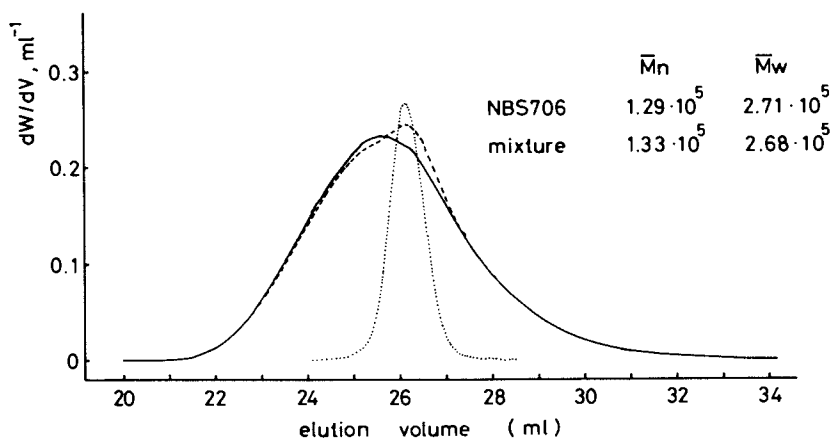


Figure 3. Normalized SEC chromatograms of NBS 706 (—), PS 200000 (·····), and the mixture of NBS 706 (97 %) and PS 200000 (3 %) (----).

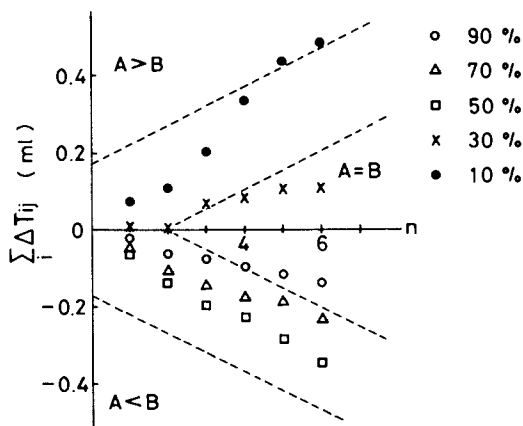


Figure 4. Sequential U test for (A) NBS 706 and (B) the mixture of NBS 706 (97 %) and PS 200000 (3 %).

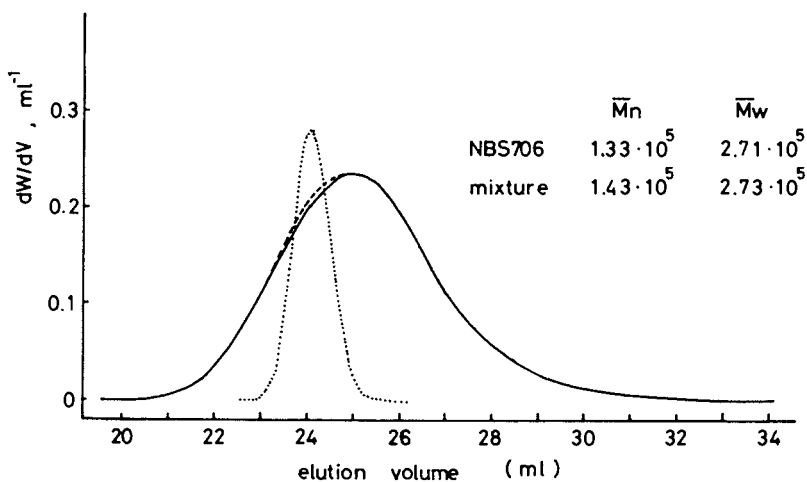


Figure 5. Normalized SEC chromatograms of NBS 706 (—), PS 411000 (·····), and the mixture of NBS 706 (98.5 %) and PS 411000 (1.5 %) (---).

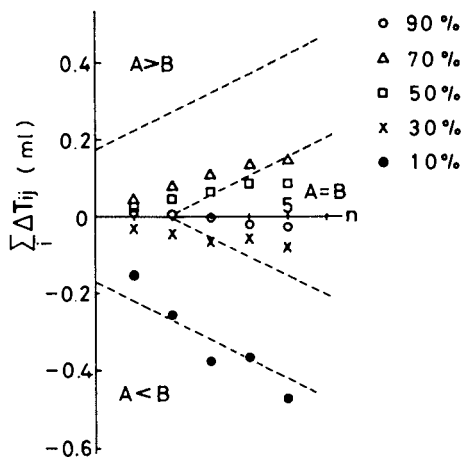


Figure 6. Sequential U test for (A) NBS 706 and (B) the mixture of NBS 706 (98.5 %) and PS 411000 (1.5 %).

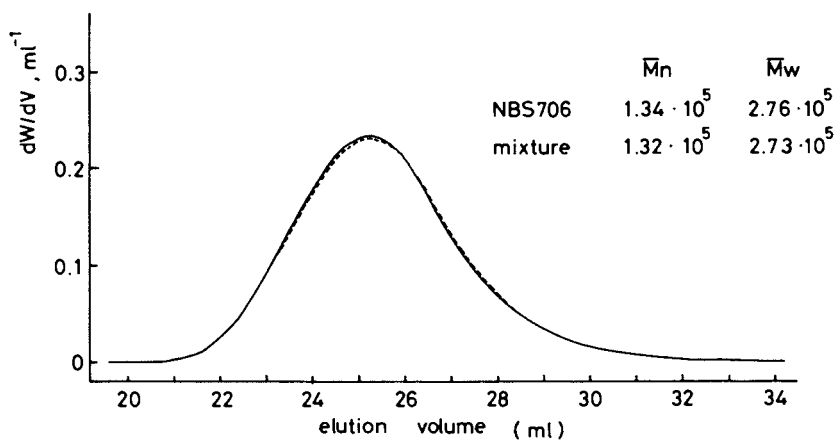


Figure 7. Normalized SEC chromatograms of NBS 706 (—) and the mixture of NBS 706 (95 %) and ESBRITE (5 %) (-----).

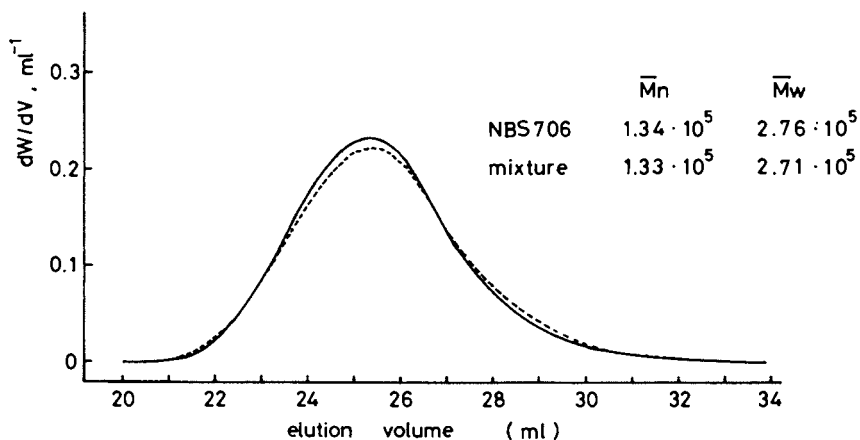


Figure 8. Normalized SEC chromatograms of NBS 706 (—) and the mixture of NBS 706 (90 %) and ESBRITE (10 %) (-----).

distinguished point at  $j = 10\%$  was located in the area  $A > B$ , it means that the MWD of the mixture was shifted to the higher molecular weights at the high molecular weight part. However, this test method could not detect the abnormality of the shape of the chromatogram at around center.

Figure 5 is the case of a mixture NBS 706 (98.5%) and PS 411000 (1.5%). The value of  $\bar{M}_w$  of the mixture is about 8% higher than that of NBS 706, but both values of  $\bar{M}_w$  are nearly the same. Both normalized chromatograms have similar shapes as in the case of Figure 1. However, the sequential U test (Figure 6) revealed after the third pair of parallel measurements that the MWD of the mixture is different from that of NBS 706.

Figures 7 and 8 show the normalized chromatograms of NBS 706 and of the mixture of NBS 706 and ESBRITE. Molecular weight averages of each pair of runs can be regarded as identical within the experimental errors. The chromatograms in Figure 7 were judged to be identical by the sequential U test of four pairs of parallel measurements. Only two pairs of runs were necessary for the decision of disagreement in the case of Figure 8.

In conclusion, the sequential U test is useful for the judgment of identity between MWDs of a pair of polymer samples whose molecular weight averages are identical within the experimental errors. Identity of MWDs of the two polymer samples was established with more than four pairs of parallel measurements, and the disagreement of MWDs with two to four pairs of parallel measurements. Though this statistical treatment is useful for the identification or differentiation of the MWDs of the pair of polymers, it can not detect small differences in shapes of the both chromatograms.

#### Literature Cited

1. Füzes, L. J. Appl. Polym. Sci. 1979, 24, 405-416.

RECEIVED September 27, 1983

## A New Family of Organic Polymer-Based High-Efficiency Gel Permeation Chromatography Columns

HERMAN S. SCHULTZ, PETER G. ALDEN, and JURIS L. EKMANIS

Waters Associates, Milford, MA 01757

The ULTRASTYRAGEL family of columns for separation by molecular size was studied using calibration curves and Probe Mixtures. The Probe Mixtures consisted of combinations of small molecules, polystyrene oligomers and high molecular weight polymer standards. Two experimental mixed pore size columns with very broad pore size distribution were also evaluated. Columns (30 cm long) were evaluated for their ability to resolve the Probe Mixtures using various combinations of one to four columns. The Probe Mixtures serve as qualitative but visually very apparent indicators of resolving power. Use of such Probe Mixtures can facilitate understanding of the interaction among amount of pores, distribution of pore sizes, number of plates, and resolving power. This in turn leads to optimum utilization of combinations of the columns. Shorter analysis times can then be attained utilizing sets of one or two columns of the proper pore size.

In 1964 Moore and Hendrickson (1,2) introduced the technique of "Gel Permeation Chromatography" (GPC) for determining molecular weight distributions of polymer samples. Moore's work introduced the use of chromatographic column packings consisting of then considered small porous spherical organic polymer particles (37-75 $\mu$ ). These particles were made from highly crosslinked copolymers of styrenes and divinyl benzenes. They became available as a family of columns under the name STYRAGEL. Subsequently, much more efficient families (3,4) of columns became available as particle sizes were reduced. The columns are generally appropriate for resolution of oligomers through very high molecular weight polymers that are soluble in organic solvents.

The mechanism of separation was by molecular volume or

0097-6156/84/0245-0145\$07.25/0  
© 1984 American Chemical Society



size. This was equated with molecular weight after calibration with very narrow molecular weight distribution standards. These standards were defined by primary molecular weight measurements such as light scattering, ultracentrifugation, osmometry, etc.. Historically, and even today, polystyrene standards are the most readily available. They are defined with least ambiguity. The subject packings exhibit little or no adsorption (non-size) effects when used to resolve compounds and polymers in appropriate mobile phases. It was noted early in the history of the subject that columns of appropriate pore size could even be used to resolve mixtures of small organic molecules (5,6,7).

Packings based on silicas for separation by molecular size are also presently available. However, the molecular size range available is more limited and possibility of encountering adsorption effects is more likely. Such columns must be thoroughly evaluated for each new type of sample for which a separation and/or molecular weight distribution is desired.

One subject of this paper is the description and illustration of the chromatographic characteristics and capabilities of a new family of styrene based GPC columns designated by the name ULTRASTYRAGEL (4,8,9,10). The possibilities created by the considerable increase in efficiency leads to the need for reassessment of how to evaluate and utilize columns of different pore size ranges. This is relative to the extended banks of columns conventionally used. Much higher speed with greater resolution than hitherto possible can now be attained in a given situation. Alternatively, extraordinary resolution is possible when time is not an issue and extended banks of these columns can be used. This new family of columns is made possible by new suspension polymerization processes for small particles (11), coupled with improved insights into the relationships of particle size distributions and the art of column packing.

Carefully constructed Probe Mixtures based on small molecules and polystyrene standards are used as standardized reference points to better define the functional capabilities of individual columns and column combinations. The result using the method of Probe Mixtures to evaluate columns is better than can be attained from calibration curves alone and is especially useful in this high resolution capability situation.

### Experimental

In most cases, calibration curves were determined at ambient or elevated temperatures using the Waters 150C High Temperature Gel Permeation Chromatograph which includes a sensitive refractive index detector. Otherwise, a modular system consisting of a Waters Model M6000A Solvent Delivery System, a Waters Model U6K Injector and a Waters Model 401 Refractometer, were used at ambient temperature. The mobile phase at room temperature was

toluene and at 140°C was 1,2,4-trichlorobenzene. Standard flow rate was 1 ml/minute. Model 401 Refractometer sensitivity was 4X or 8X. Polystyrene standards were obtained from Waters Associates, Milford, MA, and Toyo Soda Manufacturing Co., Japan. Especially great care was taken in handling standards above one million molecular weight to minimize the possibility for shear degradation. These standards were used at 0.02% concentration, prepared fresh daily, and 50-100 ul of solution was injected per column. Plates were determined using ortho dichlorobenzene and corroborated with dicyclohexyl phthalate, resulting in similar values for all columns, except with the 10<sup>6</sup>A columns where the dicyclohexyl phthalate value was used. These markers were injected as 3-5% (w/v) solutions (10 ul). Both the tangent and 5 sigma methods were used to calibrate plates (12) and both methods were used to judge the quality of a column.

Special attention was paid to minimizing band spreading due to instrumentation since this is especially deleterious to efficiency when very high plate columns are used. A measure of band spreading was determined by measuring the volume of the band width of a 10 ul injection of 3% ortho dichlorobenzene with no column in the instrument and a minimal volume connector. The length of tubing in the system was kept as short as possible and only 0.009" I.D. tubing was used between the injector and detector. Samples were injected immediately after loading into the injector to minimize diffusion of the sample in the sample loop. The volume of the band width was calculated by the equation,

$$\text{System Band Spreading (ul)} = (W_{5\sigma}) (F) (1000)/(CS)$$

where  $W_{5\sigma}$  is peak width at 4.4% peak height (cm.), F is flow rate (ml/minute), CS is chart speed (cm/minute). Typical band spreading within the instrument should be 100 ul or less. Band spreading significantly greater than 100 ul indicates an instrument problem that must be corrected.

Figure 1 defines the Probe Mixtures based on small molecules through high molecular weight polystyrene standards and the concentrations and volumes used per column. The ULTRASTYRAGEL family at ambient temperatures can be used with organic solvents such as toluene, tetrahydrofuran, methylene chloride, chloroform, etc. It has also been used at elevated temperatures with appropriate solvents such as chlorinated benzenes, cresols, and dimethyl formamide for polyolefins, polyesters and other polymers requiring elevated temperatures. All figures are based on ULTRASTYRAGEL columns.

**American Chemical  
Society Library  
1155 16th St. N. W.  
Washington, D. C. 20036**

- MIX 1** Benzene, ortho xylene, 50/50 by volume
- MIX 2** 0.5% Polystyrene Oligomer Mix "300" — 10 identified components  
MW 161-1098, peak at 370
- MIX 3** 2.0% Benzene  
0.16% Polystyrene Oligomer Mix "300"  
0.10% Polystyrene Oligomer Mix "1000"  
0.03% 2800 MW Polystyrene Standard  
0.03% 6200 MW Polystyrene Standard

<u>MIX 4 (0.03% of each)</u>		<u>MIX 5 (0.03% of each)</u>	
<u>MW</u>	<u>Ratio Successive Components</u>	<u>MW</u>	<u>Ratio Successive Components</u>
2,800	2.21X	422,000	2.99X
6,200	1.65X	1,260,000	4.35X
10,200	1.64X	5,480,000	
16,700	2.56X		
42,800	2.50X		
107,000	1.74X		
186,000	2.27X		
422,000			
		<u>MIX 6 (0.03% of each)</u>	
		1,260,000	6.68X
		8,420,000	

Injection Volume: Mix 1: 0.50  $\mu$ l / column, neat  
Mix 2: 30  $\mu$ l, 0.5% solution/column  
All Other Mixtures: 50  $\mu$ l/column

Figure 1. Definition of small molecules and polystyrene probe mixtures 1 to 6; injection volumes and concentrations.

## Results and Discussion

### Definitions of Columns Using Calibration Curves

ULTRASTYRAGEL columns (Figure 2) are available in six pore sizes ( $100\text{\AA}$  to  $10^6\text{\AA}$  designation) and are the same with respect to pore size distribution as larger particle size STYRAGEL and uSTYRAGEL columns. The total molecular weight range is from approximately 50 (small molecules) to over ten million molecular weight based on polystyrene standards. This is the approximate upper limit for valid use of such standards (13). The second column in Figure 2 tabulates a conservative estimate of the optimum molecular weight range for each column based on interpretation of calibration curves developed using small molecules and polystyrene standards. The third column in Figure 2 indicates the often broader utility range as shown by the use of standard Probe Mixtures. The fourth column in Figure 2 lists minimum column efficiencies in terms of plates. Most columns significantly exceed these minimum values.

The log molecular weight vs. elution volume calibration curves of the six individual 30 cm long columns is presented in Figure 3. The highest molecular weight polystyrene standard used was 8.4 million. For the  $10^6\text{\AA}$  column, it is apparent that the exclusion limit has not yet been reached. Figure 4 illustrates the same for banks of three columns, consisting of  $10^4\text{\AA}$ ,  $10^5\text{\AA}$  and  $10^6\text{\AA}$ , or  $100\text{\AA}$ ,  $500\text{\AA}$  and  $10^4\text{\AA}$ . Figure 5 presents calibration curves for a four column bank consisting of  $10^4\text{\AA}$  through  $10^6\text{\AA}$  and, for comparison, two sets of two columns consisting of  $10^3\text{\AA}$  plus  $10^4\text{\AA}$  and  $10^4\text{\AA}$  plus  $10^6\text{\AA}$ . The middle curve for the bank of four columns, plotted using a half scale for comparison purposes, is essentially "linear" for most of its length. This historically has been considered desirable for calibration purposes although moderately sloping curves today can be handled readily by the use of computer based methodology.

With the subject columns, the augmented resolving power, due to high plates, of a relatively smaller amount of pores in a given pore size range becomes useful for calibration purposes in non-linear portions of curves. The  $10^4\text{\AA}$  plus  $10^6\text{\AA}$  column combination in Figure 5 is a good example of this. It is relatively deficient in pore amount at the lower molecular weight end but has greater capability than the comparable  $10^3\text{\AA}$  plus  $10^5\text{\AA}$  combination at the high molecular weight end to an undetermined degree beyond the highest molecular weight standard. This is indicated by the use of Probe Mixtures to be discussed and confirmed by mercury porosimetry measurements of pore size. The  $10^3\text{\AA}$  plus  $10^4\text{\AA}$  combination in Figure 5 is close to, but not quite, linear. However, it has been used to obtain approximate molecular weight distributions.

COLUMN	OPTIMUM MW RANGE (Judged from calibration curves)	FUNCTIONAL MW RANGE (Judged from probe mixtures)	MINIMUM COLUMN EFFICIENCIES, $N_{tan}$
100 Å	50 - 1,500	50 - 1,500	10,000 ppf
500 Å	100 - 10,000	100 - 15,000	14,000 ppf
$10^3$ Å	200 - 30,000	200 - 40,000	14,000 ppf
$10^4$ Å	5,000 - 600,000	3,000 - 1,000,000	14,000 ppf
$10^5$ Å	50,000 - 4,000,000	30,000 - 8,000,000	14,000 ppf
$10^6$ Å	200,000 - $\geq$ 10,000,000	200,000 - $\geq$ 10,000,000	14,000 ppf
<b>MIXED PORE</b>			
MP-35	1,000 - 4,000,000	500 - 8,000,000	14,000 ppf

("D" Type, see text)

Figure 2. Ultrastyrigel GPC column specifications based on polystyrene standards, toluene as mobile phase (1ml/min).

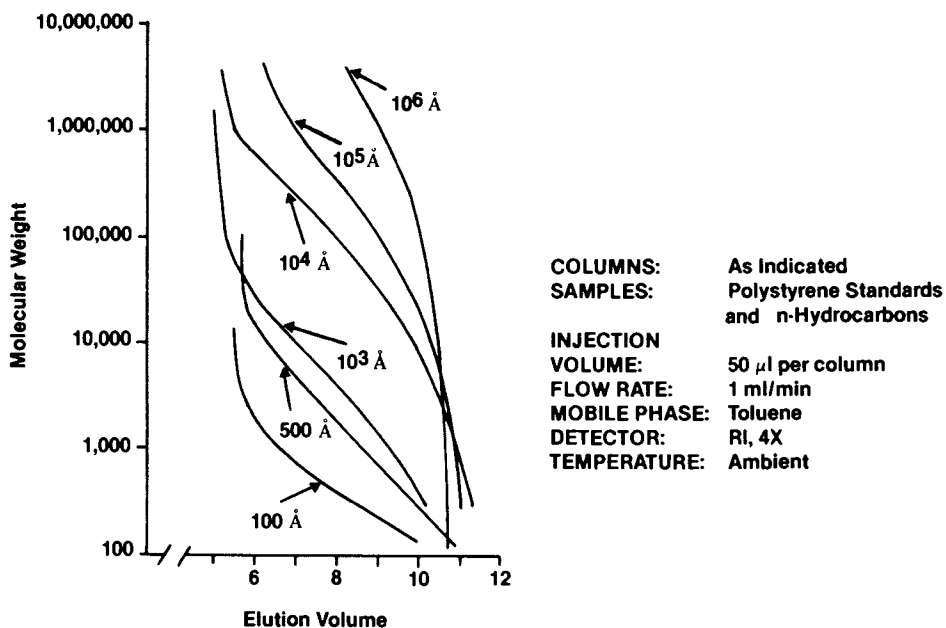


Figure 3. Individual Ultrastyrigel column calibration curves.

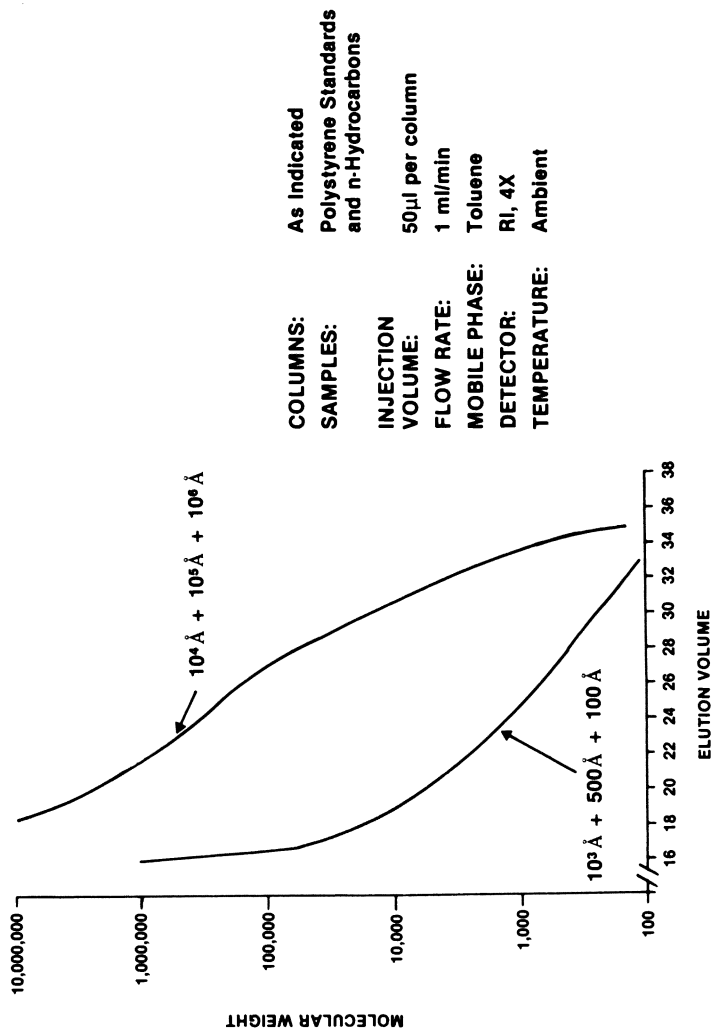


Figure 4. Calibration curves - three column sets.

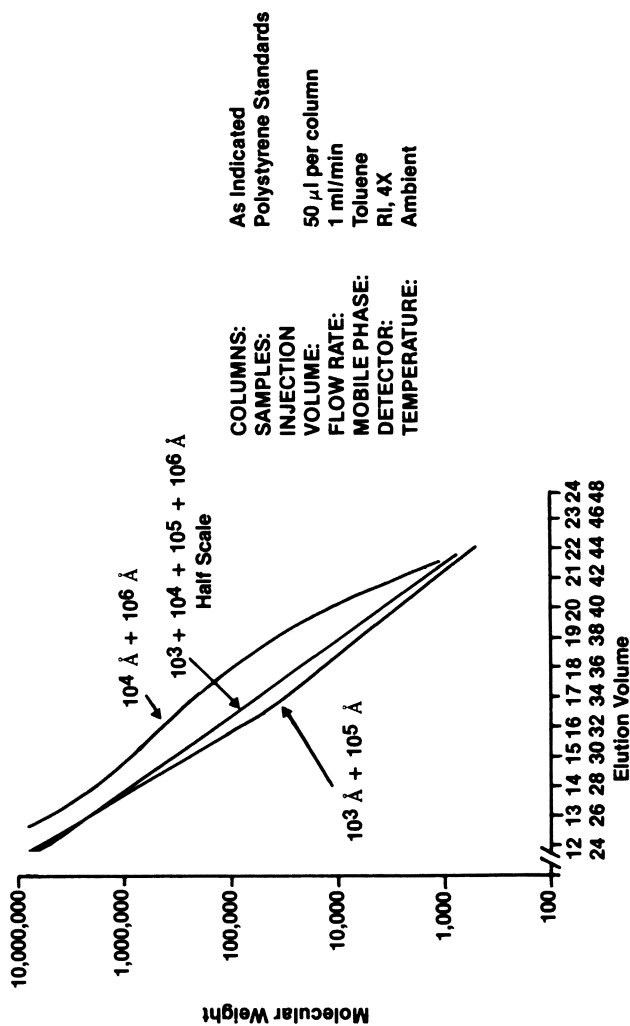


Figure 5. Calibration curves - comparison selected two column sets with four column set.

Figure 6 shows calibration curves for three other two column combinations, each representing 30,000 to 40,000 plates per set. The  $10^3 \text{Å}$  plus  $10^6 \text{Å}$  curve can be interpreted to show a deficiency in relative pore population in the range equivalent to about 50,000 to 600,000 molecular weight. The other two, properly calibrated, can conceivably be used for determination of molecular weight distributions. However, utility for resolution of specific polymodal mixtures is too difficult to assess from calibration curve alone. How much curvature of a calibration curve translates into utility or non-utility? Calibration curves indicating pore size populations all have the same shape for given column combinations whether the plate count level is 5000 plates or 20,000 plates or 80,000 plates.

Calibration curves of two column banks each consisting of two experimental mixed pore columns are presented in Figure 7. The calibration curves were determined at 140°C with trichlorobenzene as mobile phase. Each individual column in a set has exactly the same pore size distribution so that each can be used individually if the resolving capability is sufficient for a specific situation. The calibration curves for the "NW" type and the "D" type column banks should be compared respectively to the  $10^4 \text{Å}$  plus  $10^6 \text{Å}$  and  $10^3 \text{Å}$  plus  $10^5 \text{Å}$  banks in Figure 5. The comparisons indicate that it is possible to attain a very wide range of capabilities for screening and many quality control purposes with a single 30cm column. The single column is operated at 1 to 1.5 ml/minute, and between exclusion times of 4-6 minutes and total permeation time of 8-12 minutes. It should be remembered that all events take place within one volume of pores of a column or bank of columns. The "D" Type (or MP-35) mixed pore column is linear for a major portion of its length as shown in Figure 7.

The availability of calibration curves for individual columns and various combination banks of columns affords no more than a general insight, based on pore distribution, into the performance of the very high resolving power columns. The use of carefully constructed standard Probe Mixtures will now be discussed to evaluate in more detail the capability of different column combinations.

#### Use of Probe Mixtures to Define Columns and Their Performance

Probe Mixtures serve as visually very apparent indicators of resolving power. The mixtures were constructed and standardized to cover the molecular weight range from small organic molecules through high molecular weight polymodal mixtures. Figure 1 defines Probe Mixtures 1 to 6. The components of a mix were chosen so that there would not likely be baseline resolution unless there was a very favorable interplay between a high plate value and the amount of pores in a given size range, resulting



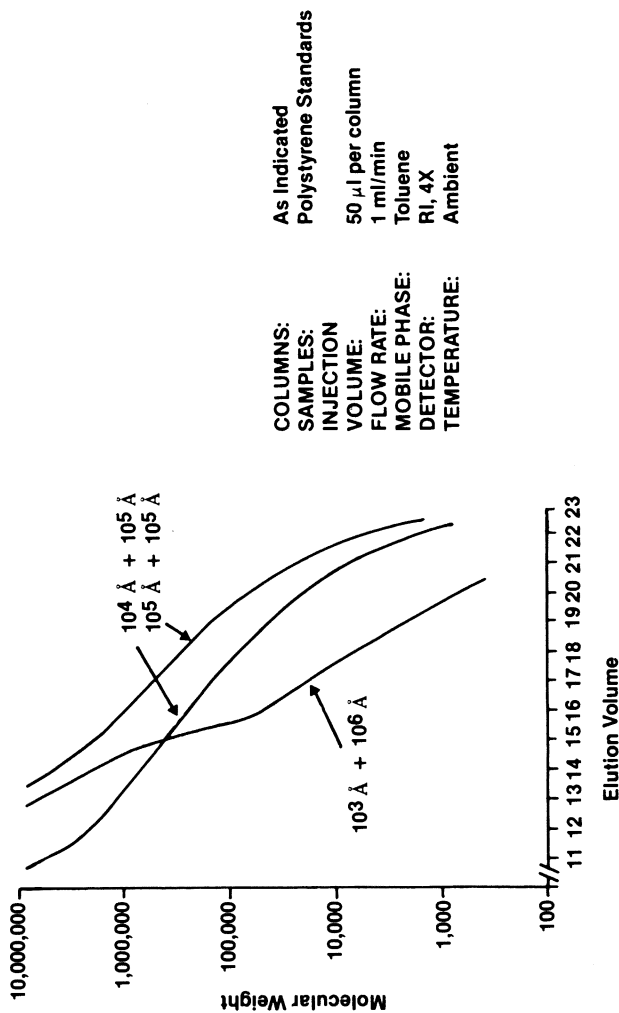


Figure 6. Calibration curves - selected two column sets.

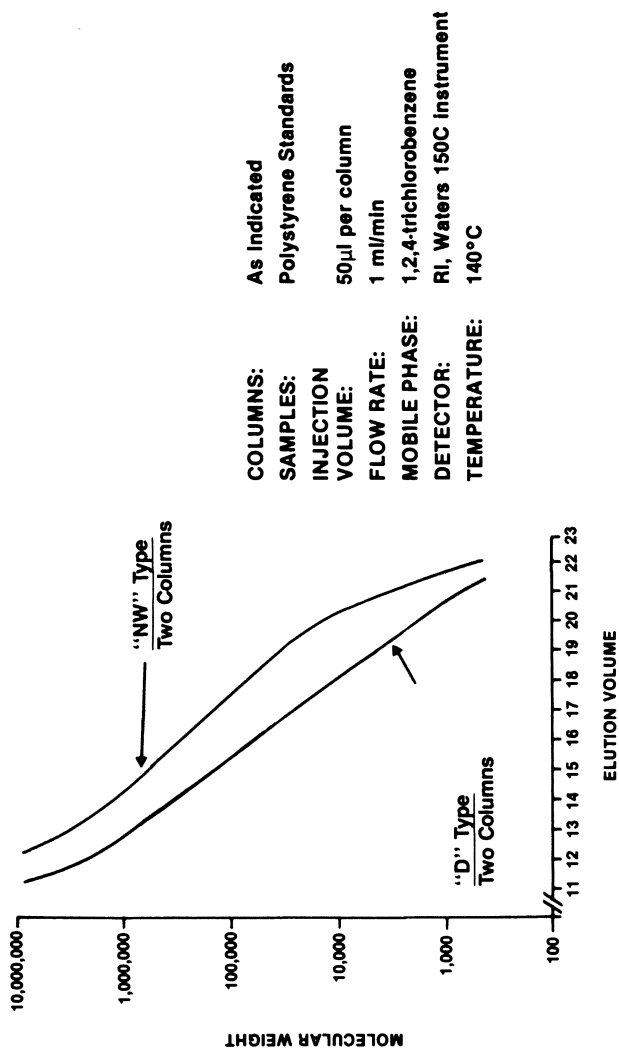


Figure 7. Calibration curves - two column sets experimental mixed pore columns.

in the needed resolving power. In Figure 1, the tabulations for Mixes 4, 5 and 6 indicate the small values chosen for the ratios of molecular weights of the adjacent standards.

The critical operational assumption that makes it possible to draw conclusions in a given comparison situation about the effect of plate and pore amount is that a constant volume and a constant absolute amount of solute was injected per column to normalize comparisons. If pore amount per column is constant, then increase in resolution with several columns of the same kind in series is due only to the increased amount of plates. Conversely, if plates of a column bank are the same, then differences in resolution are due to differences in the amount of pores of appropriate size. Also, all the other appropriate operating parameters are constant for each comparison. The following group of comparisons will illustrate different issues involving the interplay of pores, plates, and resolving power. The times on the figures are maximum values for total permeation volumes at a flow rate of 1 ml/min.

Small molecule Mix 1 (MW=78, 106) is used in Figure 8 with sets of three, two, or one  $10^3 \text{ \AA}$  columns. This figure illustrates that a large amount of plates makes up for insufficient pores to attain resolution. The resolution is functional evidence for the existence of sufficient pores of appropriate size. The previous generation of lower efficiency (i.e. 5000 plates per column)  $10^3 \text{ \AA}$  columns were never considered to have resolving power in this molecular weight range. The same probe is used in Figure 9. Two  $100 \text{ \AA}$  and two  $500 \text{ \AA}$  column banks are compared with the  $500 \text{ \AA}$  columns having twice as many plates. The  $100 \text{ \AA}$  bank having more pores in the appropriate range, resulted in approximately the same degree of resolution.

The same points are illustrated in Figure 10 using Mix 2, a polystyrene oligomer mix with components in the 161 to 1,098 range and highest population peak at 370. The bottom row across the figure is a comparison of the same amount of plates. The  $100 \text{ \AA}$  set gives the best results at the same plate level. In the top row where all sets contain three columns, the  $500 \text{ \AA}$  bank having twice as many plates, is comparable to the  $100 \text{ \AA}$  bank. It should be noted that the  $10^3 \text{ \AA}$  bank still has usefulness in this range for screening purposes due to high plates.

The remainder of this paper illustrates that families of reference chromatograms can be developed to determine if a given column combination is the best one to be used with an unknown polymer or polymer mixture, the families of chromatograms being based on the standard Probe Mixtures, one to four column combinations and different plate levels. Extended banks of lower efficiency columns would be required to attain the same degree of resolution of even one of these ULTRASTYRAGEL columns.

Figure 11 indicates the performance of three and one column banks of  $10^3 \text{ \AA}$ ,  $10^4 \text{ \AA}$  or  $10^5 \text{ \AA}$  columns using polymodal Probe Mix

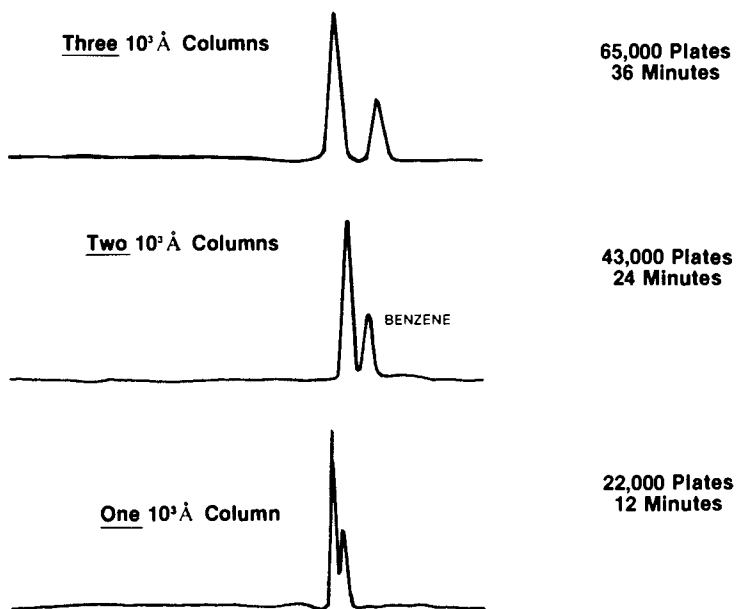


Figure 8. Comparison 3, 2, 1  $10^3 \text{ \AA}$  column sets illustration larger amount of plates makes up for insufficient pore amount; Probe Mix 1, benzene and ortho xylene.



Figure 9. Comparison  $100 \text{ \AA}$  and  $500 \text{ \AA}$  two column sets; plates versus pore amount; Probe Mix 1.

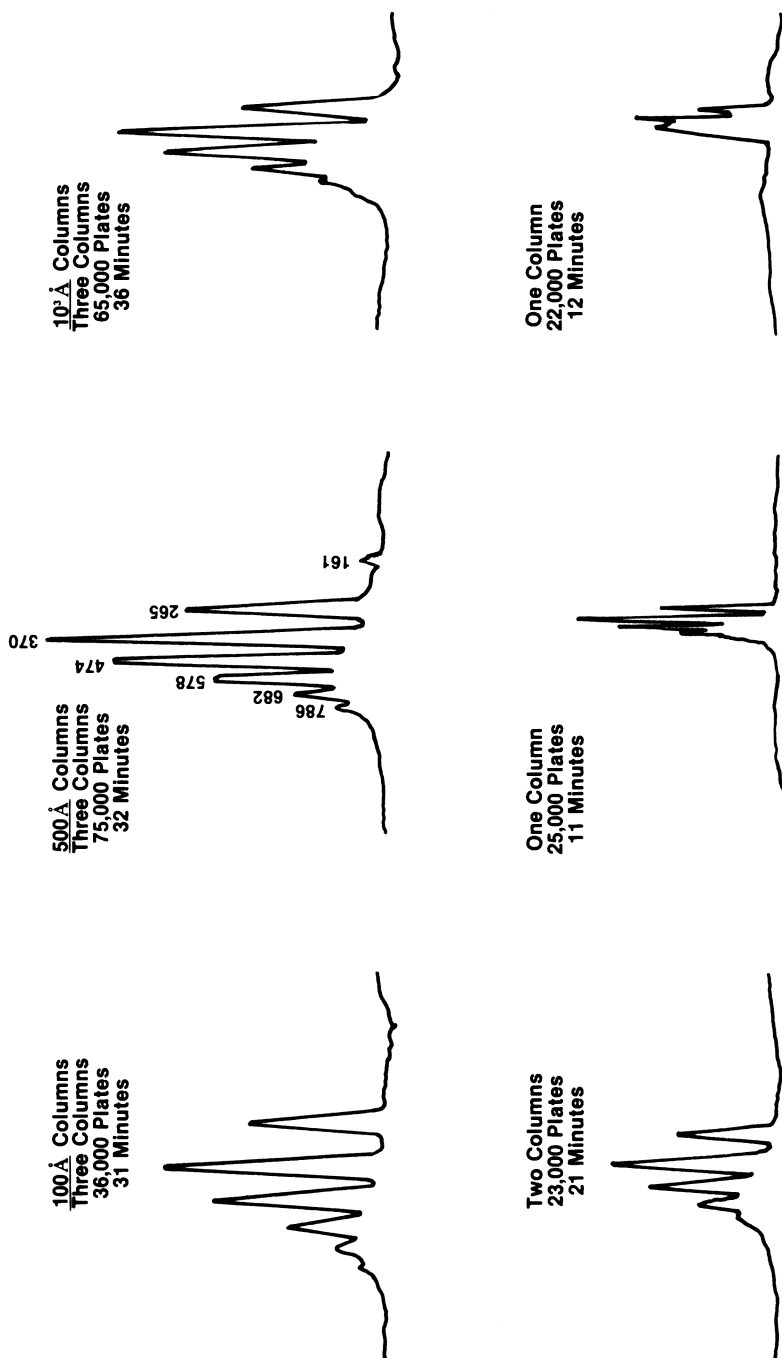


Figure 10. Comparison 3, 2, 1 column sets illustrating effect interplay of plates and pores; Probe Mix 2, polystyrene oligomer mix.

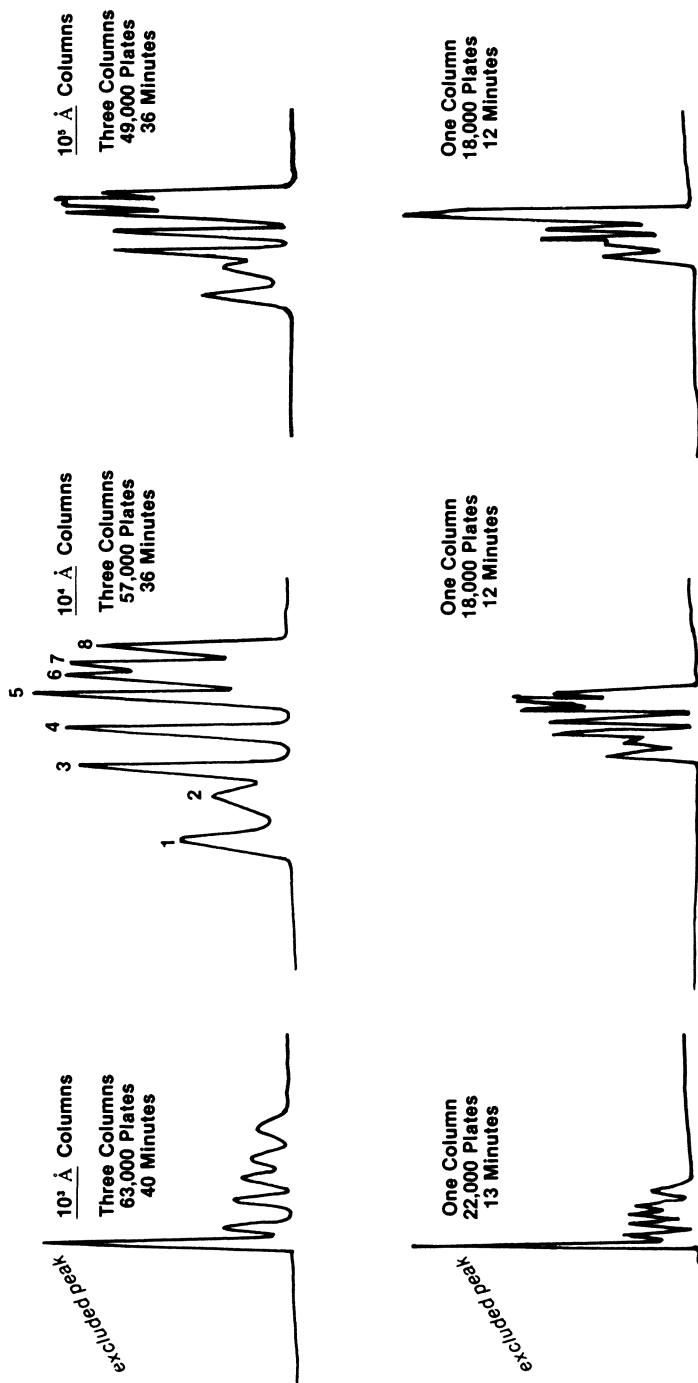


Figure 11. Comparison 3 and 1 column sets of same pore size, illustrating effect interplay of plates and pores; Probe Mix 4. MW 1 to 8 is 422,000, 186,000, 107,000, 42,000, 16,700, 10,300, 6,200, and 2,800.

4 consisting of eight polystyrene standards. The diagnostic patterns for optimum use range of each column type can be seen as a function of pore size and distribution at comparable plate levels. The  $10^3 \text{ \AA}$  columns resolve well in the 2,800-42,000 standard range. The  $10^4 \text{ \AA}$  columns are optimum in 16,700 through 422,000 standard range. The  $10^5 \text{ \AA}$  columns function to a slightly less degree in the optimum range for the  $10^4 \text{ \AA}$  columns but poorly in the  $10^3 \text{ \AA}$  range. However, any activity at all in the  $10^3 \text{ \AA}$  range would be unexpected with previously available lower plate level  $10^5 \text{ \AA}$  columns. The optimum combination for Mix 4 would consist of  $10^3 \text{ \AA}$  and  $10^4 \text{ \AA}$  columns rather than the standard mixed banks used conventionally.

A similar comparison is shown in Figure 12 using Mix 5 in the 422,000 to 5.48 million range. It can be interpreted in a similar manner to draw conclusions about effectiveness versus pore size and increased resolution due to increased plates, everything else being equal. The 16 minute marker for expected exclusion volume of the three column  $10^6 \text{ \AA}$  chromatogram indicates considerable amount of pore size volume that is available for components greater than 5.48 million standard. The  $10^4 \text{ \AA}$  and  $10^5 \text{ \AA}$  columns have better performance than previously expected.

Four banks of columns are used in Figure 13 to determine the optimum three column combination for Mix 5. Each bank has the same level of total plates (approximately 50,000). The best result is with the  $10^6 \text{ \AA}$  bank.

Patterns of capabilities are developed in Figures 14 through 18 using several Probe Mixtures for two column combinations and the full  $10^3 \text{ \AA}$ ,  $10^4 \text{ \AA}$ ,  $10^5 \text{ \AA}$  and  $10^6 \text{ \AA}$  bank calibrated in Figures 5 and 6. Comparisons reveal the power of the two column combinations and better define the preliminary ranges of use obtained from the calibration curves. The capabilities of a number of two column combinations are illustrated in Figure 14 relative to a four column conventional bank in the molecular weight range of Probe Mixture 4. For example, the  $10^4 \text{ \AA}$  plus  $10^5 \text{ \AA}$  set shows considerable  $10^3 \text{ \AA}$  activity and the  $10^4 \text{ \AA}$  plus  $10^6 \text{ \AA}$  set shows less. It can therefore be concluded that the  $10^5 \text{ \AA}$  column in the first set is contributing  $10^3 \text{ \AA}$  activity. In choosing between a  $500 \text{ \AA}$  plus  $10^5 \text{ \AA}$  set and a  $10^3 \text{ \AA}$  plus  $10^5 \text{ \AA}$  set for use in the range of the Probe Mixture, the second set has more activity (and effective pores) in the approximately 100,000 to 190,000 molecular weight range. Therefore, it would be the column set of choice.

Figures 15 through 18 should be examined as a group. Patterns of performance and comparisons are developed for Probe Mixtures 3, 4, 5 and 6 using two column sets  $10^3 \text{ \AA}$  plus  $10^4 \text{ \AA}$ ,  $10^4 \text{ \AA}$  plus  $10^6 \text{ \AA}$ , Experimental "D" Type Mixed Pore and Experimental "NW" Type Mixed Pore. They all have activity down to a surprisingly low molecular weight range. Each figure shows a comparison using a single Probe Mixture. The Probe Mixtures

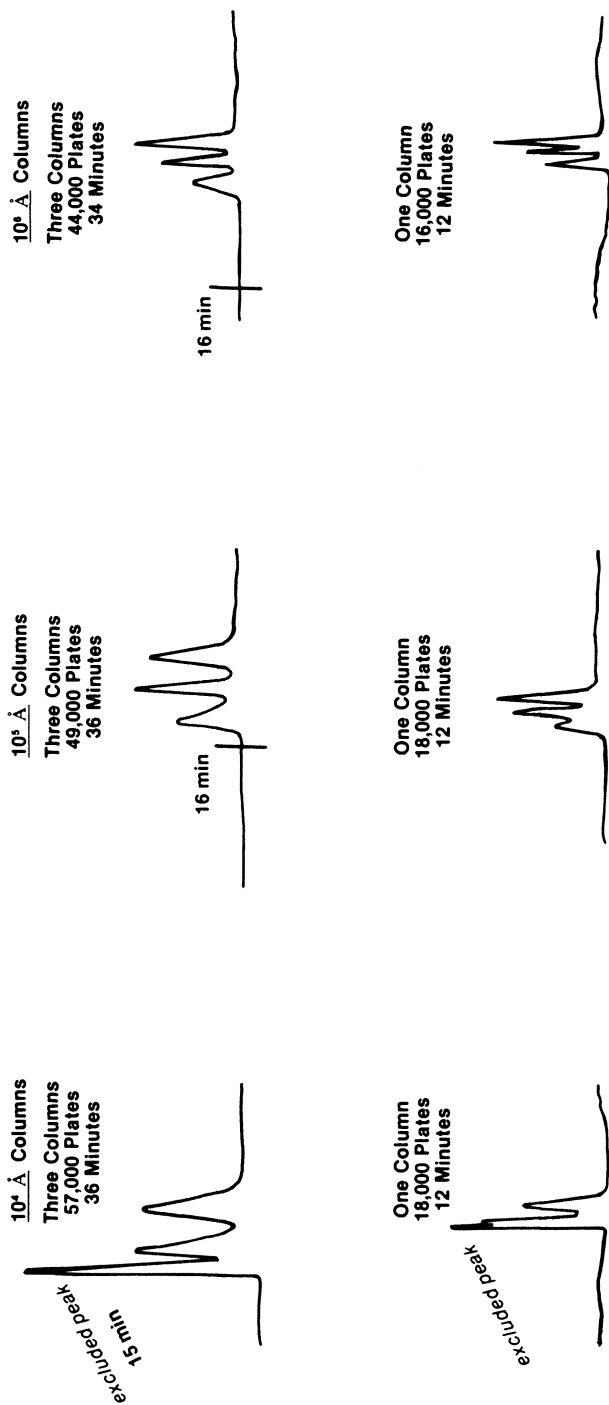


Figure 12. Comparison 3 and 1 column sets of same pore size, illustrating effect interplay of plates and pores; Probe Mix 5. MW is 5,480,000, 1,260,000, and 422,000.



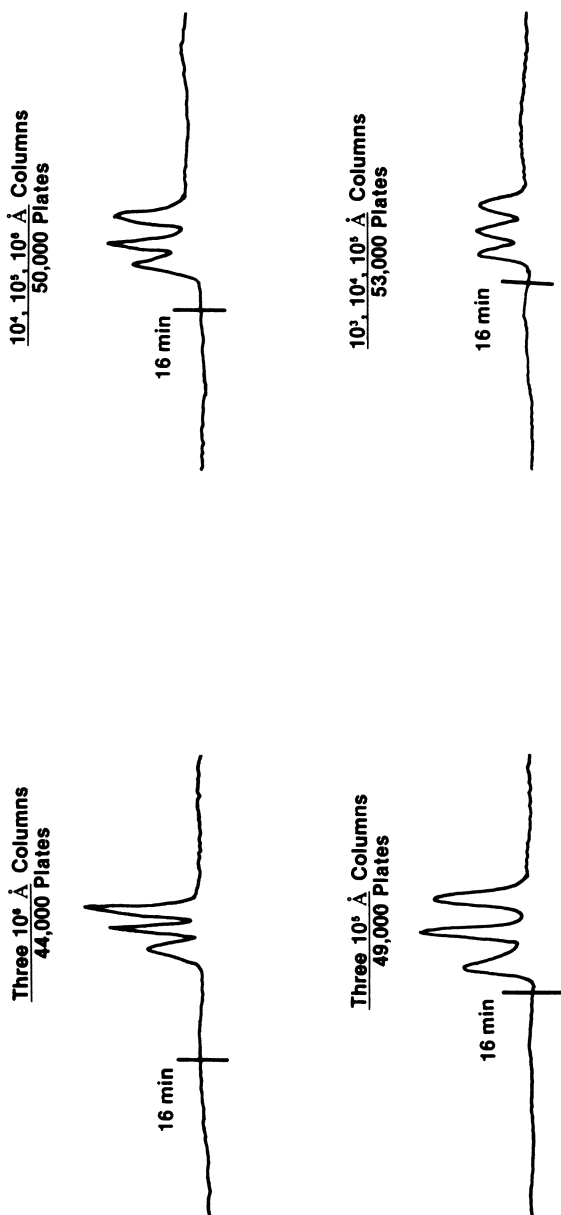


Figure 13. A comparison of 3 column sets of same and mixed pore sizes illustrating interplay of plates and pores; Probe Mix 5.

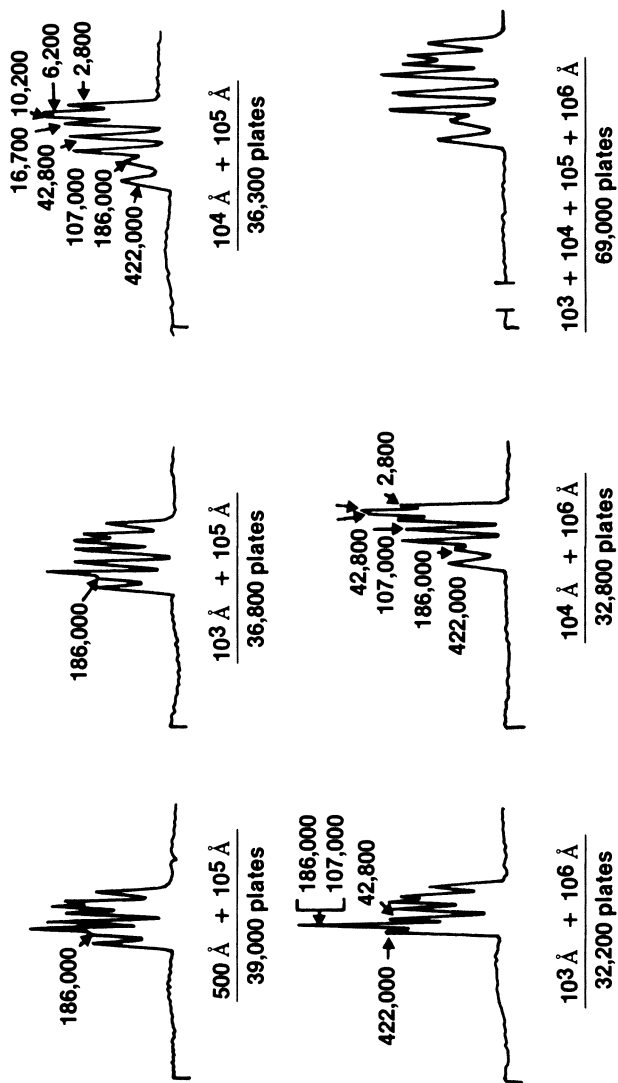


Figure 14. A comparison of capabilities of six two column sets using Probe Mix 4.

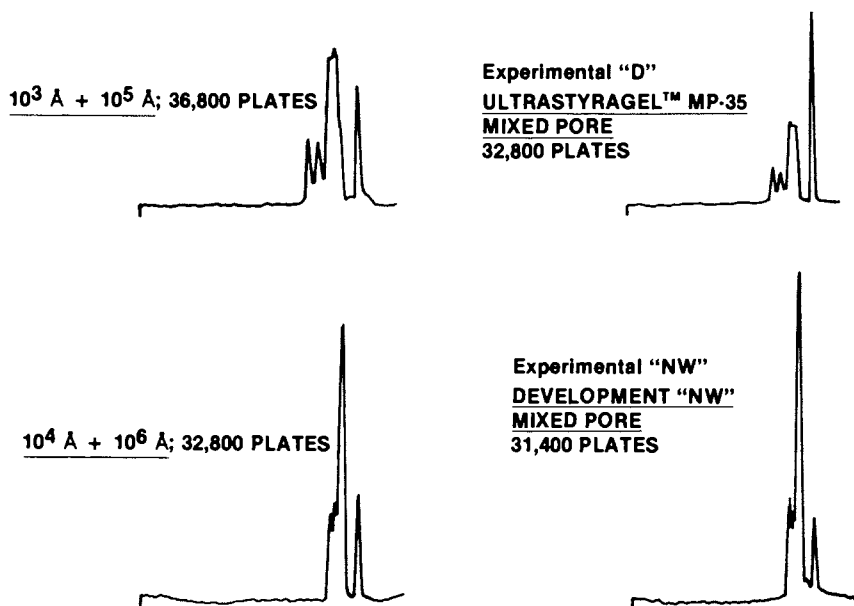


Figure 15. Patterns of capabilities; two selected individual or mixed pore column sets; Probe Mix 3.

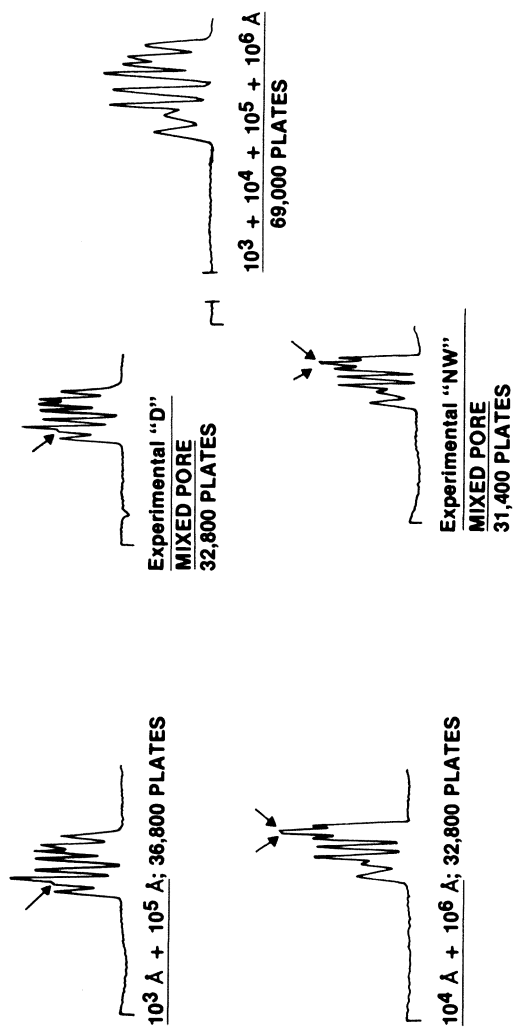


Figure 16. Patterns of capabilities; two selected individual or mixed pore column sets plus reference four column set; Probe Mix 4.

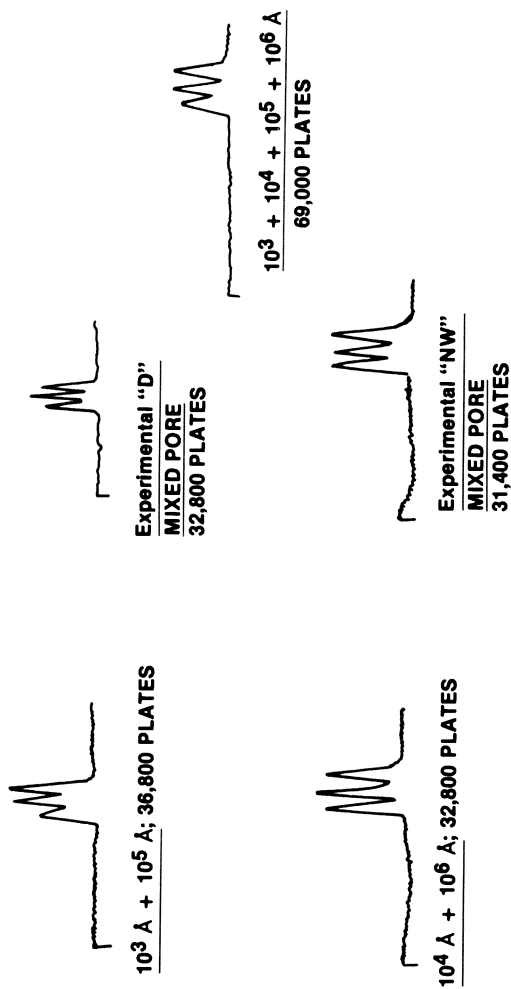


Figure 17. Patterns of capabilities; two selected individual or mixed pore column sets plus reference four column set; Probe Mix 5.

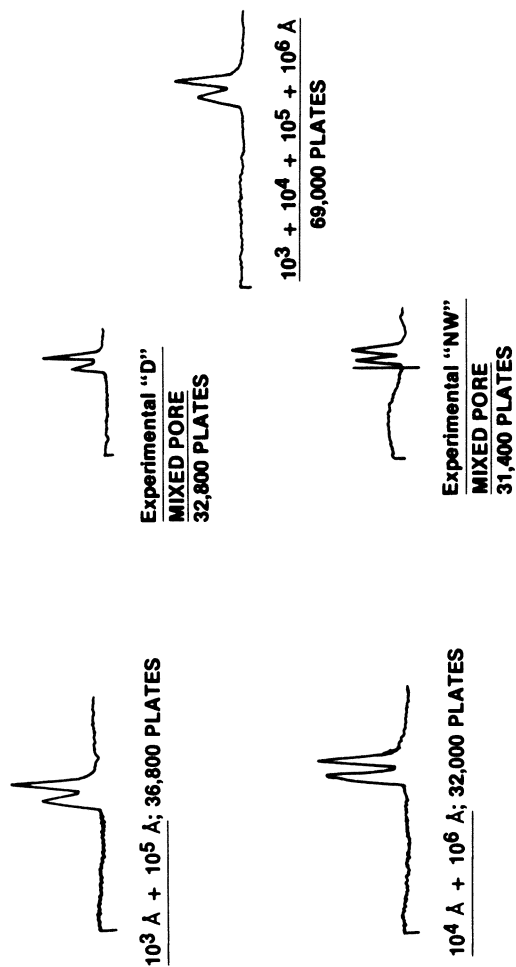


Figure 18. Patterns of capabilities; two selected individual or mixed pore column sets plus reference four column set; Probe Mix 6.

have overlapping molecular weight ranges. Together they constitute a chromatographic fingerprint for the performance of each set. Overall, the Experimental "D" Type and the  $10^3 \text{ \AA}$  plus  $10^5 \text{ \AA}$  sets have a broader molecular weight utility range than the Experimental "NW" Type and  $10^4 \text{ \AA}$  plus  $10^6 \text{ \AA}$  sets. However, the latter have somewhat more capability at the higher molecular weight pore size end. The  $10^3 \text{ \AA}$  plus  $10^5 \text{ \AA}$  set is difficult to distinguish from the Experimental "D" Type set on the basis of Probe Mixtures alone. A benefit of the Mixed Pore columns is that they combine the range of activity into one 30 centimeter very high plate count column and can be used to attain maximum speed in situations where the amount of resolution is sufficient. Another benefit of the "D" Type column is that it is "linear" over a major portion of the molecular weight range, simplifying its use for molecular weight distribution calculation purposes.

### Conclusions

It is important to understand the interplay of pore amount and pore size distribution versus plates on column resolving power. This is necessary to fully utilize the performance capabilities of the new ULTRASTYRAGEL family of columns to obtain the optimum high resolution and speed appropriate for a specific use situation. Calibration curves are useful to put one into the right separation range but the use of carefully constructed standard Probe Mixtures define more specifically the performance molecular weight range of the subject columns. Stated in other terms, if one has a large amount of plates, the less pores in a given range are required for resolution, everything else being equal. "Sufficient pore amount" is defined functionally by the ability to resolve in a specific situation. "Sufficiency" level of pore amount is less with increasing plates. Very high efficiency columns offer the capability to resolve many mixtures of small organic molecules and polymodal polymer products without the methods development needed when separations are attempted by other mechanisms.

### Literature Cited

1. Moore, J.C., J. Polym. Sci., A2 835 (1964)
2. Moore, J.C., Hendrickson, J.G., J. Polym. Sci., Part C. No. 8, 233 (1965)
3. Limpert, R.J., Cotter, R.L., Dark, W.A., Amer. Lab. 6 #5, 63 (1974)
4. Schultz, H.S., Ekmanis, J.L., Tisdale, V.R., Baptiste, A.J., Crossman, L.W., paper presented at Pittsburgh Conference on Analytical Chemistry and Applied Spectroscopy, Atlantic City, N.J., March 8-13, 1982. Abstract No. 392.

5. Smith, W.B., Kollmansberger, A., J. Phys. Chem. 69 4157 (1965)
6. Hendrickson, J.G., Moore, J.C., J. Polym. Sci., A4 167 (1966)
7. Cazes, J., Gaskill, D.R., Separation Sci., 2 421 (1967)
8. Schultz, H.S., Alden, P.G., Ekmanis, J.L., paper presented at Pittsburgh Conference on Analytical Chemistry and Applied Spectroscopy, Atlantic City, N.J., March 8-13, 1982. Abstract No. 393.
9. Schultz, H.S., Alden, P.G., paper presented at Pittsburgh Conference on Analytical Chemistry and Applied Spectroscopy, Atlantic City, N.J., March 7-12, 1983. Abstract No. 955.
10. Schultz, H.S., Alden, P.G., Ekmanis, J.L., paper presented at 185th ACS National Meeting, Seattle, WA, March 20-25, 1983. Abstract No. ORPL200; Organic Coatings and Applied Science Proceedings, 48 945 (1983)
11. Schultz, H.S., unpublished work.
12. Yau, W.W., Kirkland, J.J., Bly, D.D., "Modern Size Exclusion Chromatography" Wiley-Interscience, New York, 1979.
13. Slagowski, E.L., Fetters, L.J., McIntyre, D., Macromolecules 7 394 (1974)

RECEIVED October 13, 1983



## Optimization of Resolution in Gel Permeation Chromatographic Separation of Small Molecules

F. VINCENT WARREN, JR., BRIAN A. BIDLINGMEYER, HAROLD RICHARDSON,  
and JURIS L. EKMANIS

Waters Associates, Milford, MA 01757

Gel permeation chromatography (GPC) has mainly been used for the determination of molecular weight distributions of polymers. The potential for using GPC for the separation of discrete small molecules has long been recognized (1-7) but practical considerations have limited this application. Until recently, the efficiency of commercially available GPC columns has been relatively low, requiring the use of sets of three or four columns to separate small molecules which have a similar effective size in solution. The expense and long analysis times associated with such a bank of columns has limited the appeal of "small molecule GPC" (SMGPC).

In 1982, the ULTRASTYRAGEL family of GPC columns was introduced (8,9). These high-efficiency columns provide a two- to three-fold increase in efficiency (plates/foot) over the closely related STYRAGEL columns which have been available since 1974. Small molecule separations which once required several STYRAGEL columns can now be performed on a single ULTRASTYRAGEL column. This advance makes SMGPC considerably more attractive as a simple and effective technique for the analysis of a variety of samples (10-12). Examples presented below will illustrate the capability of single ULTRASTYRAGEL columns in applications which are not as easily solved by other modes of HPLC (e.g. reversed phase.)

Factors Which Influence Resolution. In order to effectively apply SMGPC to separation problems, the influence of three factors on the resolution of sample components must be considered. Solvent effects play a minor role, but choice of eluent can alter selectivity in some cases. Column efficiency, as noted, has a major impact on the quality of separation. The number of peaks which can be resolved within the pore volume of a given column (i.e. peak capacity) is related to the square root of the number of theoretical plates (13). Finally, the nature of the calibration curve will influence resolution. Each

0097-6156/84/0245-0171\$06.00/0  
© 1984 American Chemical Society

of these factors is further examined, with appropriate examples, in the discussion below.

Initially, it might seem that only one of the above three factors, the choice of eluent, could be readily adjusted by the user of commercial GPC columns. This is not the case since families of columns with varying efficiencies and pore size distributions are commercially available (14). An understanding of the other two factors will aid in selecting the most appropriate column(s) for a particular analysis and will facilitate the correct interpretation of the resulting separation. With a given eluent, improved resolution may be approached through either of two pathways: increased efficiency or a more favorable slope of the calibration curve.

The concept of "specific resolution" ( $R_{sp}$ ) developed by Yau and coworkers (15) reflects the dual influence of efficiency and slope on resolution:

$$R_{sp} = 0.576/(D_2\sigma) \quad (1)$$

$D_2$  is the slope of the linear portion of the calibration curve and  $\sigma$  is the standard deviation of the elution profile, as reflected in the peak width. According to the equation 1, resolution is maximized when the product of slope and peak width (an efficiency contribution) is minimized. The interplay between these two factors must, therefore, be considered in the evaluation of available GPC columns (9,16,17).

Determination of Pore Size Distributions. The shape and range of a GPC calibration curve are, in part, a reflection of the pore size distribution (PSD) of the column packing material. A consideration of the nature of PSDs for the ULTRASTYRAGEL columns to be used in this work is therefore appropriate. The classical techniques for the measurement of PSDs are mercury porosimetry and capillary condensation. The equipment required to perform these measurements is expensive to own and maintain and the experiments are tedious. In addition, it is not clear that these methods can be effectively applied to swellable gels such as the styrene-divinylbenzene copolymer used in ULTRASTYRAGEL columns. Both of the classical techniques are applied to dry solids, but a significant portion of the pore structure of the gel is collapsed in this state. For this reason, it would be desirable to find a way to determine the PSD from measurements taken on gels in the swollen state in which they are normally used, e.g. a conventional packed GPC column.

Such a technique does, in fact, exist. In a series of papers starting in 1975, Halasz described a method for the determination of PSDs by GPC (18-25). Similar techniques have since been discussed by others (26-29). In this method

polystyrene standards serve as probes of pore size. Each standard is associated with a characteristic random coil diameter in solution, and it is assumed that for each standard there will be a minimum pore diameter ( $\emptyset$ ) which allows unhindered access to that standard. An empirical equation serves to relate  $\emptyset$  to the weight-average molecular weight (MW) of a polystyrene standard:

$$\emptyset [A] = 0.62(MW)^{0.59} \quad (2)$$

The elution volume for each standard is expressed according to Equation 2:

$$R = [(V_E - V_{EX}) / (V_{IN} - V_{EX})] 100\% \quad (3)$$

where  $V_E$  is the elution volume and  $V_{EX}$  and  $V_{IN}$  are the column exclusion and inclusion volumes. For a given polystyrene standard associated with an elution volume  $V_E$  and a pore diameter  $\emptyset$ ,  $R$  is interpreted as the percentage of the total pore volume which is formed by pores having a diameter greater than  $\emptyset$ . Inspection of Equation 3 reveals that  $R/100\% = K_{GPC}$ , the distribution coefficient for GPC (13).

It is worth noting at this point that relatively little effort has been directed toward establishing a detailed relationship between PSDs determined by GPC (equations 2-3) and those obtained by classical methods. In the remainder of this discussion, all occurrences of the term "PSD" refer to the PSD as determined by GPC. We consider this method to yield an "effective PSD" for reasons discussed later. A discussion of the correlation between results of the GPC technique and classical methods is beyond the scope of this text.

In a previous report (30), we found that n-hydrocarbon standards are useful to extend the range of (small) pore sizes which may be probed. Polystyrene-equivalent molecular weights ( $MW_p$ ) are assigned to each hydrocarbon using the empirical relationship (31):

$$MW_p = 2.3 MW \quad (4)$$

which was derived from the analysis of GPC calibration curves.

GPC calibration data ( $V_E$ ,  $\log MW$ ) are transformed according to equations 2 and 3 and the resulting ( $\log \emptyset$ ,  $R$ ) values are plotted. Halasz has demonstrated (19) that this plot represents the cumulative PSD. The point-by-point derivative of the cumulative PSD is the "differential" PSD, which gives a rough outline of the PSD for the column packing material. A better way of obtaining the PSD is by fitting data from the cumulative PSD to a Gaussian distribution by a plot on probability paper.

Prediction of Calibration Curves. If the PSDs of individual columns can be accurately represented by Gaussian distributions, then it should be possible to predict the PSD and cumulative PSD

for any combination of the individual columns. The overall PSD for a set of columns is obtained by summing the Gaussian PSDs for the individuals. Before summing, the area under each individual Gaussian is made proportional to the pore volume ( $V_{IN}-V_{EX}$ ) of the related column. After summing, the overall PSD is integrated to obtain the cumulative PSD for the column set.

The cumulative PSD will accurately predict the calibration curve for the column set if a simple model for retention applies (13):

$$V_E = V_{EX} + \int_{\bar{r}}^{\infty} P(r) dr \quad (5)$$

where  $V_E$  and  $V_{EX}$  are defined as before and  $\bar{r}$  is the pore radius which is just large enough to permit unhindered access to the solute under consideration. The integral is over the pore volume consisting of all pores having a radius greater than or equal to  $\bar{r}$ . This model states that retention in GPC is simply governed by the fraction of the pore volume which is accessible to the given solute. If Equation 5 is correct, then the cumulative PSD contains sufficient information for prediction of the calibration curve, as indicated in Equation 6:

$$V_E = V_{EX} + \frac{V_p}{100} \int_{\bar{p}}^{\infty} R(p) dp \quad (6)$$

Here  $V_p$  is the column pore volume ( $V_{IN} - V_{EX}$ ) and  $R(p)$  is the cumulative PSD, where  $p = \log \bar{\theta}$  and  $\bar{p}$  is defined analogously to  $\bar{r}$  above. In actual practice, the required integration may be performed graphically or approximated by computer using a simple integration algorithm.

Previous efforts (32-34) to apply the simple model of equations 5 and 6 have not yielded accurate predictions of calibration curves. The important difference between those efforts and the present work is in the source of the PSD information. Classical methods (porisimetry, capillary condensation) have been used before, rather than the GPC method described above. When classical methods are used a more complex model is required for prediction (13):

$$V_E = V_{EX} + \int_{\bar{r}}^{\infty} K_{GPC}(\bar{r}, r) P(r) dr \quad (7)$$

This convolution equation takes into account the fact that  $K_{GPC}$ , the distribution coefficient, is a function of both the effective solute radius ( $\bar{r}$ ) and the pore radius ( $r$ ). Even if all the pores of a gel have the same diameter, solutes of

different size can be separated on the basis of their different degrees of penetration into the pores. Thus a PSD measured by classical methods will behave as a broader PSD in practice, giving a calibration curve which could not be predicted on the basis of the classical PSD alone.

For PSDs measured by GPC, we expect a greater degree of success with the simple model for retention (eq. 5). Halasz noted that the PSDs he measured were always broader than corresponding PSDs from porisimetry and capillary condensation. This is in keeping with the convolution model (eq. 7) and indicates that the PSDs measured by GPC already contain the convolution between  $K_{GPC}$  and the classical PSD. If this is the case, then the "effective PSDs" provided by the GPC method should be useful for the direct prediction of calibration curves.

### Experimental Section

Chromatographic System. The isocratic liquid chromatograph used was a Waters Associates (Milford, MA) Model 244 ALC which included a Model 6000A Solvent Delivery System, a Model 401 Differential Refractometer and a Model 440 Absorbance Detector operating at 254 nm and was fitted with a WISP automatic injector. The analog outputs of the UV absorbance detector or differential refractometer were recorded with a Model 730 Data Module (printer, plotter, integrator)(Waters). Eluent flow rate was 1.0 ml/min unless otherwise noted.

ULTRASTYRAGEL columns of 100A, 500A, and 10<sup>3</sup>A designation were obtained from Waters. The 100A column was always last in series when a column set was used. Polystyrene standards were obtained from Waters (MW=1.35K, 4K, 17.5K, 50K, 110K, 250K, 390K, and 2700K) and Toyo Soda, USA (Atlanta, GA) (2.8K). Orthodichlorobenzene, styrene monomer, and normal hydrocarbons were also used for calibration. These materials, as well as the various test solutes, were purchased from a variety of suppliers. HPLC grade THF (UV-stabilized), toluene and chloroform were obtained from Waters and degassed before use.

Sample Preparation. Calibration standards and test solutes were injected as dilute solutions in the eluent. Polystyrene standards were 0.03% (w/v). Styrene, ODCB and normal hydrocarbons were 0.15% (w/v), except for dodecane and tridecane (0.65%). Samples involving more complex matrices were prepared by crushing (if necessary), dissolving a weighed amount in the eluent, and filtering through a 0.45 Millex-SR filter cartridge (Millipore, Bedford, MA).

Data Analysis. For the determination of PSDs, the calibration data was converted to R vs log  $\phi$  by a BASIC computer program

"PORESIZE", executed on an Apple II Plus microcomputer. Plotting of the differential and cumulative PSDs was done via APPLE PLOT (Apple, Cupertino, CA). Other programs were written in BASIC to calculate Gaussian envelopes given a mean and standard deviation ("GAUSS"), to sum two or more Gaussians in any desired proportions ("COADD"), to integrate the summed distribution ("BOXES") and to transform coordinates from  $[\log \emptyset, R]$  to  $[V_E, \log (MW)]$ .

## Results and Discussion

Solvent Effects. The eluent in GPC is deliberately chosen to be a strong solvent for the solute so that retention by mechanisms other than size exclusion (e.g. adsorption) will not occur to an appreciable extent. Therefore, the choice of solvent is not expected to greatly influence the chromatographic results. Solvent effects of two kinds do occur in practice. The first is detector related. In the separation of normal hydrocarbons by GPC with THF as eluent, some peaks are positive and some are negative when detection is by differential refractometry. (See, for example, Figures 1-2 of reference 6). Since the lighter hydrocarbons have a refractive index less than that of THF, peaks for less than C10 are negative. The higher hydrocarbons show a positive response which complicates quantitation of the peaks, especially near the crossover from negative to positive. This sort of solvent effect can generally be avoided by the selection of another eluent. In the case of n-hydrocarbons, the use of toluene affords a chromatogram in which all the peaks are negative.

The second type of solvent-related effect which commonly occurs is observed when a mixture of 1-octanol and 1,8-octanediol is analyzed in two different eluents. In chloroform, the two alcohols are not resolved due to their similar molecular size. In THF, however, resolution nearly to baseline can be achieved due to differentiation of the alcohols on the basis of hydrogen bonding interactions with THF. Octanediol, having two sites for interaction, forms a species with a significantly larger effective size in solution than does octanol which has only one site for interaction. The separation is therefore enhanced.

Due to the popularity of THF as an eluent for GPC, this sort of "differential solvation" must be kept in mind, particularly when polar solutes are analyzed. This effect can also work against resolution in SMGPC, as demonstrated in Figure 1. Here BHA and BHT are fully resolved in  $\text{CHCl}_3$  but coelute in THF. Both BHA and BHT have phenolic sites, but the site on BHT is sterically hindered and apparently does not form a hydrogen bond with THF. The hydrogen bonded BHA/THF complex which does form

is apparently similar in size to BHT with the result that the two solutes coelute in THF. In chloroform, BHA and BHT are resolved due to significant differences in the molecular sizes of these solutes.

Column Efficiency. The peak capacity (13) for a GPC column used in the analysis of small molecules is related to the number of theoretical plates (N) according to:

$$n = 1 + \frac{\sqrt{N}}{4} \Delta \ln V_E \quad (8)$$

where  $\Delta \ln V_E$  specifies the elution range of interest. Since the ULTRASTYRAGEL family of columns offers almost a three-fold increase in N compared to the STYRAGEL family, a 50-70% increase is expected in the number of resolvable peaks per chromatogram. This extra resolving power makes it possible to perform a variety of SMGPC separations on single ULTRASTYRAGEL columns. Examples from application areas including foods, pesticides, pharmaceuticals, and polymer additives have recently been reported (10-12). Two advantages of SMGPC over other separation techniques (e.g. reversed-phase HPLC) are frequently observed: simple preparation of complex samples, and good chromatographic resolution of analyte peaks from interfering species.

Two representative examples of single-column SMGPC separations are presented in Figures 2 and 3. The sample for Figure 2 was a rodent bait from which the active ingredient warfarin was to be determined. Quantitation of this component by SMGPC was shown to be as reliable as for the reversed-phase method which is commonly used (35), with the advantage of a several-fold faster sample clean-up (12).

In Figure 3, the active steroid (triamcinolone acetonide) and preservative (benzyl alcohol) are determined from a steroid cream. The higher molecular weight components of the cream base are well separated from the analytes. The ability to elute all the components of a cream or ointment in a SMGPC analysis gives an important sample preparation advantage over competing separation techniques.

Calibration Curve. The calibration curves for GPC columns can provide some guidance in the selection of a column which would give the best resolution for a given analysis. Figure 4 presents calibration curves for typical 100A, 500A, and 10<sup>3</sup>A ULTRASTYRAGEL columns, based on the elution behavior of polystyrene standards and n-hydrocarbons. The slope of the linear portion of each curve is related to the resolving power of the column in that a shallower slope will yield a larger  $\Delta V_E$  for the same  $\Delta MW$ . There is a tradeoff between the slope of a calibration curve and the range of molecular weights

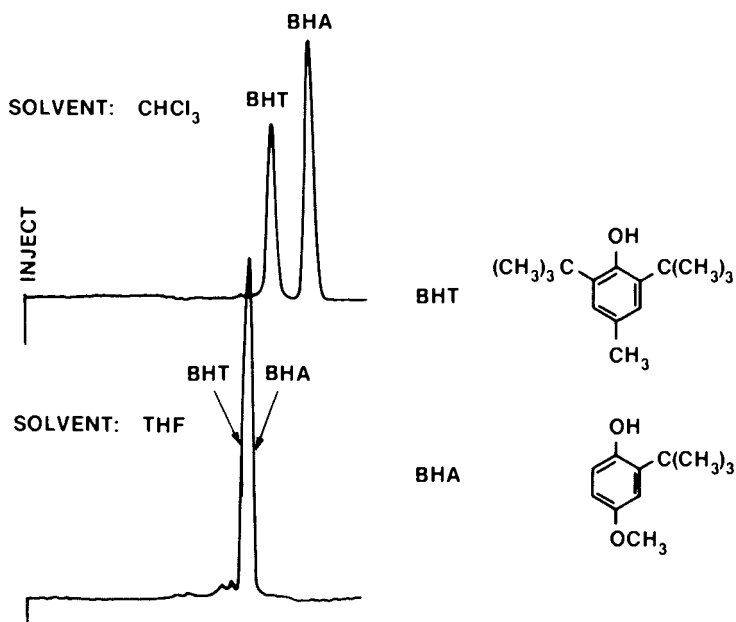


Figure 1. Separation of BHA and BHT on a 100A Ultrastyrigel column using chloroform and tetrahydrofuran. Conditions: 1 mL/min; and 254 nm.

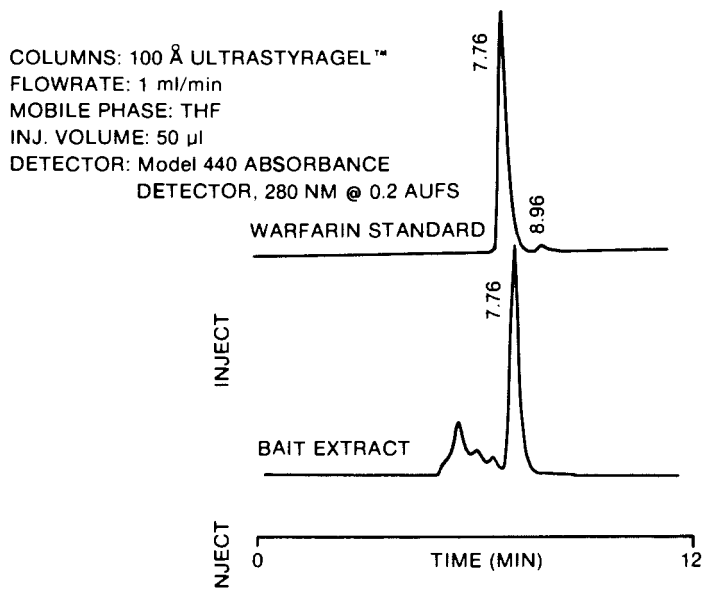


Figure 2. Determination of warfarin from grain bait by SMGPC.



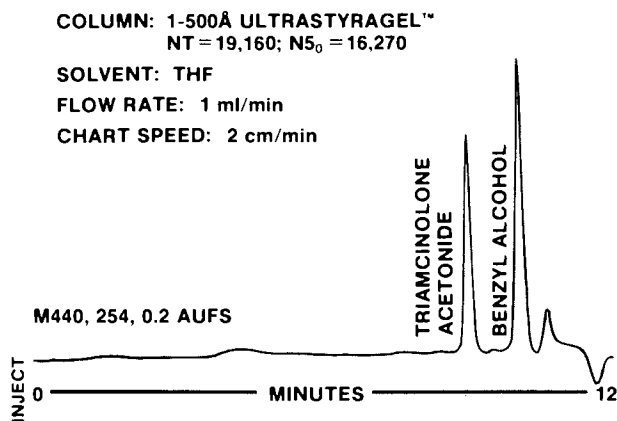


Figure 3. Determination of triamcinolone acetonide and benzyl alcohol from a steroid cream.

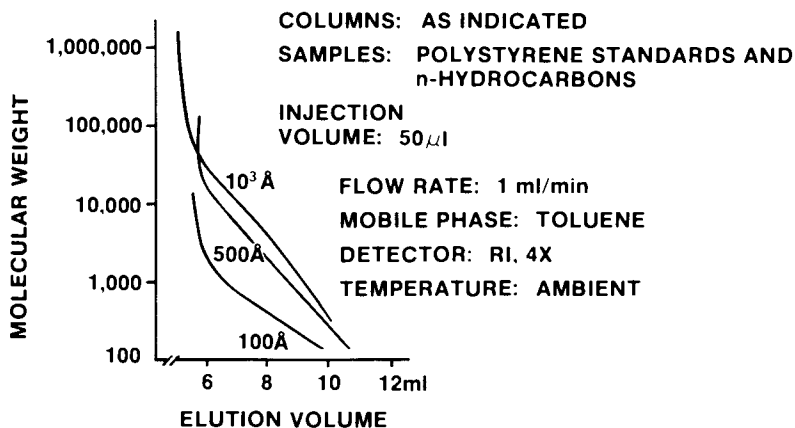


Figure 4. Typical calibration curves for 100Å, 500Å, and 10<sup>3</sup>Å Ultrastyrigel columns.

resolvable by the column. This is apparent in Figure 4, where the column with the shallowest slope (100A) also covers the narrowest molecular weight range (MW=50 to 1500). For molecules which elute within this relatively narrow range, the 100A column is preferred on the basis of slope. A more extensive range of molecular weights is served by the 500A (MW = 100 - 10,000) and 10<sup>3</sup>A (MW = 200 to 30,000) columns. The interplay between column efficiency and the slope of the calibration curve (eq. 1) should not be overlooked. A shallow slope gives a better resolution of peak centers, but for an inefficient column the peaks will be broad and significant overlap (poor resolution) may still occur.

Since the GPC separation is based on effective size in solution of the solutes, and not on molecular weight, conclusions drawn from Figure 4 will apply strictly only to polystyrene standards and n-hydrocarbons. Other compounds may exhibit a different relationship between molecular weight and size. This problem has received attention from several groups (37-41). However, in the absence of a method for assigning a polystyrene-equivalent molecular weight to each solute, the inspection of Figure 4 provides a starting point in the selection of the column which is appropriate for an analysis.

Prediction of Calibration Curves. To address a wider range of molecular weights than is possible with any one column, several columns may be joined in series. If calibration data is available for each individual column, it would be convenient to predict or calculate the calibration curve for the column set. Some rough predictions could be made on the basis of Figure 4. A more accurate answer could be obtained if the individual columns in the set have been calibrated with the same standards. In this case, simply summing the elution volumes of a given standard for each column can give a useful empirical prediction of the elution behavior of the same standard on the column set. Our experience with several examples indicates that this approach can provide accurate results.

A very different scheme for the prediction of calibration curves is presented schematically in Figure 5. This approach invokes a simple theoretical model for the GPC elution process (eq. 5,6). The example to be discussed in this case is a column set composed of two 500A and one 10<sup>3</sup>A ULTRASTYRAGEL columns. Calibration data for the individual columns is first transformed according to Equations 2 and 3. The resulting cumulative PSDs are fit to Gaussian distributions as shown in Figure 6 for the 500A column. The area under each Gaussian PSD is made proportional to the experimentally determined pore volume of the column. The Gaussian profiles are then added point-by-point to give the overall PSD of the column set. This curve is

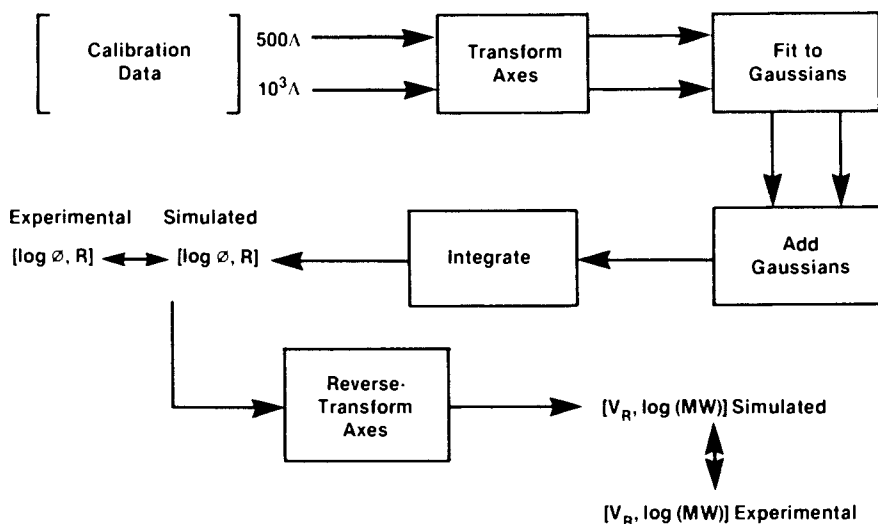


Figure 5. Scheme for prediction (simulation) of the calibration curve for a column set consisting of two 500Å and one 10<sup>3</sup>Å Ultrastyrigel columns (see text for details).

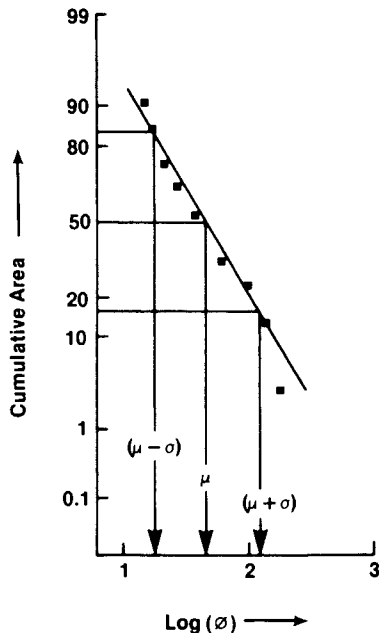


Figure 6. Plot on probability paper of cumulative PSD data for a 500Å Ultrastyrigel column. The mean ( $\mu = 1.70$ ) and standard deviation ( $\sigma = 0.42$ ) of the Gaussian PSD were determined graphically.

integrated to yield the predicted cumulative PSD. At this point, a comparison with the experimental calibration curve for the column set can be made, provided that the column set data is also transformed according to Equations 2 and 3.

In Figure 7, the predicted cumulative PSD is compared with the actual curve for the column set. It should be noted that the prediction is based on data from one 500A and one 10<sup>3</sup>A ULTRASTYRAGEL column which had been calibrated in toluene. (Previous work (19,42) has demonstrated that equivalent PSDs are obtained with several eluents including chloroform, methylene chloride, THF, and toluene.) Neither of these columns was included in the actual column set, which was independently calibrated in THF using a different instrument. Reasonably close agreement between prediction and experiment is observed in Figure 7. The predicted curve is shifted slightly to the right throughout the range, and would follow the experimental points very accurately if the shift were eliminated. The cause of the shift has not been determined, but instrumental differences (e.g. calibration of flow rate) could provide the explanation.

Alternatively, the predicted cumulative PSD can be converted to a conventional calibration curve for comparison with experimental results. This requires reversing the transformation of equations 2 and 3. To calculate values of  $V_E$  based on values of  $R$ , predicted values of  $V_{EX}$  and  $V_{IN}$  are needed. The most reasonable approach is to predict each of these as the sum of the values for the individual columns. The conversion of the cumulative PSD into a predicted conventional calibration curve may introduce additional inaccuracy through the prediction of column set values for  $V_{EX}$  and  $V_{IN}$ . As Figure 8 demonstrates, this problem is not severe, and a good prediction results.

As another example of this approach, the calibration curve for a column set containing one 100A and one 10<sup>3</sup>A ULTRASTYRAGEL column was predicted with the results shown in Figure 9 (cumulative PSD) and Figure 10 (calibration curve). For this example, the columns used for prediction were also used in the column set, with all measurements made on the same instrument. Here the good agreement between the predicted and experimental cumulative PSD (Figure 9) is lost to some extent upon conversion to the conventional calibration curve (Figure 10). The predicted exclusion volume is in error by nearly a milliliter, for reasons which are not yet clear. This error can be removed if the experimentally determined column set value for  $V_{EX}$  is used in generating the predicted calibration curve. As expected, the result of this substitution is an improved fit to the experimental data for the high molecular weight region of the curve.

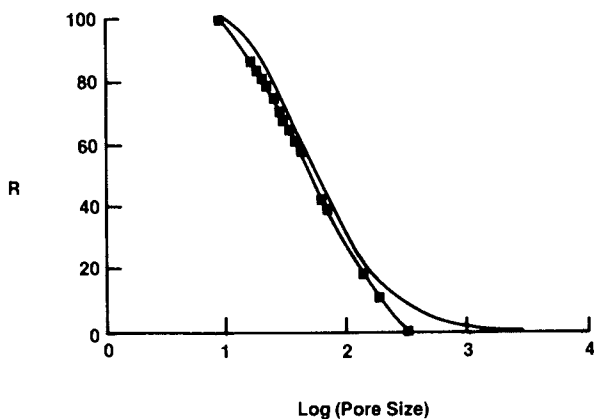


Figure 7. Predicted (smooth curve) and experimental (boxes) cumulative PSDs for a column set consisting of two 500A and one  $10^3$ A Ultrastyrigel columns.

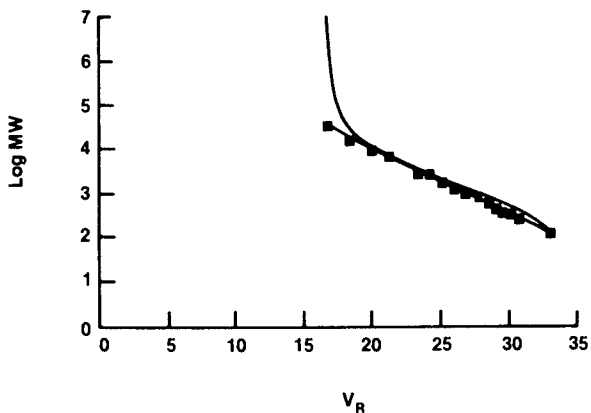


Figure 8. Predicted (smooth curve) and experimental (boxes) calibration curves for a column set consisting of two 500A and one  $10^3$ A Ultrastyrigel columns.

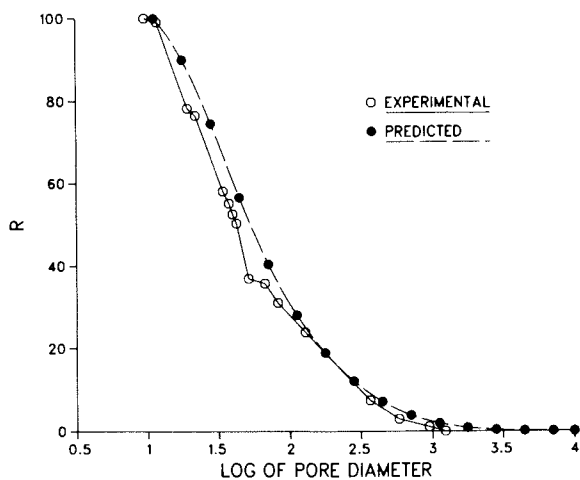


Figure 9. Predicted and experimental cumulative PSDs for a column set consisting of one 100A and one 10<sup>3</sup>A Ultrastyragel columns (see legend).

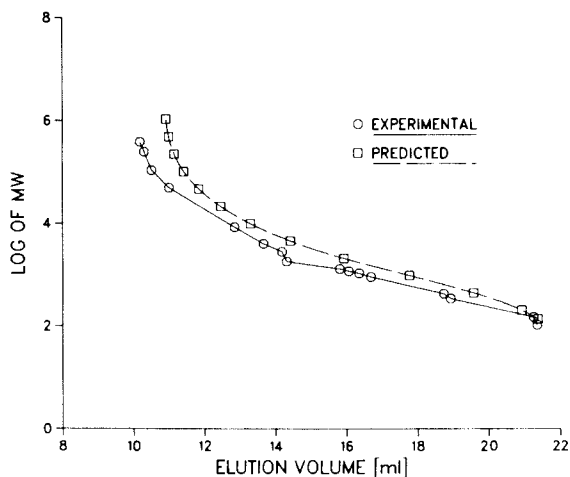


Figure 10. Predicted and experimental calibration curves for a column set consisting of one 100A and one 10<sup>3</sup>A Ultrastyragel column (see legend).

Gaussian PSDs. The two examples discussed above indicate the feasibility of the scheme outlined in Figure 5. Additional testing is needed to assure the validity of this approach. Nonetheless, the ability to accurately predict calibration curves on the basis of a simple model implies that the Gaussian PSDs generated by this method are realistic representations of the range of pores available in the columns studied. The PSDs are log normal as of function of  $\emptyset$  (eq. 2). Some workers have previously treated PSDs as log normal based on molecular weight (13,43). Figures 11 and 12 demonstrate that this view does not apply to PSDs which are measured by GPC. In Figure 11, calibration data for a  $10^3\text{A}$  column was transformed according to Equations 2 and 3 and then fit to a Gaussian. The integrated Gaussian yields a predicted cumulative PSD which compares favorably with experimental data. For Figure 12, only the  $V_E$  values were transformed. A Gaussian was fit and integrated as before. The predicted cumulative PSD in this case shows a significant deviation from experiment throughout the molecular weight range, indicating that Equation 2 is necessary to obtain a useful Gaussian PSD.

The success of this prediction scheme suggests several opportunities. It should be possible to specify the desired characteristics of a calibration curve in advance (e.g. linear from  $MW = 10^2$  to  $10^5$ ) and then predict the proper combination of available packing materials which would yield those characteristics either in a column set or a single mixed-bed column. Alternatively, the best combination of PSDs could be predicted as an aid in decisions regarding the design of new packing materials. This approach to the prediction of calibration curves may also suggest an interesting alternative to linear and polynomial curve fitting of GPC calibration data. Work is presently underway in our laboratory to pursue these opportunities.

### Conclusion

For the optimal application of GPC to the separation of discrete small molecules, three factors should be considered. Solvent effects are minimal, but may contribute selectivity when solvent-solute interactions occur. The resolving power in SMGPC increases as the square root of the column efficiency (plate count). New, efficient GPC columns exist which make the separation of small molecules affordable and practical, as indicated by applications to polymer, pesticide, pharmaceutical, and food samples. Finally, the slope and range of the calibration curve are indicative of the distribution of pores available within a column. Transformation of the calibration curve data for individual columns yields pore size distributions from which useful predictions can be made regarding the characteristics of column sets.

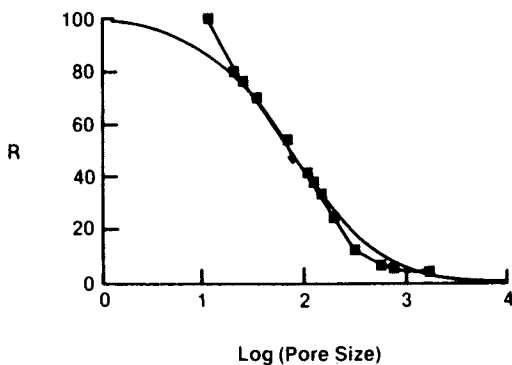


Figure 11. Predicted (smooth curve) and experimental (boxes) cumulative PSD for a  $10^3A$  Ultrastyrigel column.

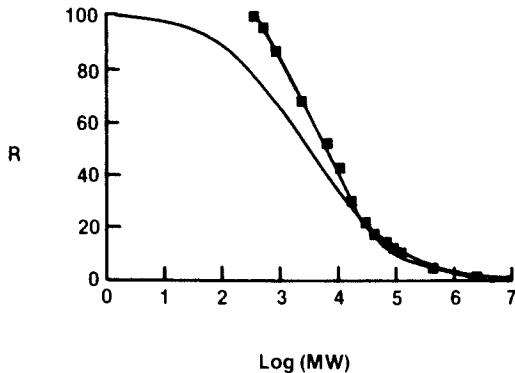


Figure 12. Predicted (smooth curve) cumulative PSD for a  $10^3A$  Ultrastyrigel column, determined incorrectly due to failure to convert log (MW) values to log 0. Experimental cumulative PSD (boxes) is shown for comparison.



Acknowledgments

The authors thank Mark Andrews, John Morawski, and Alex Newhart for performing some of the separations discussed in the text (Figures 1-2), and gratefully acknowledge the assistance of Janet Newman in the preparation of this manuscript.

Literature Cited

1. Cortis-Jones, B. Nature 1961, 79, 731.
2. Cazes, J.; Gaskill, D.R. Sep. Sci. 1967, 2, 421.
3. Bombaugh, K.J.; Dark, W.A.; Levangie, R.F. Anal. Chem. 1968, 236, 443.
4. Conroe, K.E. Chromatographia, 1975, 8, 119.
5. Vivilecchia, R.V.; Lightbody, B.G.; Thimot, N.Z.; Quinn, H.M. J. Chromatog. Sci. 1977, 15, 424.
6. Krishen, A. J. Chromatog. Sci. 1977, 15, 434.
7. Walter, R.B.; Johnson, J.F. J. Liq. Chromatogr. 1980, 3, 315.
8. Schultz, H.S.; Ekmanis, J.L.; Tisdale, V.R.; Baptiste, A.J.; Crossman, L.W. paper presented at Pittsburgh Conference on Analytical Chemistry and Applied Spectroscopy, Atlantic City, N.J. March 8-13, 1982, Abstract No. 392.
9. Schultz, H.S.; Alden, P.G.; Ekmanis, J.L. paper presented at Pittsburgh Conference on Analytical Chemistry and Applied Spectroscopy, Atlantic City, N.J. March 7-12, 1983, Abstract No. 393.
10. Richardson, H.; Tarvin, T.L. paper presented at Pittsburgh Conference on Analytical Chemistry and Applied Spectroscopy, Atlantic City, N.J. March 7-12, 1983, Abstract No. 571.
11. Morawski, J.; Cotter, R.L.; Ivie, K. paper presented at Pittsburgh Conference on Analytical Chemistry and Applied Spectroscopy, Atlantic City, N.J. March 7-12, 1983, Abstract No. 890.
12. Andrews, M.W.; Morawski, J.; Newhart, A.T. paper presented at Pittsburgh Conference on Analytical Chemistry and Applied Spectroscopy, Atlantic City, N.J. March 7-12, 1983, Abstract No. 951.
13. Yau, W.W.; Kirkland, J.J.; Bly, D.D. "Modern Size Exclusion Liquid Chromatography" Wiley: New York, 1979; Chap.2,4.
14. Majors, R.E. J. Chromatog. Sci. 1977, 15, 334.
15. Yau, W.W.; Kirkland, J.J.; Bly, D.D.; Stoklosa, H.J. J. Chromatogr. 1976, 125, 219.
16. Schultz, H.S.; Alden, P.G. paper presented at Pittsburgh Conference on Analytical Chemistry and Applied Spectroscopy, Atlantic City, N.J. March 7-12, 1983, Abstract No. 955.

17. Schultz, H.S.; Alden, P.G.; Ekmanis, J. paper presented at 185th ACS National Meeting, Seattle, WA, March 20-25, 1983, Abstract No. ORPL 200.
18. Halasz, I. Ber. Bunsenges Phys. Chem. 1975, 79, 731.
19. Halasz, I.; Martin, K. Angew. Chem., Int. Ed. Engl. 1978, 17, 901.
20. Halasz, I.; Vogtel, P. Angew. Chem., Int. Ed. Engl. 1980, 19, 24.
21. Werner, W.; Halasz, I. Chromatographia 1980, 13, 271.
22. Nikolov, R.; Werner, W.; Halasz, I. J. Chromatog. Sci. 1980, 18, 207.
23. Werner, W.; Halasz, R. J. Chromatog. Sci. 1980, 18, 277.
24. Groh, R.; Halasz, I.; Anal. Chem. 1981, 53, 1325.
25. Crispin, T.; Halasz, I. J. Chromatogr. 1982, 239, 351.
26. Freeman, D.H.; Poinasca, I.C. Anal. Chem. 1977, 49, 1183.
27. Schram, S.B.; Freeman, D.H. J. Liq. Chromatogr. 1980, 3, 403.
28. Freeman, D.H.; Schram, S.B. Anal. Chem. 1981, 53, 1235.
29. Kuga, S. J. Chromatogr. 1981, 206, 449.
30. Warren, F.V.; Bidlingmeyer, B.A. submitted to Anal. Chem.
31. Ekmanis, J.L. unpublished data.
32. Cantow, M.J.R.; Porter, R.S.; Johnson, J.F. J. Polym. Sci., Part A-1 1967, 5, 987.
33. Cantow, M.J.R.; Johnson, J.F. J. Polym. Sci., Part A-1 1967, 5, 2835.
34. DeVries, A.J.; LePage, M.; Beau, R.; Guillemin, C.L. Anal. Chem. 1967, 39, 935.
35. AOAC 6.141-2, 13 ed.
36. Smith, W.B.; Kollmansberger, A. J Phys. Chem. 1965, 69, 4157.
37. Hendrickson, J.G.; Moore, J.C. J. Polym. Sci., Part A-1 1966, 4, 167.
38. Hendrickson, J.G. Anal. Chem. 1968, 40, 49.
39. Lambert, A. J. Appl. Chem. 1970, 20, 305.
40. Lambert, A. Anal. Chim. Acta. 1971, 53, 63.
41. Krishen, A.; Tucker, R.G. Anal. Chem. 1977, 49, 898.
42. Engelhardt, H., personal communication.
43. Yau, W.W.; Ginnard, C.R.; Kirkland, J.J. J. Chromatogr. 1978, 149, 465.

RECEIVED September 29, 1983

# High-Performance High-Speed Gel Permeation Chromatography

## A Systems Approach

RONALD L. MILLER and JACK D. KERBER

The Perkin-Elmer Corporation, Main Avenue, Norwalk, CT 06856

The tremendous advances in size-exclusion column technology in the last decade have resulted in an order of magnitude reduction in analysis times in gel-permeation chromatography (GPC) since the technique was first introduced in the 1960's. The availability of highly efficient (up to 50,000 plates/meter) columns containing a broad pore-size distribution has enabled many separations to be performed using a single column, with no loss of resolution. The more recent development of 5- $\mu\text{m}$  polystyrene-divinylbenzene gel packings has resulted in capabilities for oligomer separations which were unheard of just a few years ago. As GPC separations are performed in less time, with fewer columns, the performance of other components of the chromatographic system becomes critical. A well-designed system for high-resolution, high speed GPC should embody precise control of flow rate and column temperature, minimal peak-broadening effects from both extra-column sources and the columns themselves, and sophisticated data acquisition and processing. The separation of oligomers is an application which clearly demonstrates the advantages of a systems approach to high-resolution, high-speed GPC.

Since the introduction of gel-permeation chromatography (GPC) in the 1960's, there have been tremendous advances in polymer gel size-exclusion column technology. Polystyrene-divinyl benzene copolymer gels, and the techniques by which they are packed into columns, have improved to the point where commercial columns exhibit up to 50,000 plates/meter. These 10- $\mu\text{m}$  gels are sufficiently rugged to permit flow rates of up to 3.0 ml/minute

0097-6156/84/0245-0189\$06.00/0

© 1984 American Chemical Society

with low viscosity GPC solvents such as tetrahydrofuran (THF), with little or no impact on efficiency or column lifetime. The more recent development of 5- $\mu\text{m}$  gels has resulted in columns with efficiencies of up to 80,000 plates/meter, usable at flow rates of up to 2.0 ml/minute with low viscosity solvents. The last decade has seen an order-of-magnitude increase in efficiency of GPC columns, which means a three-fold resolution increase for the same number and length of columns, or alternatively, the ability to generate equivalent resolution in a fraction of the total column length. Separations of low-molecular-weight materials may be performed in minutes using the 5- $\mu\text{m}$  gels, rather than hours, with a separation power unheard of just a few years ago.

Of course, resolution is not the only criterion for determining the optimum column set for a given separation: the column set must cover the molecular-weight range of the sample as well. A second development which minimized the number of GPC columns needed for many separations was the development of columns packed with a mixture of different pore-sized gels. Operating ranges of these columns span four to five orders of magnitude in molecular-weight units. The result is that most GPC separations can be adequately performed with either a single "mixed-bed" column, or a column set consisting of a mixed-bed column plus a second column geared to the molecular-weight range of the sample of interest. The net result is that GPC separations which required several hours to perform in the 1960's can now be performed in 15 to 20 minutes in most cases, and in 6 to 10 minutes in some cases, with better resolution than could be previously achieved. High-resolution, high-speed GPC has thus acquired a whole new meaning.

The benefits of this advanced column technology cannot be fully realized without corresponding evolution of other capabilities of the chromatographic system, however. Because the time scale of the separation is drastically shortened, factors such as constancy and reproducibility of temperature and mobile phase flow rate become much more important. As the contribution to peak broadening is lessened, extra-column contributions become more significant. More data must be taken, and taken faster; manual calculation of molecular-weight averages has already become obsolete. The increasing availability of and dependence on the laboratory microcomputer for GPC calculations has spurred development of powerful software tools using computer graphics to provide a visual dimension to GPC data reduction.

A systems approach to high-resolution, high-speed GPC takes all of these factors into consideration. Several aspects are worthy of detailed discussion.

Modern GPC Columns

The heart of a GPC separation system is, of course, the columns. As has been previously stated, column efficiencies have greatly improved over the last decade. The high efficiency of today's GPC column provides a better separation in less time. Nowhere is this more apparent than in applications which require the separation of oligomers. Low-molecular-weight condensation polymers often fall into this class. The analyst can, via judicious column selection, gain very high resolution in a reasonably short time frame. The separation of Figure 1 was obtained using only two 30-cm columns packed with 10- $\mu$ m gels, eluted with tetrahydrofuran (THF) at 1.0 ml/minute. This degree of separation, using only 60 cm of column length, was not possible a few years ago, when column efficiencies of 5,000 to 7,000 plates represented the state of the art; more columns or recycle would have been required.

Figure 2 illustrates a separation carried out using a single 5- $\mu$ m gel column, eluted with THF at a flow rate of 1.5 ml/minute. Excellent resolution is obtained with a single column; the last two compounds to elute differ by only 28 molecular-weight units. The resolution shown in Figure 2 requires a column efficiency of over 20,000 plates, generated between 4.5 and 6 minutes, or about 80 plates/second. Efficiencies of 24,000 plates at permeation and 23,000 plates at total exclusion were measured at flow rates of 1.0 ml/minute for this column. Separation speed is quite good also, but does not represent the limit which can be attained.

Bandwidth. Column efficiency may also be expressed in terms of a bandwidth. The bandwidth is defined as the volume of mobile phase containing 95% of an eluted compound, or, equivalently, four standard deviations of a statistical distribution of the same shape as the chromatographic peak:

$$\text{Bandwidth} = 4 \sigma = 4 V_R (N)^{-1/2} \quad (1)$$

Equation 1 shows that bandwidth is merely a means of expressing column efficiency,  $N$ , as a function of elution volume,  $V_R$ . Assuming an exclusion volume of 5 ml per column allows construction of Table I from Equation 1. Table I lists the bandwidth in microliters as a function of column plate number and the number of columns in series. The data assume that the plate number may be generated at total exclusion, as well as at total permeation; actual measurements made using the smaller pore size column substantiate this.

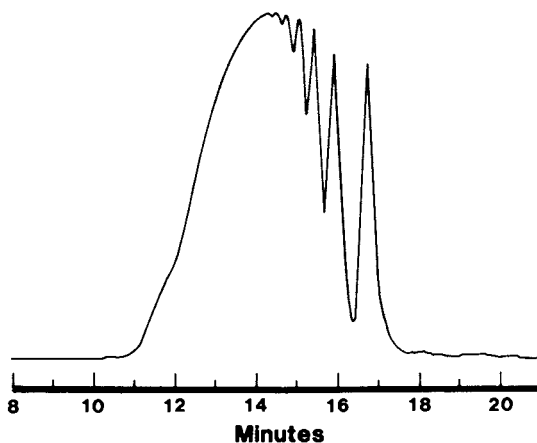


Figure 1. Separation of epoxy cresol Novolac oligomers.  
Columns: Perkin-Elmer/PL gel 10- $\mu$ m 100 A and 10- $\mu$ m 1000 A.

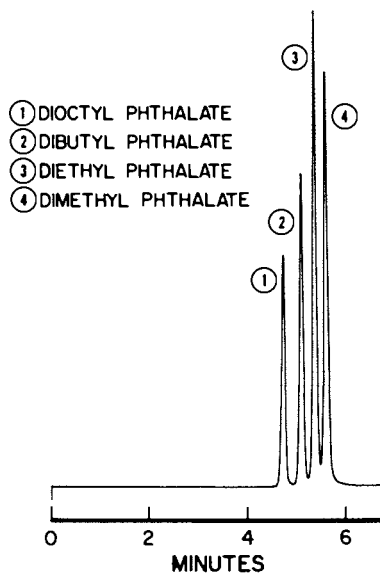


Figure 2. GPC separation of phthalate esters. Column:  
Perkin-Elmer/PL gel 5- $\mu$ m 100 A.

Table I. Bandwidths ( $\mu\text{l}$ ) of GPC columns at total exclusion

Plates per Column	Number of Columns			
	1	2	3	4
12,000	183	258	316	365
16,000	158	224	274	316
20,000	141	200	245	283
24,000	129	183	224	258

Polymer gel GPC columns packed with 10- $\mu\text{m}$  gels can exhibit efficiencies of 12,000 to 16,000 plates depending on the pore size. Single columns of this type produce bandwidths from 160 to 180  $\mu\text{l}$ . As columns are coupled in series, bandwidth increases as the square root of the number of columns, as may be seen from Equation 1. Plate number doubles, but so does the exclusion volume. The 5- $\mu\text{m}$  gel columns typically achieve 20,000 to 24,000 plates, and are represented by the bottom two rows of the table. The implications of the bandwidth values in Table I will be discussed below.

Separation Speed. Figure 3 shows chromatograms of polystyrene standards eluted with THF from a GPC column packed with a mixture of different porosity particles, the so-called "mixed-bed" column. A single column of this type covers a sufficiently broad molecular-weight range so that it alone may be used for many analyses. Furthermore, since the resistance to flow for a single column is low, higher mobile-phase flow rates may be used without generating an excessive pressure drop across the column. Figure 3 shows the separation of standards at flow rates of 1.0 and 3.0 ml/minute. The column generated 13,000 plates at the higher flow rate, compared with 12,900 at 1.0 ml/minute. Number-average and weight-average molecular weights of a polydisperse polystyrene sample run at flow rates of 1.0, 2.0, and 3.0 ml/minute were observed to vary by less than 2% when computed against calibrations obtained at the same flow rate. The variation of the molecular-weight averages with flow rate appears to be well within reason, particularly when no attempt was made to thermostat the column during these experiments; the differences between the molecular weights could easily be a consequence of small changes in column temperature between calibration and running the samples.

At high flow rates, the diffusion rates of macromolecules limit the resolution obtainable. This is apparent from Figure 3; the resolution between early eluting peaks suffers as the flow rate is increased. The resolution near the permeation limit is not greatly affected, however, and the effect on calculated molecular-weight averages was observed to be small even for large molecules. What is significant is that separation speed is limited by the nature of the sample, and not by the column.

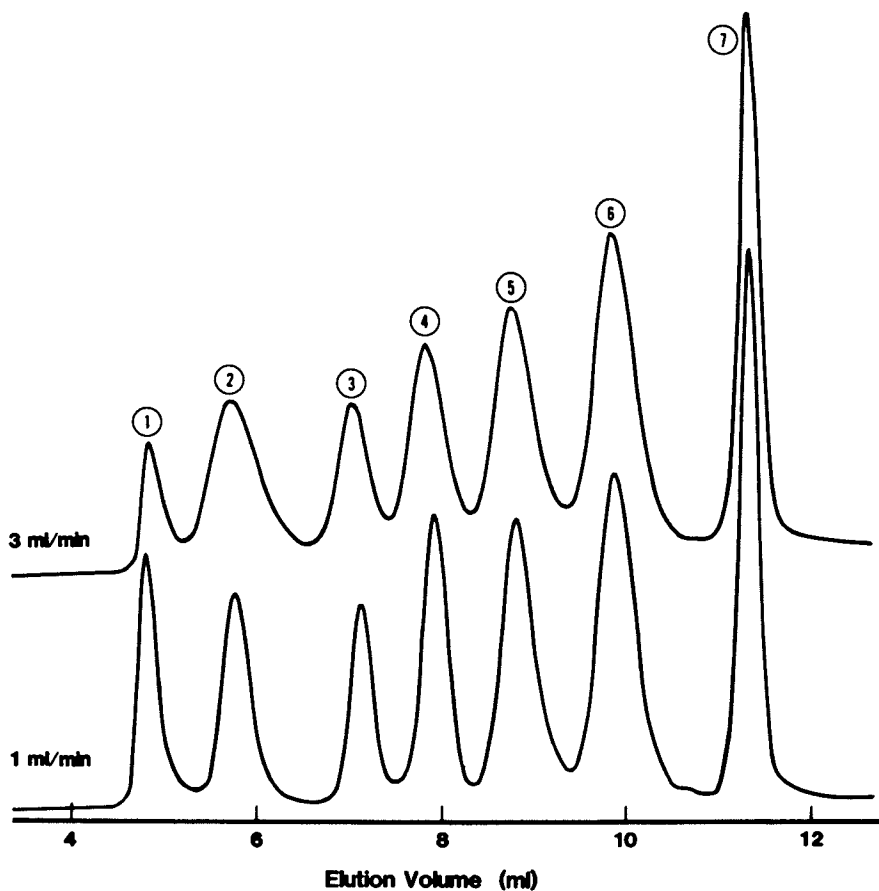


Figure 3. GPC separation of polystyrene standards at different flow rates. Column: Perkin-Elmer/PL gel 10- $\mu$ m mixed.



Instrumental Band Broadening

The data in Table I illustrates that very high-efficiency GPC columns separate compounds with a minimum of dilution. This is just another way of expressing column efficiency; the greater the plate number, the lower the dilution at a given retention volume. When the peak dilution from the column is small, i.e. when a small number of highly efficient columns are used, the degree to which other system components contribute to peak dilution and broadening becomes much more significant. DiCesare et.al. (1) have discussed extra-column contributions to bandwidth for very high speed reversed-phase liquid chromatography; most of the same considerations apply to GPC as well.

In chromatographic systems, the various contributions to peak broadening are generally independent. This means that the variance of the system is the sum of the variances from each contribution. Combining this relationship with Equation 1 yields an expression for the system bandwidth:

$$\text{Bandwidth}^2 = (4 \sigma_{\text{total}})^2 = \sum_i (4 \sigma_i)^2 \quad (2)$$

The peak broadening for the entire chromatographic system, columns plus the instrument, may thus be estimated from the bandwidth contribution of each component of the system. The effective plate number of the system may then be calculated from Equation 1.

Effect of Injection Volume. Table II shows the effect of injection volume on peak broadening and measured column efficiency. The bandwidths listed in Table II are due to injection volume alone, and were measured using an injector connected directly into the flowcell of a low-bandwidth detector. The plate reductions were then calculated for a 24,000 plate column, such as that represented by the bottom line of Table I, assuming 5 and 10 ml, respectively, for exclusion and total permeation volumes. Efficiencies of 23,000 plates at exclusion and 25,000 plates at permeation were actually measured for the column indicated in Table II. The effect of large injection volumes is thus to lose 25 to 50% of the potential column efficiency.

The injection volume chosen for analysis must represent a compromise between the amount of sample needed to properly detect the eluting material, and the amount of extra-column dispersion the analyst is willing to tolerate. It is also important that the same injection volume be used for both samples and standards, and that sample injection be properly synchronized with the start of data acquisition.

Table II. Effect of injection volume on bandwidth and realized efficiency of a Perkin-Elmer/PL Gel 5-  $\mu$ m 100 Angstrom column eluted with THF at 1.0 ml/min

Injection Volume, $\mu$ l	Injector Bandwidth, $\mu$ l	Plate Reduction at Exclusion	Plate Reduction at Permeation
3.0	30	1,132	320
6.0	31	1,204	341
10.0	36	1,595	458
23.5	47	2,592	770
50.0	86	6,863	2,397
100.0	160	13,696	6,659

Effect of Tubing Diameter. The contribution of the connecting tubing in the system to the bandwidth can also be estimated. A typical chromatograph might employ about 80 cm of connecting tubing between the injector and the detector. The bandwidth of 80 cm of .007-inch i.d. tubing has been determined to be about 31  $\mu$ l, (1) equivalent to that due to a 6- $\mu$ l injection. It may be shown that the bandwidth of the connecting tubing is proportional to the square root of the length and at least the square of the inside diameter. (2) The bandwidth due to 80 cm of .015-inch i.d. tubing is more than 140  $\mu$ l, a contribution nearly as large as that for a 100- $\mu$ l injection.

Effect of Detector Flowcell. The same considerations may be applied to the detector flowcell. For example, DiCesare et al. (1) determined that an 8- $\mu$ l flowcell in a "conventional" UV detector might have a bandwidth of 70  $\mu$ l or more. The UV detector employed in Figures 2 and 3 (LC-85B, Perkin-Elmer) has a 1.4- $\mu$ l flowcell with a bandwidth below 5  $\mu$ l. In a GPC system employing a single 24,000 plate column, a detector with a 70- $\mu$ l bandwidth would degrade efficiency by about 24% at exclusion, while the effect of the 1.4- $\mu$ l flowcell of the detector used in this work is negligible. Refractive index detectors typically have higher bandwidths, ranging from 25 to 100  $\mu$ l or more for commercial instruments.

Figure 4 illustrates the advantages of optimizing the GPC system with respect to instrumental band broadening. The lower chromatograms were obtained from a "conventional" chromatographic system employing a 10- $\mu$ l loop injector, about 80 cm of .015-inch i.d. connecting tubing, and a UV detector with an 8- $\mu$ l flowcell (LC-75, Perkin-Elmer). The sample is a liquid polystyrene resin separated using first a 10- $\mu$ m gel column (Perkin-Elmer/PL Gel 10- $\mu$ m 100 A) and then a 5- $\mu$ m gel column (Perkin-Elmer/PL Gel 5- $\mu$ m 100 A) of the same porosity. The same sample was separated on an optimized system, which employed a 6- $\mu$ l loop injector, 80 cm of .007-inch i.d. tubing, and a UV detector with a 1.4- $\mu$ l flowcell (LC-85B, Perkin-Elmer), producing the two upper

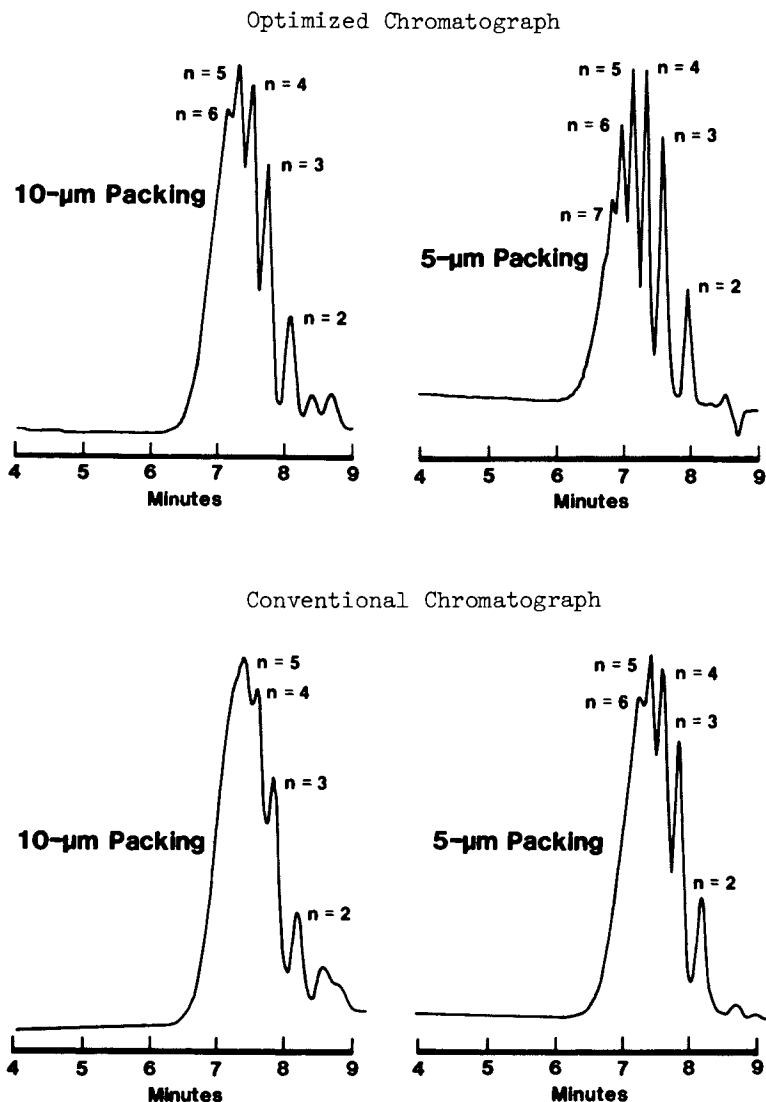


Figure 4. Separation of liquid polystyrene resin on different chromatographic systems. System configuration and column type are defined in the text.

chromatograms in Figure 3. The columns used were those used for the lower chromatograms. All four separations were performed with a THF mobile phase at 1.0 ml/minute.

The total extra-column bandwidths, calculated from Equation 2, were 195  $\mu$ l and 44  $\mu$ l, respectively, for the conventional and optimized systems. Column efficiencies were 16,000 plates for the 10- $\mu$ m gel column and 24,000 plates for the 5- $\mu$ m gel column; the column contributions to bandwidth are given in Table I. The difference in resolution obtainable between the two chromatographic systems is readily apparent from Figure 4. The optimized system produces much narrower peaks, and more of them as additional oligomer are resolved. In terms of required bandwidth, the extra-column bandwidth of the optimized system is about a third of that inherent in the 5- $\mu$ m gel column at total exclusion, while the conventional system has a bandwidth greater than that of either column. The high instrumental bandwidth of the conventional system is largely due to the contribution from the connecting tubing; the bandwidth of this system could have been reduced to about 94  $\mu$ l by substituting .007 i.d. tubing. A system bandwidth of 94  $\mu$ l is still unacceptable for work employing a single 5- $\mu$ m gel column, but may be tolerable for separations employing multiple 10- $\mu$ m gel columns.

Table III summarizes the results represented by Figure 4. The bandwidth values in the table are those calculated for the total system: the instrument plus the column. The values for number of plates are for the number of plates realized in the total system. It can be seen that the optimized system does not greatly impact column efficiency, the total loss in plates being only about ten percent at total exclusion for a 24,000 plate column. This is consistent with an instrumental bandwidth equal to a third of the bandwidth of the column. The conventional system, with a bandwidth equal to or greater than that of the column, exhibited a severe loss in realized efficiency, particularly at or near exclusion.

Table III. Effect of instrumental bandwidth on column efficiency

Inherent Column Efficiency	Conventional System		Optimized System	
	Total System Bandwidth, $\mu$ l	Effective Plates	Total System Bandwidth, $\mu$ l	Effective Plates
16,000 plates				
at permeation	372	11,600	319	15,700
at permeation	256	6,300	164	14,800
20,000 plates				
at permeation	344	13,500	286	19,500
at permeation	255	6,900	148	18,200
24,000 plates				
at permeation	324	15,200	261	23,300
at permeation	234	7,300	136	21,500

The data of Table III represent calculated bandwidths and efficiencies. Actual realized efficiencies were measured for the four chromatograms of Figure 4. For the 10- $\mu\text{m}$  gel column, the conventional system produced an effective efficiency of 11,000 plates, compared with an effective efficiency of 16,000 plates for the optimized systems. These values are in excellent agreement with the calculated values shown on the top line of Table III. Similar measurements on chromatograms obtained from the 5- $\mu\text{m}$  gel columns yielded values of 16,000 and 20,000 plates, respectively, for the conventional and optimized systems. This also represents good agreement with calculated effective efficiencies at total exclusion for a 24,000 plate column.

The 5- $\mu\text{m}$  gel GPC columns are seen to produce tremendous efficiencies, but these efficiencies are only realized when the chromatographic system is optimized with respect to bandwidth. This also holds true to a lesser degree for a well-packed 10- $\mu\text{m}$  gel column.

Effect of Detector Response Time. The speed of response of the detector electronics can also affect resolution. Response times can also be expressed as bandwidths by multiplying by the flow rate in the appropriate units. In the previous discussion, this effect was ignored, as the time constant bandwidths were negligible: less than 12.5  $\mu\text{l}$  for either detector. Figure 5 shows an example of what can happen when the time constant bandwidth is too large. The chromatographic system used for the separations shown in Figure 5 is an optimized system incorporating a refractive index detector; bandwidth contributions from the flowcell, tubing, and injector combine to produce a volume bandwidth of 52  $\mu\text{l}$  for this system. The time constants of 5 and 0.5 seconds equate to bandwidths of 167 and 16.7  $\mu\text{l}$ , respectively, for total system bandwidths of 174 and 55  $\mu\text{l}$ . The effect on resolution is readily apparent; the faster response time produces a total bandwidth acceptable for all applications except where maximum resolution for a single 5- $\mu\text{m}$  gel column is required near total exclusion. The 5 second response time, on the other hand, is of little use except when several of the 10- $\mu\text{m}$  gel columns are used. It is interesting to point out, however, that a system bandwidth of 174  $\mu\text{l}$  was thought to be quite suitable a few years ago, when column efficiencies were significantly lower, and more columns were used.

#### Data Acquisition and Processing

The data acquisition rate can also contribute to the integrity of GPC data. Chromatograms traced on a recorder are in response to an analog signal, and are continuous traces. Calculation of molecular weights, however, requires digitized data. The frequency of measurement used when digitizing an analog signal is

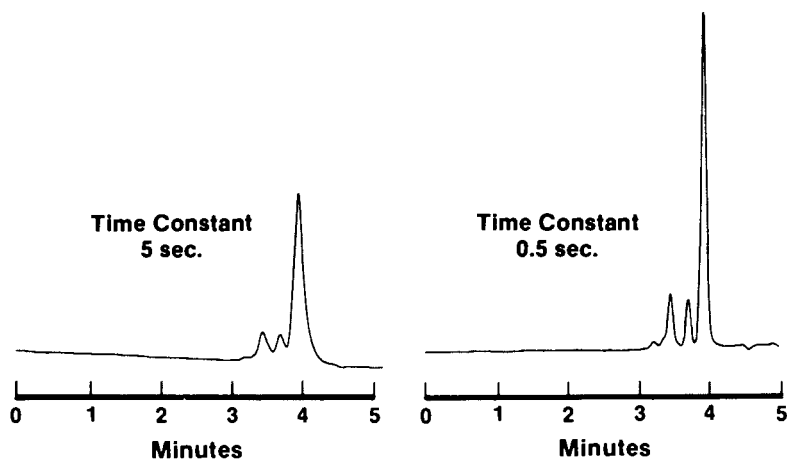


Figure 5. The effect of detector time constant on the GPC separation of a liquid epoxy resin. Column: Perkin-Elmer/PL gel 5- $\mu\text{m}$  100 Angstrom. Eluent: THF at 2.0 ml/min. Injection volume: 6  $\mu\text{l}$ . Detector: LC-25 RI detector (Perkin-Elmer).

known as the information bandwidth, and can also be converted to volume units. Table IV shows the quantitative effect of the size of the information bandwidth. The sample and conditions are those of Figure 5, except that flow rate was 1.5 ml/minute, and the 0.5 second detector response time was used throughout. Separations of the liquid epoxy resin were performed at various data acquisition rates, and molecular-weight averages calculated against calibration data obtained at a data rate of 0.1 seconds/point.

Table IV. Effect of sampling rate on GPC results

Data Rate, Seconds/point	Time of Largest Data Point, Min.	Molecular-Weight Averages*		
		No. Ave.	Wt. Ave.	Z Ave
0.1	4.93	377	400	435
0.2	4.94	375	398	433
0.5	4.95	372	395	430
1.0	4.97	366	387	420
2.0	5.00	360	379	408
5.0	5.17	328	343	375

\* Relative to calibration data taken at 0.1 seconds/point.

The data rates in Table IV correspond to information bandwidths varying from 2.5  $\mu$ l to 125  $\mu$ l. The retention times of the largest peak, when taken as the time of the largest data point in the digitized data, show a definite trend, increasing as the time between measurements increases. This is entirely a consequence of the information bandwidth; the analog chromatograms were identical. Table IV also shows the effect on the calculated molecular-weight averages, when calculations were performed relative to calibration data taken from a digitized chromatogram for which a very fast data rate was used. The decreasing molecular-weight averages also varies as the slope of the calibration curve, and would be much greater for a broader range column.

Thus, data rates of 0.5 seconds/point are required to suppress band-broadening contributions from data acquisition. This does not define the limiting requirement of the data system, however. Between 50 and 100 data points are desired to accurately define a molecular-weight average for a single peak, particularly an average representing a higher statistical moment such as the Z-average. The chromatograms of Figure 3 contain seven peaks; 400 to 800 data points are optimum for this chromatogram, when sufficient data points are included to adequately define baseline. The chromatogram of Figure 3 obtained at a flow rate of 3 ml/minute thus requires data rates of 100 to 200 points per minute (300 points per minute were actually used).

Needless to say, processing this data in a time frame compatible with the time needed for chromatography cannot be done without the aid of a computer; this is true for even the 20-minute separations of Figure 1. Since the polymer chemist working with GPC is becoming more dependent on the computer programmer, it is pertinent to include software as an integral part of the GPC data system.

The sheer volume of data generated by high resolution, high speed GPC mandates some type of media storage for raw data, together with the ability to recall, replot, and rework any of this raw data. Automation of both data acquisition and data processing is required to keep pace with the speed at which samples can be run. This alone may be sufficient for the quality control laboratory, but the research laboratory also requires the ability to deal with a particular chromatogram in greater detail in a more leisurely manner.

The advantages of interactive computer graphics in GPC come into play here. If the molecular weight averages of two samples differ, the replotting of chromatograms or distributions on the CRT of a computer terminal permits a fast, easy comparison of just how the samples differ. Given appropriate software, screen graphics can be used to not only redisplay, but also to rescale, expand, and even subtract chromatograms and distributions, to plot and manipulate GPC calibrations, and to define baseline and summation limits to be used in numerical computations. These capabilities provide a visual dimension not available from mere numbers, and enable the chemist to solve problems faster and easier.

The most important consideration of software, however, is that it must provide the correct answers. This requires that the appropriate molecular weight be associated with each data point, which relates to the techniques and algorithms used in constructing the calibration curve. Calibration curves are generated from chromatographic data obtained on standards of known molecular weight; both monodisperse and polydisperse standards have been used. A discussion of the relative merits of each technique is beyond the scope of this paper; suffice it to say that the model used by the software should reflect the true calibration as closely as possible.

### Temperature Control

The importance of temperature control of the GPC column cannot be overstated. The use of temperatures above ambient results in lower mobile-phase viscosity, which in turn reduces the back pressure generated by the column. Column life is prolonged, and in some cases higher flow rates may be employed. The reduction in mobile-phase viscosity improves both the rate and efficiency of mass transfer processes, enhancing column performance. While



the benefits of elevated temperature are certainly desirable, the use of constant temperature is critical. Mark-Houwink coefficients, the parameters which describe the relationship between molecular weight and hydrodynamic volume (and therefore elution volume), are significantly temperature dependent. Polymer solubility improves with increasing temperature; polymer molecules in solution uncoil to a greater degree, and hence occupy larger volume and elute earlier from the GPC column.

The effect of changing temperature on GPC results is illustrated in Table V for a polystyrene sample; a column was calibrated using monodisperse polystyrene standards. The standards and the sample were both run at 25 and 30 C. The detrimental effect of a change in temperature between calibration and sample analysis is obvious; a five-degree C change in temperature was seen to produce errors of 11-14% in the weight-average molecular weight. In this case the sample and the standards were identical chemically. If they are not, their Mark-Houwink coefficients may show differences in temperature dependency, and the errors become compounded. If the goal of the chemist is to attain reproducibility to within 1%, the column temperature must be maintained to within 0.5 C or better throughout the course of the experiments.

Table V. Effect of temperature on weight average molecular weight

Analysis Temperature	Calibration Temperature	Weight-Average Molecular Weight
25 C	25 C	357,000
25 C	30 C	313,000
30 C	25 C	400,000
30 C	30 C	352,000

An air-bath oven is an excellent choice for GPC in that a substantial number of columns may be accommodated by a single unit. Costs are low and temperature stability and reproducibility quite good. Some type of heat-exchange device should be placed in the oven to raise the temperature of the mobile phase to the desired point before it reaches the column; this practice helps eliminate temperature gradients along the column axis. Injectors can be mounted directly on (or even in) an oven, minimizing the amount of heat exchange between the mobile phase and the injector.

#### Solvent Delivery

Effect of Flow Rate Errors. The effect of flow rate errors on molecular-weight averages calculated from GPC data has been

discussed by Bly, et al.(3) These workers concluded that flow rate repeatability of better than 0.3%, flow rate drift of less than 1% over the time of the chromatogram, and short-term random variation (noise) of better than 4%, are all required to reproduce molecular-weight averages to within 6%. Thus, the most important criteria for a GPC pumping system are, respectively, resettability, drift, and pulsation. Absolute accuracy of flow rate must also be considered if comparison of results obtained on different instruments is also important.

The exact magnitude of flow-rate induced errors in the molecular-weight averages depends on the slope of the calibration curve: the steeper the slope, the more a given flow rate variation affects reproducibility of the averages. GPC separations employing a single 25- to 30-cm mixed bed column probably represent the worst case. Table VI illustrates the effect of a one percent error in the flow rate resettability for a column of this type. Using a given set of calibration data and a given set of raw slice areas for a polystyrene sample, reference values of the various molecular-weight averages were computed. The mobile phase was THF at 1.0 ml/minute flow. A flow rate increase of one percent between the time of calibration and sample analysis was then simulated by multiplying each of the retention times in the calibration data set by 1.01, and repeating the molecular-weight calculations. A decrease in flow rate was simulated in a like manner. The results indicated that even a small error in flow rate generates very large errors in molecular weight, particularly for a column with a steep calibration curve.

Table VI. Effect of flow rate errors on molecular-weight averages

Molecular Weight	No Change	1% Increase	1% Decrease
Number-Average	125,000	141,700 (+13%)	110,100 (-12%)
Weight-Average	384,900	452,800 (+18%)	331,000 (-14%)
Z-Average	1,621,000	2,628,000 (+62%)	1,078,000 (-27%)

While the effects of flow rate drift or noise at the one percent level over the duration of the separation are not nearly as disastrous as the case illustrated in Table VI, the data serve to demonstrate the need for flow rate stability and repeatability. The absolute accuracy of flow rate is of lesser importance, as this type of variation only manifests itself when comparing raw data obtained on different instruments, all of which should be calibrated independently of each other in any case. It should be pointed out that the GPC calibration should always be redetermined whenever any component of the system is changed; this is simply good laboratory practice.

Pumps for GPC. The most important considerations when selecting a solvent delivery system are those involving flow rate resettability, drift, and noise. Reciprocating-piston pumps, either in single-piston or multiple-piston configurations, are by far the most commonly used solvent delivery devices for GPC. In a dual-head pump, for example, each pump head operates essentially 180 degrees out of phase with the other, so that one pump head is always delivering solvent; pulsation occurs only at the point of "crossover" between one pump head and the other. Advanced designs of single-piston pumps minimize pulsation by refilling the piston at a much faster rate than it delivers solvent. In either case, some additional pulse-dampening capability is generally provided to further reduce short term flow rate fluctuations, or flow rate "noise". Since the pumps used for GPC tend by and large to be those designed for "conventional" chromatography, their pulse dampeners may be optimized for applications producing higher back pressures than GPC. In this case, placing a flow restrictor between the pump and injector may improve flow rate reproducibility. In this work, 3 to 9 meters of coiled tubing, 0.007" i.d., was used as a flow restrictor. This coil was placed inside the oven, and also served to preheat the mobile phase.

A final aspect of GPC solvent delivery relates to the solvent reservoirs themselves. The ability to perform in situ helium degassing of solvents, provide inert gas blankets over solvents, and protect solvents from contamination from external sources are worth consideration from the standpoints of convenience and safety alone. If these features are provided for, it is a small step to also provide a small positive pressure, say 10 psi or so, to the solvent reservoir. This positive pressure helps minimize the formation of solvent vapors in the pump chamber during the refill part of the pump stroke, and improves the flow rate reproducibility of rapid-refill type pumps delivering high-vapor-pressure solvents.

System Reproducibility. Table VII describes the reproducibility achievable with an optimized GPC system. Twelve consecutive analyses of the same polystyrene sample were analyzed to produce these data. The pump used was a single-piston rapid-refill type reciprocating pump (Series 10, Perkin-Elmer) equipped with reservoir pressurization and restrictor coil as discussed above. The mobile phase was THF at 1.0 ml/minute, and the reservoir pressure 11 psi. The column temperature was controlled at 40 C by placing the column (Perkin-Elmer PL Gel 10- $\mu$  MIXED) and the restrictor coil in an air bath oven (LC-100, Perkin-Elmer) to reduce any variability due to temperature. Samples were injected with an autosampler (Model 420B, Perkin-Elmer) containing a fixed-volume loop injection valve. A variable wavelength UV detector (LC-75) operating at 265 nm was used as the detector. Molecular-weight averages were calculated for all twelve

injections using the same baseline times, calibration curve, and summation limits. The results, summarized in Table VII, illustrate the precision which can be routinely obtained when all sources of variation are controlled. Relative standard deviations lower by about a factor of three have been obtained using this system for low-molecular-weight polyethoxylated phenol, separated using a column with a less "steep" calibration curve.

Table VII. Summary of results from twelve repetitive analyses of polystyrene.

Parameter	Mean	Standard Deviation	Relative Standard Deviation, %
Number-Average Mol. Wt.	140,010	970	0.69
Weight-Average Mol. Wt.	381,500	2,799	0.73
Z-Average Mol. Wt.	1,211,000	13,872	1.15

#### Summary

We have demonstrated the benefits which can be obtained from high-efficiency GPC column technology when the chromatographic system is properly optimized. Band broadening from extra-column sources must be minimized to realize the full efficiency of modern GPC columns. Proper control of both flow rate and column temperature is vital to maximizing reproducibility in GPC.

#### Literature Cited

1. DiCesare, J. L.; Dong, M. W.; Atwood, J. G. J. Chromatogr. 1981, 217, 369-85.
2. Martin, M.; Eon, C.; Guiochon, G. J. Chromatogr. 1975, 108, 229-41.
3. Bly, D. D.; Stoklosa, H. J.; Kirkland, J. J.; Yau, W. W. Anal. Chem. 1975, 47, 1810-3.

RECEIVED September 12, 1983

## Deuterium Oxide Used to Characterize Columns for Aqueous Size Exclusion Chromatography

HOWARD G. BARTH

Research Center, Hercules Incorporated, Wilmington, DE 19899

FRED E. REGNIER

Department of Biochemistry, Purdue University, West Lafayette, IN 47907

In order to characterize size-exclusion chromatographic (SEC) columns, both the interstitial volume and the pore volume of a packed column must be determined. This information is required for the construction of a calibration curve as well as to obtain SEC distribution coefficients. In aqueous SEC, either glucose or deuterium oxide ( $D_2O$ ) are commonly used to measure the total permeation volume of a column. Using LiChrospher silica packings with a glycerylpropyl silane bonded phase (SynChropak GPC), we found that the elution volume of  $D_2O$  was significantly greater than the results obtained for glucose. Controlled-pore glass packings which have narrower pore-size distributions did not exhibit this property. From these results, it appears that the silica packing contains a population of micropores which are accessible only to low molecular weight probes.

Size exclusion chromatography (SEC) is a separation process by which molecules are fractionated by size on the basis of differential penetration into porous particulate matrices. Elution volume ( $V_e$ ) of any given molecular species relative to another of different size is dependent on the pore diameter of the matrix, pore-size distribution, pore volume ( $V_i$ ), interstitial volume ( $V_o$ ) and column dimensions. Use of SEC to estimate molecular size is achieved by plotting the log of the molecular weight of a series of calibrants against their elution volume. Since  $V_e$  is a function of  $V_o$  and  $V_i$ , its magnitude will be dependent on the geometry of a column.

A more useful and fundamental parameter than elution volume is the dimensionless size exclusion distribution coefficient ( $K_D$ ) which is related to  $V_i$  and  $V_o$  by the equation:

0097-6156/84/0245-0207\$06.00/0

© 1984 American Chemical Society

$$K_D = \frac{V_e - V_o}{V_i} \quad (1)$$

Use of  $K_D$  instead of  $V_e$  in the calibration of columns produces a calibration curve that is independent of column dimensions and pore volume. To obtain  $K_D$  for any species requires the determination of  $V_o$  and  $V_i$  in addition to  $V_e$ .  $V_o$  is usually taken as the elution volume of an excluded polymer while  $V_i$  is equal to  $V_T - V_o$ . The volume  $V_T$  is the total permeation volume of the column and is measured with a low molecular weight compound that totally permeates particle matrices.

Deuterium oxide ( $D_2O$ ) has been used to determine  $V_T$  in SEC columns because its low molecular weight assures high matrix permeation and its high diffusion coefficient is useful in determining column efficiency (1-3). (It should be noted that in aqueous mobile phases, DHO would be present after injecting  $D_2O$  into a column because of hydrogen exchange.) In addition to  $D_2O$ , tritiated water (THO) has been used as a low molecular weight probe of  $V_T$  in SEC (1,4-7). Marsden (4,8), however, cautions that tritium exchange within the crosslinked polysaccharide matrix could result in errors when THO is used to determine  $V_T$ . From  $V_T$  measurements with  $H_2^{18}O$ , Marsden found that  $K_D$  for THO was 1.09 (8).

The assumption has generally been made in SEC with matrices greater than 100Å pore diameter that there is little, if any, size discrimination of molecules less than 500 daltons, i.e., they would all elute at  $V_T$ .

During our studies with SynChropak, a high-performance SEC packing consisting of LiChrospher silica with a glycerylpropyl silane bonded phase, we found to our surprise that the elution volume of  $D_2O$  was significantly greater than that of glucose which we had previously used as a low molecular weight calibrant (9-11).

The problem of determining  $V_T$  in SEC is similar to that of determining zero retention time ( $t_o$ ) in other liquid chromatography columns. Recently, there have been several papers dealing with the determination of retention time of a retained peak in HPLC (12-19). In high-performance reversed-phase chromatography, McCormick and Karger (15) and Berendsen, et al., (16) have employed  $D_2O$  to measure  $t_o$ . Neidhart et al., (12,14) took a different approach by determining the retention times of a solute as a function of temperature. Since the enthalpy of adsorption of a solute onto a stationary phase is negative, the elution time of a retained species should decrease with increasing temperature.

However, none of these methods rigorously examines the possibility that microporosity may also cause differences in  $t_o$  between solutes. This paper describes the extent of retention time differences between  $D_2O$  and glucose on bonded phase inorganic supports.

### Experimental

**Apparatus.** Pumping systems used in these studies for high-performance columns were a Varian 8500 syringe pump and a Varian 5000 isocratic pump. An Altex 110A was employed for the controlled-pore glass (CPG) columns. Waters Associates model 401 refractometers were used on all instruments. Stagnant mobile phase was kept in the reference side of the refractometer. Samples were injected with a Rheodyne 70-10 injection valve using a 20 $\mu$ l loop (100 $\mu$ l for CPG columns).

**Columns.** The packing materials were 10 $\mu$ m SynChropak and 37-74 $\mu$ m controlled-pore glass with glyceryl silane bonded phase. SynChropak columns were purchased prepacked in 25 cm x 4.1 mm ID stainless steel columns from SynChrom (Linden, IN). Nominal pore sizes were 100, 300, 1000 and 4000 $\text{\AA}$ .

CPG was dry packed into stainless steel columns using the tap-fill procedure (20). Column dimensions were 100 cm x 4.6 mm ID for the 1000, 1400, 2000 and 3000 $\text{\AA}$  material and 50 cm x 4.6 mm ID for the 75 $\text{\AA}$  packing. A description of these packings is given in Table I. Values listed in the table were obtained from the manufacturer (Electronucleonics Inc.).

---

TABLE I. GLYCERYL-CPG COLUMN PACKING MATERIAL (200/400 mesh)

---

Nominal Pore Size, $\text{\AA}$	Mean Pore Diameter, $\text{\AA}$	Pore Size Distribution, +%	Pore Volume, cc/g	Surface Area, $\text{m}^2/\text{g}$
75	75	6.0	0.47	140
1000	1038	7.3	1.22	28
1400	1489	6.4	1.16	17.6
2000	1902	10	0.80	10
3000	3125	10	1.25	7.9

---

**Chemicals.** Urea (99+%), glucose and D<sub>2</sub>O (99.8%) were obtained from Aldrich Chemical Co. (Gold Label).

**Mobile Phase Preparation.** Distilled water and 6M urea were filtered under vacuum using a 0.22 $\mu$ m membrane filter (Type GS, Millipore).

**Sample Preparation in 6M Urea.** Solutions of glucose were prepared directly in 6M urea. D<sub>2</sub>O solutions were prepared by diluting equal volumes of D<sub>2</sub>O and 12M urea and the resulting solution was then diluted 1:1 with 6M urea.

**Elevated Temperature Studies.** The Varian 5000 liquid chromatograph and a Waters Associates 401 differential refractometer were employed. The column was heated with a Varian universal heater block at an estimated accuracy of  $\pm 0.5^\circ\text{C}$ . About 15–30 minutes were allowed for column equilibration for a given temperature. The recorder employed was a Varian 9176.

A 25 cm x 4.6 mm ID long 300Å SynChropak column was used to evaluate temperature effects. Injections were made with 5% D<sub>2</sub>O and 1.3 mg/ml glucose solutions. D<sub>2</sub>O gave a negative refractive index response.

Because of some peak tailing, the number of theoretical plates was based on peak width at one-half peak height:  $N=5.54 (t_r/w_{1/2})^2$ . The pooled standard deviation (all temperatures) of retention time measurements (df=34) was  $\pm 0.007$  minutes.

**Physical Measurements on Supports.** Pore diameter and volume were determined by mercury porosimetry. Micropores were estimated by the BET and t-curve methods (21, 22).

## **Results and Discussion**

**Elution Volume of D<sub>2</sub>O and Glucose on Controlled-Pore Glass and SynChropak Columns.** The elution volumes of D<sub>2</sub>O and glucose on 100, 300 and 4000Å pore-size SynChropak columns are given in Table II. As indicated, the elution volume of D<sub>2</sub>O was greater than that of glucose in all cases. Because of the smaller hydrodynamic volume of D<sub>2</sub>O, as compared to glucose, this trend was expected.

However, the sizable elution volume difference between D<sub>2</sub>O and glucose exhibited by the 100 and 300Å columns is surprising. On the basis of total pore volume,  $V_t$ , the percentage of micropore volume that was available to D<sub>2</sub>O and not glucose was high:  $17.4 \pm 1.7\%$  and  $8.4 \pm 1.5\%$ , respectively, for the 100 and 300Å packings. The result obtained with the 4000Å column was within experimental error.

Glucose and D<sub>2</sub>O were also tested on five glycerylpropyl CPG packings of 75, 1000, 1400, 2000 and 3000Å and the results are presented in Table III. The percentage of micropore volume that was available to D<sub>2</sub>O and not glucose was close to or within the experimental error of  $V_e$  determination for all columns.



TABLE II. ELUTION CHARACTERISTICS OF D<sub>2</sub>O  
AND GLUCOSE ON SYNCHROPAK COLUMNS\*

<u>Pore Diameter</u>	<u>100Å</u>	<u>300Å</u>	<u>4000Å</u>
D <sub>2</sub> O, V <sub>r</sub> (ml)	2.58	2.82	2.62
Glucose, V <sub>r</sub> (ml)	2.34	2.68	2.60
Δ, ml	+0.24	+0.14	+0.02
V <sub>i</sub> , ml**	1.38	1.66	1.47
Micropore volume, %***	17.4±1.7	8.4±1.5	1.4±1.7

\* Chromatographic conditions: Mobile phase: H<sub>2</sub>O; Flow: 0.5 ml/min; Chart Speed: 1 in/min; Volume injected: 20μl; Sample concentrations: 1 mg/ml glucose and 5% D<sub>2</sub>O; Columns: 25 cm x 4.1 mm ID; RI detector sensitivity: X4.

\*\* V<sub>i</sub> = V<sub>T</sub> - V<sub>O</sub> where V<sub>T</sub> is the elution volume of D<sub>2</sub>O. For 4000Å columns, V<sub>O</sub> = 0.35 (π·r<sup>2</sup>·L). For 100 and 300Å columns, V<sub>O</sub> was obtained from 2 x 10<sup>6</sup> dalton dextran (1.20 and 1.16 ml, respectively).

\*\*\* Propagated error assuming flow rate precision of ± 1%.

TABLE III. ELUTION CHARACTERISTICS OF D<sub>2</sub>O  
AND GLUCOSE ON GYCERYL - CPG COLUMNS\*

<u>Pore Diameter</u>	<u>75Å</u>	<u>1000Å</u>	<u>1400Å</u>	<u>2000Å</u>	<u>3000Å</u>
D <sub>2</sub> O, V <sub>r</sub> (ml)	5.75	14.25	14.20	13.70	13.38
Glucose, V <sub>r</sub> (ml)	5.65	14.15	14.18	13.65	13.30
Δ, ml	0.10	0.10	0.02	0.05	0.08
V <sub>i</sub> , ml**	2.15	8.43	8.38	7.88	7.56
Micropore volume, %***	4.6±2.7	1.2±1.7	0.2±1.7	0.6±1.8	1±1.8

\* Chromatographic conditions: Mobile phase: 0.5 M NaOAc; Flow: 0.5 ml/min; Chart Speed: 0.5 cm/min; Volume injected: 100μl; Sample concentrations: 2 mg/ml glucose (X4) and 5% D<sub>2</sub>O (X8); Columns: 100 cm x 4.6 mm ID (50 cm x 4.6 cm ID for 75Å); Pump: Altex 110A.

\*\* V<sub>i</sub> = V<sub>T</sub> - V<sub>O</sub> where V<sub>T</sub> is the elution volume of D<sub>2</sub>O. For 1000, 1400, 2000 and 3000Å columns, V<sub>O</sub> = 0.35 (π·r<sup>2</sup>·L). For 75Å columns, V<sub>O</sub> was obtained from 2 x 10<sup>6</sup> dalton dextran.

\*\*\* Propagated error assuming flow rate precision of ± 1%.

Mercury porosimetry data of these packings are given in Table IV. It is of interest to note that the pore-size distribution of CPG is significantly more narrow than that of SynChropak, a surface-modified porous silica (LiChrospher). These different physical characteristics may help to explain the existence of micropores in SynChropak. Because of the wide pore-size distribution of this packing, it seems reasonable that this material also contains a population of micropores which are only accessible to D<sub>2</sub>O. In mercury porosimetry measurements, the lower pore size limit is about 30Å.

TABLE IV. PHYSICAL CHARACTERISTICS OF SEC PACKINGS FROM MERCURY POROSIMETRY

Support Pore Diameter	SynChropak (10µm diam.)			Glyceryl-CPG (37-74µm diam.)		
	100Å	1000Å	4000Å	75Å	1000Å	3000Å
Pore-size distribution, µm	0.0044-0.06	0.02-0.30	0.14-0.9	0.006-0.009	0.09-0.18	0.25-0.35
Dead-end volume, cc/g	1.66	1.55	0.84	0.125	0	0
V <sub>i</sub> , cc/g*	0.92	0.96	0.82	0.33	1.35	0.89
V <sub>0</sub> , cc/g**	1.10	1.10	1.25	0.90	1.65	1.4
Surface area, m <sup>2</sup> /g	294	48.4	12.0	181	50	9.5

\* Pore volume

\*\* Interstitial volume (measured to 100 psi)

Comparison of surface areas as determined by the BET and t-curve methods (21) is another measure of microporosity since the latter technique will estimate the surface area of pores under 15Å in diameter. A SynChropak GPC-100 sample gave 201 m<sup>2</sup>/g by the BET method and 216 m<sup>2</sup>/g by the t-curve method. The 15 m<sup>2</sup>/g difference is attributed to micropores less than 15Å. In contrast, 75Å pore diameter Glycophase CPG was found to have 137 m<sup>2</sup>/g of surface area by both the BET and t-curve methods indicating the absence of micropores.

Dead-end volume is estimated from mercury porosimetry by measuring the amount of mercury liberated from the packing when the applied pressure is released. This measurement approximates the volume occupied by blind channels or pockets within the interstitial and pore volumes. Assuming that the interstitial volume of the bed consists totally of blind channels, then the minimum percentage of dead-end volume within the pores of the packing is 61 and 47%, respectively, for the 100 and 1000Å

SynChropak materials. The minimum percentage of dead-end pores within the 4000Å SynChropak is 0%. Because of the much larger particle diameter of the CPG packings, one would expect that blind channels within the packed bed would be negligible. In view of this, the 75Å CPG packing would have a maximum of 38% of dead-end volume. The 1000 and 3000Å CPG packings have no dead-end pores. The implication of these findings in terms of column efficiency will be presented in a future paper (23).

Effect of Flow Rate on Elution Volume of D<sub>2</sub>O and Glucose. In order to rule out the possibility that the increased retention volume of D<sub>2</sub>O was caused by deuterium exchange on either residual silanol groups on the packing or hydroxyl groups on the glycerylpropylsilyl stationary phase, the elution volume of DHO was determined as a function of flow rate. As shown in Figure 1, there was no significant difference in elution volume when the flow rate was varied from 0.10 to 2.0 ml/min (23.4 to 1.2 minute residence time, respectively). For a control, the elution volume of glucose is also given. It should be emphasized that even if deuterium exchange were occurring, the resulting H<sub>2</sub>O molecules would not be detected. Furthermore, DHO peaks were symmetrical; the absence of a tailed peak is further confirmation that secondary equilibrium was not occurring.

Effect of D<sub>2</sub>O Concentration on Elution Volume. If deuterium exchange were occurring, one would also expect that the exchange equilibrium would be dependent on D<sub>2</sub>O concentration. In view of this, 0.625 to 10% D<sub>2</sub>O was injected and the resulting retention times and peak heights are shown in Table V. The results clearly demonstrate that there was no D<sub>2</sub>O concentration dependency of either retention volume or peak height.

TABLE V. EFFECT OF INJECTION CONCENTRATION ON PEAK HEIGHT AND RETENTION VOLUME OF D<sub>2</sub>O\*

D <sub>2</sub> O Concentration, %	V <sub>r</sub> , ml**	Height, cm**	DRI Attenuation
10	2.55	14.1	16
5	2.52	14.2	8
2.5	2.54	14.3	4
1.25	2.54	14.1	2
0.625	2.54	14.2	1

\* Chromatographic conditions: See Table II, 100Å column

\*\* Average of triplicate 20µl injections

6M Urea as the Mobile Phase. The only possible partitioning mechanism that could be responsible for D<sub>2</sub>O retention is hydrogen bonding to the glycerylpropylsilyl stationary phase which is highly unlikely because of competition between D<sub>2</sub>O and the H<sub>2</sub>O mobile phase. However, to rule this out, D<sub>2</sub>O and glucose were chromatographed in a 6M urea mobile phase using a 100Å column. The results, given in Table VI, are similar to the data obtained using water as the mobile phase (Table II), indicating that the urea mobile phase had no significant effect on elution volume of D<sub>2</sub>O.

It is of importance to note that it was difficult to prepare a 5% D<sub>2</sub>O solution in 6M urea so that the concentration of urea would be identical to that of the mobile phase. Because of the high urea content, a relatively small difference between the urea concentration in the injected solution and in the mobile phase, produced a urea peak. In view of this, the urea content of the injected solution was adjusted to minimize interference.

---

TABLE VI. ELUTION OF D<sub>2</sub>O IN 6M UREA\*

---

D <sub>2</sub> O, V <sub>r</sub> (ml)	2.59
Glucose, V <sub>r</sub> (ml)	2.32
Δ, ml	0.27
V <sub>i</sub> , ml	1.38
Micropore volume, %	19.3 ± 1.7

\* Chromatographic conditions: Flow: 1.0 ml/min; Chart speed: 2.5 in/min; 100Å Synchronapak column. See Table II for other conditions.

---

Effect of Temperature on Elution Volume. The heat of solution of a solute (ΔH) (heat loss when 1 mole of solute is transferred from the mobile phase to the stationary phase) is related to the partition coefficient (K) as follows:

$$\text{Log } K = \frac{-\Delta H}{2.30 RT} + C \quad (2)$$

Since  $K = k' V_M / V_S$  where  $k'$  is the capacity factor [ $k' = (t_r - t_0) / t_0$ ],  $t_r$  and  $t_0$  are the elution times of a retained and unretained peak, respectively,  $V_M$  is the volume of mobile phase,  $V_S$  is the volume of stationary phase and  $C$  is a constant, then

$$\text{Log } k' = \frac{-\Delta H}{2.30 RT} + C' \quad (3)$$

Thus,  $\Delta H$  can be readily determined by plotting  $\log k'$  versus  $1/T$ . If  $\Delta H$  is zero, there are no solute-packing interactions other than an entropic contribution (size separation).

Since, by definition,  $k' \geq 1$ , the retention time of glucose was used for  $t_0$  and the retention time of  $D_2O$  was used for  $t_r$ . The retention times of glucose and  $D_2O$  as a function of column temperature using a 300Å SynChropak column are in Table VII. As indicated, the percent difference in retention time between  $D_2O$  and glucose was about 4.5% for all temperatures. These results were close to the 5.2% difference obtained from Table II. The smaller value obtained in this study was probably caused by differences in the two lots of silica used in the columns.

TABLE VII. EFFECT OF COLUMN TEMPERATURE ON THE ELUTION TIME OF  $D_2O$  AND GLUCOSE USING A 300Å SYNCHROPAK COLUMN\*

Column Temp., °C	Pressure, psi	tr, min		Difference, %	k', $D_2O$
		Glucose	$D_2O$		
29	420	6.512	6.802	4.4	0.0445
39	348	6.496	6.776	4.3	0.0431
49	290	6.468	6.752	4.4	0.0439
60	246	6.436	6.732	4.6	0.0459
70	218	6.422	6.712	4.5	0.0451

\* Chromatographic conditions: Mobile phase:  $H_2O$ ; Flow: 0.5 ml/min; Chart Speed: 5 cm/min; Volume injected: 20 $\mu$ l; Sample concentrations: 1.3 mg/ml glucose and 5%  $D_2O$ ; Detector: RI X8; Column: 25cm x 4.6mm ID SynChropak 300Å.

The decrease in solute retention time with column temperature was caused in part by the expansion of mobile phase as it entered the heated column. For example, there was a 1.3-1.4% increase in flow rate when the temperature was increased from 29 to 70°C. The predicted value based on the expansion coefficient of water is 0.8%.

As shown in Table VII there appears to be no significant change of  $k'$  with respect to temperature. These data were plotted using Equation 3 and from linear regression analysis, the heat of solution was +0.18 Kcal/mole. Since  $\Delta H$  should be negative, this low value is obviously caused by experimental error. Furthermore, the  $\Delta H$  calculated from the standard error of the estimate ( $\pm 1$  standard deviation units) of the linear regression line is  $\pm 0.17$  Kcal/mole. Since  $\Delta H$  is zero or is very close to zero, Equation 3 reduces to

$$\log k' = C' \quad (4)$$

and the free energy change when DHO is transferred from the mobile phase to the stationary phase is of the form  $G=TS$ . Thus the retention time of  $D_2O$  is caused by entropic rather than enthalpic interactions with the packing. These results confirm that the existence of micropores must be responsible for the difference in elution volume between glucose and  $D_2O$ .

The effect of temperature on column efficiency is also shown in Figure 2. As expected, the number of theoretical plates generated by  $D_2O$  was significantly greater than for glucose because of its higher diffusion coefficient. The temperature dependency of glucose appears to be significantly greater than for  $D_2O$ . For example, a column temperature change from 29 to 70°C, results in a 50% increase in efficiency for glucose as compared to only 10% for  $D_2O$ . Since the relationship between temperature and diffusion coefficient is linear as predicted by the Wilke-Chang equation, one would expect a much higher plate count for  $D_2O$ . A possible explanation for these relatively low values for  $D_2O$  could be disruption of the packed column bed at elevated temperatures which would affect the narrower  $D_2O$  peak more than the glucose peak.

### Conclusions

From these studies with SynChropak SEC packings and controlled porosity glass, it is concluded that the silica packing contains a population of micropores which are differentially accessible to low molecular weight probes of total permeation volume. It is not known, however, if the microporosity in the 100 and 300Å SynChropak SEC packings is the result of the rather wide pore-size distribution and whether all silicas contain micropores.

The existence of micropores in a SEC packing and the fractionation of low molecular weight probes presents a dilemma as to what should be used as  $V_T$  in calculating  $K_D$  of high molecular weight species. It is recommended that the corresponding monomer (except in the case of proteins) be used when constructing a calibration curve for a given polymer. For example, in the case of cellulosics, glucose would be the low molecular weight calibrant of choice.  $D_2O$  is best used to determine column efficiency because of its sensitivity toward chromatographic peak broadening and extracolumn effects (23). However  $D_2O$  may still be used to estimate  $V_T$  in some cases.

In view of Freeman's studies on the use of normal alkanes and polystyrenes to probe the macroporosity of porous materials (24), the results presented here would suggest that low molecular weight species ranging from twenty (deuterium oxide) to several thousand daltons may be used to define microporosity of a SEC support. The ease with which this is achieved may allow routine examination of microporosity in new support materials and a more exact definition of total permeation volume in SEC.

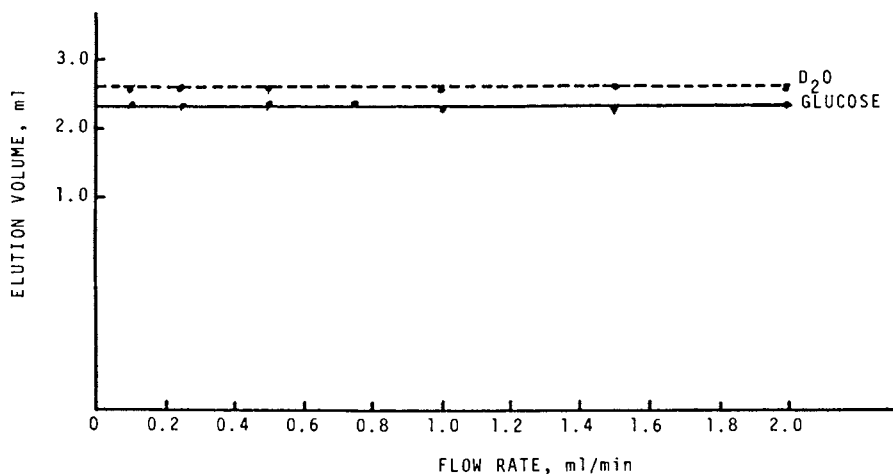


Figure 1. Influence of flow rate on elution volume of D<sub>2</sub>O and glucose. The column was a SynChropak 100Å column. See Table II for conditions.

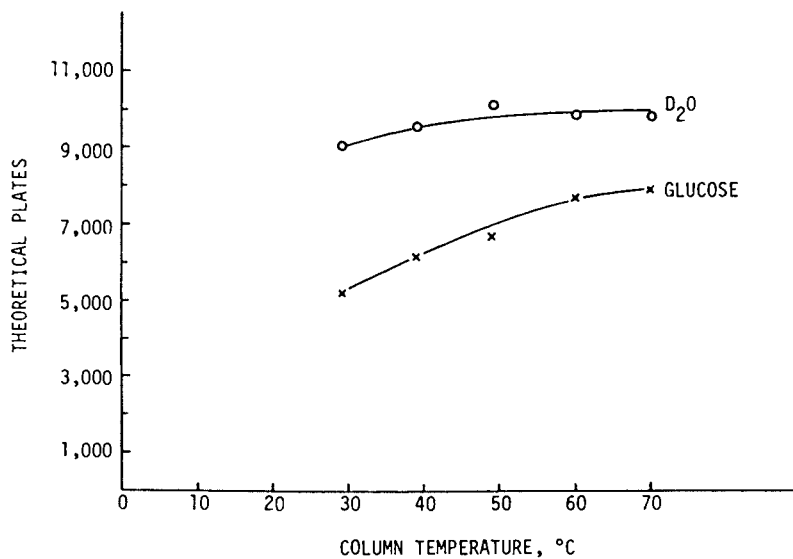


Figure 2. Influence of temperature on column efficiency using a SynChropak 300Å column. See Table VII for conditions.

### Acknowledgments

The helpful discussions with Walter J. Freeman and the excellent technical assistance of David Allen Smith are appreciated. We also thank James F. Carre for providing and interpreting the porosimetry and BET data.

### Literature Cited

1. Bio-Rad Laboratories "A Laboratory Manual on Gel Chromatography"; Richmond, CA, 1971.
2. Karch, K.; Sebestion, I.; Halasz, I.; Engelhardt, H. J. Chromatogr. 1976, 122, 171.
3. Rochas, C.; Domard, A.; Rinaudo, M. Eur. Polym. J. 1980, 16, 135.
4. Marsden, N.V.B. Ann. N. Y. Acad. Sci. 1965, 125, 428.
5. Yoza, N.; Ohashi, S. J. Chromatogr. 1969, 41, 429.
6. Ohashi, S.; Yoza, N. J. Chromatogr. 1966, 24, 300.
7. Obrink, B.; Laurent, T.C.; Rigler, R. J. Chromatogr. 1967, 31, 48.
8. Marsden, N.V.B. J. Chromatogr. 1971, 58, 304.
9. Barth, H.G.; Regnier, F.E. J. Chromatogr. 1980, 192, 275.
10. Barth, H.G. J. Liq. Chromatogr. 1980, 3, 1481.
11. Barth, H.G.; Smith, D.A. J. Chromatogr. 1981, 206, 410.
12. Neidhart, B.; Kringe, K.P.; Brockmann, W. J. Liq. Chromatogr. 1981, 4, 1875.
13. Grushka, E.; Colin, H.; Guiochon, G. J. Liq. Chromatogr. 1982, 5, 1391.
14. Neidhart, B.; Kringe, K.P.; Brockmann, W. J. Liq. Chromatogr. 1982, 5, 1395.
15. McCormick, R.M.; Karger, B.L. Anal. Chem. 1980, 52, 2249.
16. Berendsen, G.E.; Schoenmakers, P.J.; Galen L.D.; Vigh, G.; Puchory, Z.V.; Inczeczy, J. J. Liq. Chromatogr. 1980, 3, 1669.
17. Slaats, E.H.; Markovski, W.; Fekete, J.; Poppe, H. J. Chromatogr. 1981, 207, 299.
18. Kristulovic, A.M.; Colin, H.; Guiochon, G. Anal. Chem. 1982, 54, 2438.
19. Billet, H.A.H.; van Dalen, J.P.J.; Schoenmakers, P.J.; Galan, L.D. Anal. Chem. 1983, 55, 847.
20. Snyder, L.R.; Kirkland, J.J. "Introduction to Modern Liquid Chromatography"; J. Wiley and Sons: New York, 1979; p. 207.
21. Lippens, B.C.; Linsen, B.G.; de Boer, J.H. J. Catalysts 1964, 3, 32.
22. Unger, K.K. "Porous Silica"; Elsevier Scientific Publishing Co.: Amsterdam, 1979.
23. Barth, H.G., results to be published.
24. Freeman, D.H.; Poinescu, I.C. Anal. Chem. 1977, 49, 1183.

RECEIVED December 20, 1983



## Methylene Chloride-Hexafluoroisopropyl Alcohol (70/30)

### Use in High-Performance Gel Permeation Chromatography of Poly(ethylene terephthalate)

JAMES R. OVERTON and HORACE L. BROWNING, JR.

Research Laboratories, Eastman Chemicals Division, Eastman Kodak Company, Kingsport,  
TN 37662

The solvent system 70/30 methylene chloride/hexafluoroisopropanol has been in use in our laboratory since 1977 as a solvent for poly(ethylene terephthalate) (PET) and other semicrystalline polar polymers. Some advantages of this solvent are: it provides rapid room temperature solubilization; it is transparent at 254 nm (U.V.); it is a solvent for polystyrene; and it is a minimum boiling azeotrope. Disadvantages are its low boiling point (36°C) and the potential safety hazard it represents. The combination of appropriate HPGPC equipment and this solvent system reveals heretofore unrecognized features of the molecular weight distributions of polyesters.

Poly(ethylene terephthalate) (PET) has been analyzed by gel permeation chromatography (GPC) routinely for many years.<sup>(1-7)</sup> During this time, satisfactory results have been obtained with several solvent systems, the most common being *m*-cresol. The high viscosity of *m*-cresol requires that it be used at elevated temperatures, and the associated handling difficulty is sufficient reason for finding a replacement. This paper will present some of our experience with the solvent system 70/30 (v/v) methylene chloride (MeCl<sub>2</sub>)/hexafluoroisopropanol (HFIP). Some comments regarding the use of *m*-cresol are included.

0097-6156/84/0245-0219\$06.00/0  
© 1984 American Chemical Society

### Solvent System Properties

The ratio of 70/30 (v/v) MeCl<sub>2</sub>/HFIP was chosen because it is a minimum-boiling (37°C) azeotropic mixture. The exact composition can be reproduced by distillation from a mixture of approximately the correct ratio, and one can easily reclaim >90% of the solvent used by simple distillation. In view of the cost of HFIP the ability to reclaim solvent is an important consideration.

In a kinetic sense, the system is a better solvent than HFIP alone. We postulate that MeCl<sub>2</sub> swells the amorphous regions of PET thereby providing HFIP with an easy access to the crystalline regions. This swelling action does not occur with HFIP alone, and the dissolution process takes much longer. At room temperature, amorphous PET is instantaneously solubilized by this solvent system. PET that has been annealed for >24 hr at 220°C to yield maximum crystallinity dissolves in <4 hr at room temperature. PET annealed in this manner does not dissolve in pure HFIP after 14 days at room temperature. Poly(butylene terephthalate) and aliphatic polyamides are soluble in this solvent system. Polystyrene is also soluble, which permits conventional calibration and the use of the universal calibration approach. We have determined the Mark-Houwink relationships for PET and polystyrene in 70/30 MeCl<sub>2</sub>/HFIP to be

$$\left\{ \eta \right\}_{\text{PET}} = 4.034 \times 10^{-4} \bar{M}_w^{0.691}$$

$$\left\{ \eta \right\}_{\text{PSTY}} = 7.998 \times 10^{-4} \bar{M}_w^{0.54}$$

where  $\left\{ \eta \right\}$  is the inherent viscosity determined at 0.5 g/dl and 25°C.

The solvent system, which is transparent at 254 nm, permits the use of a UV detector system. This is a distinct advantage for high performance GPC where low sample loadings are necessary and refractive index detectors may provide only marginal sensitivity.

There are two disadvantages with this solvent system. First, the low boiling point (37°C) can lead to handling difficulty. We found it necessary to replace the Waters 6000A pump in the Waters Model 244 high performance liquid chromatograph (HPLC) with a Waters M45 pump to avoid an occasional interruption in flow which we assured to be caused by vapor lock. Second, there are health hazards associated with the use of HFIP, and hygienic laboratory procedures should be followed. The system should not be used prior to consulting the HFIP Product Information and Material Safety Data Sheet from Du Pont.

### Experimental

This work was done with a Waters Model 244 liquid chromatograph having two Du Pont Bimodal IIS columns (29,000 plates/meter) and a Linear dual-pen recorder. Also used was a Waters Model 440 UV absorbance detector. Samples were run at 0.1% (w/v) using an injection volume of 25- $\mu$ L and a flow rate of 1 mL/min. The system was calibrated with polystyrene standards from Pressure Chemical Co. according to the universal calibration procedure. Data collection and computation were done with an Intel 80/30 microprocessor.

### Results

A typical GPC curve for PET prepared by melt-phase polymerization is shown in Figure 1. The small peak on the low molecular weight side of the distribution is caused by the cyclic trimer of PET that is present at  $\sim 1.5$  wt % in melt-phase polymer.(8) A sample prepared by solid-phase polymerization is shown in Figure 2. This sample has a higher molecular weight than the melt phase sample, and the presence of cyclic tetramer and cyclic dimer, as well as the cyclic trimer, can be distinguished. The identities of these peaks were verified by spiking the samples with knowns. These features cannot be seen on chromatograms run on Styragel columns in m-cresol at 100°C because of inadequate resolution. Such a curve is shown in Figure 3. Solid-phase polymerization of PET reduces the cyclic oligomer content. This is because the polymer crystallizes to  $\sim 50\%$  during polymerization, with cyclics being excluded from the crystalline phase. The thermodynamic equilibrium concentration is then reestablished in the amorphous regions (during solid phase build up), and therefore, based on whole polymer, there is approximately a 50% reduction in cyclic oligomer content. Since cyclic oligomers (cyclic trimer) are known to cause processing difficulties, the determination of the cyclic trimer content of PET is often desirable. By monitoring the 0-2 v integrator output of the detector with the second pen of the dual-pen recorder, we can simultaneously generate a chromatogram at two sensitivities. This is illustrated in Figures 4 and 5. By taking the ratio of the cyclic trimer peak from the high-gain signal to the polymer peak from the normal signal, the cyclic trimer content of the sample can be calculated. The values calculated from Figures 4 and 5 are 1.5% and 0.8%, respectively.

The Waters Model 244 liquid chromatograph is not equipped with a thermostated oven and, therefore, operates at ambient temperature. We have observed some variations in flow rate due to laboratory temperature changes. Flow rate variations can be illustrated by comparing the cyclic trimer elution volume in

Figure 1. Melt-phase  
PET (a) cyclic trimer.

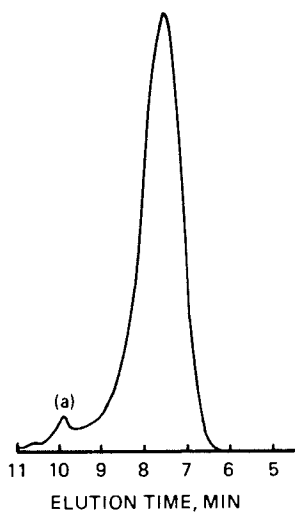
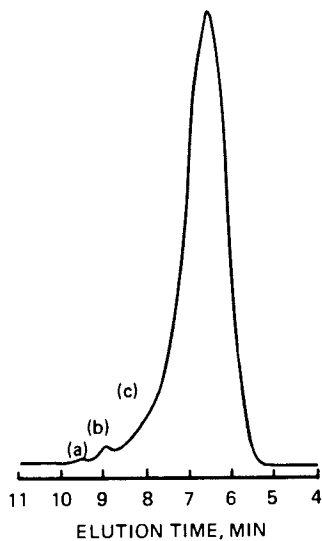


Figure 2. Solid-phase  
prepared PET, (a) cyclic  
dimer, (b) cyclic trimer,  
and (c) cyclic tetramer.



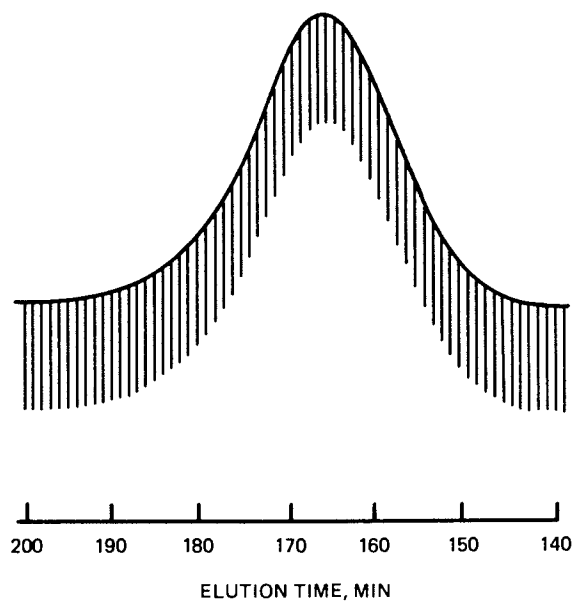


Figure 3. Melt-phase PET, *m*-Cresol, 100 °C.



Figure 4. Melt-phase PET run at two gains simultaneously (a) cyclic trimer.

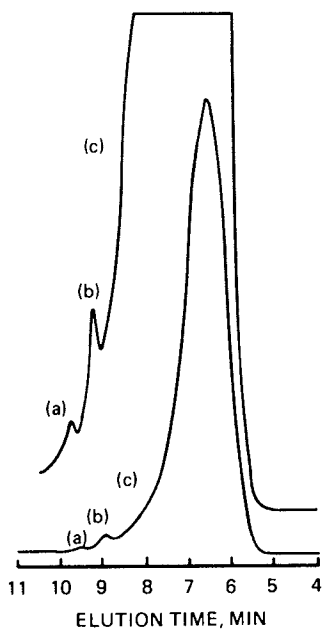


Figure 5. Solid-phase prepared PET, (a) cyclic dimer, (b) cyclic trimer, and (c) cyclic tetramer.

Figure 4 to that in Figure 5. Our computer software has been modified to allow for these changes by using the elution time of cyclic trimer as a measure of flow rate for a given run. The system is calibrated by using polystyrene spiked with cyclic trimer. For each run, elution volumes are normalized on the basis of cyclic trimer elution. This technique assumes constant flow rate during each run and compensates for run-to-run variations.

Distributions to date yield values of  $\bar{M}_w/\bar{M}_n > 2.0$ . The theoretical value of  $\bar{M}_w/\bar{M}_n$  and the often-quoted experimental value of 2.0 are only for linear species.<sup>(9)</sup> Consider the effect of 1.5% cyclic trimer (ignoring the low concentration of other cyclics) on the value of  $\bar{M}_w/\bar{M}_n$ . For  $\bar{M}_w = 40,000$ ,  $\bar{M}_n$  (linear) = 20,000. The presence of 1.5% cyclic trimer ( $M=576$ ) lowers  $M_n$  to 13,000 with essentially no effect on  $\bar{M}_w$  and  $\therefore \bar{M}_w/\bar{M}_n \approx 3$ . Because of the compact structure of the cyclic trimer it elutes later than the linear species of equivalent mass. The perceived mass of cyclic trimer by the GPC column is actually  $\sim 275$ . In the example cited, the presence of 1.5% of mass 275 lowers  $M_n$  to about 10,000 and  $\therefore \bar{M}_w/\bar{M}_n \approx 4$ .

Other workers have suggested that in a polar solvent such as *m*-cresol or hexafluoroisopropanol, PET will undergo rapid ester interchange leading to the "equilibrium distribution" having a ratio of  $\bar{M}_w/\bar{M}_n=2.0$ .<sup>(6, 7)</sup> These workers failed to recognize that the equilibrium distribution in a dilute solution is not the same as equilibrium distribution in the absence of a diluent.<sup>(10, 11, 12)</sup> In dilute solution, intramolecular ester interchange dominates, and the equilibrium distribution consists mostly of cyclic species. In our laboratory, we have been able to show under conditions where ester interchange does occur in solution that at a concentration of 1% polymer (w/v) the equilibrium distribution contains >75% cyclic trimer. The result of ester interchange in solution is, therefore, to broaden the distribution by the generation of cyclic species.

### Conclusions

The azeotrope 70/30 MeCl<sub>2</sub>/HFIP is an excellent solvent for PET and similar polymers, as well as for polystyrene. This combination, along with its UV transparency, makes it an excellent GPC solvent. The Du Pont Product Information and Material Safety Data Sheet on HFIP should be consulted before using this system.

Literature Cited

1. J. R. Overton, J. Rash, and L. D. Moore, Jr., Sixth International GPC Seminar Proceedings, Miami Beach, Florida October 7-8, 1968, p. 422.
2. G. Shaw, Seventh International GPC Seminar Proceedings, Monte Carlo, 1969, p. 309.
3. L. D. Moore, Jr., and J. R. Overton, J. Chromatogr., 55, 137 (1971).
4. Y. Ishida and K. Kawai, Shirnadzu Hyoron, 29112, 89 (1972).
5. J. R. Overton and S. K. Haynes J. Polym. Sci. Part C, 43 9 (1973).
6. E. E. Paschke, B. A. Bidlingmeyer, and J. G. Bergmann, J. Polym. Sci. Polym. Chem., 15 983 (1977).
7. M. Sang, N. Jin, and E. F. Jiang, J. Liq. Chromatog., 5 (9), 1665 (1982).
8. S. Jabarin and D. C. Balduff, J. Liq. Chromatog., 5 (10), 1825 (1982).
9. P. J. Flory, J. Chem. Phys., 12, 425 (1944).
10. H. L. Browning, Jr. and J. R. Overton, Polymer Prepr., 18 237 (1977).
11. H. Jacobson and W. H. Stockmayer, J. Chem. Phys. 87, 931, (1965).
12. H. Jacobson, C. D. Beckmann, and W. H. Stockmayer, J. Chem. Phys., 18, 1607 (1950).

RECEIVED October 20, 1983



## Shear Degradation of Very High Molecular Weight Polymers in Gel Permeation Chromatography

D. MCINTYRE, A. L. SHIH, J. SAVOCA, R. SEEGER, and A. MACARTHUR

Institute of Polymer Science, The University of Akron, Akron, OH 44325

The degradation of very high molecular polymers in GPC is demonstrated to occur in the gel columns, to begin at a critical molecular weight depending on the polymer structure, and to follow a power law dependence on MW after the onset of degradation. A loop model of entanglement is advanced to explain the degradation, and guidelines to minimize degradation are explicitly described.

An earlier experiment in these laboratories reported that very high molecular weight polystyrene (PS) was degraded in gel permeation chromatography (GPC) columns operating at relatively low pressures (125 psi) and low elution rates (1ml/min) (1). The degraded very high molecular weight polystyrene (MW  $44 \times 10^6$ ) was recovered from the eluent, and its molecular weight was determined by intrinsic viscosity measurements. The molecular weight of the original polymer,  $44 \times 10^6$ , had been decreased to  $19 \times 10^6$ . Thus the original polymer chain had on the average been cut to less than one-half its size in its passage through the GPC column. When the degraded molecular weight was used as the correct molecular weight, the degraded polymer nearly fit the GPC calibration curve of elution volume-molecular weight that had been established with much lower molecular weight polystyrenes. Since earlier work (2) had shown that a  $10 \times 10^6$  MW polystyrene did obey the GPC calibration curve, the onset of measurable degradation had to occur at a molecular weight greater than  $10 \times 10^6$ .

It seemed worthwhile to explore the generality of the earlier finding of chain degradation in PS at very high molecular weights, since the degradation only had been shown to occur with polystyrene in a given set of columns, using a conventional mechanical configuration, while operating at a low shear rate (or equivalently elution rate). Consequently, both the physical set-up of the GPC columns and the chemical structure of the chromatographically separated polymers were varied in this study. High molecular

0097-6156/84/0245-0227\$06.00/0

© 1984 American Chemical Society

weight polydimethylsiloxane (PDMS) and PS over a range of molecular weights were examined. Benzene was used as a solvent.

The flow rate and mechanical constrictions in the tubing were varied while attempting to measure degradation in the GPC. The change in flow rate is related to the pressure drop and therefore to the shear rate in the columns. The operating pressure was varied only over a narrow range (50 psi to 150 psi, or an equivalent flow rate of 1ml/min to 0.25 ml/min). Severe constrictions to the flow of liquids in the column occur in the 10  $\mu$ m fritted filter at both the inlet and the outlet of each packed column and also in the interstices of the packing in the column. Either of these constrictions might be the source of the shearing stresses for polymer degradation. Since a 44 million MW polystyrene has an unperturbed radius of gyration of 0.25 micron(3) and therefore would have some instantaneous chain segment end-to-end distances that would approach the size of some of the pores in the fritted filter, the effect of the filter on the degradation was carefully examined first.

PDMS was chosen to determine if polymers other than polystyrene degrade during GPC analyses, and, if so, at what molecular weights. PDMS was chosen because it is an even more flexible chain and also has a large chemical difference in the chain backbone structure. Although the exact relation between chain flexibility, chain entanglements, and shear degradation is not well understood, these experiments use dilute polymer solutions so that the entanglements ought to be related to the characteristic parameter (or relative unperturbed size) of the single polymer chain. Consequently the degradation of high molecular weight PDMS in GPC columns ought to be different from the degradation of the less flexible and purely hydrocarbon backbone of PS. Also, it was felt that the PDMS backbone rupture would not involve a free radical mechanism and subsequent chain transfer reactions. These findings are particularly timely now because there has recently been speculation that there is extensive degradation of all polymer chains in the newer and faster, high-pressure GPC instruments(3,4). Other polymers with a greater range of flexibility were also studied.

### Experimental

**Polymers** - The PS, PDMS, polyhexylisocyanate (PHIC), and polyisoprene (PI) samples had been extensively characterized to determine molecular weights, molecular sizes, and thermodynamic parameters (5, 6, 7). The samples were anionically polymerized using butyllithium as the initiator. The pertinent data are shown in Table I. Polyisobutylene/PIB polymers were obtained by fractionation of commercial polymers and their molecular weights were measured (8).

**Solvents**. Benzene - Baker, reagent grade; Cyclohexane - Matheson, Coleman and Bell (MCB), reagent grade; Tetrahydrofuran - Fisher Scientific, reagent grade.

Table I. Identification and Molecular Weight of Polymers

Polymer		$M_w$	Source
PS	13	$4.4 \times 10^7$	Ref. 5
	18	$2.72 \times 10^7$	
	11	$9.6 \times 10^6$	Waters Associates
	9	$4.5 \times 10^6$	
	25166	$4.11 \times 10^5$	
	61970	$2.6 \times 10^6$	
	25167	$8.67 \times 10^5$	
41995	$9.82 \times 10^4$		
PIB	B	$1.5 \times 10^6$	Ref. 8
	E	$1.2 \times 10^6$	
	F	$6.5 \times 10^5$	
	PIIA	$1.5 \times 10^5$	
PDMS	5-1	$2.0 \times 10^7$	Ref. 6
	5	$1.2 \times 10^7$	
	A	$6.8 \times 10^6$	
	B	$4.4 \times 10^6$	
	A-1	$1.46 \times 10^6$	
	A-2	$5.5 \times 10^6$	
PHIC	11	$4.24 \times 10^4$	Ref. 7
	22	$5.8 \times 10^4$	
	33	$1.33 \times 10^5$	
	44	$2.30 \times 10^5$	
	66	$1.31 \times 10^6$	
PI	2E7	$7.2 \times 10^6$	Ref. 7
	20M	$1.8 \times 10^6$	
	7E5	$7.6 \times 10^5$	

### GPC Instrument Operation

1. High Molecular Weight Polymers in Routine Degradation Experiments. Waters Associates Ana-Prep and 501 GPC were used for separation of high molecular weight PS, PDMS, PI, and PIB fractions. Five four-foot Styragel columns were connected in the following sequences (Set A) using a differential refractometer as the detector.

#### Set A

one:  $7 \times 10^5$  to  $5 \times 10^6 \overset{\circ}{\text{A}}$   
 one:  $7 \times 10^5$  to  $5 \times 10^6 \overset{\circ}{\text{A}}$   
 one:  $7 \times 10^5$  to  $5 \times 10^6 \overset{\circ}{\text{A}}$   
 one:  $1.5 \times 10^5$  to  $7 \times 10^5 \overset{\circ}{\text{A}}$   
 one:  $5 \times 10^4$  to  $1.5 \times 10^5 \overset{\circ}{\text{A}}$

The size designations are those given by Waters Associates. This set had a plate count of 680 PPF when o-dichlorobenzene was the solute. Samples were prepared on a weight-to-volume basis. Each sample was run at several different concentrations in the range of 0.05 - 0.2 g/dl in order to extrapolate the peak position to zero concentration. Full loop injections were used for all solutions. A 2.5 ml siphon was used at the elution end.

PS 13 and PS 18 were also run through Set A at a reduced flow rate of 0.5 ml/min and reduced concentration. No significant changes occurred in the peak position and in the shapes of the curves.

2. High Molecular Weight Polymers in Cyclohexane and also in Special Column Arrangements. Waters Associates Ana-Prep and 501 GPC were used. One four-foot Styragel column of  $5 \times 10^6$  pore size was connected to a pump and a differential refractometer detector to determine the effect of fritted discs on degradation.

Single columns of different pore size were used to determine the effect of gel pore size on degradation.

Single columns were used to determine the effect of solvent power on degradation.

Samples were prepared on a weight-to-volume basis. Full loop injections were used for all solutions, and polymer from the GPC eluent was recovered for characterization by taking all eluent solution 2 counts before and 2 counts after the polymer elution peak.

Viscosity Measurements. A Zimm-Couette type low shear viscometer was used. The intrinsic viscosities were estimated from single concentration viscosity measurements using the equations for the concentration dependence of the specific viscosity (5,6). The Mark-Houwink equation was used to determine  $M_v$  (5,6).

### Experimental Design

a) Measurement of Degradation. The experiments were carried out to elucidate the roles of both physical and chemical variables in

the GPC degradation of high molecular weight polymers to lower molecular weight polymers. Therefore, a measure of degradation had to be chosen that was independent of GPC. Although viscosity, light scattering, and sedimentation measurements of molecular weight have been made, only the viscosity measurements are reported here. Although the whole molecular weight distribution is desirable for analysis, only the single viscosity - average moment of the molecular weight distribution was determined. A simple measurement of degradation was determined as:

$$\% \text{ Degradation} = \% D = (100 - \% \text{ Decrease MW}) = 100 \left[ 1 - \frac{(\text{MW}) \text{ after GPC}}{(\text{MW}) \text{ before GPC}} \right]$$

b) Physical Variables. The effect of shear rate on degradation was evaluated by changing flow rates, pore size, packing geometry, column length, solution viscosity, and frits in the columns.

c) Chemical Variables. The effect of the backbone bond strengths and the flexibility of the polymeric chain was evaluated by studying the degradation of polymers of different backbone structures [ $\text{C-C}$ ], [ $\text{Si-O}$ ], of flexible polymers with different chain flexibilities at constant backbone structure [PIB, PS], and of rigid polymers [PHIC].

d) Physico-Chemical Effects. Polymer concentrations were kept low in order to reduce the solution viscosities and measure only the effect of the GPC on single polymer chains. At the highest MW's the concentrations were always <0.02%. Both poor and good solvents were used to decrease solution viscosities and in some cases enhance adsorption of the polymers to the packing.

## Results and Discussion

Physical Variables. Very dilute solutions of the PS and PDMS in a syringe were pushed through a 10  $\mu\text{m}$  fritted filter similar to the filter in the GPC columns. The relative viscosities of the filtered and unfiltered (original) solutions were determined in a low shear viscometer. The values of the relative viscosity are given in Table II. The data indicate that there is no degradation within the experimental error of  $\pm 2\%$ . In separate experiments a single Styragel column without the fritted filter at the inlet end was used to analyze the polymer in the conventional manner, but the eluent containing the polymer was collected and analyzed. The measured relative viscosities and the estimated intrinsic viscosities and molecular weights are given in Table III. Both the PS and PDMS of similar molecular weight have comparable degradation in the single GPC column. Degradation occurred even when the flow rate was reduced from 1 ml/min to 0.25 ml/min.

It is clear that the packed Styragel column is responsible for the degradation of the polymer. In all cases the pores of the packing are sufficiently large to accommodate portions of the

polymer chain, since the flow time of the PS and PDMS is longer than the time required for plug flow of solvent. Since the  $10 \times 10^6$  MW PS sample falls on the linear portion of the log MW - elution volume calibration curve, the degradation at even this high molecular weight cannot be greater than a few percent - which would be an acceptable level in many polymer characterization studies. Similarly the  $7 \times 10^6$  MW PDMS sample falls on its empirically established GPC calibration curve using low molecular weight samples. Since the radii of gyration of the PS and PDMS molecules used in these experiments are of comparable magnitude [ $3460\text{\AA}$  (PS),  $2750\text{\AA}$  (PDMS)], and since the molecular weights of the repeat units [ $104$  (PS),  $74$  (PDMS)] are not too different, it appears that a molecular weight of  $10 \times 10^6$  or a radius of gyration of  $2000\text{\AA}$  represents a limit for the reliable estimate of the molecular weight by GPC of a flexible polymer chain with stable main chain bonds like C-C or Si-O.

Table II. Relative Viscosities and ( $\eta_{rel}$ ) and Reduced Specific Viscosities ( $\eta_{sp}/c$ ) of Polymer Solutions Passed Through Fritted Filter ( $10\mu$ )

Polymer (MW)	Conc.(g/dl)	$\eta_{rel}$	$\eta_{sp}/c$ (dl/g)	$\langle S^2 \rangle^{1/2}$ ( $3460\text{\AA}$ )
<u>PS</u> ( $27 \times 10^6$ )				
unfiltered	0.024	2.159	47.3	
filtered	0.024	2.130	48.3	
<u>PDMS</u> ( $20 \times 10^6$ )				( $2750\text{\AA}$ )
unfiltered	0.030	1.631	21.0	
filtered	0.030	1.629	20.9	

Table III. Measured Relative and Reduced Viscosities. Estimated Molecular Weight, Intrinsic Viscosities of Polymers Passed Through GPC Columns in Benzene

Polymer (MW)	C(g/dl)	$\eta_{rel}$	$\eta_{sp}/C$	$[\eta]$ dl/g	$M_v$	%degradation
PS (27)	0.0074	1.182	24.6	23.1	$17 \times 10^6$	33 (see note)*
PDMS (20)	0.0077	1.111	14.4	13.8	$14 \times 10^6$	30

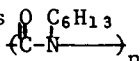
\*in THF, degradation of PS was also 33%

These experiments were made using benzene as a solvent. The earlier experiments (1) were made using THF, with an added antioxidant, as a solvent. Other experiments (2) had shown that THF without an antioxidant induced drastic degradation of PS solutions.

Earlier data on the GPC degradation of  $27 \times 10^6$  MW PS in THF were compared with the current data in benzene. The degradation

in both solvents is comparable. Consequently the degradation cannot be attributed to a solvent-induced degradation. This observation is reinforced by the new observation that both PDMS and PS have comparable chain degradation. If the degradation were to come from radicals generated in the solvent, then PDMS would degrade much less than PS.

PHIC was chromatographed with the same columns and solvents as PS and PDMS. The results of this experiment are shown in Table IV, and the comparison with earlier PS and PDMS results is summarized in the same table. The MW of PHIC did not change during the chromatographic separation with an experimental error of  $\pm 5\%$ . The composition of PHIC is  $\text{O C}_6\text{H}_{13}$  and the backbone is rigid.



Consequently, a relatively low molecular weight polymer ( $\text{MW}=1.39 \times 10^6$ ) has an intrinsic viscosity (25.6 dl/g) equivalent to a PS or PDMS more than 10x higher in MW. (Earlier GPC work on PBIC (9) and PHIC (7) had shown no deviations from the universal calibration curve for GPC at high molecular weights). The primary role of chain flexibility in GPC degradation rather than simple molecular hydrodynamic volume is conclusively shown by these results.

Table IV. Comparative Degradation of Stiff (PHIC) and Flexible Chains (PS, PDMS)

PHIC	$[\eta]$ dl/g	$M_v$ (g/mol)	
before GPC	25.6	$1.39 \times 10^6$	
after GPC	25.0 ( $\pm 5\%$ )	$1.32 \times 10^6$	
Comparison	MW	$[\eta]$ dl/g	%D
PS	$27 \times 10^6$	36	33
PDMS	$20 \times 10^6$	20.5	30
PHIC	$1.4 \times 10^6$	25.6	$\sim 0$ (<3%)

In order to evaluate the role of chain flexibility on GPC degradability when the backbone has a constant chemical structure, namely  $\langle \text{C}-\text{C} \rangle$ , high molecular weight PIB was chromatographed. Unfortunately the highest molecular weight fraction available had a molecular weight of  $3 \times 10^6$ . Nevertheless, the degradation at the highest MW was 25%, although there was no degradation at  $1.5 \times 10^6$  MW. These data are graphically shown in Figure 1 in which all of the data for PS, PDMS and PIB are shown. These PIB data are supported by the data of Huber and Lederer (3) on the GPC degradation of PIB using a different GPC experimental arrangement.

An unusual backbone structure occurs in polyisoprene (PI). The alternating single and double bonds,  $\langle \text{CH}_2-\text{C}(\text{CH}_3)=\text{CH}-\text{CH}_2 \rangle$ , can give rise to additional chemical enhancement of the primary degradation by free radical chain transfers and branching--even though the flexibility of the monomer segment is similar to PIB. The degradation is extensive in PI. For a seven-column set the

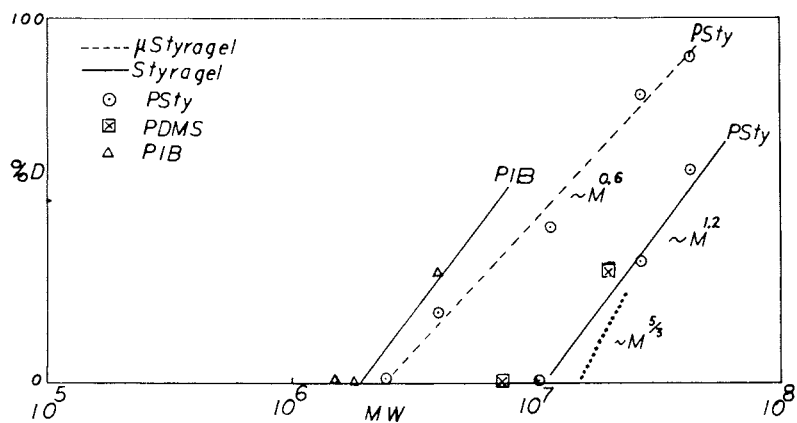


Figure 1. Per cent degradation (%D) as a function of Molecular Weight (MW) to determine onset of degradation (critical MW) and power law dependence of degradation on MW.



degradation begins below  $5 \times 10^5$  and is about 70% at  $10 \times 10^6$  MW. These data are being rerun under various experimental arrangements and will be reported in detail later. The significant fact is that the degradation begins at  $(2-5) \times 10^5$  MW and there is extensive degradation at low MW's. As a result PI can be used as a test-probe polymer to evaluate the physical variables that affect degradation by enhancing the primary degradation and therefore the detection capability.

GPC degradation of polymers has been shown in four polymeric systems using Styragel packing. Chain flexibility is an important parameter. The degradation appears to occur in the column packing and not in the frit, although no attempt was made to change the injection loop plumbing. Work is planned to evaluate the effect of the shear stresses in the injection loop. The following investigations were carried out to discover those variables in a given GPC set-up that might lessen the degradation and lead to practical ways to minimize the degradation for routine analyses.

It is possible to alter the pore size, packing swelling, and bead size of Styragel type packing by using different porosities, different solvents (swelling and non-swelling), and Styragel and  $\mu$ -Styragel. Although the experiments were not exhaustive, they attempted to sort out the variables in a rough manner. PI was used to magnify the effect with the realization that the chemical degradation is not simple in PI. Tables V, VI, and VII present the scope of the survey of physical variables.

Table V. Effect of Pore Size on GPC Degradation

Polystyrene

<u>Expt'l conditions:</u>	<u>% Degradation</u>	
(Solvent: THF); (Styragel)	MW: $44 \times 10^6$	$27 \times 10^6$
a) 6-col., large pores (no $10^3$ col.)	58	33
b) 1-col., $10^3$ por.	86	78

Polyisoprene

<u>Expt'l conditions:</u>	<u>% Degradation</u>	
(Solvent: THF); (Styragel)	MW: $10 \times 10^6$	$3 \times 10^6$
a) 1-col ( $10^7$ )	18	15
b) 1-col ( $10^3$ )	37	21

From Table V it is an inescapable fact that a small pore enhances the degradation. For PS the 7-column set had no  $10^3$  pore-size column, and yet the whole extra battery of 6 higher pore-size columns degraded PS less than the one low pore-size column. The PI results are similarly illustrative. When just one low

pore-size column was used the degradation is twice that of the degradation with a large pore-size column.

Table VI. Effect of Gel Swellant on GPC Degradation

Polyisoprene

<u>Expt'l conditions:</u>	<u>% Degradation</u>
Solvent: (Styragel)	(MW: $1.8 \times 10^6$ )
Cyclohexane	69
THF	36

From Table VI the influence of swelling (THF) and non-swelling (cyclohexane) solvents on the GPC degradation is clear. A non-solvent for the packing enhances the degradation almost two-fold for PI. Obviously the better the gel swellant, the more likely the lessening of degradation. An explanation of this effect can only be reconciled to be the combination of two related factors. First, the non-swellant increases the surface adsorption of a chemically similar polymer solute and gel. Second, the bead pore will have a lower overall size in the non-swellant. Both of these factors would lead to increased degradation as discussed later, although a change of the texture of the pore surface might alter the dependence on the average pore size alone.

Finally Table VII demonstrates the effect of the bead size on the GPC degradation of polymers. The small bead size (10 $\mu$  vs 60 $\mu$ ) would decrease the interstitial volume. Unfortunately, the increased pressure also increases the shear rate so that both decreased interstitial volume and high shear rates occur simultaneously. However, it is clear that both the MW at the onset of degradation and the amount of degradation are higher. From an analytical chemist's viewpoint, lower pressures and larger interstitial volumes are to be preferred if the goal is to decrease systemic errors in the GPC analysis of high MW polymers. It is interesting to compare the results of Rooney and VerStrate (4) in which polystyrene of  $4 \times 10^6$  MW at a flow rate of 1ml/min showed a 40% degradation @ 135° in TCB with Showdex 800. The 22% degradation in Table VII, run at 1ml/min but with  $\mu$ -Styragel at 40°C, would be expected to be smaller than that at 135°C so that the difference between 22% and 40% is not unreasonable. Rooney and VerStrate also describe a strong dependence of degradation on flow rates. In the Styragel results described earlier in this paper, there is no apparent decrease in degradation when the flow rate is lowered from 1.0 to 0.25 ml/min. The dependence of degradation on concentration was not explicitly measured in this work because the lowest detectable concentrations were used. Comparative experiments at a fixed molecular weight were carried out at approximately the same composition. There is a rapid rise of the solution

viscosity of very high molecular weight polymers at low concentrations ( $\sim 0.1\%$  g/dl), called the entanglement region. Concentrations above this region must be avoided.

Table VII. Effect of Styragel Bead Size on GPC Degradation

<u>Polystyrene</u>	<u>% Degradation</u>	
	Styragel (R=60 $\mu$ ) (100 psi)	-Styragel (R=10 $\mu$ ) (1000 psi)
<u>Expt'l conditions:</u>		
MW		
Solvent: THF		
7-column set (Type A)		
40°C		
44x10 <sup>6</sup>	58	88
27	33	78
10	0	-
8	-	22

Recommended Analytical Procedure. A protocol to eliminate or at least minimize any systematic error in the GPC determination of high molecular weights would be:

1. Use concentrations well below the entanglement region and as low as can be detected.
2. Use the lowest possible flow speeds and pressures.
3. Use the largest interstitial volumes (large bead sizes).
4. Use swelling solvents.
5. Avoid low pore sizes.
6. Use the lowest injection speeds.
7. Avoid polymer - substrate adsorption.
8. Avoid, if possible, high temperatures or reactive solvents.

A Loop Entanglement Model Rationalization of GPC Chain Degradation. These experimental results suggest that there are large enough shear stresses in GPC columns to break the backbone chemical bonds of polymers. The large stresses on the chain likely occur because the fast moving solvent outside the pore and the slow moving solvent inside the pore causes a velocity gradient on a portion of the large flexible chain molecule which may have appreciable portions of its chain segments both inside and outside the pore. Since the equilibrium chain segment distribution at these high molecular weights would be expected to have appreciable loop entanglements, the shear stress due to the velocity gradient would cause a locking of the loops on the time scale required for the repositioning of the segments either totally inside or totally outside the pore of the gel. As a result the chain backbone is broken. If there were adsorption of segments in the interstitial passages, the same mechanism would lead to degradation. If the

shear field were sufficiently strong at any point in the apparatus, the degradation would occur whether or not there were pores or adsorption. But the mechanism would still involve a loop entanglement to concentrate the stress, unless the stress were given as a very short time impulse in which very short chain segments could not respond immediately. Consequently, it is conjectured that most flexible polymers will be degraded in GPC experiments if the polymer size is sufficiently large to allow considerable loop formation in the distribution of the chain segments.

The loop entanglement model has been discussed elsewhere (10-12). A brief pictorial representation of the "locking of loops" is given in Figure 2. The entangling of loops leads to the possible "locking of loops" when the tangle is under stress. Figure 2 illustrates three conditions for "locking". The degree of entangling depends on the number of loops,  $n_l$ . Since the number of loops depends on the length of the chain, the number of loops depends on a power of  $M$ . Let that power of  $M$  be  $M^{5/3}$  (10,12). As a pair-wise process the interacting of pairs to produce "locked" loops,  $n^*$ , depends on the square of the number of loops between two identical MW neighboring chains A and B. That is  $n^*$  is proportional to  $(n_l)_A (n_l)_B$ , or  $(n_l)^{10/3}$ . In Figure 2a the thin strand from B is locking the thick strands from A. In an adsorbed chain the "locking" is proportional to  $[(n_l)_A(\text{adsorbed wall sites})]$  for the molecule A in the GPC column as shown in Figure 2b. For interaction with polymer loops from the gel the "locking" is due to  $[(n_l)_A(n_l)_{\text{gel}}]$  as shown in Figure 2c. Since the number of adsorbing sites or the number of loops in the gel is a constant for a given GPC experiment, the "locking" is proportional to  $(n_l^{5/3})_A$  or  $M^{5/3}$ .

Of course the number of "locked" loops fundamentally depends not on the MW but on the number of statistically independent chain segments. The loops therefore depend on the chain flexibility or the characteristic parameter of Flory,  $C_\infty$ , and the degree of polymerization (DP). Thus a stiff chain like PHIC does not easily degrade, a flexible polymer like PS, ( $C_\infty \sim 10$ ), degrades less than PIB, ( $C_\infty \sim 6$ ). There ought to be a critical size (or MW) below which degradation in GPC does not occur. Figure 1 gives an indication of these critical values ( $M$ )<sub>GPC</sub>, where degradation in GPC first begins. Also the discussion of PI leads to a value of  $(M_c)_{\text{GPC}}$  in the region of  $(2-5 \times 10^5 \text{ g/mol})$ . The direct relationship between  $(M_c)_{\text{VISC}}$  and  $(M_c)_{\text{GPC}}$  is discussed elsewhere (12) and appears to be approximately  $(M_c)_{\text{VISC}}^2 \sim (M_c)_{\text{GPC}}$ .

As a consequence of this model it is qualitatively easy to anticipate when degradation will occur if  $(M_c)_{\text{VISC}}$  is known. That is,  $(M_c)_{\text{GPC}}$  is  $(M_c)_{\text{VISC}}^2$ . A rough dependence of degradation on  $M_{\text{exp}}^{1.2}$  or  $M_{\text{theo}}^{2.3}$  will not be far from the correct result for PS or PIB if  $(M_c)_{\text{GPC}}$  is estimated correctly. At high shear stresses the  $(M_c)_{\text{GPC}}$  for  $\mu$ -Styragel is lower and the power law dependence in  $M$  is lower ( $\sim M^{0.6}$ ). A more exact description of these phenomena is currently under investigation, theoretically and experimentally(15).

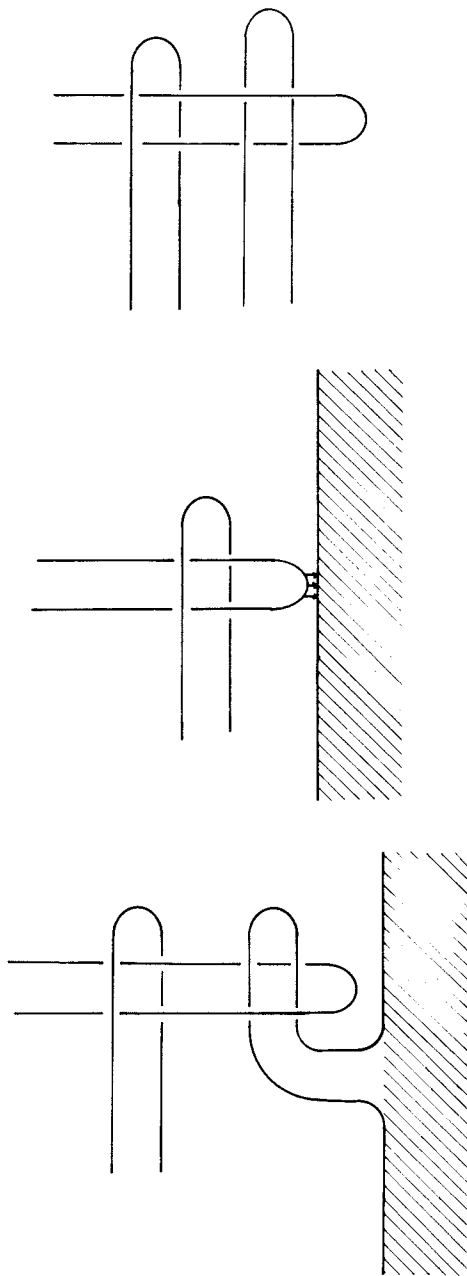


Figure 2. Loop entanglements that could lead to "locking" under stress: (a) locking of free loops; b) locking of loops by adsorption on substrates; c) locking of loops by interpenetration into loops on substrate.

Further experiments are in progress to locate the  $(M_c)_{GPC}$  for the onset of chain degradation in GPC and also to determine the quantitative relationships between flexibility, entanglement, and backbone bond strengths on the GPC degradation. However, it is clear in the experiments so far that no significant chain degradation occurs in saturated hydrocarbon polymers unless the molecular weights are 5-10 million. Therefore, most MW measurements on polymers less than  $(5-10) \times 10^6$  in MW can be safely carried out with a low pressure GPC apparatus, unless (1) the polymer is known from other observations to be especially susceptible to shear degradation, or (2) the MW's must be determined to accuracies better than 3%. But at very high molecular weights it is clear that the estimated GPC MW can easily be one-half or less that of the true MW. For unsaturated chains the secondary chemical reactions hasten the degradation as soon as the  $(M_c)_{GPC}$  threshold is passed.

Qualitatively all of the observed GPC degradation characteristics can be rationalized by the above loop model. Reasonable estimates of the onset of degradation in GPC can be made, and estimates of the percent degradation can be made cautiously.

#### Literature Cited

1. Slagowski, E.L.; Fetters, L.J.; McIntyre, D.; Macromol. 1974, 7, 394.
2. McIntyre, D.; Fetters, L. J.; Slagowski, E. L.; Science 1972, 176, 1042.
3. Huber, C.; Lederer, K. H.; Polymer Letters 18, 535 (1980).
4. Rooney, J. G.; VerStrate, G.; in "Liquid Chromatography of Polymers", Cazes, J., Ed.; Dekker, New York, 1981; p. 207.
5. Slagowski, E. L.; Ph.D. Thesis, The University of Akron (1972).
6. Shih, A. L.; Ph.D. Thesis, The University of Akron (1972).
7. Kuo, C. C.; Ph.D. Thesis, The University of Akron (1980).
8. Shih, A. L.; M.S. Thesis, The University of Akron (1968).
9. Ambler, M. R.; McIntyre, D.; Polymer Letters, 13, 589 (1975).
10. MacArthur, A.; M.S. Thesis, The University of Akron (1978).
11. MacArthur, A.; Stephens, H. L.; J. Appl. Polymer Sci., 1983, 28, 1561.
12. MacArthur, A.; McIntyre, D.; Rubber Division, Toronto, May (1983), Paper #7.
13. Flory, P. J.; "Statistical Mechanics of Chain Molecules"; Wiley: New York, 1968.
14. Ferry, J. S.; "Viscoelastic Properties of Polymers" (second ed.); Wiley: New York, 1970.
15. McIntyre, D.; MacArthur, A.; Polymer Preprints, 24, August 1983, p. 102.

RECEIVED October 13, 1983

## High-Efficiency Gel Permeation Chromatography Applications for the Analysis of Oligomers and Small Molecules

A. KRISHEN

Chemical Research and Development Division, The Goodyear Tire & Rubber Company,  
Akron, OH 44316

High efficiency columns currently available for gel permeation chromatography of small molecules and oligomers provide high speed separations. The use of multiple detectors provides additional information which facilitates characterization and determination of the separated species.

High efficiency gel permeation chromatography in the low molecular weight range is based on the same mechanism of separation as gel permeation chromatography for high molecular weight polymers. The solute components are selectively retarded according to the degree of their permeation into the solvent filled pores in the column packing. Larger molecules are excluded from the pores of the packing due to their physical size and thus elute before the smaller molecules. Beyond this similarity however, the resemblance between the two is minimal. Molecular weight distributions are the main concern for polymers while retention volumes and distinct separation of individual species are of importance in high-efficiency gel permeation chromatography in the low molecular weight range. This technique has greater similarity to both gas chromatography and high performance liquid chromatography than to gel permeation chromatography of polymers.

Gel permeation chromatography for small molecules is a relatively recent development in chromatographic techniques. In 1968 Hendrickson (1) predicted, "It appears likely that GPC for small molecules will become a new basic tool that could be called a liquid phase size spectrometer."

0097-6156/84/0245-0241\$06.00/0  
© 1984 American Chemical Society

### Advantages

In contrast to gas chromatography and other forms of liquid chromatography, gel permeation chromatography is applicable even when there are no differences in the solubility, polarity, adsorption, ionic characteristics or volatility of the molecules. Furthermore the following three characteristics of the technique are responsible for its increasing utility:

1. Separations are achieved with a single solvent.
2. Elution of all the components of a mixture normally takes place in a finite volume controlled by the column characteristics.
3. Additional important information on the size of the separated compounds can be obtained easily by comparison with known compounds having similar characteristics; furthermore the characterization of the separated compounds is facilitated by the use of multiple detection systems.

### Columns

The number of suppliers of the polymeric gels of the polystyrene-divinylbenzene type suitable for the analysis of small molecules has been increasing over the years. Packed columns - usually 30 cm x 8 mm i.d. or gels are currently available from many sources (2) although some of them sell only the packed columns.

Columns range in theoretical plate efficiency from 12,000 to 40,000 plates per meter as measured by chromatographing acetone at a flow rate of 1 ml per minute. The molecular weight range covered by each column depends on the pore size of the gel. It is quite common to use either a combination of columns of different pore sizes or columns with beds of mixed pore gels to obtain the desired range for the application at hand. A typical chromatogram obtained for a mixture of n-alkanes is shown in Figure 1. Alkanes of sufficient purity to serve as standards are available up to about  $C_{44}H_{90}$  (M.W. 618) and low molecular weight polystyrenes are useful as standards in the higher molecular weight range. Most of the columns provide sufficient resolution to separate the lower molecular weight polystyrene standard samples into their individual oligomeric components.



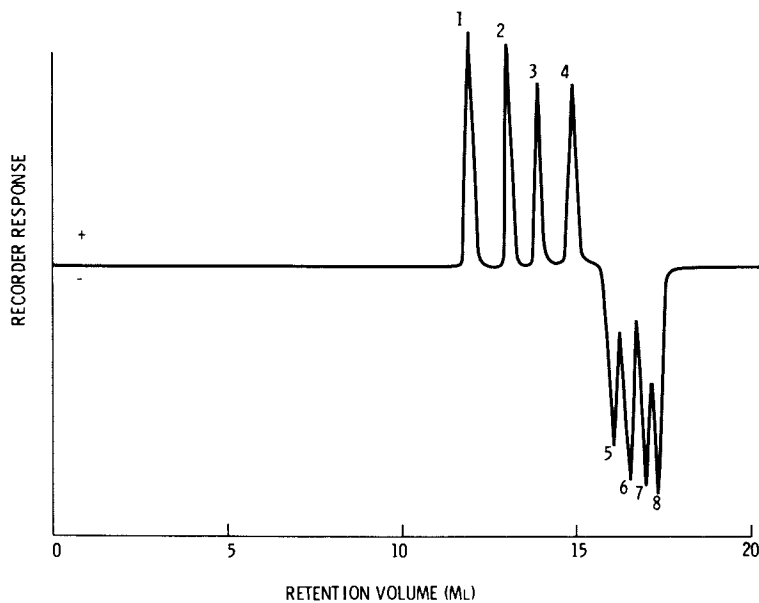


Figure 1. Gel permeation chromatogram of *n*-alkanes. Conditions: 610 mm x 8 mm TSKG 2000 H8 column; and tetrahydrofuran eluant at 0.5 mL/min. Key: 1,  $n\text{-C}_{36}\text{H}_{74}$ ; 2,  $n\text{-C}_{24}\text{H}_{50}$ ; 3,  $n\text{-C}_{18}\text{H}_{38}$ ; 4,  $n\text{-C}_{12}\text{H}_{26}$ ; 5,  $n\text{-C}_8\text{H}_{18}$ ; 6,  $n\text{-C}_7\text{H}_{16}$ ; 7,  $n\text{-C}_6\text{H}_{14}$ ; and 8,  $n\text{-C}_5\text{H}_{12}$ .

### Calculation of Molecular Sizes

The high efficiency columns separate individual components as distinct peaks similar to those obtained in gas chromatography. It has been recognized that the separation is predominantly based on the size that the molecule exhibits in the eluting solvent under the experimental conditions. Geometrical shape, molecular association and solvolysis due to hydrogen bonding are some of the factors which control the effective size of a molecule. Hendrickson and Moore (3) and Hendrickson (1) considered the chain length of a molecule as the controlling factor for the elution volume. The chain lengths of the molecules were calculated from the bond angles and atomic radii. n-Hydrocarbons were used as standards. Their chain lengths can also be calculated as follows:

Chain Length (Angstroms) =  $2.5 + (1.25 \times \text{Number of Carbons})$ .

The chain lengths of different molecules were then compared with the chain lengths of hydrocarbons to calculate the carbon number which relates the elution volume of the compound to the elution volume of a real or imaginary n-hydrocarbon. The "effective" carbon number for benzene based on its elution volume was experimentally found to be 2.85 - i.e. it eluted near the elution volume for propane which has a carbon number of 3.0 while the calculations based on bond angles and radii of atoms indicated that benzene would have a carbon number of 3.55. Thus corrections to the calculations for carbon number were required. These were derived from the experimentally observed elution behavior of various molecules.

Smith and Kollmansberger (4) introduced the concept of molar volumes as "fundamental in determining the degree of separation." Molar volumes were calculated for a number of compounds from their density and were expressed as ml/mol. Chang (5), Cazes and Gaskill (6,7) and Edwards and Ng (8) provided further understanding of the basic factors involved in the separation process in gel permeation chromatography. Lambert (9,10) combined the data from various investigators and attempted to recalculate the results for a large number of compounds on a common basis. The n-hydrocarbons were used as standards and their molar volumes were found to conform to the following equation

$$\text{Molar Volume (ml/mol at } 20^{\circ}\text{C)} = 33.02 + 16.18 \times (\text{CAU}) + 0.0041 \times (\text{CAU})^2$$

where CAU is the size of the hydrocarbon in carbon atom units. Lambert's (9,10) summary of the factors to be considered for predicting the elution volumes for small molecules in tetrahydrofuran pointed out the generalizations.

The elution volumes for n-hydrocarbons show a straight line relationship vs the logarithms of their molar volumes. Molar volumes, calculated from the densities of compounds other than n-hydrocarbons, must be modified to have the elution volumes of these compounds conform to the same calibration line (elution volume vs log molar volume) as that for the n-hydrocarbons. W. W. Schulz (11) related the elution behavior of branched alkanes in the range of C<sub>7</sub>-C<sub>11</sub> to the average numbers of gauche arrangements (Z<sub>g</sub>) which the molecule can assume.

The molecular weights of oligomeric species corresponding to chromatographic peaks and their identification are usually more useful than their molar volumes or their carbon numbers. The interpretation of experimental data can be simplified by using the logarithm of the molecular weights rather than the logarithms of molar volumes for standardization. Larson (12) indicated that the elution volumes for aliphatic hydrocarbons, aromatic hydrocarbons and aliphatic alcohols formed three different parallel straight lines when plotted against the logarithms of their molecular weights. These relationships are similar to those observed in gas chromatography for different homologous series. The line for the aromatic hydrocarbons was displaced higher than that for the n-alkanes, indicating that the "effective" molecular weight of the aromatic hydrocarbons was smaller than their actual molecular weight while the alcohols exhibited larger effective molecular weights due to their hydrogen bonding with the solvent, tetrahydrofuran.

We have recently reported (13) the use of this technique for characterization of various compounds. Experimental data obtained for a number of compounds are shown in Figure 2. We calculated the "size factors" for a number of small molecules and oligomers. This factor is a measure of the deviation of the elution volume of a given species from the calibration curve for n-alkanes which is assigned a size factor of 1. This size factor, F, is defined to be equal to A/M, where M is the molecular weight of the compound and A is the molecular weight of a real or hypothetical n-alkane which will elute at the same retention volume as the compound. Size factors for a number of

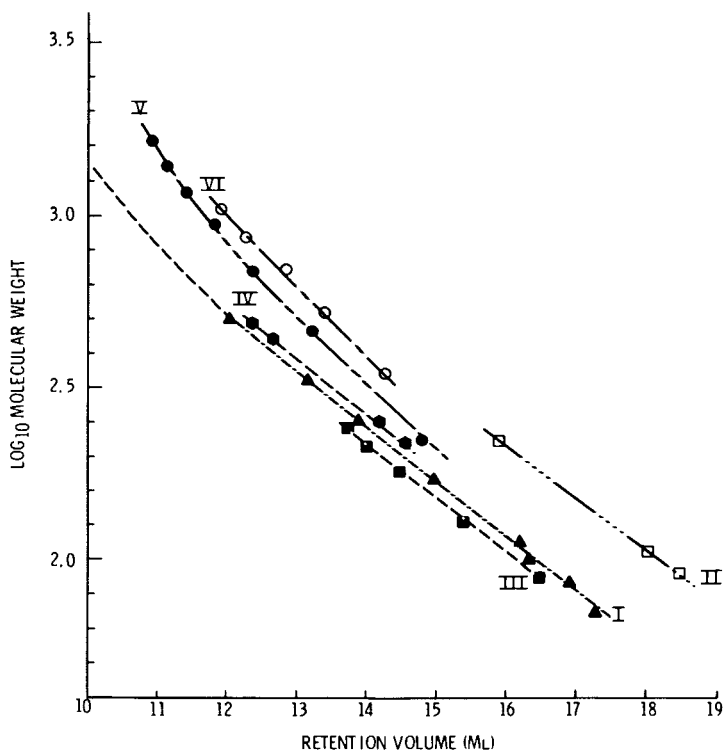


Figure 2. Molecular weight vs. retention volume relationships. Key: I, n-alkanes ( $C_5H_{12}$  to  $C_{36}H_{74}$ ); II, toluene, p-xylene, and diethylphthalate; III, n-alcohols ( $C_4H_9OH$  to  $C_{16}H_{33}OH$ ); IV, 2,6-di-tert-butyl-p-cresol, dibutyladipate, n-didecyl phthalate, and n-didodecyl phthalate; V, nonylphenol-formaldehyde adducts; and VI, TMDQ oligomers (dimer to hexamer).

compounds along with their molar volumes have been calculated (13).

### Applications:

While the mechanism of retention for various compounds can be only partially understood, the application of the technique provides much needed information for characterization of different types of materials. Some of these applications, including those requiring the use of multiple detectors, are presented here.

Phenol - Formaldehyde Resins. Oligomeric species produced by interlinking of phenolic molecules with  $-CH_2-$  moieties result in complex mixtures which cannot be resolved by gas chromatography. The GPC system provides ample information on the individual components for comparison of different batches of resins specially when a dual detector system consisting of a differential refractive index and a UV absorption detector (254 nm) is used (Figure 3). Each of the peaks observed in the chromatogram represents individual oligomers produced by addition of a monomeric unit consisting of the phenol and  $-CH_2-$  since a plot of the retention volume versus the logarithm of the molecular weight of the oligomers produces a straight line (Figure 1; V).

2,2,3-Trimethyl-1, 2-Dihydroquinoline. (TMDQ). The advantage of the GPC approach becomes evident when examining the chromatogram of TMDQ oligomers (Figure 4). This material is a common antioxidant made from the reaction of aniline and acetone and then polymerized. If the observed peaks are assigned the normal sequence - dimer, trimer, tetramer etc., the plot of the retention volume versus the logarithm of the molecular weights does not produce a smooth line. The peaks representing the normal oligomeric sequence can be selected by trial and error and then a different series of peaks is discovered where the oligomerization follows a different route. The characterization of this second series of peaks has been achieved by mass spectroscopy and reported by Lattimer et. al. (14).

Butylated p-Cresol-Dicyclopentadiene Product. A complex non-staining oligomeric antioxidant marketed by Goodyear as "Wingstay L" is the butylated reaction product of p-cresol and dicyclopentadiene. After trying various analytical techniques, we found that GPC provides the best approach for following the reaction

**American Chemical  
Society Library**

1155 16th St. N. W.

In Size Exclusion Chromatography: Provder, T.;  
Washington, D. C. 20036  
ACS Symposium Series 311, American Chemical Society, Washington, DC, 1984.

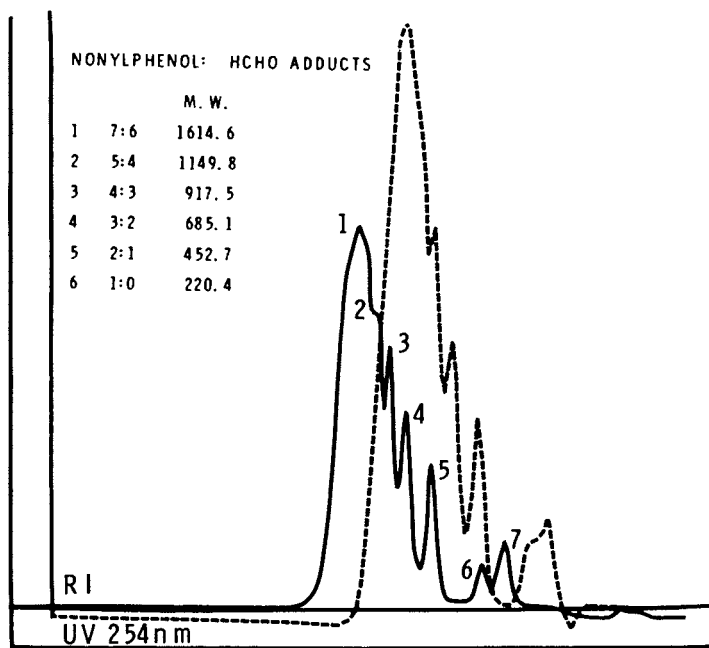


Figure 3. Gel permeation chromatogram of nonylphenol-formaldehyde adducts with dual detectors.

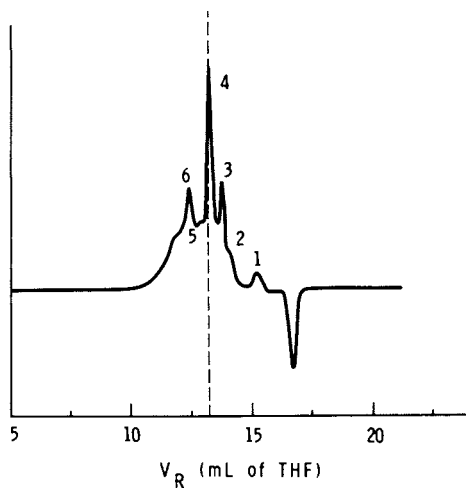


Figure 4. Gel permeation chromatogram of polymerized acetone-aniline condensation products. Key: 3,5- and 6-TMDQ oligomers; and 1,2- and 4-oligomeric series from a different addition route.

products. Both the unbutylated and butylated oligomers are well separated (Figure 5) and they all fall on a simple straight line when their retention volumes are plotted against the logarithm of their molecular weights. In this case both the differential refractive index and the UV 254 nm detectors provide essentially the same information.

Plasticizers. Some of the common plasticizers used for PVC applications consist of esters of phthalic acid, epoxidized soya oils and esters of dibasic alkyl acids. While gas chromatography can resolve some of the lower boiling materials, a complete analysis can be obtained by GPC using two detectors. When a complete characterization of the mixture of plasticizers is required, the use of a UV 254 nm and a differential refractive index detector is essential. While all the plasticizers including epoxidized oils respond in the RI detector, detection of esters with phthalate aromatic moieties is achieved with the UV 254 nm detector. In a recent problem where plasticizers were extracted from a polymer were being examined by GPC, we observed a peak corresponding to di-2-ethylhexyl phthalate. There was nothing unusual and the identification was confirmed by GC. A careful examination of the UV and RI responses, however, showed that the UV response was lower than expected. The UV/RI ratio for di-2-ethyl-hexyl-phthalate is about 2.0 but the sample peak gave a ratio of only about 1.0.

This information suggested the presence of an additional component co-eluting with di-2-ethylhexyl-phthalate. With the information at hand it was possible to surmise that this component had the following characteristics:

1. It had only minimal response in UV.
2. It had a molecular weight of about 400.
3. It was too high boiling for gas chromatography.

It was then possible to screen some possible candidates and come up with the probable presence of a chlorinated paraffin. This material was found to elute at the same retention volume as di-2-ethylhexyl-phthalate and showed no response at 254 nm (Figure 6). For quantitation UV/RI response ratio provided all the data required. However, in order to confirm the presence of this additional component, the sample was hydrolyzed and the acid converted to its dimethyl ester. The products were then examined by GPC. The UV response for the peak of interest was completely

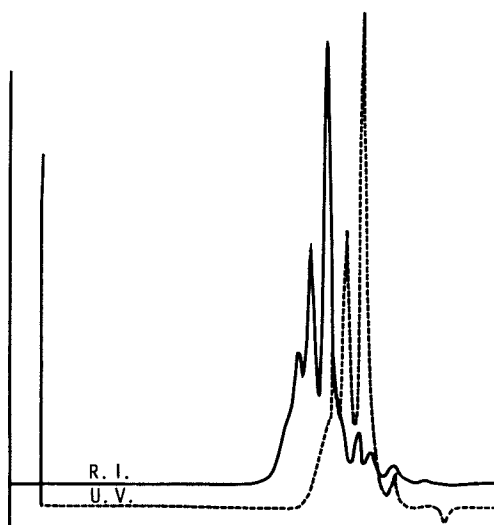


Figure 5. Gel permeation chromatogram of butylated p-cresol-dicyclopentadiene reaction products.



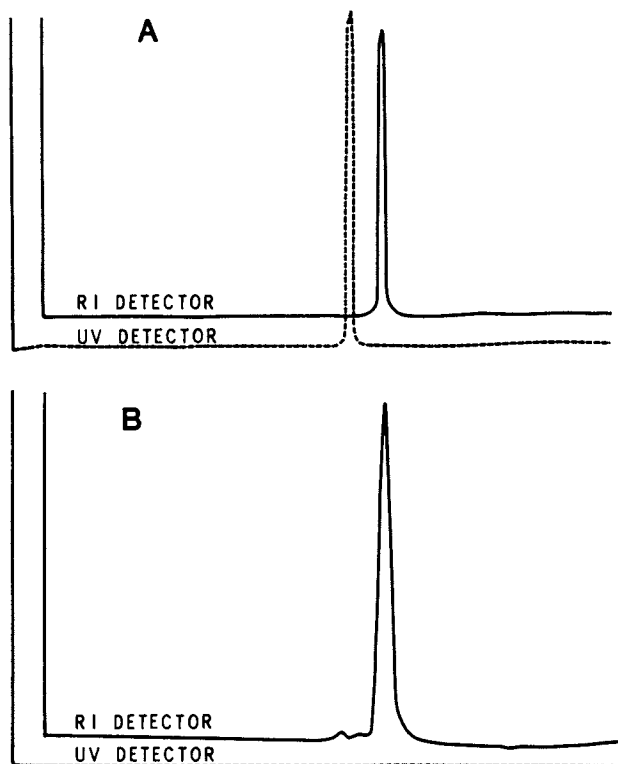


Figure 6. Gel permeation chromatograms with dual detectors. Key: A, di-2-ethylhexyl phthalate; and B, chlorinated paraffin.

eliminated but the RI response due to unhydrolyzable chlorinated paraffin was still there. The dimethyl ester of phthalic acid eluted later and showed the expected UV response.

Quinones and Hydroquinones. In the analysis of quinones and hydroquinones, the use of two different dual detector systems was required. The retention data for hydroquinones shows the normal behavior of hydroxyl groups associating with the solvent, THF. Thus octyl quinone and hydroquinone elute almost together. Similarly dioctylquinone and octyl hydroquinone elute together (Figure 7). The UV/RI response ratio for benzoquinone is 3.75. Hydroquinone and dioctylquinone show similar disparities in the UV/RI responses. This information provides a very good method for detecting impurities in dioctyl hydroquinone.

The reverse problem of detecting hydroquinone impurities in quinones requires the use of an electrochemical detector. The hydroquinones are oxidized at 1.2V to quinones to give very strong responses. The quinones have no response in this detector.

Poly Chlorinated Biphenyls. The photoconductivity detector provides good responses for polychlorinated biphenyls separated by GPC. The normal matrix components are detected by RI and UV detectors while the polychlorinated species show high responses in the electrochemical detector (Figure 8).

A comprehensive listing of the applications of this technique in the coatings industry has been presented in recent publications (15,16).

### Conclusions

High-efficiency gel permeation chromatography offers a very useful technique for the characterization and analysis of oligomers and small molecules particularly when multiple detector systems are used.

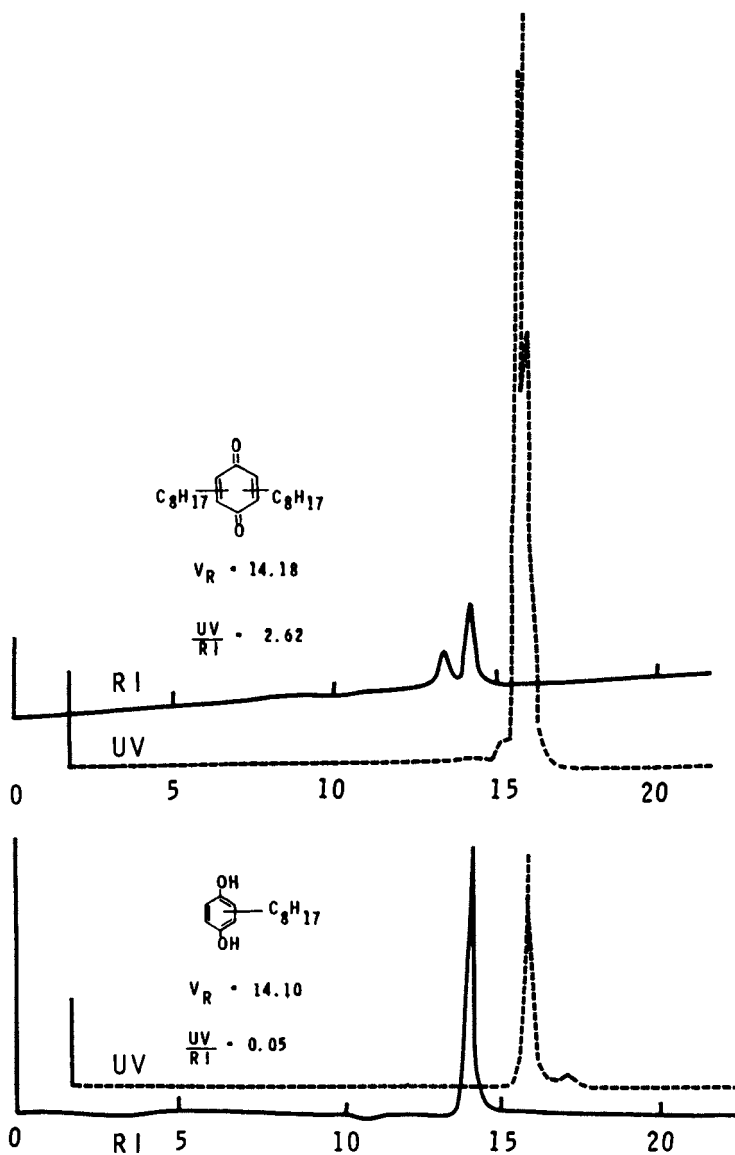


Figure 7. Gel permeation chromatograms with dual detectors. Key: top, dioctyl quinone; and bottom, octyl hydroquinone.

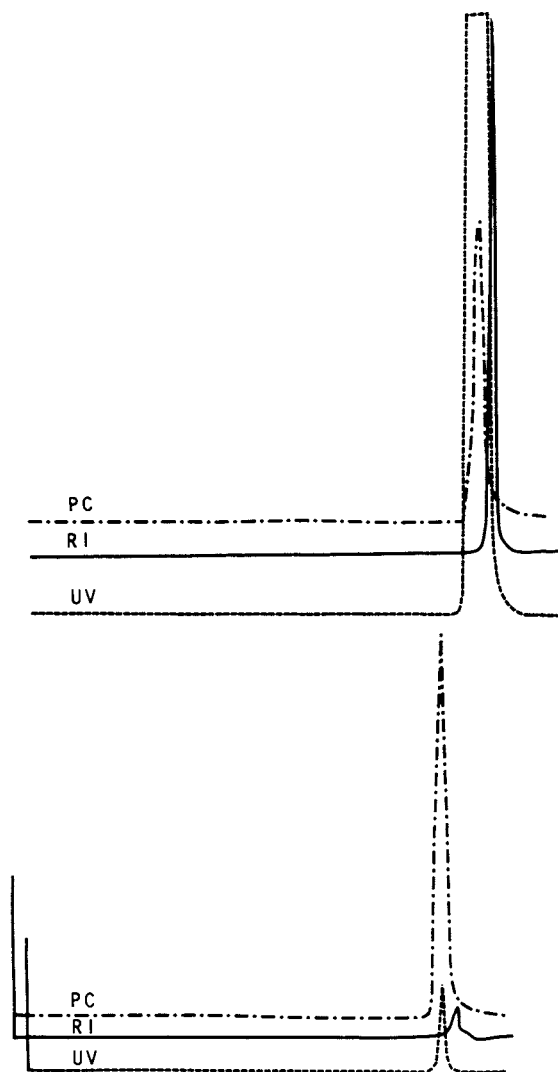


Figure 8. Gel permeation chromatograms with refractive index, UV 254, and photoconductivity detectors. Key: top, p-chlorobiphenyl; and bottom, decachlorobiphenyl.

Acknowledgment

The permission of The Goodyear Tire & Rubber Company to publish this paper is gratefully appreciated.

Literature Cited

1. Hendrickson, J. G., Anal. Chem. 40: 49-53 (1968)
2. Majors, R. E. J., Chromatog. Sci. 18: 488-511 (1980).
3. Hendrickson, J. G. and Moore, J. C., J. Polym. Sci. Part A-1 4:167-88 (1966).
4. Smith, W. B. and Kollmansberger, K., J. Phys. Chem. 69: 4157-61 (1965).
5. Chang, Teh-Liang, Anal. Chim. Acta. 39: 519-21 (1967).
6. Cazes, J. and Gaskill, D. R., Sep. Sci. 2: 421-30 (1967).
7. Cazes, J and Gaskill, D. R., Sep. Sci. 4: 15-24 (1969)
8. Edwards, G. D., and Ng, Q. Y., J. Polym. Sci. Part C. 21: 105-17 (1968).
9. Lambert, A., J. Appl. Chem. 20: 305-306 (1970).
10. Lambert, A, Anal. Chim. Acta. 53: 63-72 (1971).
11. Schulz, W. W., J. Chromatog. 55: 73-81 (1971).
12. Larsen, F. N., App. Polym. Symp. 8: 111-24 (1969)
13. Krishen, A. and Tucker, R. G., Anal. Chem. 49: 898-902 (1977).
14. Lattimer, R. P., Hooser, E. R., and Zakriski, P. M. Rubber Chem. Technol. 53: 346-356 (1980)
15. Kuo, C., and Provder, T. ACS Symposium Series, No. 138: 207-224 (1980).
16. Kuo, C., Provder, T., and Kah, A. F., Paint & Resin, March/April 1983: 26-33.

RECEIVED October 13, 1983

# Analysis of Petroleum Crude and Distillates by Gel Permeation Chromatography

C. V. PHILIP and RAYFORD G. ANTHONY

Kinetics, Catalysis and Reaction Engineering Laboratory, Department of Chemical Engineering, Texas A&M University, College Station, TX 77843

The currently available high efficiency columns with 5 micron size polystyrene/divinylbenzene copolymer packing, have extended the capability of size exclusion chromatography for the separation of smaller molecular size species in addition to the large polymeric species. Petroleum crude and its refinery products are composed of both larger and smaller molecular components (asphaltenes and distillates). Gel permeation chromatography (GPC) using a 100A PL Gel column and tetrahydrofuran (THF) separates petroleum crude or the refinery product into fractions containing different chemical species such as nonvolatiles (asphaltenes), long chain alkanes and aromatics. GPCs of petroleum crude as well as its distillation cuts are used to illustrate the use of GPC for the analysis of petroleum crude and its refinery products.

Currently most refineries are capable of processing different petroleum crudes and can increase the yield of the selected products on demand. The composition of the crudes varies depending on factors such as geographical origin, the well location and depth. Certain ASTM specifications such as API gravity, viscosity, distillation temperatures, and flash point are generally used for the evaluations of crude as well as its refinery products. A number of studies have reported certain physical and chemical properties of refinery products (1-5). It appears that the ASTM specifications, some of them are a few decades old, are both time consuming to obtain as well as not adequate enough to guide the crude through the refinery process to obtain optimum production of desired distillation cuts. Thus, other analytical tools to characterize both the crude and its refinery products are needed.

0097-6156/84/0245-0257\$06.00/0  
© 1984 American Chemical Society

Gel permeation chromatography (GPC) has been extensively used for molecular size determinations of large molecular weight species such as polymers (6), coal liquids (7-14), and petroleum asphaltenes (15,16,17). GPC data on a number of compounds such as straight-chain alkanes, amines, alcohols, multi-ring aromatics, etc. (7) show that the retention volume is mainly a function of the length of the molecule rather than molecular volume, molecular weight or any other molecular size parameter. The steady increase in the retention volumes of large straight-chain alkanes suggests that they exist in the solution in a stretched state rather than in a coiled state. It is appropriate to say that GPC separations are mostly on the basis of linear molecular size rather than any other molecular size parameter. Longer molecules elute faster than shorter molecules because longer molecules are less likely to diffuse into the liquid trapped inside the pores. The retention volume  $V_t$  in a GPC column is given by the equation:

$$V_t = V_i + KV_p \quad (1)$$

where:  $V_i$  = the column interstitial volume;  $V_p$  = the total pore volume; and  $K$  = the partition coefficient, the ratio of the accessible pore volume to the total pore volume. All solutes elute between  $V_i$  and  $V_i + V_p$ . For most gel columns the value of the ratio of  $V_i$  to  $V_p$  is in the order of 1 to 1.3. Consequently the total number of peaks that can be resolved by GPC is limited compared to other modes of liquid chromatography. Some molecules are too large for pores of the column and they are eluted without separation at  $V_i$  (total size exclusion) and some other molecules are too small and they elute at  $V_i + V_p$  (total permeation). By selecting the correct pore size for the molecular size distribution of species in the sample, the resolution of peaks can be increased. Compared to other modes of liquid chromatography relatively larger samples can be separated, without significant loss in resolution. The new columns packed with 5 micron particles have increased the theoretical plate counts (manufacturers claims 40,000 plates/meter) significantly and hence analysis can be accomplished in 10-25 minutes depending on column size and flow rates.

Linear Molecular Sizes from Valence-Bond Structures. In the absence of any interactions between solute and solvent such as hydrogen bonding between solute and solvent molecules resulting in a larger molecular size, and any interactions between solute and gel particles such as adsorption which is the basis for liquid chromatography, the molecular length can be obtained from the valence bond structures. Figure 1 illustrates the fact that rigid molecules such as aromatics are expected to have smaller linear molecular sizes, and consequently, larger retention

volumes than straight-chain hydrocarbons of similar molecular weight.

"Effective" Linear Molecular Size in Solutions. When THF is used as the mobile liquid phase, certain species can form hydrogen bonds with THF effectively producing a complex molecule which exhibits a greater linear molecular size (Figure 2) and lower retention volume. When non-polar solvents such as toluene are used, the molecular size is essentially unaffected. Phenol forms hydrogen bonds with THF (Figure 3) resulting in a 1:1 complex and an increase in effective linear molecular size. GPC is widely used for the size separation as well as for the molecular weight distribution of typical polymers. Since molecular length is the main basis for the GPC separation and the fact that the solute size can increase in certain solvents, GPC achieves class separation of species which normally have similar molecular sizes, in some complex mixtures (8,14). Use of GPC for separation of coal liquids into fractions enriched with distinct class of chemical species such as aromatics, phenols, asphaltenes mixed with alkanes, is discussed elsewhere (14).

### Experimental

Samples of crude oil and refinery products used in this study were obtained from commercial as well as from local sources. The GPC separations were performed on a Waters Associates Model ALC/GPC 202 liquid chromatograph equipped with a refractometer (Model R401). A Valco valve injector was used to load about 50 microliter samples into the column. A 5 micron size 100A PL gel column (7.5 mm ID, 600 mm long) was used in this study. Reagent grade tetrahydrofuran (THF) which was refluxed and distilled with sodium wire in a nitrogen atmosphere, was used as the GPC carrier solvent. Flow rate was 1 ml per minute. THF was stored under dry nitrogen, and all separations were conducted in a nitrogen atmosphere to prevent the formation of peroxides.

Straight chain alkanes from Applied Science, aromatics from Fisher Scientific Company and polystyrene standards from Waters Associates were used without purification for the linear molecular size calibration of the GPC. Since the solubility of the larger alkanes in THF is very low, approximately 0.2 -1 mg of each standard was dissolved in 50 microliters of the THF for the molecular size calibrations.

The samples of crude and distillate for GPC analysis were prepared by dissolving the sample in dry additive-free THF to obtain a 25% solution and the solution was filtered through micro-pore filters (Millipore, 0.5 micrometer size). A solution containing both the calibration standard and the sample was used to determine the molecular size distribution of the sample.



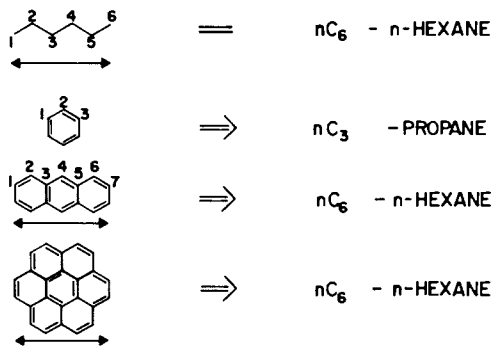


Figure 1. Linear molecules size in straight-chain alkane carbon units with comparable aromatic structures (Fuel, 1982) (14).

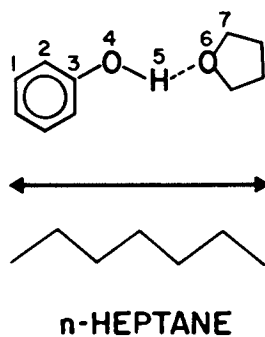


Figure 2. Phenol-THF Complex (Fuel 1982) (14).

### Results and Discussions

The separation of coal liquids by gel permeation chromatography using 100A Styragel columns and solvents such as THF and toluene has been reported elsewhere (7,8,9,13,14). Coal liquids and petroleum crude are similar in their physical appearance as well as the complexity in composition. The major difference between the two is that petroleum crude does not contain oxygenated compounds, such as alkylated phenols, in substantial quantity. In addition, the average linear molecular size of petroleum derived asphaltenes (15,16) is much larger than that of coal derived asphaltenes (9).

Linear Molecular Size: The Best Available Basis for the GPC Separation. The elution pattern of the GPC using 5 micron 100A PL gel column is illustrated in Figure 4 where the GPC separation of a standard mixture containing straight chain alkanes and aromatics is shown. The polystyrene standard (mol. wt. 2350 and chain length 57A) gave a broad peak at 11 ml retention volume. The peak position is marked in the figure rather than using the polystyrene standard in the mixture in order to save the  $nC_{44}H_{80}$  peak from the enveloping effect of the broad polystyrene peak. The retention volume of several aliphatic and aromatic compounds in THF and toluene have been reported (7). It is clear that aromatic compounds, as expected from their valence bond structures, have smaller linear molecular sizes compared to n-alkanes of similar molecular weight. It is expected that most of the condensed ring aromatics such as naphthalene, anthracene and even big ones like coronene (seven fused rings with molecular weight of 300.4) are smaller than n-hexane (14) and hence have retention volumes larger than that of n-hexane.

The Effect of "Aromatic" Gel on the Size Separation of Aromatic Species. Certain aromatics such as anthracene, benzopyrene and coronene produce GPC separation patterns which deviate from what is expected from their molecular lengths. All aromatic species have a slightly shorter effective molecular length compared to their valence bond structures. Although anthracene is about the size of n-hexane, it has a retention volume close to that of n-butane. Benzopyrene (five fused rings) has a retention volume equivalent to propane. The retention volume of coronene (Figure 1) shows that its effective size is slightly smaller than that of propane. This type of anomalous behavior is expected for a limited number of compounds due to their structures associated with extreme aromaticity. The GPC columns are packed with swelled polymer particles of controlled pore size formed by the co-polymerization of styrene and divinylbenzene. Every other carbon atom on the polymer chain has a phenyl group freely hanging. The species with aromatic structures can interact with the phenyl groups of the polymer chains of the gel. The inter-

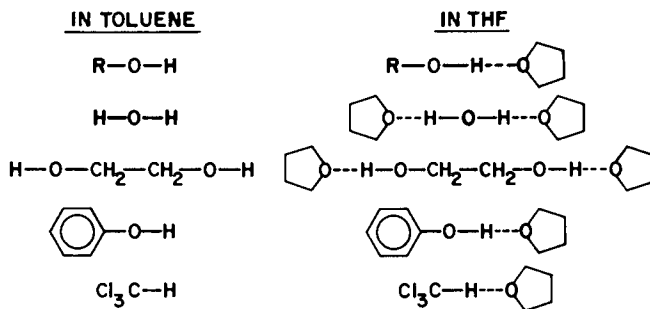


Figure 3. Effect of solvent on the effective linear sizes of molecules in solution (Fuel 1982) (14).

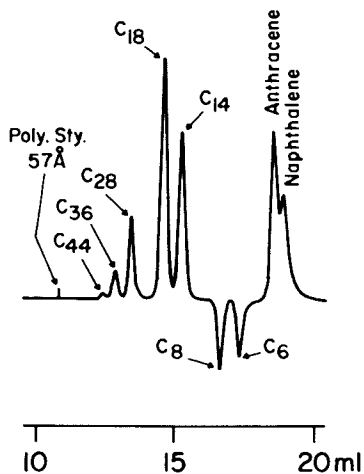


Figure 4. Calibration of GPC retention volume using known compounds.

action between gel particles and the aromatic species can increase the retention volume slightly which may indicate smaller "effective" molecular length. For samples containing species with non-uniform structures, the molecular parameter which can be predicted from the GPC separation pattern is molecular length.

Based on elution volume, the polystyrene standard with a size of 57A appears to be larger than expected from the alkane standard. The large number of phenyl groups on the main polymer chain (57A) make the molecule into a large cylindrical structure with a large steric hinderance for getting through the pores of the gel. The two terminal phenyl groups also contribute to an increase in chain length. The polystyrene peak (57A) is very close to the total exclusion limit of the 100A PL gel column.

Petroleum crude and its refinery products have two major component based on distillation. The portion that can be distilled under refinery conditions can be called volatiles and the nondistillables are the nonvolatiles. The volatiles can be analyzed by GC or GC-MS. The crude has both components. The distillate as the names applied, such as naphtha and kerosene contain only volatiles. When GPC is used for analyzing various distillates, the fractions separated by GPC can be characterized by GC or GC-MS. These data can be used to verify the nature of components present in various distillation cuts as a function of GPC elution volume. If the samples such as crude contains both volatiles as well as nonvolatiles, the samples should be separated into volatiles and nonvolatiles. The GPC of both components should be used to calibrate the GPC of the total crude. The parameter that can be obtained from GPC is effective molecular length. It can be used to relate other molecular parameters of interest after calibration.

The GPC of a local crude (Bryan, Texas) sample spiked with a known mixture of n-alkanes and aromatics is shown in Figure 5 and the GPC of the crude is shown in Figure 6. The hydrocarbon mixture is used to calibrate the length of the species which separates as a function of retention volume. The molecular length is expressed as n-alkane carbon units although n-alkanes represent only a fraction of the hydrocarbons in the crude. In addition to n-alkanes, petroleum crude is composed of major classes of hydrocarbons such as branched and cyclic alkanes, branched and cyclic olefins and various aromatics and nonvolatiles namely asphaltenes. Almost all of the known aromatics without side chains elute after n-hexane ( $C_6$ ). If the aromatics have long side chains, the linear molecular size increases and the retention volume is reduced. Cyclic alkanes have retention volumes similar to those of aromatics. GPC separates crude on the basis of linear molecular size and the species are spread over 10 to 20 ml retention volume range and almost all of the species are smaller than the polystyrene standard (57A). In other words, the crude has very little asphaltenes. The linear

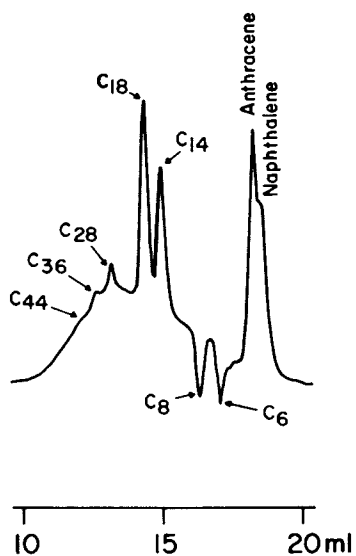


Figure 5. GPC of petroleum crude spiked with known compounds.

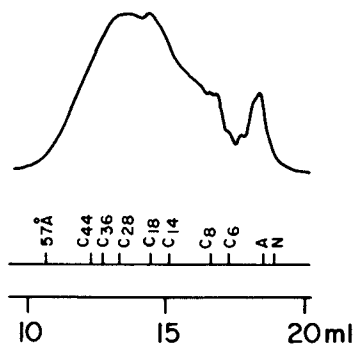


Figure 6. The separation of petroleum crude by GPC.

molecular size distribution of petroleum asphaltene ranges from 50 to 500A with a peak at 100A on the basis of polystyrene standard (15). The bulk of the crude is composed of species with molecular size smaller than that of n-tetradecane ( $nC_{14}H_{30}$ ). The crude contains a small fraction of aromatics, which is the last peak and has retention volume of 18 ml.

The GPCs of refinery products are shown in Figures 7 to 12. The retention volume, as well as the linear molecular size expressed in n-alkane carbon units are marked in these figures. The refinery products picked for illustrative purpose represent a wide range of distillation cuts as well as nonvolatiles (road asphalt). The commercial grade naphtha (Figure 7) and regular leaded gasoline (Figure 8) have a similar molecular size range, however, regular gasoline has slightly more long molecules. The aromatic regions of the two GPCs may include cyclic alkanes and cyclic olefins in addition to aromatics. Because of the low distillation temperatures of the two, the heavy aromatics are not expected.

GPC of charcoal lighter fluid (Figure 9) shows the increase in the linear molecular size of the cut similar to the ASTM distillation pattern. Lubricating oils are narrower cuts.

The GPC of three oils are shown in Figures 10 and 11. Transmission oil (Dextron II) has a GPC with peaks at  $n-C_{16}H_{34}$  with a small amount of polymeric additive which separates from the bulk of the oil as a shoulder before the polystyrene mark (57 A). Figure 11 shows the GPCs of two motor oils. Single weight SAE 30 W motor oil has a GPC with a peak at  $n-C_{24}H_{50}$  with no peaks due to the polymeric species showing the absence of such additives. The multiviscosity motor oil SAE 10-30 W has a GPC peak at  $n-C_{17}H_{36}$  and a small peak due to added polymeric species. The multiviscosity oil is prepared by adding polymeric additives which make it behave like heavy weight oil at higher temperatures. All these lubricating oils represent narrow distillation cuts from refineries, and it is interesting to note that they have GPCs showing a linear molecular size distribution similar to their distillation temperature distributions or molecular weight distributions. It could be interpreted that these lubricating oils are composed of very similar hydrocarbon species.

The road asphalt used in this study was obtained from the road as a fresh sample. The road asphalt is composed of asphaltenes (GPC peak at 100A and petroleum residual oils (15) (GPC peak at  $n-C_{40}H_{82}$ ). The GPC of road asphalt is shown in Figure 9. Since petroleum asphaltenes cannot be separated by a 100A pore size gel column, the asphaltene appears without any separation at the total size exclusion limit of the column. But the nonasphaltene components are separated showing a peak at  $n-C_{40}H_{82}$ . The performance of the road asphalt depends on the asphaltene content as well as on the molecular size distribution of the nonasphaltenic fraction.

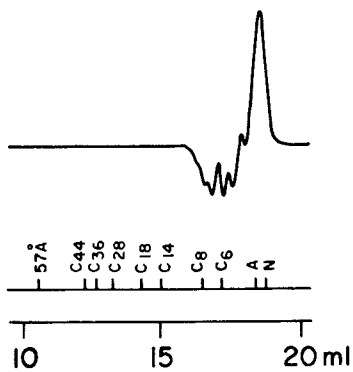


Figure 7. GPC of naphtha.

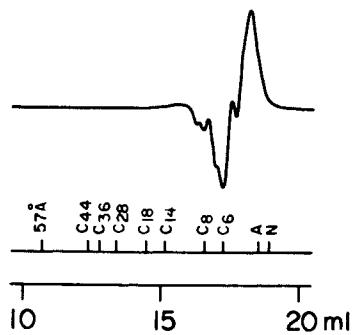


Figure 8. GPC of regular gasoline.

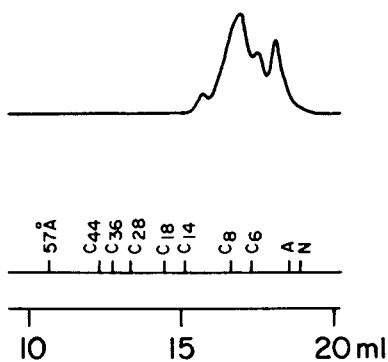


Figure 9. GPC of charcoal lighter.

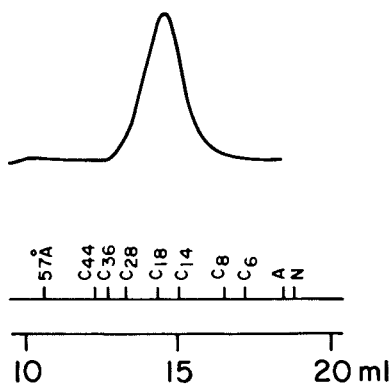


Figure 10. GPC of transmission oil.



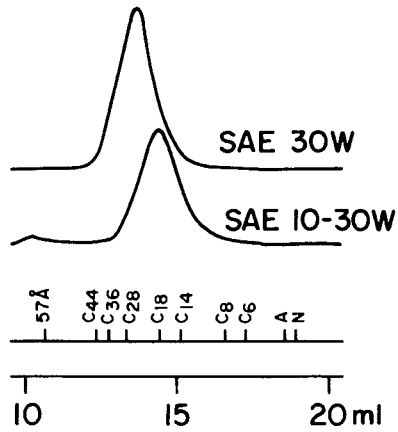


Figure 11. GPC of motor oils a) SAE 30W, b) SAE 10-30W.

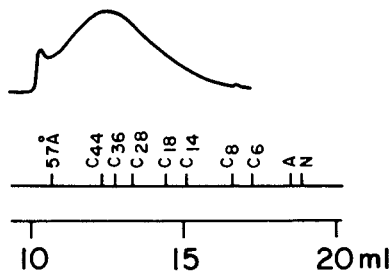


Figure 12. GPC of road asphalt.

### Conclusions

Recently available 5 micron columns such as PL gel columns have increased the efficiency of GPC separations. A single 67 cm column packed with 5 micron size 100A PL gel can separate both petroleum crude as well as its refinery products in about 20 minutes consuming about 20 ml of THF. Currently used ASTM specification, especially the most widely used ASTM distillation temperature specifications can be complemented or even substituted by simpler GPC analysis. By comparing the GPC of the crude (Figure 3) with GPCs of various distillation cuts (Figures 4-9) the prediction of the quality of the crude as well as its likely conversion into various cuts could be feasible. The hydrocarbon species eluting at various retention volumes can be identified by the established techniques such as Fourier Transform Nuclear Magnetic Resonance Spectroscopy (FT NMR). The GPC determines the molecular length; FT NMR can continuously monitor effluents for its chemical nature. By using GPC with the appropriate combination of detectors, a very precise evaluation of petroleum crude and predictions of product yield, as well as suitable processing conditions appears to be feasible.

### Acknowledgments

The financial support of the Texas Engineering Experiment Station and the Texas A&M University Center for Energy and Mineral Resources is very much appreciated. The authors are grateful to Dr. Jerry A. Bullin for helpful suggestions.

### Literature Cited

1. Dice, M. J. "Approximate Calorific Value of California Fuel Oil," Chem. Metal Eng. 1926, 8, 499.
2. Geniesse, J. C. "A Comparison of Viscosity-Index Proposals," A.S.T.M. Bulletin 1956, 7, 81-84.
3. Kryiacopoulos, G. B. "Viscosity Index of Lube Oil Blends," Scien. Lubrication 1962, 5, 27.
4. Kryiacopoulos, G. B. "Blending Oil for Viscosity Index," Hydrocarbon Proc. 1975, 9, 137-138.
5. Woodle, R. A. "Figures Solvent Extract of Heavy Oils," Hydrocarbon Proc. 1966, 45, 133-136.
6. Snyder, R. L.; Kirkland, J. J. "Introduction to Modern Liquid Chromatography"; John Wiley and Sons, Inc., New York, 1974.
7. Philip, C. V.; Anthony, R. G. Am. Chem. Soc. Div. Fuel Chem. Preprints 1979, 24, (3), 204.
8. Philip, C. V.; Zingaro, R. A.; Anthony, R. G. Am. Chem. Soc. Fuel Chem. Preprints 1980, 25, (1), 47.

9. Philip, C. V.; Zingaro, R. A.; Anthony, R. G. in "Upgrading of Coal Liquids"; Sullivan, R. F., Ed.; ACS SYMPOSIUM SERIES No. 156, American Chemical Society: Washington, D.C., 1981; p. 239.
10. Farnum, S. A.; Olson, E. S.; Farnum, B. W.; Willson, W. G. Am. Chem. Soc. Div. Fuel Chem. Preprints 1980, 25 245.
11. Philip, C. V.; Anthony, R. G. Am. Chem. Soc. Div. Fuel Chem. Preprints 1977, 22, (5), 31.
12. Philip, C. V.; Anthony, R. G. in "Organic Chemistry of Coal"; Larsen, J. W., Ed.; American Chemical Society: Washington, D.C., 1978; p. 258.
13. Philip, C. V.; Anthony, R. G. Fuel 1982, 61, 351.
14. Philip, C. V.; Anthony, R. G. Fuel 1982, 61, 357.
15. Philip, C. V.; Bullin, J. A.; Anthony, R. G. "Separation of Heavy Fuel Oils by Gel Permeation Chromatography"; submitted for publication.
16. Long, R. B. in "Chemistry of Asphaltenes"; Bunger, J. W.; Li, N. C., Eds.; ADVANCES IN CHEMISTRY SERIES No. 195, American Chemical Society: Washington, D.C., 1981; p. 17.
17. Hall, G.; Herron, S. P. "Chemistry of Asphaltenes"; Bunger, J. W.; Li, N. C., Eds.; ADVANCES IN CHEMISTRY SERIES No. 195, American Chemical Society: Washington, D.C., 1982; p. 137.

RECEIVED October 13, 1983

# High-Temperature Size Exclusion Chromatography of Polyethylene

V. GRINSHPUN, K. F. O'DRISCOLL, and A. RUDIN

Guelph Waterloo Centre for Graduate Work in Chemistry, University of Waterloo, Waterloo, Ontario, Canada, N2L 3G1

The use of dilute polymer solutions for molecular weight measurements requires the macromolecules to be in a true solution, i.e., dispersed on a molecular level. This state may not be realized in certain instances because stable, multimolecular aggregates may persist under the conditions of "solution" preparation. In such cases, a dynamic equilibrium between clustered and isolated polymer molecules is not expected to be approached and the concentration and size of aggregates are little affected by the overall solute concentration. A pronounced effect of the thermal history of the solution is often noted under such conditions.

Stable aggregates have been shown to present a problem in the characterization of polyvinyl chloride (1,2) and it has been suggested that residues of crystalline structures may persist in polyethylene solutions at temperatures below the polymer's crystalline melting point (3-5).

This paper shows the need and describes a method for eliminating aggregates in solutions of polyethylene. In doing so we have developed a simple technique for establishing when polymer solutions are molecularly dispersed. This research is directed toward Size Exclusion Chromatography (SEC) measurements, but low angle laser light scattering (LALLS) has been the primary tool for assessing the quality of the solutions studied.

## Experimental

A Chromatix KMX-16 laser differential refractometer and a KMX-6 LALLS photometer attached to a Waters 150C high temperature gel permeation chromatograph were employed in this work. However, since we were only interested in establishing solution quality, no columns were used in the 150C; only its pump, and automatic injector being employed. Samples of polyethylene solutions, prepared as described below, were injected into the SEC unit at 145°C and their light scattering properties measured as they flowed through the KMX-6, also at 145°C. The KMX-6 was used at

0097-6156/84/0245-0273\$06.00/0  
© 1984 American Chemical Society

an angle of 6-7° with a 0.15 mm field stop to minimize background. The lasers in both the Chromatix light scattering photometer and differential refractometer operate at 632.8 nm. The KMX-6 has a heated flow cell and a heated, insulated tube through which the sample flows from the liquid chromatograph.

The samples investigated initially were commercial high pressure low density, linear low density and high density polyethylenes and had properties given in Table 1. Solutions of these polymers were prepared in concentrations of 0.8 to 3.5 g/l by dissolving the polymer over a time period of two hours in an oven maintained at 145°C. To avoid degradation 0.05% 4,4'-thiobis(3-methyl-6-tert-butyl phenol) was used as an anti-oxidant in the solutions.

A second set of solutions were prepared from aliquots of the first solutions by subjecting them to a further thermal treatment of 160°C for 1 hour in an oven.

All solutions were filtered through a 0.5 µm Fluoropore poly(tetrafluorethylene) filter (FHUP, Millipore Corp.). The solvents trichlorobenzene (TCB), o-dichlorobenzene (ODCB) and α-chloronaphthalene (αCN) were used as received without further purification.

Refractive index increments (dn/dc) were measured using the Chromatix KMX-16 differential refractometer and its heated cell at 145°C; the values obtained are given in Table II. Refractive index increments are essentially identical for all the polyethylene types in a given solvent.

### Results and Discussion

Figure 1A shows a typical observation of the LALLS for a polymer solution prepared at 145°C. The many spikes are evidence of aggregates which have survived the "solution" preparation and filtering. Heating this solution to 160°C for 1 hour removed almost all traces of large scatterers (Fig. 1B). This is circumstantial evidence for the elimination of supermolecular aggregates. The procedure described below shows quantitatively that such entities have indeed been removed. It also provides a criterion for determining if a particular solution history has provided aggregate-free mixtures.

This is made possible by considering the second virial coefficients of polymers in the various solvents after different solution histories. The second virial coefficient,  $A_2$ , can be determined experimentally from the expression

$$\frac{Kc}{R_\theta} = \frac{1}{M_w} + 2A_2c \quad (1)$$

where  $c$  is the solution concentration,  $K$  is the polymer optical constant and is a function of  $dn/dc$ , and  $R_\theta$  is the

Table I. Polyethylene Sample Properties

Designation	Type	Melt Index (g/10 min)	Density (g/ml)
A	High Density	0.25	0.951
B	High Pressure Low Density	0.80	0.921
C	Linear Low Density	1.0	0.920

Table II. Refractive Index Increments (ml/g)

Polymer	Solvent		
	TCB	ODCB	$\alpha$ CN
A	-.112	-.056	-.189
B	-.108	-.051	-.185
C	-.106	-.048	-.180

excess Rayleigh scattering of the solution over the solvent as measured by the maximum of the ordinate in Figure 1, not considering the pikes, and  $\bar{M}_w$  is the weight average molecular weight.

If the average molecular weight of the sample is known its second virial coefficient can be predicted using the Kok-Rudin method (6). Input parameters for this calculation are  $\bar{M}_w$ , obtained from LALLS data according to Equation 1, and the Mark-Houwink constants for the polymer in the particular solvent and under Theta conditions. The Mark-Houwink constants used in these calculations are listed in Table III.

The existence of aggregates is evidenced by virial coefficients which are lower than the theoretical values, for the measured  $\bar{M}_w$ . This is because the second virial coefficient decreases with increasing molecular weight. Supermolecular aggregates appear to have very high effective molecular weights.  $\bar{M}_w$  is relatively little affected by such aggregates in the concentrations at which they seem to be present. Higher averages are changed, however, and so is the light scattering second virial coefficient of the solution.

Experimental and theoretical values of  $A_2$  are compared in Table IV. The predictions of  $A_2$  and the experimental observations are in good agreement for those experiments in TCB and ODCB where the sample received the 160°C treatment and the "spikes" disappeared.

It was not possible to remove the "spikes" in  $\alpha$ CN solutions by 160°C treatment. Discoloration occurred if higher temperatures were used with this solvent. We conclude that  $\alpha$ CN is too poor a solvent for polyethylene to be amenable to this solution preparation method. In support of this inference, it may be noted that  $\bar{M}_w$  measured in a  $\alpha$ CN is always consistently lower than in the other two solvents. This is presumably because higher molecular weight molecules are aggregated and appear in the light scattering trace as "spikes" which do not contribute to the excess Rayleigh scattering used to measure  $\bar{M}_w$ . It will also be noticed that the second virial coefficient of  $\alpha$ CN solutions remains much lower than in the other two solvents, even after the prescribed thermal treatment.

Table V compares  $\bar{M}_n$ ,  $\bar{M}_w$  and  $\bar{M}_z$  values for two polyethylenes analyzed by SEC in TCB solution at 145°C. Sample C is a linear low density material listed in Table 1. NBS 1476 is low density polyethylene which is stated to be a low conversion tubular reactor product with density 0.931 gcm<sup>-3</sup> and melt index 1.2 (11).  $\bar{M}_n$  and  $\bar{M}_w$  are little affected by the existence of aggregates in these two samples but  $\bar{M}_z$  values are more severely influenced. It can also be expected that any calculations of long chain branching frequency (12,13) will be severely compromised by errors resulting from supermolecular structures. This is because the frequency of long branches resulting from chain transfer to

Table III. Parameters for Calculation of Second Virial Coefficients\*

Solvent	K (cm <sup>3</sup> /g)	a	Ref.
TCB	5.96 x 10 <sup>-2</sup>	0.70	(7)
ODCB	5.06 x 10 <sup>-2</sup>	0.70 (LDPE)	(8)
ODCB	5.05 x 10 <sup>-2</sup>	0.693 (HDPE)	(9)
αCN	4.3 x 10 <sup>-2</sup>	0.67	(9)
Theta	315 x 10 <sup>-3</sup>	0.5	(10)

\*Calculation method is given in (6).

Table IV. Molecular Weights and Virial Coefficients as a Function of Thermal History

Polymer	Solvent	at 145°C		at 145° with 160° treatment		
		M <sub>w</sub>	A <sub>2</sub>	M <sub>w</sub>	A <sub>2</sub>	A <sub>2</sub> (theor.)
C	TCB	220,000	4.2x10 <sup>-4</sup>	217,400	1.50x10 <sup>-3</sup>	1.4 x10 <sup>-3</sup>
	ODCB	216,100	3.1x10 <sup>-4</sup>	213,700	1.05x10 <sup>-3</sup>	1.09x10 <sup>-3</sup>
	αCN	178,700	3.7x10 <sup>-4</sup>	168,900	7.9 x10 <sup>-4</sup>	3.2 x10 <sup>-4</sup>
B	TCB	212,300	5.1x10 <sup>-4</sup>	208,300	3.05x10 <sup>-3</sup>	1.51x10 <sup>-3</sup>
	OCDB	215,100	4.2x10 <sup>-4</sup>	210,200	1.71x10 <sup>-3</sup>	1.11x10 <sup>-3</sup>
	αCN	174,200	3.9x10 <sup>-4</sup>	167,300	8.7 x10 <sup>-4</sup>	3.4 x10 <sup>-4</sup>
A	TDB	-	-	233,600	2.00x10 <sup>-3</sup>	1.41x10 <sup>-3</sup>
	ODCB	-	-	230,800	1.41x10 <sup>-3</sup>	1.05x10 <sup>-3</sup>
	CN	-	-	189,100	6.8 x10 <sup>-4</sup>	2.9 x10 <sup>-4</sup>

Table V. Comparison of SEC Measurements\*

Polymer	145°C solution			145°C solution after 160 treatment		
	M <sub>n</sub>	M <sub>w</sub>	M <sub>z</sub>	M <sub>n</sub>	M <sub>w</sub>	M <sub>z</sub>
C(LLDPE)	48,900	188,000	546,500	46,500	185,000	606,800
NBS 1476	27,900	92,400	3,388,000	28,400	93,100	3,722,000

\*SEC measurements with 500 Å, 104 Å and 10<sup>5</sup> Å Ultrastayragel columns; polymer concentrations were 3.5-5.5 mg/mL in samples injected into TCB at 0.5 mL/min flow rate.



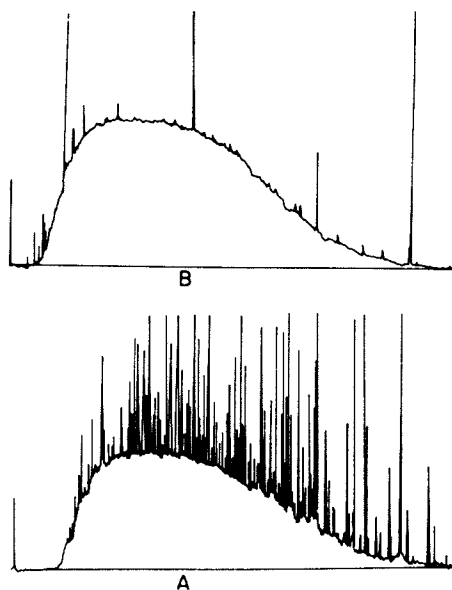


Figure 1. Strip chart recording of LALLS output for sample (A) without and (B) with 160°C treatment. Ordinate is scattering an arbitrary units. Sample is polyethylene A in TCB at 2.2 g/l and a flow rate of 0.1 ml/min with an injection volume of 0.5 ml at 145°C.

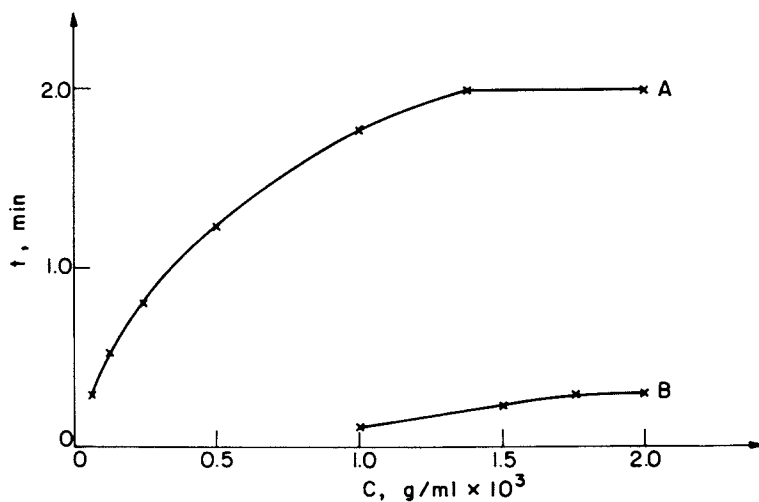


Figure 2. Time required for maximum scattering to return to solvent scattering baseline as a function of polymer concentration and flow rate. A flow rate 0.1 ml/min. B flow rate 0.5 ml/min.

polymer will probably be greater for higher molecular weight polyethylenes in the high pressure free radical production of this polymer

It is of interest to note in Figure 1 that there is a lag in the response of the LALLS with time caused by mixing in the cell. This is an artifact of the relatively higher viscosity and density of the solution flowing into the cell and displacing the less viscous solvent in the cell. This effect can be seen readily in this work because the solution concentrations were deliberately made high and the flow rate slow. Figure 2 shows the effect of flow rate and concentration on the time required for the cell to be completely emptied of polymer. In conventional SEC measurements this artifact could be of importance, but should not be observed unless very slow flow rates are used. A recent observation on this appears in the work of Rand and Mukherji (14) who used slow flow rates to observe degradation of polymer in an SEC column.

### Conclusions

A thermal treatment at 160°C for 1 hour has proved to be adequate for the removal of aggregates that persist at 145°C in TCB or ODCB solutions of polyethylene. Such a treatment enables one to obtain true solutions for use in SEC. Solution of polyethylene in  $\alpha$ CN appears to be incomplete even after the 160°C treatment and  $\alpha$ CN is therefore not recommended for use in SEC with polyethylene, despite the favorable specific refractive index increment of its solutions.

The 1 hour treatment at 160°C will be more severe than necessary for some samples and inadequate for others. We have observed that storage at 160°C for as much as a day may be required to remove detectable aggregates in solutions of very high molecular weight linear polyethylene samples. In any event, the appropriate duration of such treatments can be assessed by the method described here. That is to say, the solution history should be adjusted so that direct measurements of  $\bar{M}_w$  by LALLS (without the SEC columns) yields clean recorder traces (as in Figure 1) and second virial coefficients which are in accord with Kok-Rudin predictions of such values for the measured  $\bar{M}_w$ .

### Acknowledgment

Support of this research by the Natural Sciences and Engineering Research Council of Canada is appreciated.

### Literature Cited

1. Doty, P, Wagner, H and Singer, S, J. Phys. Chem., 1947, 51, 32.

2. Rudin, A and Benschop-Hendrychova, I, J. Appl. Polym. Sci., 1971, 15, 2881.
3. Trementozzi, Q.A., J. Polym. Sci., 1959, 36, 113.
4. Schreiber, H.P. and Waldmann, M.H., J. Polym. Sci., Pt. A, 1964, 2, 1655.
5. Stejskal, J. Horska, J. and Kratochvil, P., J. Appl. Polymer Sci., 1982, 27, 3929.
6. Kok, C.M. and Rudin, A, J. Appl. Polym. Sci., 1981, 26, 3583.
7. Ram, A and Miltz, J., Appl. Polym. Sci., 1971, 15, 2639.
8. Dawkins, J.V. and Maddock, J.W., Eur. Polym. J., 1971, 7, 1537.
9. Kotera, A., Saito, T., Takamisara, K. and Kiyasara, Y., Rept. Progr. Polym Phys. Japan, 1960, 3, 58.
10. Chiang, R., J. Phys. Chem. 1966, 70, 2348.
11. Wild, L., Ranganath, R. and Barlow, A., J. Appl. Polym. Sci., 1977, 21, 3331.
12. Foster, G.N., MacRury, T.B. and Hamielec, A.E., in "Liquid Chromatography of Polymers and Related Materials II", Cazes, J. and Delamare, X., eds., Marcel Dekker, New York, 1980.
13. Axelson, D.E. and Knapp, W.C., J. Appl. Polym. Sci., 1980, 25, 119.
14. Rand, W.G. and Mukherji, A.K., J. Polym. Sci. Polym. Letters Ed., 1982, 20 501.

RECEIVED September 22, 1983

# Development of a Continuous Gel Permeation Chromatography Viscosity Detector

## For the Characterization of Absolute Molecular Weight Distribution of Polymers

F. B. MALIHI, C. KUO, M. E. KOEHLER, T. PROVIDER, and A. F. KAH

Glidden Coatings and Resins, Division of SCM Corporation, Strongsville, OH 44136

A continuous capillary viscosity detector has been developed for use in High Performance Gel Permeation Chromatography (HPGPC). This detector has been used in conjunction with a concentration detector (DRI) to provide information on the absolute molecular weight, Mark-Houwink parameters and bulk intrinsic viscosity of polymers down to a molecular weight of about 4000. The detector was tested and used with a Waters Associates Model 150 C ALC/GPC. The combined GPC/Viscometer instrumentation was automated by means of a micro/mini-computer system which permits data acquisition/reduction for each analysis.

This work describes the design, operation and application of the continuous GPC viscosity detector for the characterization of the molecular weight distribution of polymers. Details of the design and factors affecting the precision and accuracy of results are discussed along with selected examples of polymers with narrow and broad molecular weight distribution.

Recent developments in gel permeation chromatography (GPC) have focused on three major areas including the introduction of high performance columns, instrument automation and the development of molecular weight sensitive detectors. The last area has resulted in the development of laser light scattering photometers,<sup>(1,2)</sup> and continuous viscosity detectors.<sup>(3-5)</sup> These detectors when combined with a concentration detector such as a refractive index or an optical density detector in a GPC system, can provide quantitative absolute molecular weight distribution and branching information for polymers. The viscosity detector, although not commercially available, particularly is attractive due to its relative simplicity in design, ease of data reduction and low cost compared to the light scattering detector.

0097-6156/84/0245-0281\$06.00/0

© 1984 American Chemical Society

### Instrumentation

A schematic diagram of the GPC/Viscometer system is shown in Figure 1. The viscometer is coupled to a Waters Associates Model 150°C ALC/GPC. The key component of the viscometer is a differential pressure transducer (Model P-7D CELESCO, Canoga Park, California) with a +25 psi pressure range. The transducer monitors the pressure drop across a section of stainless steel capillary tubing (length: 2 ft., I.D.=0.007 in.). The geometric detector volume is about 15  $\mu$ l.

The viscometer assembly is placed in the constant temperature column compartment of the chromatograph between the column outlet and the refractometer. A combination of two Waters Associates M-45 hydraulic filters in series with a capillary tubing coil (length: 10 ft., I.D.:0.01 in.) is used to dampen the line pressure fluctuations caused by the pump. With the above pressure damping modifications the overall system noise was reduced to less than 1 millibar at 1.0 ml/min flow rate in tetrahydrofuran (THF) for a set of six  $\mu$ -Styragel columns; 10<sup>6</sup>, 10<sup>5</sup>, 10<sup>4</sup>, 10<sup>3</sup>, 500, 100Å (Waters Associates, Milford, MA.). The column compartment temperature was set at 50°C.

The automation of the HPGPC/Viscometer system is achieved by interfacing the differential refractometer (DRI) and viscosity detector to a microcomputer for data acquisition. The raw data subsequently, are transferred to a minicomputer (DEC PDP-11/44) for storage and data analysis. Details of the instrument automation are given elsewhere.(6)

### Materials

The column set was calibrated with a series of polystyrene standards with weight average molecular weights ( $\bar{M}_w$ ) between  $2 \times 10^5$  and  $4.1 \times 10^6$ . The standards were supplied by Pressure Chemical Co., Pittsburgh, Pa. and ArRo Laboratories, Inc., Joliet, Ill. Other systems used in this work included the NBS-706 polystyrene standard and an emulsion polymerized polymethyl methacrylate sample.

### Data Reduction

Details of the data analysis for the GPC/Viscometer system have been reviewed by Ouano.(7) The data reduction scheme is summarized in Figure 2 and briefly will be discussed here. The intrinsic viscosity of the effluent at a given retention volume  $[\eta](v)$  is determined from the DRI and continuous viscosity detector responses according to the following equation

$$[\eta](v) = \frac{1}{C(v)} \ln \left( \frac{\Delta E(v)}{\Delta E_o} \right) C \rightarrow 0 \quad (1)$$

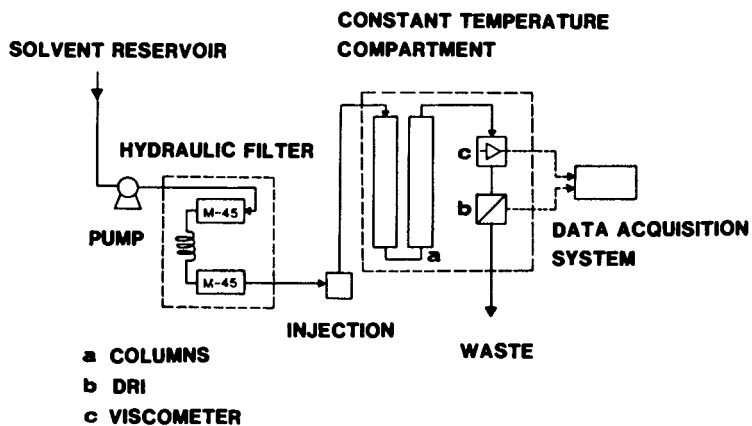


Figure 1. Schematic of GPC/Viscometer system.

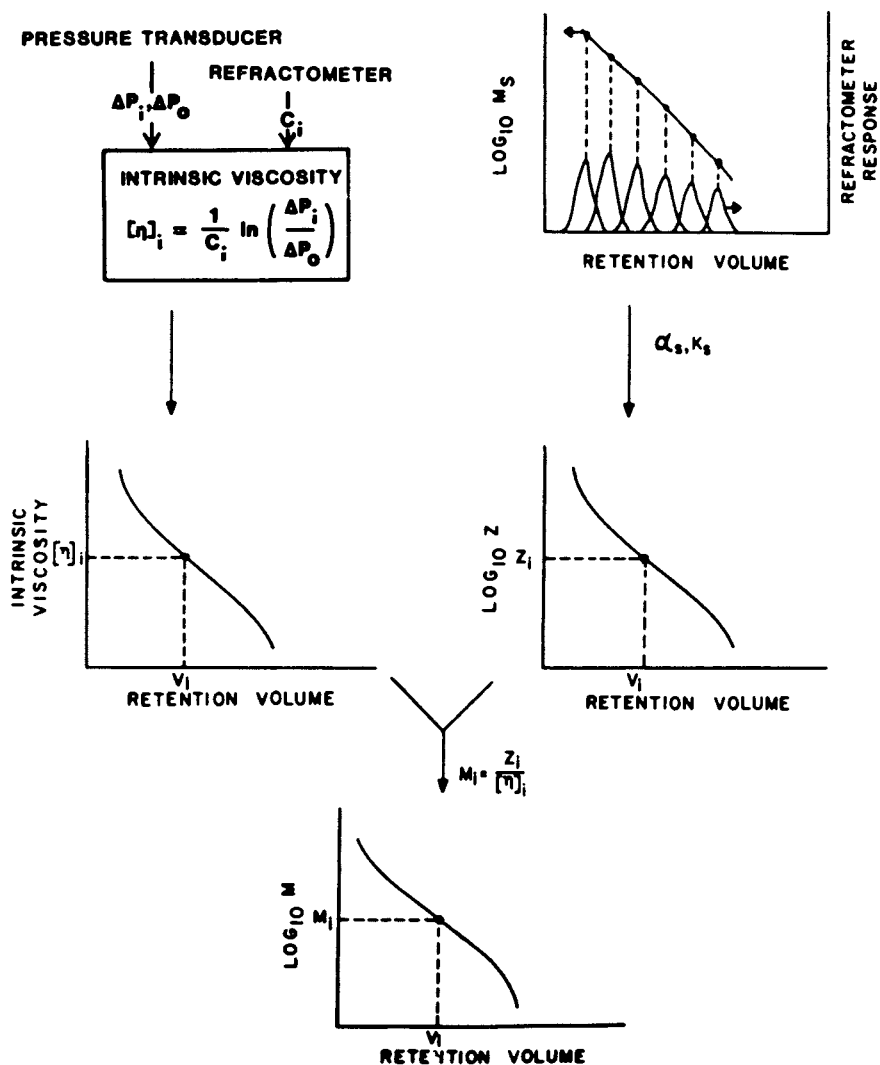


Figure 2. Data reduction scheme for analysis of DRI/Viscometer chromatograms.

where  $\Delta E_p$  and  $\Delta E(v)$  are the viscosity detector responses (millivolts) at constant flow rate corresponding to solvent and to sample having concentration  $C(v)$ , respectively. For a linear transducer,  $\Delta E(v)$  is proportional to the pressure drop across the capillary,  $\Delta P(v)$ . The concentration  $C(v)$  is given by

$$C(v) = W \cdot f(v) / \int_{v_L}^{v_H} f(v) dv \quad (2)$$

where  $W$  (grams) is the weight of the sample injected, and  $f(v)$  is the concentration detector (DRI) response at the retention volume  $v$ . The parameters  $v_L$  and  $v_H$  represent the lowest and highest retention volume in the chromatogram.

From the primary calibration curve based on polystyrene standards and the Mark-Houwink constants for polystyrene ( $K, \alpha$ ) a universal calibration curve ( $Z$  vs.  $v$ ), based on hydrodynamic volume is constructed.  $Z$  is calculated from

$$Z(v) = [\eta](v) \cdot M(v) = KM(v)^{\alpha+1} \quad (3)$$

Using the intrinsic viscosity data and the universal calibration curve(8) a secondary molecular weight calibration curve can be constructed for the polymer of interest as shown by the following equation:

$$M_x(v) = Z(v)/[\eta]_x(v) \quad (4)$$

From this information the absolute molecular weight distribution and the intrinsic viscosity-molecular weight plot can be constructed. From this plot the solvent and temperature dependent Mark-Houwink coefficients for linear polymers and information for polymer chain-branching of non-linear polymers can be obtained.

#### Effect of Operational Parameters

Successful operation of the viscometer depends on good control of possible sources of flow variations in the system which include pump pulsations, temperature variations and restrictions in the GPC columns and fractional sections of tubing.



### Pump Pulsations

The noise due to the reciprocating action of the dual-headed pump in the 150C ALC/GPC has a constant frequency pattern and can be reduced by hydraulic filters as shown in Figure 3. A 60% reduction in the peak-to-peak noise is achieved by using a Mark II dampener (Laboratory Data Control, River Beach, Florida), while the M-45 filters under same conditions have reduced the noise by 90%.

### Flow Rate

Figure 4 shows the effect of flow rate on the stability of the viscometer baseline signal. Results indicate that the increase in flow rate reduces the high frequency noise (pump noise) while increasing the low frequency noise, apparently caused by imperfections in the flow system (e.g., column packing condition, end fittings, adsorbed sample impurities, etc.). Optimum operating conditions can be established for flow rates between 1 to 1.5 ml/min. Similar results were obtained when DuPont Zorbax Bimodal columns (DuPont Co., Wilmington, DE.) and Varian MicroPak TSK columns (Varian Associates Inc., Palo Alto, Calif.) were used with the GPC/Viscometer system.

### Imperfections in the Hydraulic System

The low frequency baseline noise of the viscometer can be substantially reduced by careful filtration of samples and regular checking and maintenance of column end fittings and fractional sections of tubing in the system. Figure 5 shows the effect of column screen replacement on the stability of the baseline signal at a flow rate of 1.0 ml/min.

### Sensitivity of the Viscometer

Once the major sources of the viscometer baseline noise are eliminated the viscometer detector can be used for the analysis of polymers with molecular weights as low as 2000. The precision of the GPC/Viscometer analysis is influenced to a great extent by the signal-to-noise ratio (S/N) of the viscometer response at each point on the chromatogram. An estimate of the S/N ratio for this viscometer system is provided in the chromatograms shown in Figures 6 and 7. In these Figures the viscometer response is shown for two narrow MWD standard polystyrene samples with average molecular weights of 4,000 and 97,000, with injected mass of 1.50 mg and 0.690 mg, respectively.

At a flow rate of 1 ml/min with THF as mobile phase at 50°C, initially a baseline pressure of 664 millibars is established for both samples. For the 4,000 molecular weight polystyrene a maximum pressure of 668 millibars is reached at the peak position

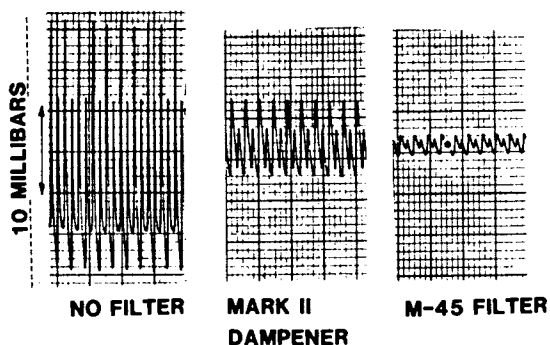


Figure 3. Effect of the commercial hydraulic filters on the baseline noise of the viscometer trace (Mobile Phase: THF, Flow Rate: 0.5 ml/min, Temperature: 30°C)

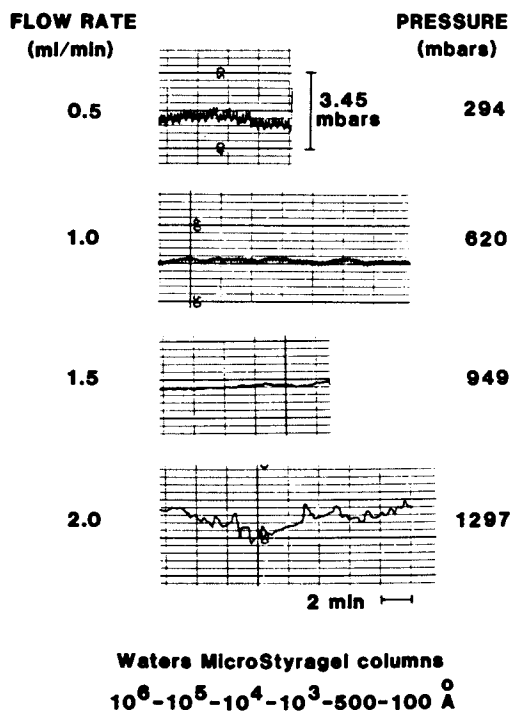
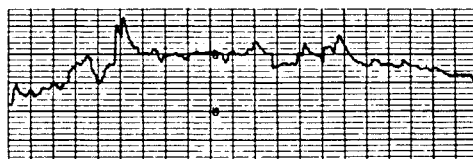
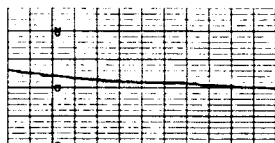


Figure 4. Effect of flow rate on the baseline noise of the viscometer trace (Mobile Phase: THF, Temperature: 30°C)



BEFORE SCREEN REPLACEMENT



AFTER SCREEN REPLACEMENT

Figure 5. Viscometer trace before and after the column screen replacement.

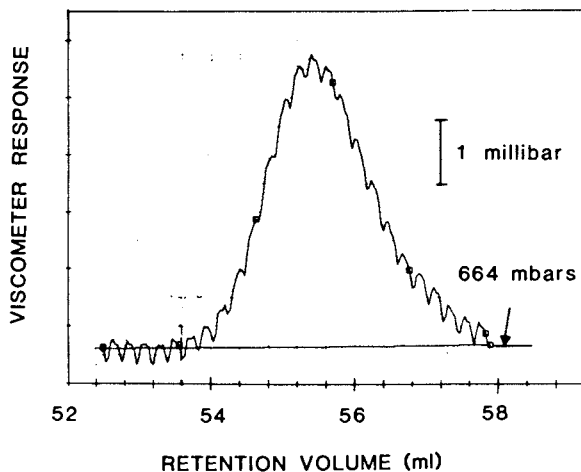


Figure 6. Viscometer chromatogram of narrow MWD standard polystyrene. ( $M_w$ :4000, Injected Mass: 1.50 mg, Flow Rate: 1 ml/min, Temperature: 50°C, Column: as in Figure 4)

with 0.32 millibar peak-to-peak baseline noise. Results for the 97,000 molecular weight sample indicate a maximum pressure of 679 millibars, with a peak-to-peak noise of 0.45 millibar. At the point of maximum pressure the S/N for the 4000 molecular weight sample is 10.5 and for the 97000 molecular weight sample is 32 indicating good S/N performance for both systems.

The high sensitivity of the viscosity detector to the high molecular weight fractions is demonstrated in the analysis of a sample of very high molecular weight poly(methyl methacrylate) shown in Figure 8. A shoulder at 3,000,000 molecular weight detected by the DRI becomes a peak when detected by the viscometer detector.

#### Determination of the Dead Volume Between the Viscometer and the Concentration Detector

Another requirement for accurate GPC/Viscometer data analysis is accounting for the dead volume ( $\Delta V$ ) between the viscometer and the concentration detector.

Reported literature<sup>(10)</sup> and our own experience have shown that an estimate of  $\Delta V$  based on the geometry of the connecting tubing is not reliable for this purpose. This primarily is due to the variation in the internal diameter of the commercially available tubing. In this work we have applied a semiempirical experimental method to determine  $\Delta V$ . The method recently has been implemented by Lesec and coworkers.<sup>(10)</sup>

In this method one injects a known amount of a high molecular weight polymer on to low porosity GPC columns. From the viscometer and DRI chromatograms, as shown in Figure 2, the apparent intrinsic viscosity  $[\eta](v)$  is determined and plotted against retention volume  $v$ . A series of  $[\eta](v)$  vs.  $v$  plots are then constructed assuming a range of dead volumes. The slope of each plot is determined by linear regression and is plotted against the assumed  $\Delta V$ . The correct  $\Delta V$  corresponds to the zero slope.

To implement this technique a combination of two  $\mu$ -styrigel columns with 100Å and 500Å porosity was used. A sample size of 50 $\mu$ l of 0.1% (W/V) standard narrow distribution polystyrene with  $\bar{M}_w = 1.8 \times 10^6$  was injected on to the columns. THF was used as the mobile phase at a flow rate of 1 ml/min and temperature of 50°C. Using the data analysis routine described above, a value of 115 $\mu$ l was obtained for  $\Delta V$  as shown in Figure 9.

#### Quantitative Analysis

Figure 10 shows DRI and viscometer traces for the NBS 706 polystyrene standard. Based on the information from these two chromatograms in conjunction with the universal calibration curve, one can calculate the intrinsic viscosity  $[\eta](v)$  and molecular weight  $M(v)$  at each retention volume as shown in

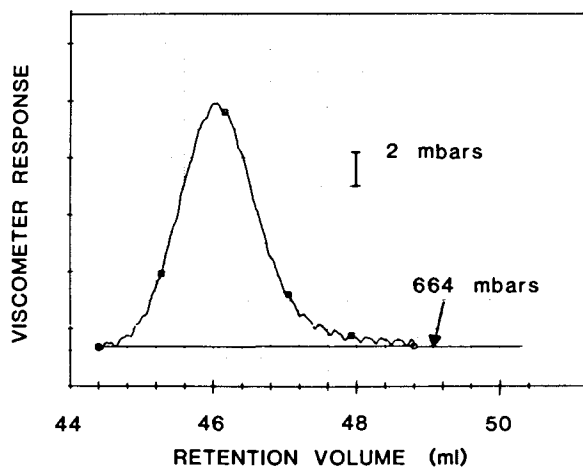


Figure 7. Viscometer chromatogram of narrow MWD standard polystyrene. ( $M_w$ :97,000, Injected Mass: 0.690 mg, Other conditions: same as in Figure 6.)

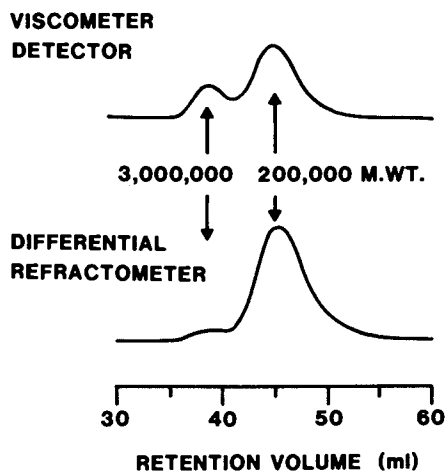


Figure 8. DRI and viscometer chromatograms for a high molecular weight polymethyl methacrylate sample.

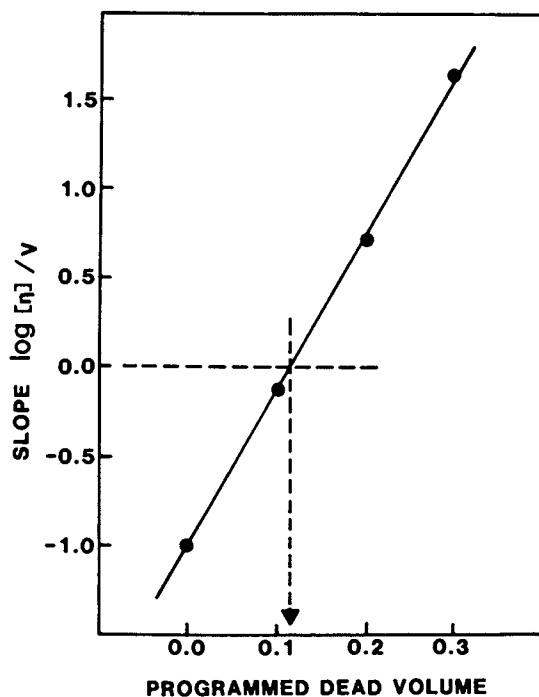


Figure 9. Slope versus  $\Delta V$  plot for the determination of the dead volume between DRI and viscometer detectors.

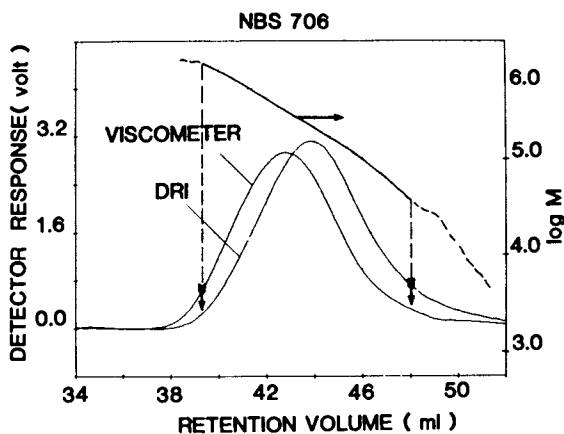


Figure 10. DRI and viscometer chromatograms, and  $\log (M)$  vs.  $(v)$  for NBS-706. (Mobile Phase: THF, Flow Rate: 1.0 ml/min, Temperature: 50°C, Injected Mass: 2.15 mg, Column Set: as in Figure 4.)

Figures 10 and 11. The molecular weight  $M(v)$  can then be used to generate molecular weight distribution statistics as summarized in Table I.

Table I. Molecular Weight Distribution Statistics For NBS-706

	$\bar{M}_n$	$\bar{M}_w$	$\bar{M}_w/\bar{M}_n$
From Secondary Calibration	133,900	278,400	2.08
From NBS Data Sheet	136,500	257,800	1.89

Figure 12 shows the classical method of obtaining the Mark-Houwink coefficients,  $K$  and  $\alpha$ , by plotting the  $\log [\eta](v)$  vs.  $\log M(v)$  for this polymer in THF at  $50^\circ\text{C}$ . The data points used for the plot in Figure 12 are indicated by the area between the arrows in Figure 10. Linear regression analysis of the data resulted in  $K_{50^\circ\text{C}}=1.86 \times 10^{-4}$  and  $\alpha_{50^\circ\text{C}}=0.662$  with a correlation coefficient of  $R=0.9996$  for NBS 706 polystyrene.

Table I indicates good agreement between the molecular weight distribution statistics obtained by coupled GPC/Viscometer method and the nominal values for NBS 706. The discrepancy between the Mark-Houwink parameters obtained here and the reported values for polystyrene standard (9) in THF at  $25^\circ\text{C}$  (i.e.,  $\alpha = 0.706$  and  $k = 1.60 \times 10^{-4}$ ) may in part be due to the uncertainty involved in the determination of the dead volume between DRI and viscometer detectors. Our simulation studies over a range of dead volume values (0 to  $120\mu\text{l}$ ) showed that  $\alpha$  and  $k$  are quite sensitive to the dead volume between the detectors. Larger dead volume results in smaller  $\alpha$  and larger  $k$  values. This is a direct result of a clockwise rotation of  $\log [\eta]$  vs.  $\log M(v)$  curve (Figure 12) which occurs when the dead volume correction is applied in quantitative analysis. The effect on the molecular weight statistics, however, appeared to be small with  $\bar{M}_n$  being more sensitive to this correction.

This simulation study also indicated that the result of the experimental determination of dead volume (as described above) may be overestimated by as much as 50%. A possible reason for this could be due to the lack of complete exclusion of the high molecular weight polystyrene used in this technique. Further refinement of this semi-empirical experimental technique for the determination of the dead volume is needed. Details on the simulation studies will be reported in future communications.

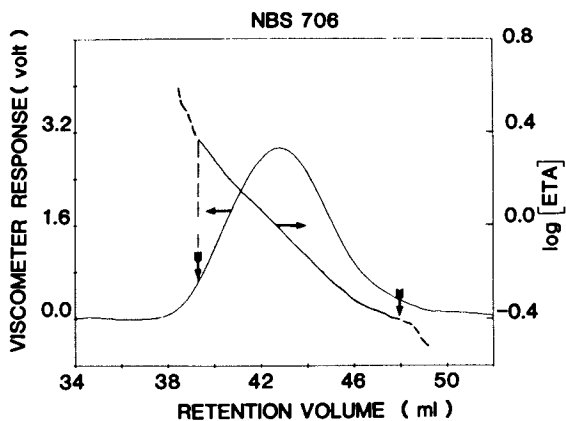


Figure 11. Viscometer chromatogram and  $\log [ETA]$  vs. (v) for NBS-706. (Conditions as in Figure 10).

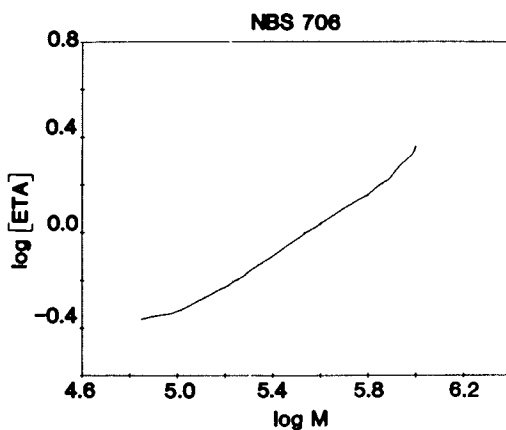


Figure 12.  $\log [ETA]$  vs.  $\log M$  for NBS-706. (Conditions as in Figure 10).



Other possible reasons for the discrepancy in the Mark-Houwink parameters may be due to the band spreading effects and inadequate signal-to-noise quality at the tails of the viscometer chromatogram. These subjects will be the topic of our future investigations in this area.

### Summary

The use of a continuous GPC viscosity detector in conjunction with a DRI detector permits the quantitative determination of absolute molecular weight distribution in polymers. Furthermore, from this combination one can obtain Mark-Houwink parameters and the bulk intrinsic viscosity of a given polymer with a GPC calibration curve based only on polystyrene standards. Coupling these two detectors with ultraviolet and infrared detectors then will permit the concurrent determination of polymer composition as a function of molecular weight and branching. This work will be reported in future communications.

### Literature Cited

1. A. C. Ouano and W. Kaye, J. Polym. Sci. Polym. Chem. Ed., 12, 1151 (1974).
2. M. L. McConnell, Am. Lab., 10(5), 63 (1978).
3. A. C. Ouano, J. Polym. Sci., A-1, 10, 2169 (1972).
4. L. Letot, J. Leseq, C. Quivoron, J. Liq. Chromatogr. 3, 427 (1980).
5. F. B. Malihi, M. E. Koehler, C. Kuo, and T. Provder, 1982 Pittsburgh Conference, Paper No. 806.
6. M. E. Koehler, A. F. Kah, T. F. Niemann, C. Kuo and T. Provder, "An Automated Data Analysis System for A Waters Model 150C ALC/GPC System with Multiple Detectors", This Volume.
7. A. C. Ouano, J. Macromol. Sci., Revs. Macromol. Chem., C9(1), 123 (1973).
8. T. Provder and E. M. Rosen, Separation Sci., 5 (4), 437 (1970).
9. T. Provder, J. C. Woodbrey, J. H. Clark, E. E. Drott, Advances in Chemistry Series No. 125 "Polymer Molecular Weight Methods", Ed. E. Ezrin 117 (1973).
10. D. Lecacheux and J. Leseq, J. Liq. Chromatogr., 12, 2227, (1982).

RECEIVED October 4, 1983

# Size Exclusion Chromatography with Low-Angle Laser Light-Scattering Detection

## Application to Linear and Branched Block Copolymers

R. C. JORDAN, S. F. SILVER, R. D. SEHON, and R. J. RIVARD

3M—3M Center, P.O. Box 33221, St. Paul, MN 55133

Linear block polymers of styrene-co-isoprene and styrene-co-butadiene were prepared via anionic polymerization and subsequently were coupled with divinyl benzene to give multi-arm macromolecules. Low-angle laser light scattering (LALLS) was used for molecular weight measurement both in the stand-alone (static) mode and as a detector coupled to SEC. No dependence of the weight average molecular weight ( $\bar{M}_w$ ) on solvent was found, which is consistent with light scattering theory for compositionally homogeneous block polymers. Comparison of SEC/LALLS data for both the linear and branched species shows the strong effect of branching upon the hydrodynamic volume/molecular weight relationship. The data indicate the multi-arm samples are of relatively small molecular weight polydispersity, with a weight-average branching functionality of 16-18. Use was made of the universal calibration and SEC/LALLS data to calculate the branched/linear intrinsic viscosity ratio through the molecular weight distribution of the multiarm samples; an anomalous dependence on molecular weight was found. Difficulties with the universal calibration procedure or sample viscosity effects are discussed as possible causes.

The deliberate introduction of multifunctional branching into anionically prepared polydiene and poly(diene-co-styrene) polymers produces materials with unique morphological and viscoelastic properties (1-3). Work has included synthesis of symmetric star polymers produced by reaction of living polyanionic "arms" with multi-functional chlorosilane (4-9),

0097-6156/84/0245-0295\$07.50/0  
© 1984 American Chemical Society

and less well defined structures have been obtained using divinyl benzene (DVB) as the linking agent (10-16).

Dilute solution studies on such materials have been carried out in an attempt to gain some understanding of molecular structure/property relationships (6, 7, 14, 17-19), and the work has benefited from elegant theoretical frameworks developed by several workers (20-24). Molecular weight characterization is critical to fundamental investigations, as well as to development of controlled production processes in commercial applications.

Several studies have been published which utilize size exclusion chromatography (SEC) for characterization of the molecular weight distribution of multi-arm structures of polystyrene, polyisoprene, and block copolymers of styrene/butadiene and styrene/isoprene (1, 2, 8, 17, 25-26). An interesting phenomenon of direct consequence to work presented here was recorded by Bi and Fetters (1) as a result of their work on DVB-linked "star" block copolymers of poly(styrene-co-polybutadiene) and poly(styrene-coisoprene): they found that the universal calibration procedure gave anomalous molecular weight values for several samples. These workers noted that the sample intrinsic viscosity ( $[\eta]$ ) was insensitive to the number of arms, when the arm composition and molecular weight was held constant, and it was suggested that this characteristic might underlie the unusual chromatographic behavior. However, it was noted that some degree of SEC separation by number of arms was achieved. These authors suggest that unique hydrodynamic properties conferred by a "core/shell" structure may be responsible for the SEC behavior, and also it is not clear what relative effects the number of arms and arm length have on the SEC separation.

The observations and questions raised by these workers helped stimulate the experiments which are presented here. In this work, size exclusion chromatography with low angle laser light scattering detection (SEC/LALLS) was used to probe the distribution of branching functionality in multiarm macromolecules of styrene/isoprene and styrene/butadiene block copolymers and to evaluate the applicability of universal calibration to analysis of such materials. The SEC process separates via hydrodynamic volume, not molecular weight, so that use of conventional calibration methods (e.g., calibration with linear polystyrene standards) suffers from the inherent hydrodynamic volume/molecular weight differences between sample and calibrant. In general, branching decreases the hydrodynamic volume of a macromolecule relative to its linear homolog, so that conventional SEC analysis of branched species is especially precarious. Use of LALLS with SEC can circumvent such difficulties since connection of a LALLS detector in series with a concentration detector allows determination of the correct molecular weight

at each increment in the polymer chromatogram without recourse to use of calibration techniques (27-29). The SEC/LALLS method has proved to be a valuable tool for the study of branched polymers, with several excellent publications appearing on this subject (17, 26, 30-33).

Synthetic copolymers often present a fundamental difficulty for molecular weight measurement by light scattering, since compositional heterogeneity can be superimposed on the distribution of molecular weights. Whereas a dilute solution light scattering measurement from a homopolymer which is polydisperse in molecular weight yields the weight-average molecular weight of the sample ( $M_w$ ), a compositionally heterodisperse polymer sample gives an apparent molecular weight which depends on the solvent (34). The copolymer difficulty arises from the change of the specific refractive index increment ( $dn/dc$ ) with polymer composition, while a value of  $dn/dc$  measured on the entire sample is used to calculate molecular weights from light scattering data. In cases without compositional variation among polymer chains, the light scattering molecular weight is independent of solvent identity.

The experimental samples used in this work should, however, be amenable to straightforward light scattering analysis since the constituent polymers possess backbone block microstructures which guarantee compositional uniformity throughout the sample. The synthetic route utilizes "living" anionic polymerization of polystyrene, followed by isoprene or butadiene addition; divinyl benzene (DVB) linkage of these species gives multiarm structures (MA) containing arms which are homogeneous with respect to composition and molecular weight. The light scattering average molecular weight of both the linear block (LB) copolymer and MA should be independent of solvent identity, with an identical  $dn/dc$  for both materials.

The SEC/LALLS method was 1) used to study a commercially available linear block copolymer: Kraton 1107 brand elastomer (Shell Chemical Company), and 2) to study the starting "arm" block copolymer and resultant DVB-linked MA of several experimental samples.

## Theory

Dilute Solution Light Scattering: Homopolymers and Copolymers. The theoretical basis for polymer molecular weight measurement by light scattering has been developed in detail, and only the concepts relevant to SEC/LALLS studies of copolymers are presented here.

Proper use of LALLS to measure polymer molecular weight requires a dilute solution of optically isotropic flexible macromolecules whose dimensions are of the same

order as the wavelength of scattering radiation (35-37). For chains which are compositionally and molecular-weight monodisperse, in the limit of vanishingly small observation angle ( $\theta$ ):

$$\frac{Kc}{\bar{R}_\theta} = \frac{1}{M} + 2A_2c \quad (1)$$

where  $\bar{R}_\theta$  is the "excess" Rayleigh factor calculated from the excess scattering of polymer solution over solvent, and  $A_2$  and  $c$  are the second virial coefficient and polymer concentration, respectively. The quantity  $K$  is an optical constant, defined for the polarized laser light source and particular annular collection optics of the commercially available LALLS detectors as:

$$K = \frac{2\pi^2 n_0^2}{\lambda_0^4 N_A} (1 + \cos^2 \theta) \left(\frac{dn}{dc}\right)^2 = K' \left(\frac{dn}{dc}\right)^2 \quad (1a)$$

where  $n_0$ ,  $\lambda_0$ , and  $N_A$  represent the solvent refractive index, in vacuo scattering wavelength, and Avogadro's number, respectively (38, 39).

The quantity  $dn/dc$  is the specific refractive index increment and it represents the incremental change in solution refractive index with sample concentration at the wavelength, temperature, and pressure of the LALLS measurements. Since  $dn/dc$  reflects the optical characteristics of the polymer and solvent (their different optical polarizabilities), its value strongly depends on the chemical composition of both components (40).

In block copolymers containing monomers A and B, to a good approximation the overall  $dn/dc$  is (40):

$$\left(\frac{dn}{dc}\right) = W\left(\frac{dn}{dc}\right)_A + (1-W)\left(\frac{dn}{dc}\right)_B \quad (1b)$$

where the subscripted parameters refer to the  $dn/dc$  of homopolymers of A and B, measured in the same solvent and at the same temperature and wavelength as the copolymer. The weight composition  $W$  is:

$$W = \frac{M_A}{M_A + M_B}$$

where  $M_A$  is the molecular weight of the polymer of only the A subunits of the copolymer and  $M_B$  is the corresponding quantity for B subunits.

The  $dn/dc$  can show a dependence on polymer tacticity (41) and molecular weight, but these effects usually are minor relative to that of polymer composition (40). Also, the

magnitude of  $dn/dc$  increases with decreasing wavelength (42) as  $(1/\lambda_0)^2$ , and it shows a small dependence on temperature; the quantity must be measured at the same wavelength and temperature as used in the scattering measurement (40).

Next, consider a polymer sample which is heterodisperse both in molecular weight and composition. In the limit of vanishing concentration, Equation 1 gives, for independent scatterers, i:

$$(\bar{R}_\theta)_i = K' c_i M_i \left(\frac{dn}{dc}\right)_i^2 \quad (2)$$

where from Equation 1a we see that:

$$K' = \frac{2\pi^2 n_0^2}{\lambda_0^4 N_A}$$

which is independent of molecular identity. Assuming that the total excess Rayleigh factor is the sum of individual scatterers, Equation 2 gives:

$$\bar{R}_\theta = K' \sum_i c_i M_i \left(\frac{dn}{dc}\right)_i^2$$

or

$$\bar{R}_\theta = K' c \left(\frac{dn}{dc}\right)^2 \left[ \frac{\sum_i c_i M_i \left(\frac{dn}{dc}\right)_i^2}{c \left(\frac{dn}{dc}\right)^2} \right] = K' c \left(\frac{dn}{dc}\right)^2 M^* \quad (3)$$

where  $c$  and  $(dn/dc)$  are the sample concentration and specific refractive index increment, respectively. The quantity  $M^*$  is an apparent average molecular weight, and it will vary with solvent identity because of the compositional (and associated  $dn/dc$ ) differences in individual molecular species  $i$ .

The light scattering equation for molecular weight-heterodisperse samples which are compositionally homogeneous simplifies if  $dn/dc$  is constant for all species:

$$\bar{R}_\theta = K' c \left(\frac{dn}{dc}\right)^2 \bar{M}_w = Kc \bar{M}_w \quad (4)$$

The derivation of Equation 4 utilizes the definition of the weight-average molecular weight:

$$\bar{M}_w = \frac{\sum c_i M_i}{\sum c_i}$$

Hence the equation for LALLS measurement of the  $\bar{M}_w$ :

$$\frac{Kc}{R_{\theta}} = \frac{1}{M_w} + 2A_2c \quad (5)$$

For copolymers, the above development shows that LALLS molecular weight measurements can be carried out in several solvents in order to check for compositional polydispersity. Polymers which are compositionally homogeneous will give a  $\bar{M}_w$  which is independent of solvent identity.

Size Exclusion Chromatography with Low-Angle Laser Light Scattering (SEC/LALLS). A size exclusion chromatograph with both LALLS and concentration detectors gives the correct weight-average molecular weight  $M_w(v)$  of polymers with concentration  $c(v)$  in elution volume  $v$  (28-31, 33). With adequate SEC resolution,  $M_w(v)$  represents the molecular weight of a species which is monodisperse in molecular weight  $M$ . In all that follows, we assume that the latter condition is approximated and that  $M_w(v) = M(v)$ . The reasonableness of this assumption will be examined in the context of data for samples analyzed in this work. The fundamental LALLS equation (Equation 5) forms the basis of the SEC/LALLS method.

Universal Calibration. One of the goals of this work was to evaluate the applicability of the universal calibration technique (43) to SEC analysis of these multi-arm macromolecules. This technique assumes a unique calibration relationship

$$[\eta](v) \cdot M(v) = J(v) \quad (6)$$

for the SEC system which describes the elution behavior of all samples. In Equation 6,  $[\eta](v) \cdot M(v)$  is the product of the intrinsic viscosity ( $[\eta]$ ) and molecular weight ( $M$ ) of a molecular-weight monodisperse polymer eluting in  $v$ . The relationship in Equation 6 first was proposed and demonstrated by Benoit et al. (44) and shown to hold for polymers with a spectrum of configurations, including rod-like, branched, and linear random coil structures. However, as noted above, studies of multi-arm stars of linear poly(diene-co-styrene) arms suggest deviation from universal calibration behavior (1).

Branching Parameter  $g'$  from SEC/LALLS. The effect of polymer branching upon the dilute solution configuration of polymers is conveniently expressed as the ratio of intrinsic viscosities of branched and linear polymers of the same chemical composition and molecular weight (35), i.e.,

$$g' = \frac{[\eta]_b}{[\eta]_l M} \quad (7)$$

where subscripts b and l refer to branched and linear material, respectively, and the subscript M denotes constant molecular weight.

In order to determine  $g'$  as a function of molecular weight, one approach is to use universal calibration with SEC analysis of molecular-weight polydisperse samples (31-33). For a multiarm (MA) branched material, the intrinsic viscosity of polymer eluting in  $v$  is:

$$[\eta]_{MA}(v) = \frac{J(v)}{M_{MA}(v)} \quad (8)$$

where  $M_{MA}(v)$  is the light scattering molecular weight in  $v$ . Also, from the Mark-Houwink relationship (43):

$$J(v) = K_{PS}(M_{PS}(v))^{1+a_{PS}} \quad (9)$$

where  $K_{PS}$  and  $a_{PS}$  denote the Mark-Houwink parameters for polystyrene calibrants in the chromatographic solvent, and  $M_{PS}(v)$  is the molecular weight (weight-average) of a narrow distribution standard with peak elution volume  $v$ .

Now consider MA materials which consist of linked arms of identical linear block copolymers (LB). Define the ratio:

$$k = \frac{M_{PS}(v)}{M_{LB}(v)} \quad (10)$$

which represents the difference in molecular weight/elution volume behavior for polystyrene calibrants and LB. We assume  $k$  is constant over the calibration range. These relationships can be used to calculate the intrinsic viscosity of LB material which has the same molecular weight as MA eluting in  $v$  ( $M_{MA}(v)$ ); the LB will elute in some earlier volume  $v_e$ . The molecular weight of polystyrene eluting at  $v_e$  is  $k \times M_{MA}(v)$ , and the universal calibration relationship gives:

$$[\eta]_{LB}(v_e) = \frac{K_{PS}(k \times M_{MA}(v))^{1+a_{PS}}}{M_{MA}(v)} \quad (11)$$

The viscosity ratio  $g'(v)$  then can be defined for MA eluting in  $v$ . Using Equations 11 and 10 in Equation 7 gives:



$$g'(v) = \left[ \frac{M_{PS}(v)}{k \times M_{MA}(v)} \right]^{1+a_{PS}} M_{MA}(v) \quad (12)$$

The above derivation rests on three assumptions:

- 1) Validity of the universal calibration,
- 2) SEC system performance sufficient to resolve the polymer sample into discrete molecular weight species at each  $v$ ; i.e., band spreading is negligible and chromatographic artifacts such as "viscous streaming" (43) are absent, and
- 3) a constant value of the polystyrene/LB molecular weight ratio through the chromatogram.

### Experimental

Polymer Synthesis/Materials. Multiarm samples were prepared via anionic polymerization in cyclohexane at 50–60 deg C. Polystyrenyl lithium anions of desired molecular weight were prepared with *S*-butyl lithium initiation, followed by addition either of isoprene or butadiene to give block polydienyl anion. A sampling of the latter was taken, terminated, and used as representative LB arm. The MA samples were synthesized by addition of DVB at a mole ratio of 4.5 DVB:1 anion. The polymerization was terminated by methanol addition. Four styrene/isoprene LB samples (SI-X) of different molecular weight and composition were prepared along with the corresponding MA: (SI-X) DVB; one styrene/butadiene (SB-1) and its MA ((SB-1) DVB) was made. Proton NMR gave the following weight percent styrene for each LB: SI-1 (9%), SI-2 (23%), SI-3 (26%), SI-4 (48%), and SB-1 (53%).

Homopolymers of butadiene, isoprene, and styrene were prepared under similar conditions. It should be noted that DVB was a commercial grade and, therefore, consisted of meta/para isomers and ethyl vinyl benzene.

Kraton 1107 brand elastomer was from Shell Chemical Co., and it is synthesized by coupling the isoprenyl anion ends of a styrene/isoprene (SI) block copolymer to give styrene/isoprene/styrene (SIS). Proton NMR analysis indicated 84% (wt.) isoprene and 16% (wt.) styrene.

Polystyrene calibration standards were from Pressure Chemical Co. and all had polydispersities ( $M_w/M_n$ ) less than 1.1.

SEC System, Data Processing, and Chromatography Procedures. The SEC/LALLS system contained a Model 110A pump (Altex), Model 7125 injector (Rheodyne), KMX-6 Low-Angle Laser Light Scattering Photometer (LDC/Milton Roy), and a Model 98.00

Refractive Index Detector (Knauer). The KMX-6 scattering intensity was measured with the 6-7 degree forward-scattering annulus. A series of Zorbax PSM columns (DuPont) was used: PSM 60, PSM 1000, PSM 1000, PSM 60, PSM 1000. Tetrahydrofuran (THF) from Baker was filtered through a 0.22 micrometer Fluoropore filter (Millipore Corp.) before use in chromatography, and a flow rate of 0.7 ml/min was used.

Analog detector data were acquired via analog/digital Instrument Interface Modules (LDC/Milton Roy) connected in series to a Minc 11/23 (Digital Equipment Corp.) computer. Software packages for run-scheduling and data acquisition ("RTDAS-1"), conventional calibration SEC ("GPC-11"), and SEC/LALLS data processing ("MOLWT-11") were from LDC/Milton Roy.

The MOLWT-11 program calculates the molecular weight of species in retention volume  $v(M(v))$ , where  $v$  is one of 256 equivalent volumes defined by a convenient data acquisition time which spans elution of the sample. Moments of the molecular weight distribution (e.g.,  $\bar{M}_z$ ,  $\bar{M}_w$ ,  $\bar{M}_n$ ) are calculated from summation across the chromatogram. Along with injected mass and chromatographic data, such as the flow rate and LALLS instruments constants, one needs to supply a value for the optical constant  $K$  (Equation 1a), and second virial coefficient  $A_2$  (Equation 1). The value of  $K$  was calculated for each of the samples after determination of the specific refractive index increment ( $dn/dc$ ) for the sample in the appropriate solvent. Values of  $A_2$  were derived from off-line (static) determinations of  $\bar{M}_w$ .

A universal calibration curve was developed, using the retention volume  $v_m$  corresponding to the DRI detector peak maximum of eluting polystyrene calibrants. Data were fitted with the GPC-11 program to an equation of the form:

$$\ln J(v_m) = D_1 - D_2 v_m + D_3 v_m^2 - D_4 v_m^3 + D_5 v_m^4 \quad (13)$$

where values of  $J$  corresponding to  $v_m$  were calculated from the corresponding polystyrene calibrant molecular weight via Equation 9 using:

$$J(v_m) = (1.14 \times 10^{-4})(M_{PS}(v_m))^{1.72}$$

where we have used published values of  $K_{PS}$  and  $a_{PS}$  for polystyrene in THF at 25 deg C (45).

Stock solutions of samples were prepared with a known concentration ( $w/v$ ) in THF in the range of  $4 \times 10^{-3}$  to  $5 \times 10^{-3}$  gm/ml. These stock solutions were filtered through a 0.22 micrometer Fluoropore filter prior to injection, and an injection size of 50 microliters was used. Of all the input

parameters for MOLWT-11, a large potential source of error resides in the value used for the injected mass; loss of sample during prefiltration or adsorption on the SEC column packing can introduce significant error into the SEC/LALLS molecular weight data. Comparison of off-line and on-line  $\bar{M}_w$  values is one check for full sample recovery, and this test was satisfied for the LB samples.

Mass recovery of MA samples was checked by using the concentration (DR1) detector response (mass/area ratio) of the corresponding LB arm; it was assumed that the detector response was identical for compositionally similar samples. Corrections for 38% and 9% sample loss were applied to the "mass injected" in the SEC/LALLS data for (S1-1) DVB and (S1-2) DVB, respectively.

Differential Refractometry (dn/dc). Stock solutions of polymer were prepared with known concentrations (w/v) in the solvent of choice, and the specific refractive index increment (dn/dc) was measured at 26 deg C with a KMX-16 Laser Differential Refractometer (LDC/Milton Roy). Sample concentrations typically were ca.  $5 \times 10^{-3}$  gm/ml.

Static Light Scattering. Off-line (static) values of the weight-average molecular weight ( $\bar{M}_w$ ) were measured using solutions prepared with toluene, THF, and chloroform. Four or five solutions in the range  $1.0 \times 10^{-3}$  to  $5.0 \times 10^{-3}$  gm/ml for the LB and  $0.1 \times 10^{-3}$  to  $0.5 \times 10^{-3}$  gm/ml for MA samples were prepared via serial dilution of a stock solution which was prefiltered through a 0.22 micrometer Fluoropore filter. Also, a similar 0.22 micron filter was placed in the sample inlet line to the KMX-6 LALLS cell. The LALLS measurements were performed at 6-7 degrees forward scattering angle, and data were processed and plotted in the standard fashion as  $Kc/\bar{R}_\theta$  vs. c (Equation 5); the intercept and slope of the best (visual) linear fit to the data gave the weight-average molecular weight ( $\bar{M}_w$ ) and second virial coefficient ( $A_2$ ), respectively.

## Results

Off-Line  $\bar{M}_w$  Measurements in Several Solvents. Table 1 shows results of dn/dc (column 3) and off-line  $\bar{M}_w$  measurements (column 6) which were carried out in THF, toluene, and chloroform. The dn/dc also was calculated via Equation 1b using the weight fraction of each monomer (from proton NMR, "Experimental") and the dn/dc for the corresponding homo polymers. Values of the homopolymers in THF: styrene (0.190), isoprene (0.127), butadiene (0.132); toluene: styrene (0.108), isoprene (0.031), butadiene (0.032); chloroform: styrene (0.155), isoprene (0.093), butadiene (0.094). Values of dn/dc derived in this manner are presented in column 4.

Table I. Specific Refractive Index and Off-Line LALLS Data

Sample	Solvent	dn/dc (ml/gm)		$\bar{M}_w \times 10^{-3}$	$\bar{M}_w \times 10^{-3}$	$A_2 \times 10^4$
		Meas.	Calc.	SEC/LALLS	Static LALLS	(mol-cm <sup>3</sup> /gm <sup>2</sup> )
SB-1 (53% S)	THF	0.159	0.162	58.2	62.3	12.6
	Tol.	0.072	0.072	-	57.5	11.4
	Chlor.	0.124	0.126	-	58.1	13.2
(SB-1) DVB	THF	0.160	-	671	746	4.0
	Tol.	-	-	-	749	4.0
	Chlor.	-	-	-	892	4.7
K1107 (~16% S)	THF	0.137	0.137	154	163	9.9
	Tol.	0.041	0.043	130	194	2.9
	Chlor.	0.101	0.103	-	205	10.3
SI-1 (9% S)	THF	0.136	0.133	210	249	11.0
	Tol.	0.037	0.038	-	214	10.8
	Chlor.	0.101	0.099	-	222	10.4
(SI-1) DVB	THF	0.133	-	1770	-	-
SI-2 (23% S)	THF	0.140	0.141	143	138	8.8
	Tol.	0.049	0.048	-	135	10.0
	Chlor.	0.105	0.107	-	149	9.0
(SI-2) DVB	THF	-	-	1490	-	-
SI-3 (26% S)	THF	0.143	0.143	109	124	11.2
	Tol.	0.051	0.051	-	124	12.4
	Chlor.	0.108	0.109	-	115	11.9
(SI-3) DVB	THF	-	-	1110	-	-
SI-4 (48% S)	THF	0.155	0.157	59.4	64.6	11.2
	Tol.	0.068	0.068	-	60.0	11.4
	Chlor.	0.117	0.123	-	71.5	12.5
(SI-4) DVB	THF	-	-	870	1320	3.6
	Tol.	-	-	-	1250	2.8
	Chlor.	-	-	-	1300	3.1

For several of the DVB-linked multi-arm structures, it was impossible to obtain acceptable static LALLS data: solutions were extremely difficult to filter, and they exhibited noisy and unstable LALLS baselines.

The off-line measurements of the linear block copolymer "arm" samples were not difficult. However, in most cases, chloroform solutions demonstrated noticeably more LALLS baseline instability than those prepared in THF and toluene; intensity readings changed as much as 10% within several minutes regardless of the amount of solution prefiltration.

SEC Data. Tables I and II present data from the SEC/LALLS runs. Overall sample  $\bar{M}_w$  values are given in Table I, while Table II shows  $\bar{M}_w$  and polydispersity data for the major peak in each chromatogram along with the molecular weight of the "kill" polystyrene component in each LB sample. Table II includes results from both the SEC/LALLS and linear polystyrene calibration treatments; this table shows also the ratio ( $k$ ) of the polystyrene-equivalent  $\bar{M}_w$  to the value from SEC/LALLS for the major peak in the chromatogram. The eighth column in Table II gives the weight-average number of arms ( $f_w$ ) for the MA samples, calculated from the  $\bar{M}_w$  value of the major peak in the MA and LB chromatograms. In the case of the LB samples, the  $\bar{M}_w$  from SEC/LALLS agrees favorably with that from off-line measurements. The approximately 19% higher off-line  $\bar{M}_w$  obtained in toluene vs. THF for K1107 reflects aggregation; note the significantly lower  $A_2$  in toluene.

In cases where static LALLS results were obtained for the DVB-linked samples, poor agreement was found with SEC/LALLS. In both cases shown in Table I ((SI-4) DVB) and ((SB-1) DVB), the SEC/LALLS  $\bar{M}_w$  is considerably less than the off-line  $\bar{M}_w$ . The concentration detector (DR1) response showed no significant sample loss ("Experimental") following injection, and this discrepancy possibly results from breakup of sample aggregates during chromatography ("Discussion", below).

The SEC/LALLS chromatograms for LB samples K1107, SI-3, and SI-4 are shown in Figures 1, 2a, and 3a, respectively, with the chromatograms for (SI-3) DVB and (SI-4) DVB presented in Figures 2b and 3b, respectively. The corresponding  $\log M(v)$  vs.  $v$  plots for (SI-3) DVB and (SI-4) DVB are given in Figures 2c and 3c, respectively, with representative values for the intrinsic viscosity ratio  $g'(v)$  included in the latter figures. The polystyrene calibration curve is included for comparison. Samples (SI-1) DVB and (SI-2) DVB showed sign inflections similar to (SI-3) DVB in the  $\log M(v)$  vs.  $v$  plots, while (SB-1) DVB demonstrated behavior similar to (SI-4) DVB.

Table II. SEC Data

Sample	SEC/LALLS <sup>(1)</sup>		Polystyrene Calibration <sup>(2)</sup>			$k$ <sup>(3)</sup>	$f_w$ <sup>(4)</sup>
	$\bar{M}_w \times 10^{-3}$	$\bar{M}_w/\bar{M}_n$	$\bar{M}_w \times 10^{-3}$	$\bar{M}_w/\bar{M}_n$	$M_{KILL} \times 10^{-3}$		
SI-1	198	1.01	231	1.04	15.0	1.17	15.6
(SI-1) DVB	$3.09 \times 10^3$	1.19	$1.44 \times 10^3$	1.28	-	0.47	
SI-2	143	1.02	142	1.05	30.0	0.99	18.0
(SI-2) DVB	$2.57 \times 10^3$	1.15	$1.05 \times 10^3$	1.27		0.41	
SI-3	108	1.02	115	1.04	25.0	1.06	15.9
(SI-3) DVB	$1.72 \times 10^3$	1.03	786	1.30		0.46	
SI-4	60.0	1.01	63.0	1.02	34.0	1.05	17.2
(SI-4) DVB	$1.03 \times 10^3$	1.11	491	1.16		0.48	
SB-1	60.0	1.01	76.0	1.02	31.0	1.27	15.8
(SB-1) DVB	946	1.16	507	1.20		0.54	
K1107	166	1.01	175	1.03	13.6	1.05	-

(1) Calculated for the major polymer peak of the chromatogram.

(2) Calculated for the major polymer peak of the chromatogram.  
"M<sub>KILL</sub>" is the peak mol. wt.

(3) Ratio of the polystyrene  $\bar{M}_w$  (col. 4) to SEC/LALLS  $\bar{M}_w$  (col. 2).

(4) Weight average branching functionality, using values in column 2.

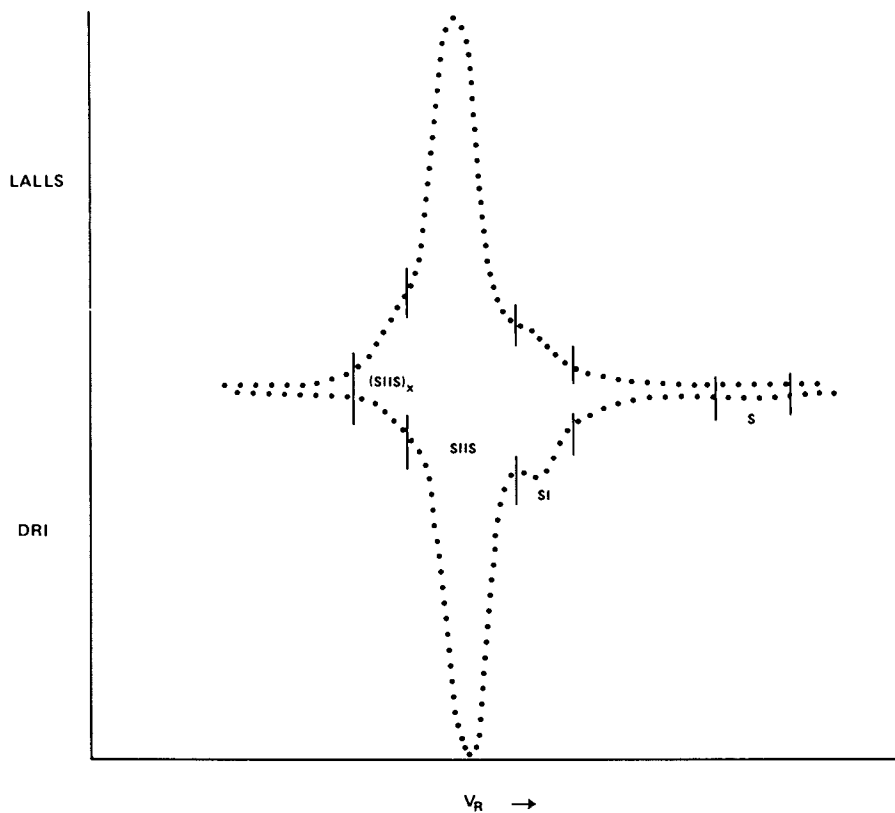


Figure 1. SEC/LALLS data for K1107. Peak S is "kill" polystyrene, while peaks SI, SIIS, and (SIIS)<sub>x</sub> are block copolymer, coupled block copolymer, and an unknown high molecular weight species<sup>4</sup>, respectively<sup>5</sup>. Values of  $\bar{M}_w$  from SEC/LALLS are  $8.26 \times 10^4$  and  $2.79 \times 10^5$  for SI and (SIIS)<sub>x</sub>.

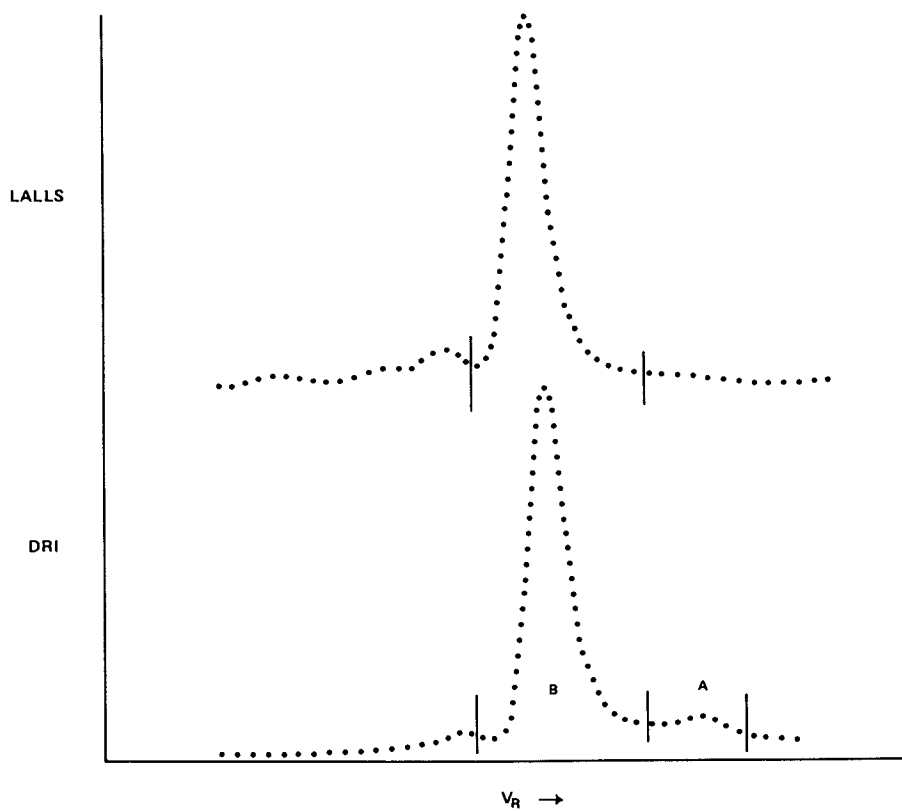


Figure 2a. SEC/LALLS chromatogram. Sample SI-3. Peak A is "kill" polystyrene; and peak B is LB.



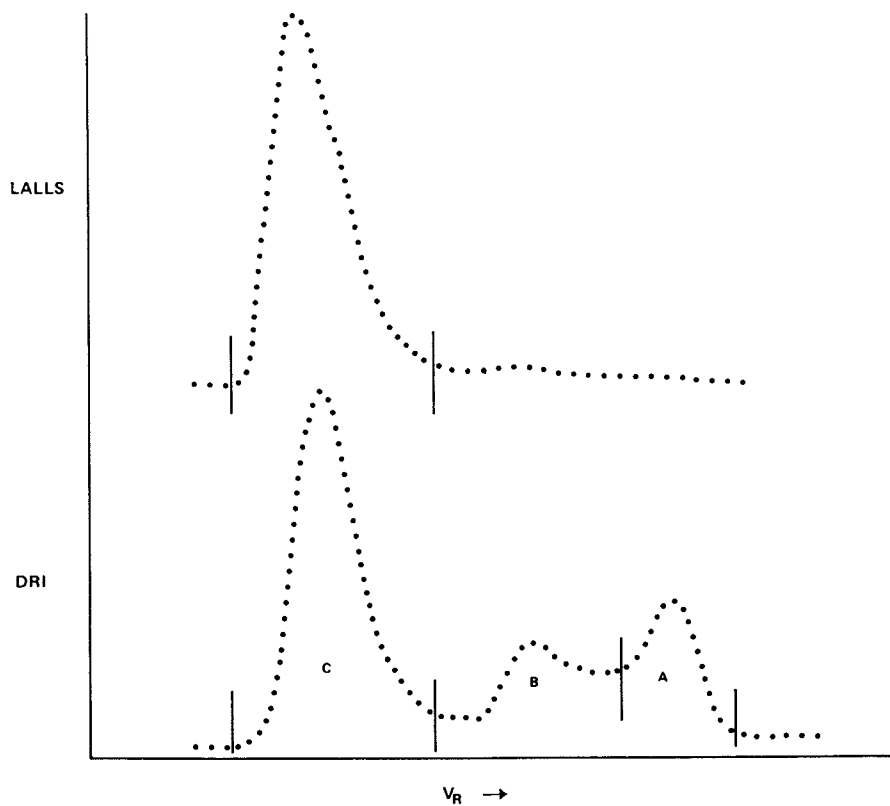


Figure 2b. SEC/LALLS chromatogram. Sample (SI-3) DVB. Peak A is "kill" polystyrene; peak B is LB; and peak C is DVB-linked MA.

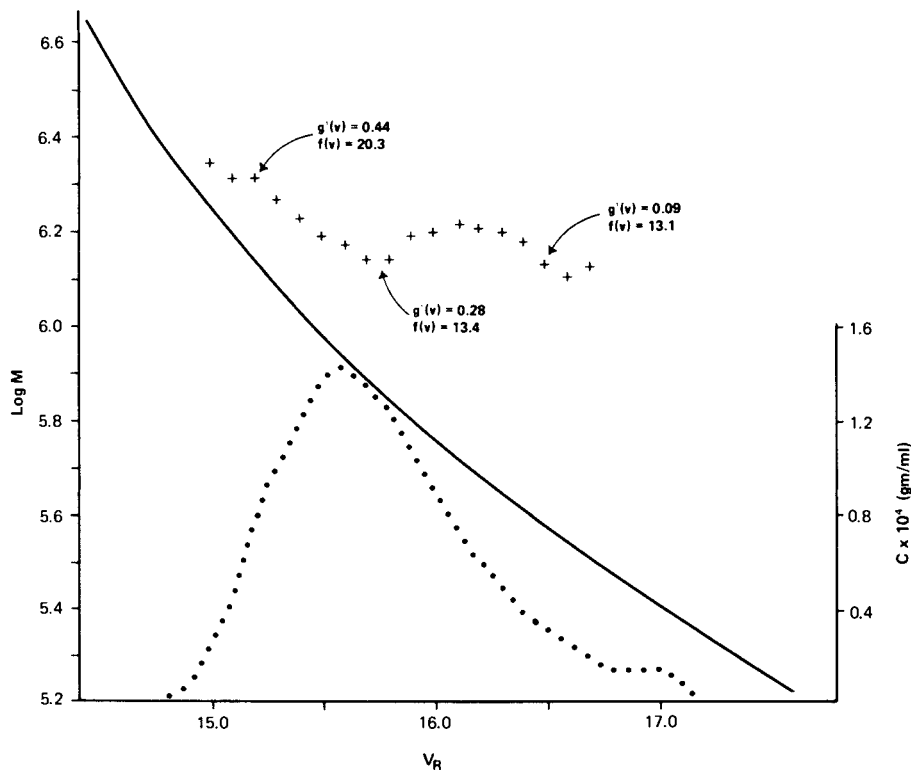


Figure 2c. Plots of  $\log M$  and concentration ( $c$ ) vs. retention volume ( $v$ ) for sample (SI-3) DVB. Values of the viscosity ratio  $g'(v)$  and branching functionality  $f(v)$  are given for several retention volumes.

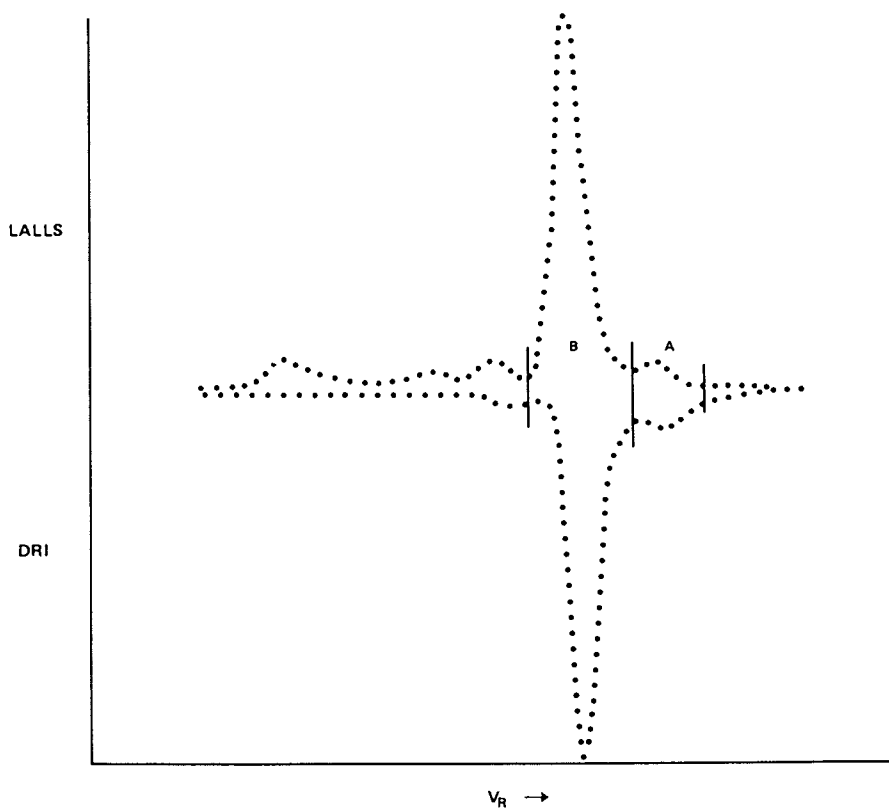


Figure 3a. SEC/LALLS chromatogram. Sample SI-4. Peak A is "kill" polystyrene; peak B is LB.

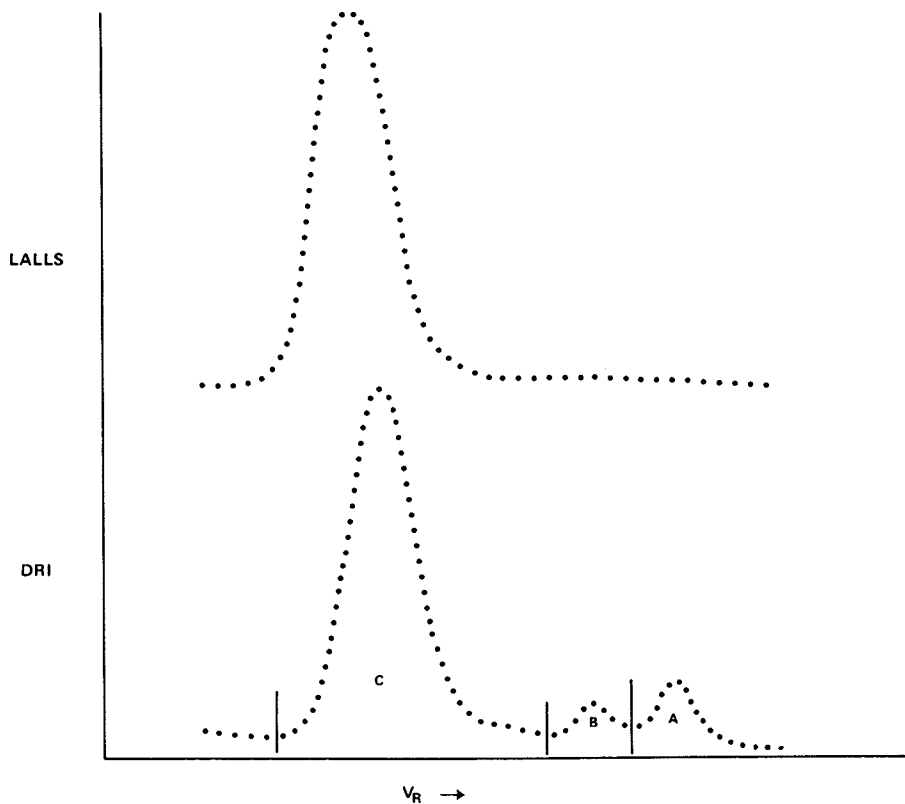


Figure 3b. SEC/LALLS chromatogram. Sample (SI-4) DVB. Peak A is "kill" polystyrene; peak B is LB; and peak C is DVB-linked MA.

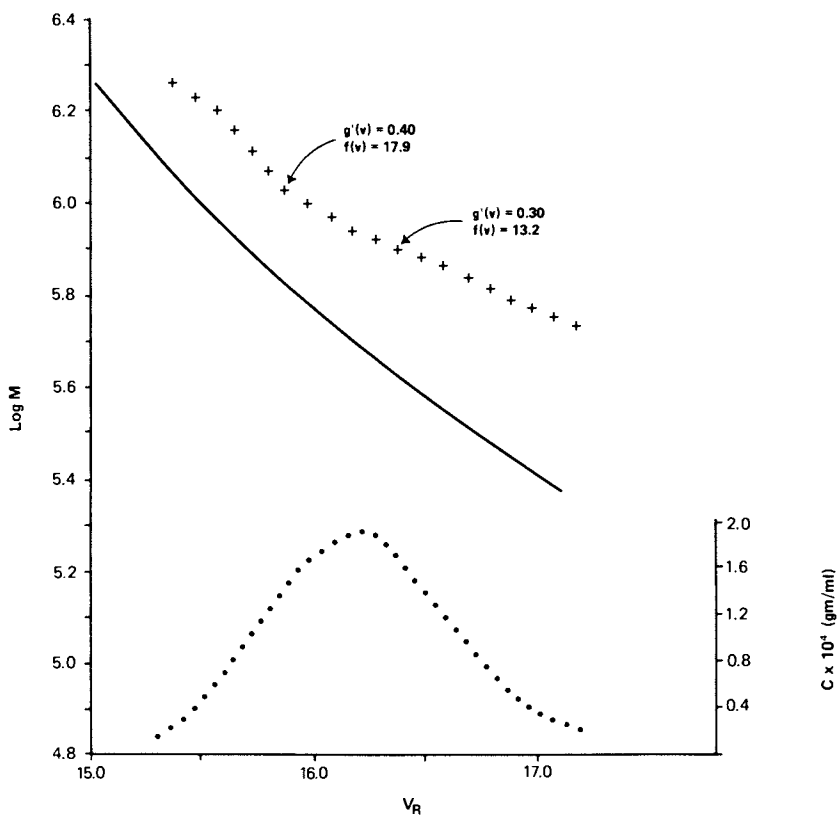


Figure 3c. Plots of  $\log M$  and concentration ( $c$ ) vs. retention volume ( $v$ ) for sample (SI-4) DVB. Values of the viscosity ratio  $g'(v)$  and branching functionality  $f(v)$  are given for several retention volumes.

The chromatogram of Kraton 1107 shows the other components of the sample besides the major coupled diene S-1-1-S: small amounts of "kill" polystyrene, uncoupled S-1 block copolymer, and material with higher molecular weight than that of SIIS are indicated. As indicated in Figures 2a and 3a, the LB polymers all showed a small polystyrene "kill" component and a high molecular weight shoulder on the block copolymer peak with a molecular weight of about twice that of the block copolymer.

The DVB-linked MA polymers showed evidence of "kill" polystyrene and block copolymer arm with peak elution volumes at the same position as in the LB chromatograms. Note that in Figure 2b, the LALLS chromatogram has a shoulder on the major peak which is not observable in the DRI chromatogram; this corresponds to a sign change in the slope of the  $\log M(v)$  vs.  $v$  relationship.

The most remarkable feature about the data from the LB and MA materials is the dramatic upward shift in the  $\log M(v)$  vs.  $v$  relationship which is induced by the multi-arm branching (Figures 2c and 3c). This is reflected by the change in  $k$  from values of ca. 1.0-1.3 to 0.5 for the LB and MA samples, respectively (Table II).

## Discussion

Off-Line (Static Measurement and  $\bar{M}_w$ . Congruence of the off-line  $\bar{M}_w$  measurement in the three solvents is consistent with compositional homogeneity of the LB arms ("Theory", above). Confirmation of the LB arm compositional uniformity was essential to the use of SEC/LALLS for investigation of the molecular weight/retention volume behavior of the MA polymers, since the  $dn/dc$  measured for the sample must correspond to that of polymer eluting in retention volume  $v$ . Agreement of the calculated and measured  $dn/dc$  (Table I) for the bulk sample is expected for block copolymers ("Introduction"). Off-line  $\bar{M}_w$  measurement of MA samples were beset with experimental difficulties. For example, the (SI-4) DVB sample showed good  $\bar{M}_w$  agreement in all three solvents, while (SB-1) DVB gave the same value in THF and toluene, but a significantly larger  $\bar{M}_w$  in chloroform. Considerable LALLS baseline instability indicated aggregation/association behavior in the chloroform solutions of (SB-1) DVB.

The second virial coefficients ( $A_2$ ) shown in Table I do not show significant dependence upon solvent for most of the LB samples. The only exception is K1107 which yielded an anomalously low  $A_2$  value in toluene; this sample exhibited marginal solubility in toluene, and the low  $A_2$  suggests unfavorable polymer-solvent interaction. The  $A_2$  values for MA polymers, however, are consistently lower than their LB

precursors. This decrease of  $A_2$  with increased molecular weight (and branching) is consistent with dilute solution polymer theory (35).

SEC/LALLS Measurements:  $\bar{M}_w$  Values. For most of the LB samples, SEC/LALLS  $\bar{M}_w$  data are in reasonable agreement with off-line (static) values. This supports the validity of the SEC/LALLS experimental data since it shows that the calculated mass injected probably equals the eluting mass. Loss of mass via column adsorption, insoluble gel, etc., usually is manifested by a low value of the SEC/LALLS  $\bar{M}_w$  relative to the off-line value. The off-line  $\bar{M}_w$  values which were obtained for the MA samples were significantly larger than the SEC/LALLS values ((S1-4) DVB and (SB-1) DVB). The detector response characteristics of these MA samples, compared to the starting LB polymers, indicated no loss of mass during sample preparation and chromatography. A possible source of the  $\bar{M}_w$  discrepancy is the presence of a small fraction of undissolved microgel in the stock solution along with a high proportion of loosely associated aggregates. The microgel probably is removed by filtration and column frits, while the aggregates would be dissociated in the strong shear fields in the flowing SEC solvent. The detector response data would not show sample loss from removal of a very small number of microgel particles and dissociation of the aggregated material. Such behavior is strongly suggested by the difficult filtration behavior of the MA sample, and the presence of microgel and aggregates will have a disproportionate effect on the LALLS response.

The differences in polystyrene-equivalent and absolute molecular weight for the LB and MA polymers are represented by the  $k$  values in Table II; they demonstrate dissimilarities in hydrodynamic volume/molecular weight which are conferred by monomeric composition and polymeric backbone structure. The decrease in  $k$  from ca. 1.0-1.3 for LB materials to about 0.5 for the corresponding MA reflects the much higher polymer segment density in the MA species.

The LB behavior can be compared with Tung's data (46) for styrene/butadiene block copolymers as well as with that author's presentation of Duc and Prud'homme's polystyrene/isoprene block copolymer data (47). The styrene/butadiene materials (45% styrene) exhibited polystyrene-equivalent molecular weights about a factor of 1.35 larger than their true molecular weight. Although he did not carry out experiments with block copolymers of polystyrene/isoprene, Tung did study homopolymers of isoprene and butadiene; these data suggest that the polystyrene-equivalent molecular weight of styrene/isoprene block copolymers would be closer to the true value than in the case of styrene/butadiene. The  $k$  value for SB-1 (1.27) agrees with Tung's data for

styrene/butadiene block copolymers of similar composition, and the lower values (1.0-1.17) for the styrene/isoprene block copolymers are consistent with Tung's homopolymer results.

The weight-average branching functionality ( $f_w$ ) for the major MA peak (Table II) falls between 16 and 18 for all the samples. This probably reflects the constancy of experimental preparation conditions: temperature, concentration, solvent, and the ratio  $[DVB]/[RLi]$ .

The dramatic upward shift in the MA molecular weight/elution volume curve was accompanied, in several of the samples, by changes in the sign of the slope. Figure 2c illustrates this. Such a sign inflection was found in the molecular weight/elution volume behavior of samples (SI-1) DVB, (SI-2) DVB, and (SI-3) DVB, and it is manifested by appreciably smaller  $\bar{M}_w/\bar{M}_n$  for SEC/LALLS compared with polystyrene calibration data (Table II). The polystyrene calibration forces any chromatogram to yield identical elution volume/molecular weight characteristics. (The SEC/LALLS method typically gives a slightly lower polydispersity than linear polystyrene calibration, due to detector response differences and opposite effects of column/hardware band spreading on the molecular weight calculation (28, 29, 31). However these effects generally are small relative to the polydispersity differences shown here.) The SEC/LALLS data for the lowest molecular weight MA samples, (SI-4) DVB and (SB-1) DVB, showed continually decreasing molecular weight with retention volume and a smaller slope than the polystyrene calibration. The latter difference contributes to the smaller polydispersity ( $\bar{M}_w/\bar{M}_n$ ) given by SEC/LALLS. A sign inflection was noted in the SEC/LALLS molecular weight/elution volume behavior of cellulose tricarbonyl (48), and these workers have ascribed it to "branching"; the qualitative rationale is that branched polymer with a high segment density can elute after a less-branched polymer with a larger hydrodynamic volume and smaller molecular weight. Such SEC/LALLS data for the cellulose derivatives and some of the MA samples in this work may reflect distributions of branching structure. Further studies are necessary to elucidate this.

The representative viscosity ratio ( $g'(v)$ ) values shown in Figures 2c and 3c reflect considerably higher segment density of the MA species relative to their linear homolog of identical molecular weight. However, the variation of  $g'(v)$  with  $M$  is contrary to that expected from theory, which predicts an increase in this parameter with decreasing molecular weight (21). The variation of  $g'(v)$  with  $M$  is qualitatively predictable from comparison of the polystyrene calibration curve and data shown in Figures 2c and 3c: Equation 12 shows that if  $M_{PS}(v)/M_{MA}(v)$  decreases with molecular weight, as with data shown here,  $g'(v)$  must



decrease. This result casts doubt on the validity of the universal calibration as well as assumption of a constant ratio ( $k$ ) for  $M_{PS}/M_{LB}$ . The latter certainly may be in error, and further work with LB materials of constant composition and a range of molecular weights would be necessary to evaluate the appropriateness of the assumption. Also, the SEC behavior of the MA materials may not conform to the universal calibration curve; the work of Bi and Fetters (1) on similar samples containing butadiene-styrene and isoprene-styrene block copolymer arms showed that the universal calibration method gave erroneous molecular weight information for high molecular weight samples. The structure which Bi and Fetters ascribe to the DVB-linked block copolymers, i.e., an inner "core" poly(diene) surrounded by a "shell" of polystyrene, might confer unusual SEC elution behavior which is related to their finding that the intrinsic viscosity depends on arm length and not branching functionality. (Similar MA materials prepared with homopolymer arms of isoprene or butadiene gave accurate molecular weights via the universal calibration (8, 15).)

Finally, chromatography artifacts may contribute to failure of universal calibration. At high sample concentrations, so-called "viscous streaming" (43) retards SEC elution of high molecular weight polymers. This may in fact account for the inflection in the molecular weight/elution volume behavior shown by the three higher molecular weight MA samples: this viscosity/concentration effect might be selectively retarding elution of some higher molecular weight species within the same sample. The effect may be operating to a lesser extent in the SEC behavior of the two lower molecular weight MA samples. In the latter case, it will tend to decrease the slope of the  $\log M/V_R$  curve.

In summary, the approach outlined here is a straightforward method for determining representative values of viscosity ratios  $[\eta]_{MA}/[\eta]_{LB}$ ; certainly  $g'$  values significantly less than 1.0 are expected for such highly branched polymers (33). However, the anomalous dependence of  $g'(v)$  on  $M_{MA}$  suggests that 1) the core/shell hydrodynamic configuration and/or chromatographic artifacts invalidate universal calibration, and/or 2) the LB elution behavior does not conform to that of polystyrene in the assumed, constant manner. Further work is necessary to elucidate these points.

### Literature Cited

1. Bi, L. K.; Fetters, L. J. Macromolecules 1976, 9, 732.
2. Von Meerwall, E.; Tomich, D. H.; Hadjichristidis N.; Fetters, L. J. Macromolecules 1982, 15, 1157.
3. Raju, V. R.; Menezes, E. V.; Marin, G.; Graessley, W. W.; Fetters, L. J. Macromolecules, 1981, 14, 1668.

4. Morton, M.; Helminiak, T. E.; Gadkary, S. D.; Bueche, F. J. Polym. Sci., 1962, 57, 471.
5. Zelinski, R. P.; Wofford, C. F. J. Polym. Sci., Part A, 1965, 3, 93.
6. Roovers, J. L.; Bywater, S. Macromolecules, 1972, 5, 385.
7. Roovers, J. L.; Bywater, S. Macromolecules, 1974, 7, 443.
8. Hadjichristidis, N.; Guyot, A.; Fetters, L. J. Macromolecules, 1978, 11, 668.
9. Hadjichristidis, N.; Fetters, L. J. Macromolecules, 1980, 13, 191.
10. Decker, D.; Rempp, P. C. R. Acad. Sci., Ser. C., 1965, 261, 1977.
11. Worsfold, D. J.; Zilliox, J. G.; Rempp, P. Canad. J. Chem., 1969, 47, 3379.
12. Bi, L. K.; Fetters, L. J. Macromolecules, 1975, 8, 90.
13. Kohler, A.; Polacek, J.; Koessler, T.; Zilliox, J. G.; Rempp, P. Eur. Polym. J., 1972, 8, 627.
14. Zilliox, J. G. Makromol. Chem., 1972, 156, 121.
15. Quack, G.; Fetters, L. J.; Hadjichristidis, N.; Young, R. N. Ind. Eng. Chem. Prod. Res. Dev., 1980, 19, 587.
16. Martin, M. K.; Ward, T. C.; McGrath, J. E. in "Anionic Polymerization"; McGrath, J. E., Ed.; ACS SYMPOSIUM SERIES No. 166, American Chemical Society: Washington, D.C., 1981; p. 558.
17. Roovers, J.; Hadjichristidis, N.; Fetters, L. J. Macromolecules, 1983, 16, 214.
18. Hadjichristidis, N.; Roovers, J. J. Polym. Sci. (Polym. Phys. Ed.), 1974, 12, 2521.
19. Bauer, B. J.; Hadjichristidis, N.; Fetters, L. J.; Roovers, J. L. J. Am. Chem. Soc., 1980, 102, 2410.
20. Benoit, H. J. Polym. Sci., 1953, 11, 507.
21. Zimm, B. H.; Stockmayer, W. H. J. Chem. Phys., 1949, 17, 1301.
22. Candau, F.; Rempp, P.; Benoit, H. Macromolecules, 1972, 5, 627.
23. McCrackin, F. L.; Mazur, J. Macromolecules, 1981, 14, 1214.
24. Stockmayer, W. H.; Fixman, M. Ann. N. Y. Acad. Sci., 1953, 57, 334.
25. Roovers, J. Polymer, 1979, 20, 843.
26. Roovers, J.; Toporowski, P. M. Macromolecules, 1981, 14, 1174.
27. Ouano, A. C.; Kaye, W. J. Polym. Sci. (Polym. Chem. Ed.), 1974, 12, 1151.
28. McConnel, M. L. Am. Lab., 1978, 10 (5), 63.
29. Jordan, R. C. J. Liquid Chromatog., 1980, 3, 439.
30. Hamielec, A. E.; Ouano, A. C.; Nebenzahl, L. L. J. Liquid Chromatog., 1978, 1, 527.

31. Jordan, R. C.; McConnel, M. L. in "Size Exclusion Chromatography (GPC)"; Provder, T., Ed.; ACS SYMPOSIUM SERIES No. 138, American Chemical Society: Washington, D.C., 1979; pp. 107-129.
32. Axelson, D. E.; Knapp, W. C. J. Appl. Polym. Sci., 1980, 25, 119.
33. Agarwal, S. H.; Jenkins, R. F.; Porter, R. S. J. Appl. Polym. Sci., 1982, 27, 113.
34. Benoit, H.; Froelich, D. in "Light Scattering from Polymer Solutions"; Huglin, M. B., Ed.; Academic: New York, 1972; p. 468.
35. Flory, P. J. in "Principles of Polymer Chemistry"; Cornell University Press: Ithaca, New York, 1953.
36. Stacey, K. A. in "Light Scattering in Physical Chemistry"; Academic Press: New York, 1956.
37. Tanford, C. in "Physical Chemistry of Macromolecules"; John Wiley and Sons: New York, 1961.
38. Kaye, W. Anal. Chem., 1973, 45, 221A.
39. Kaye, W.; Havlik, A. J. Appl. Opt., 1973, 12, 541.
40. Huglin, M. B. in "Light Scattering from Polymer Solutions"; Huglin, M. B., Ed.; Academic: New York, 1972; p. 165.
41. Schulz, G. V.; Wunderlich, W.; Kirste, R. Makromol. Chem., 1964, 75, 22.
42. Machtle, W.; Fischer, H. Angew. Makromol. Chem., 1969, 7, 147.
43. Yau, W. W.; Kirkland, J. J.; Bly, D. D. in "Modern Size Exclusion Chromatography"; John Wiley and Sons: New York, 1979.
44. Grubisic, Z.; Rempp, P.; Benoit, H. J. Polym. Sci., 1967, B 5, 753.
45. Hellman, M. Y. in "Liquid Chromatography of Polymers and Related Materials"; Cazes, J., Ed.; Marcel Dekker: New York, 1977; p. 31.
46. Tung, L. H. J. Appl. Polym. Sci., 1979, 24, 953.
47. Ho-Duc, N.; Prud'homme, J. Macromolecules, 1973, 6, 472.
48. Cael, J. J.; Cannon, R. E.; Diggs, A. O. in "Solution Properties of Polysaccharides"; Brant, D. A., Ed.; ACS SYMPOSIUM SERIES No. 150, American Chemical Society: Washington, D.C., 1980; p. 43.

RECEIVED December 20, 1983

# Determination of Thermoset Resin Cross-link Architecture by Gel Permeation Chromatography

A. J. AYORINDE, C. H. LEE, and D. C. TIMM

University of Nebraska, Lincoln, NE 68588-0126

W. D. HUMPHREY

Brunswick Corporation, Lincoln, NE 68504

Gel permeation chromatography is the method of choice for analysis of thermoplastic resin systems. Corrected for imperfect resolution, chromatogram interpretation yields accurate molecular descriptions, including theoretical, kinetic distributions (1,2). The current research is designed to extend the utility of this analytical tool to the analysis of thermoset resins.

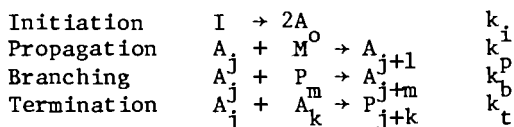
Kinetic mechanisms (3) are such that low molecular weight species are present in a cured resin; in fact, the molar concentration of dimers, trimers, etc. usually exceeds that for higher molecular weight species. An exception is a Poisson distribution, but oligomeric species are still abundant. If a cured thermoset resin is prepared such that a large surface area to volume ratio is achieved, solvent leaching provides an effective method for sample preparation. Analysis of extracts (4,5) provides data descriptive of monomeric content and oligomeric, molecular distributions. Such extracts contain definitive information with respect to the extent of cure as well as a description of the crosslink architecture. Average molecular weights between crosslink sites plus crosslink density within the insoluble, resin fraction can be determined.

Observations for cured epoxy resins and resins derived from 1,2-polybutadiene crosslinked with *t*-butylstyrene are reported. These resins find applications in aerospace industry, including high performance, Kevlar 49, filament wound, pressure vessels on Skylab and the Space Shuttle.

## Population Density Distributions

Chain-growth polymerization. A 1,2-polybutadiene polymer is crosslinked with *t*-butylstyrene, utilizing a free radical initiator. Reaction rates include

0097-6156/84/0245-0321\$06.00/0  
© 1984 American Chemical Society



The 1,2-polybutadiene initially formulated is a commercially available material supplied by Colorado Specialty Company and Nippon Soda. An anionic polymerization, initiated by a butyl lithium, is likely used in its manufacture. This results in a molar distribution of constitutive molecules defined by a Poisson distribution for batch polymerizations. Thus, the number and weight average molecular weights are nearly equal. The current research further assumes that this distribution is sufficiently narrow such that all polybutadiene molecules are of the same molecular weight, which is described by the degree of polymerization  $n$ . This constraint greatly simplifies the mathematical description to be developed for the population of molecules during the subsequent chain-growth cure initiated by dicumyl peroxide.

Fisher (6), in a discussion of relative rates of reaction, states that the styrenic free radical is more likely to react with a styrene molecule than with the polyunsaturated 1,2-polybutadiene. The relative rates are expected to differ by orders in magnitude. Therefore, the propagation reaction rate is expressed in terms of the molecularly mobile monomer, *t*-butylstyrene. The consequence is that the 1,2-polybutadiene will be crosslinked primarily by *t*-butylstyrene segments.

The extracts from a quality resin contain oligomeric molecules of a degree of polymerization less than that for the 1,2-polybutadiene. These species are a consequence of simultaneous propagation and termination reactions. Their population density distribution is also descriptive of that portion of molecules which react with polymeric species, initially forming a branched, and later a crosslinked, structure within the resin. Research shows that the average molecular weight of the oligomeric fraction correlates with the crosslink average molecular weight within the insoluble, crosslinked resin fraction (7). Such is a kinetic consequence of the competition between branching and termination reactions in the above reaction model.

For free radical species of degree of polymerization less than that for the 1,2-polybutadiene used in the formulation, a kinetic reaction analysis results in the following relationships expressed in terms of the molar concentration of primary free radicals  $A_0$ .

$$\frac{dA_0}{dt} = 0 = 2k_i I - (k_p^M + k_b^P_{TOT} + k_t A_{TOT}) A_0$$

$$A_0 = 2k_i I / (k_p^M + k_b^P_{TOT} + k_t A_{TOT})$$

$$\frac{dA_1}{dt} = 0 = k_p M A_o - (k_p M + k_b P_{TOT} + k_t A_{TOT}) A_1$$

$$A_1 = A_o (k_p M)^1 / (k_p M + k_b P_{TOT} + k_t A_{TOT})^1 = \frac{A_o}{D^1}$$

The cumulative molar concentrations of polymeric and activated intermediates are  $P_{TOT}$  and  $A_{TOT}$ , respectively. The denominator is  $D = (k_p M + k_b P_{TOT} + k_t A_{TOT}) / k_p M$ . The analysis recognizes that these activated intermediate species must be saturated and, therefore, do not experience generation through branching/crosslinking reactions which normally require unsaturation. For primary free radicals  $A_o$ , conservation of population includes initiation, propagation, branch formation and termination reactions. The latter is assumed to be by combination. For free radicals that contain monomer segments  $j$ ,  $0 < j < n$ , the initiation rate is superseded by a propagation rate. The rate of accumulation or depletion within the batch reactor is negligible for these activated intermediates. These expressions are representative of a recurring type relationship.

For molecules at a degree of polymerization  $n$  or larger, the mathematical model incorporates branch formation reactions which include a free radical of size  $j$  and a polymeric specie of degree of polymerization  $m \geq n$ . The consequence is the formation of a free radical of molecular size  $j + m$ . Furthermore, due to the relatively high concentration initially of the 1,2-polybutadiene constituent at  $j = n$ , the derivation assumes that all polymeric species of size  $j \geq n$  are unsaturated and are capable of branch and/or crosslink formation. Polymeric species are denoted by  $P_j$ ; free radical intermediates are described by  $A_j$ . Therefore, the first activated intermediate capable of formation by branching reactions is  $A_n$  via  $A_o + P_n \rightarrow A_n$ . Conservation laws yield

$$\frac{dA_n}{dt} = 0 = k_p M A_{n-1} - (k_p M + k_b P_{TOT} + k_t A_{TOT}) A_n + k_b A_o P_n$$

$$A_n = A_o / D^n + k_b A_o P_n / k_p M D$$

As the degree of polymerization increases, all possible combinations of reactions forming a free radical via branching must be considered. Thus

$$\frac{dA_{n+1}}{dt} = 0 = k_p M A_n - (k_p M + k_b P_{TOT} + k_t A_{TOT}) A_{n+1} + k_b (A_o P_{n+1} + A_1 P_n)$$

Previous expressions for  $A_n$  and  $A_1$  can be substituted, yielding

$$A_{n+1} = \frac{A_o}{D^{n+1}} + \frac{k_b A_o}{k_p M D} \left( P_{n+1} + \frac{2P_n}{D} \right)$$

The factor 2 is a consequence of the second term in the expression for  $A_n$  and the term  $k_b A_1 P_n$  in the conservation expression  $dA_{n+1}/dt$ . At a degree of polymerization  $j = n + 2$

$$\frac{dA_{n+2}}{dt} = 0 = k_p M A_{n+1} - (k_p M + k_t A_{n+2} + k_b P_{TOT}) A_{n+2} + k_b (A_o P_{n+2} + A_1 P_{n+1} + A_2 P_n)$$

Substitution of the several expressions for  $A_{n+1}$ ,  $A_1$ ,  $A_2$  and a collection of similar terms yields

$$A_{n+2} = \frac{A_o}{D^{n+2}} + \frac{k_b A_o}{k_p M D} (P_{n+2} + \frac{2P_{n+1}}{D} + \frac{3P_n}{D^2})$$

This type of recurring formula represents the molar concentration of free radicals up to a degree of polymerization  $j=2n-1$ . At molecular weights twice that of the initial 1,2-polybutadiene,  $j=2n$ , the initial substitution of the expression for  $A_n$  in the rate of formation due to branching occurs and results in a second major change in the overall functionality of the descriptive relationship for the concentration of activated intermediates. Consider the conservation laws at this degree of polymerization

$$\frac{dA_{2n}}{dt} = 0 = k_p M A_{2n-1} - (k_p M + k_b P_{TOT} + k_t A_{2n}) A_{2n} + k_b \{ A_o P_{2n} + A_1 P_{2n-1} + \dots + A_{n-1} P_{n+1} + A_n P_n \}$$

Solving this expression for  $A_{2n}$  after expressing  $A_j$ ,  $1 \leq j \leq n$  and  $A_{2n-1}$  in terms of  $A_o$  yields

$$A_{2n} = \frac{A_o}{D^{2n}} + \frac{k_b A_o}{k_p M D} (P_{2n} + \frac{2P_{2n-1}}{D} + \frac{3P_{2n-2}}{D^2} + \dots + \frac{(n+1)P_n}{D^n}) + (\frac{k_b}{k_p M})^2 A_o (P_n P_n)$$

Thus, the addition of a third function occurs for the first time at  $j=2n$ . Continuation of the derivation will result in a series of rather complex functionality, but one which will be mathematically defined.

The degree of polymerization intervals of interest are, therefore, comprised of distinct regions determined by the initial molecular weight of the 1,2-polybutadiene,  $n$ .

$$\begin{aligned} j < n & \quad A_j = A_o / D^j \\ n \leq j < 2n & \quad A_j = A_o / D^j + \frac{k_b A_o}{k_p M D} \sum_{k=1}^{j-n+1} k P_{j+1-k} / D^{k-1} \end{aligned}$$

$$\begin{aligned}
 2n \leq j \quad A_j = & A_o / D^j + \frac{k_b A_o}{k_p MD} \sum_{k=1}^{j-n+1} k P_{j+1-k} / D^{k-1} \\
 & + \left( \frac{k_b}{k_p MD} \right)^2 A_o \sum_{m=n}^{m=j-n} \frac{(m+1-n)(m+2-n)}{2} \sum_{k=n}^{k=j-m} P_{j-k-m+n} / D^{m-n} \quad (1)
 \end{aligned}$$

A set of first order differential equations descriptive of the molar concentrations for polymeric species is given. Species, less than size  $n$ , are saturated and, therefore, accumulate only within the batch reactor and do not participate in branch/cross-link reactions. Molecules greater in size than  $n$  are unsaturated and will experience the reaction described by branch formation. As the extent of cure progresses, this reaction forms chain networks within the resin. Representative equations are

$$\begin{aligned}
 j < n \quad \frac{dP_j}{dt} = & A_o^2 k_t (j+1) / 2D^j \\
 n \leq j < 2n \quad \frac{dP_j}{dt} = & A_o^2 k_t (j+1) / 2D^j + \frac{A_o^2 k_t k_b}{2k_p MD} \sum_{k=0}^{j-1} \frac{(k+1)(k+2)}{D^k} P_{j-k} \quad (2)
 \end{aligned}$$

An expression for macromolecules greater than twice that of the initial 1,2-polybutadiene will necessarily be more complex due to the last equation of Expression (1).

Experimentally, macromolecules greater than  $2n$  are usually crosslinked to an extent that they are essentially insoluble, being attached to the network resin structure. The intent of the model is to explain comparative observations in oligomeric population density distributions obtained through analysis of extracts of thermoset resins. The model clearly shows that for activated intermediates  $A_j$  and for polymeric species  $P_j$  frequency distributions are comprised of additive functions for distinct regions in molecular weight. The functionality at a lower degree of polymerization is contained within the distribution at a larger degree of polymerization, relative to the size of the initial polybutadiene component.

The term  $D^j$  can be expressed in terms of the relative rates of branch formation plus termination compared to propagation. Since this relative rate is numerically small, a truncated series of  $\ln(1+x)$  results in the valid approximation

$$D^{-j} = \exp\left(- \frac{k_b P_{TOT} + k_t A_{TOT}}{k_p M} j\right) \quad (3)$$

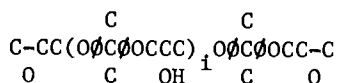
The argument of the exponential is  $x$ . Therefore, molar distributions of oligomeric species leached from cured resins will be presented on semilogarithmic graphs.



Data observed for cured resins are presented by Figure 1. Formulations and cures were identical except for the molecular weight of the 1,2-polybutadiene. The functionality of the oligomeric fraction leached from cured resins clearly shows expected dependency of the population density distribution on molecular weight of the original polymer. Numerical chromatogram analysis (1) corrects for imperfect resolution. The calibration utilized a set of linear, epoxy resins formed from the step-growth polymerization of nadic methyl anhydride and phenyl glycidyl ether. The molecular distributions of these materials are a Poisson (8) distribution of different average molecular weight. The calibration and subsequent interpretation has been extensively tested using thermoplastics (9,10) of known, kinetic distribution. However, the effects of hydrodynamic volume on molecular weight on the present nonlinear oligomeric fraction of varying chemical composition is unknown. Thus, the assignment of degree of polymerization is on a relative basis.

Figure 1 is graphed consistent with the functionality of Equations 2. The degree of polymerization 329 is a constant of calibration. The 450-1200 molecular weight, 80% 1,2-polybutadiene resin has an initial inflection point at about 700 molecular weight, a second at 2,570 molecular weight. Equations 1 and 2 predict such, though the second break point is somewhat greater than the simplified model predicts. Integration and Trommsdorff (11) effects are expected to influence precise locations. The extracts were leached from quality cured resins being evaluated for aerospace applications. The initial break points for the 2,000 molecular weight, 80% 1,2-polybutadiene resin and for the 4,400 molecular weight, 70% 1,2-polybutadiene resin show expected dependency on molecular weight (see Table I). The initial and second break points for the 3,000 molecular weight, 90% 1,2-polybutadiene and the second break point for the 2,000 molecular weight specimens are absent, primarily due to low oligomeric resin content at expected degrees of polymerization. Less than one percent of the former resin is soluble. The second break points for the two, highest molecular weight specimens are in the regions of insoluble, crosslinked structures. Observations are tabulated, see Table I.

Step-growth polymerization. Epoxy resins were prepared from nadic methyl anhydride and Epon 828. This bifunctional oxirane also supplies reactive hydrogen sites. The major component is at  $i=0$ , minor components include oligomers with  $i=1,2,3$ . Their concentrations rapidly diminish as degree of polymerization increases.



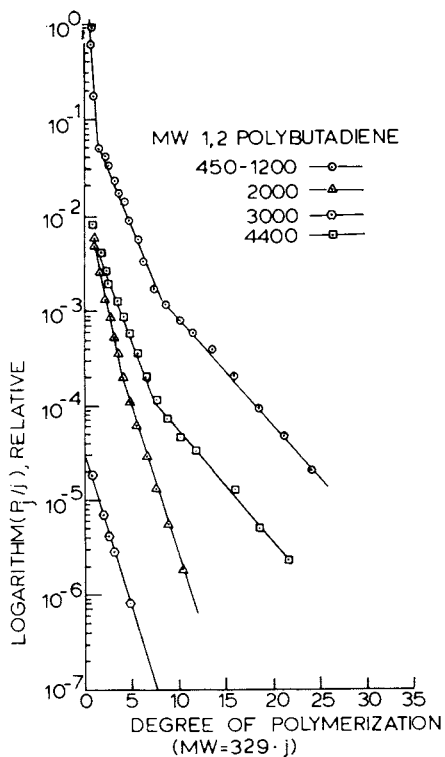


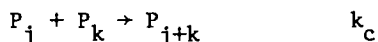
Figure 1. Oligomeric frequency distribution, chain-growth polymerization.

Table I: Hydrocarbon Resin Formulation

$\overline{MW}$	1,2-polybutadiene		t-butyl- styrene Parts	Dicumyl Peroxide Parts	Figure 1	
	Parts	% 1,2			Break Point 1st	2nd
450-1200	70	80	30	1.9	660	2570
2000	80	80	20	1.9	1410	--
3000	80	90	20	1.9	--	--
4400	80	70	30	1.9	2500	--

Cure at 24 hours, 140°C

Basic industrial catalysts were utilized. The ionic, polymerization mechanism (12) results in the reactive hydrogen site alternately reacting with the anhydride and oxirane groups. The chemistry of the reaction is such that an alcohol end group reacts with monomeric anhydride, forming an acid group. This group will then react with an oxirane group, forming an alcohol. Thus, the reactive hydrogen site is conserved. The molecule's backbone structure will contain anhydride residuals alternating with oxirane residuals coupled via ester linkages. The molecule will also contain pendent side chains terminated by oxirane groups. Acid end groups on one molecule will, therefore, react with monomeric or oligomeric species containing the oxirane functionality. Both reactions result in the coupling of two molecules



If one of the species is monomeric oxirane, then  $j = 1$ . Likewise, if one of the polymeric species supplied the oxirane, then  $j > 1$ . The molecule with the acid group is at degree of polymerization  $k$ . The degree of polymerization indexes the number of oxirane residuals within the macromolecule. Though the reaction sequence is simplified, it retains the essence of one molecule reacting with every other molecule. This step-growth mechanism (13) develops the thermoset resin microstructure.

For batch polymerizations initially void of polymeric species, the molar distribution of polymeric species is expressed by

$$P_j(\tau) = P_1(\tau) \{1 - \exp(-\tau)\}^{j-1}$$

An excellent approximation for small values of  $\exp(-\tau)$  is

$$P_j(\tau) = P_1(\tau) \exp(-\exp(-\tau)(j-1)) \quad (4)$$

The time variable  $\tau$  is the eigenzeit transform

$$\tau = \int_0^t k_c P_{TOT}(t) dt$$

The first moment of the distribution is  $P_{TOT}$ , the total, cumulative molar concentration of polymeric material. As the molecular weight of polymeric species increases, branching and crosslinking reactions yield a thermoset resin. Chromatography analysis of epoxy resin extracts confirms the expected population density distribution described by Equation 4, as is shown in Figure 2. Formulations and cure cycles appear in Table II.

Three of the four resins yield extracts of the functionality of Equation 4. The slope of the exponential decay allows for the evaluation of  $\tau$ . The resin, see Table II, initiated by benzyl dimethyl amine (BDMA) at the stated cure cycle, when subjected to leaching yields an extract of low solubility and a distribution of oligomeric molecules of low number average molecular weight.

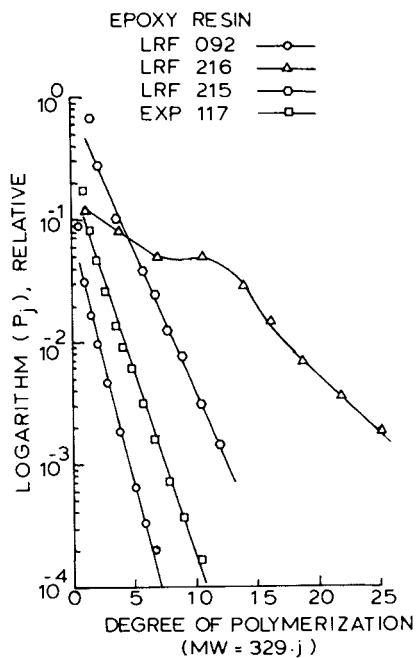


Figure 2. Oligomeric frequency distribution, step-growth polymerization.

Table II: Epoxy Resin Formulation

Resin	Anhydride	Epoxy	Catalyst	HDT, °F
LRF-216	NMA	Epon 828	ATC 3	107
*LRF-215	Polyoxypropyleneamine	DER 332	---	139
EXP-117	NMA	Epon 828	EMI-24	211
LRF-092	NMA	Epon 828	BDMA	276
Anhydride Cure	12 hrs., 125°F; 2 hrs., 225°F; 4 hrs., 290°F			
* Amine Cure	16 hrs., 80°F; 2 hrs., 150°F			

Such a resin is highly crosslinked. The resin Exp 117 is more soluble and the oligomeric species are of a greater average molecular weight. Thus, the average extent of crosslink development has diminished. The resin LRF 215 is an amine cured epoxy; thus, its relative placement will depend, in part, on the specific refractive index increment contribution of the amine component compared to the anhydride segment. This is not expected for this resin to be substantially different. The slope of the population distribution of oligomeric species contained in the resin's extract is of a still higher molecular weight. Thus, the extent of crosslinked development is less than the previous two resins discussed. The system LRF 216 is the least cured of the four resins.

The emphasis of the current research is on molecular structure of oligomeric fractions leached from quality cured, industrial resins. However, the potential for applications in quality control should not be overlooked. Chromatography analysis provides positive feedback capable of molecular descriptions of extent of cure actually achieved. Oligomeric distributions coupled to kinetic reaction analysis allows for detailed estimates of crosslink architecture within the resin (7).

### Molecular Architecture

For quality cured thermoset resins, approximately one percent of the mass is soluble when subjected to long-term leaching with tetrahydrofuran. Equilibrium is approached in two weeks; resin swell is not visually noticeable. The monomeric, chemical structures are such that the hydrocarbon resins exhibit more pronounced viscoelastic properties; whereas, the epoxy resins are similar to elastic bodies when subjected to tensile testing at room temperature. Therein, LRF 216 is less sensitive to flaws and is more nonlinear in tensile or compressive stress-strain analysis.

Data in Table II for the epoxy resin sets are ordered according to increasing extent of crosslink development. Heat distortion temperatures are an indication of molecular weight between crosslink sites. The average degree of polymerization of the soluble oligomeric fraction reported was obtained by gel permeation chromatography. In conjunction with Figure 2, results show that as the average molecular weight of the oligomeric fraction diminishes and as the resin becomes less soluble, the number average molecular weight between crosslinks decreases and the crosslink density increases within the insoluble network fraction. Similar data for the hydrocarbon resins have been reported (14).

### Acknowledgments

Financial and technical support from the Brunswick Corporation and the Engineergin Research Center are appreciated.

<u>Nomenclature</u>	<u>Units</u>
$A_j$ concentration of free radical, degree of polymerization $j$	moles/volume
$A_{TOT} = \sum_{j=0}^{\infty} A_j$ , cumulative molar distribution	moles/volume
$D = (k_p M + k_t A_{TOT} + k_b P_{TOT}) / k_p M$	
$j$ degree of polymerization, $j = 0, 1, 2, 3, \dots$	
$k$ degree of polymerization, $k = 0, 1, 2, 3, \dots$	
$k_b$ rate constant, branch formation	vol/mole time
$k_c$ rate constant, molecular combination	vol/mole time
$k_i$ rate constant, initiation	vol/mole time
$k_p$ rate constant, propagation	vol/mole time
$k_t$ rate constant, termination	vol/mole time
$M$ monomer concentration	moles/volume
$m$ degree of polymerization, $m = n, n+1, n+2, \dots$	
$n$ degree of polymerization of 1,2-polybutadiene	
$P_j$ concentration of polymeric specie of degree of polymerization $j$	moles/volume
$P_{TOT} = \sum_{k=1}^n P_k$ for hydrocarbon resin	moles/volume
$P_{TOT} = \sum_{x=1}^x P_k$ for epoxy resin	
$t$	time

Literature Cited

1. Timm, D.C.; Rachow, J.W., *J. Poly. Sci.* 1975, **13**, 1401.
2. Pickett, H.E.; Cantow, M.J.R.; Johnson, J.F., *J. Poly. Sci.* 1968, **C-21**, 23, 67.
3. Flory, P.J. "Principles of Polymer Chemistry"; Cornell University Press: Ithaca, NY, 1953.
4. Yen, H.C.; Tien, C.S.; Timm, D.C., *Proc. 2nd World Congress of Chemical Engineering* 1981, **VI**, 381.
5. Plass N.C.; Timm, D.C.; Liu, S.H.; Humphrey, W.D., *Proc. Conference International du Caoutchouc* 1982, **I**, 1.
6. Fisher, J.P., *Angew. Makromol. Chem.* 1973, **33**, 35.
7. Timm, D.C.; Ayorinde, A.J.; Huber, F.K.; Lee, C.H., submitted to *International Rubber Conf.* '84, Moscow.
8. Adesanya, B.A.; Yen, H.C.; Timm, D.C.; Plass, N.C., ACS symposium "Recent Advances in Size Exclusion Chromatography", in press.
9. Timm, D.C.; Kubicek, L.F., *Chem. Engr. Sci.* 1974, **29**, 2145.
10. Scamehorn, J.F.; Timm, D.C., *J. Poly. Sci.* 1975, **13**, 1241.
11. Trommsdorff, E.; Kohle, H.; Legarrly, Pl, *Makromol. Chem.* 1947, **1**, 169.
12. Feltzin, J., *Am. Chem. Soc. Mtg. Chicago* 1964, No. 40.
13. Yen, H.C., M.S. Thesis, University of Nebraska-Lincoln, Lincoln, NE, 1981.
14. Humphrey, W.D.; Liu, S.H.; Timm, D.C.; Plass, N.C., *Proc. 6th Conférence Européenne des Plastiques* 1982, **II**, 28.

RECEIVED September 12, 1983

## Size Exclusion Chromatography Analysis of Epoxy Resin Cure Kinetics

GARY L. HAGNAUER and PETER J. PEARCE<sup>1</sup>

Polymer Research Division, Army Materials & Mechanics Research Center, Watertown, MA 02172

Liquid size exclusion chromatography (SEC) is applied to investigate the isothermal cure kinetics of the reaction between pure N,N'-tetraglycidyl methylene dianiline (TGMDA) and 4,4'-diaminodiphenyl sulfone (DDS) monomers over the temperature range 121° to 187°C. Intermediate reaction products are isolated by preparative SEC, identified and used as standards for SEC calibration. Monomer and soluble reaction product concentrations, molecular weight averages, and gel content are monitored as functions of reaction time by analytical SEC. A 3rd order rate expression describing the early stages of cure is established and Arrhenius relationships describing the temperature dependence of the rate constant and the onset of gelation are determined. Reaction mechanisms are discussed and the effects of variations in stoichiometry of TGMDA/DDS resins on the network structure and properties of the cured resin are considered.

Epoxy resins containing N,N'-tetraglycidyl methylene dianiline (TGMDA) and 4,4'-diaminodiphenyl sulfone (DDS) are widely used in the manufacture of fiber-reinforced structural composites for aircraft. However, the commercial resin formulations are generally quite complex and may include several different types of epoxy resins, additional curing agents, catalysts, organic solvents, and additives to facilitate processing or modify properties of the cured resin. An accurate assessment of the cure kinetics is virtually impossible since the resins are often partially reacted or "staged" during their formulation and "prepregging" which generates a host of ill-defined, intermediate reaction products and because a variety of reactions which proceed at different rates and by different mechanisms may occur during cure. Indeed impurities

<sup>1</sup>Current address: Materials Research Laboratories, Ascot Vale, Victoria, Australia

This chapter not subject to U.S. copyright.  
Published 1984, American Chemical Society

and synthesis by-products present in commercial TMDA are found to have a significant effect on curing behavior when DDS alone is added as the curing agent (1). To begin to understand the curing behavior of the commercial resins it is essential first to investigate and understand the curing chemistry of simpler model systems. Preliminary studies have shown that it is possible to accurately monitor cure kinetics and, at least during the early stages of cure, to elucidate the curing chemistry if pure TGMDA and DDS monomers are used (2).

In this paper liquid size exclusion chromatography (SEC) is applied to investigate the isothermal cure kinetics of the reaction between pure TGMDA and DDS monomers over the temperature range 121° to 187°C. The objective is to gain a better understanding of the epoxy resin curing chemistry and to evaluate the temperature dependence of the curing reaction. Intermediate reaction products are isolated by preparative SEC, identified and used as standards for SEC calibration. Monomer and soluble reaction product concentrations, molecular weight averages and gel content are monitored as functions of reaction time by SEC. From stoichiometric studies a rate expression describing the early stages of cure is developed and an Arrhenius relationship is determined from the temperature dependence of the rate constant.

### Experimental

Preparative liquid chromatography techniques were applied to purify the TGMDA monomer (1). The monomer used for this study is a pale yellow liquid with a viscosity of approximately 1300 centipoise at 50°C and an epoxy equivalent weight (EEW) of 108g/eq. The theoretical EEW of the TGMDA monomer is 105.5g/eq. The curing agent DDS is a white, crystalline (mp, 162°C) powder and was highly pure (approx., 99%) as received from Aldrich Chemical Co. TGMDA/DDS resin formulations were prepared by heating the weighed components to 90°C and then mixing to form homogeneous solutions (approx., 30g). Except during sampling the resin formulations were stored in sealed containers at -13°C. Chromatographic and spectroscopic analyses showed that no reaction occurred during mixing and that upon storage the formulations remained unreacted for at least 6 months.

A Perkin-Elmer DSC 1B instrument was used to study the isothermal cure (polymerization) behavior of the resin formulations. Samples (5-10mg) were weighed in aluminum DSC sample pans on a microbalance and transferred to the DSC heating stage. The temperature of the heating stage was preset at the curing temperature and the cures were conducted in a nitrogen atmosphere. About 10-20 samples per resin formulation were partially cured over a range of time intervals. The reactions were terminated by rapidly lowering the temperature and transferring the sample pans to 25 mL volumetric flasks and adding



tetrahydrofuran (THF). To facilitate dissolution the flasks were agitated and the samples allowed to soak for 1-4 days. Except for through a 0.2  $\mu\text{M}$  Millipore membrane filter in preparation for SEC analysis. Only soluble components were analyzed by SEC.

A Waters Associates ALC/GPC-244 instrument with M6000A solvent delivery system, M720 system controller, M730 data module, 710B WISP auto-injector and M440 UV detector was used for the SEC analyses and operated under the following conditions:

Column Set:  $\mu\text{Styragel}$  (2 x 500 $\text{\AA}$ , 3 x 100 $\text{\AA}$ )  
Sample Concentration: 0.2-0.5  $\mu\text{g}/\mu\text{L}$   
Injection Volume: 20-60  $\mu\text{L}$   
Mobile Phase: THF (UV grade, Burdick & Jackson Labs)  
Flow Rate: 1 mL/min  
Detector: UV 254nm  
Run Time: 45 min

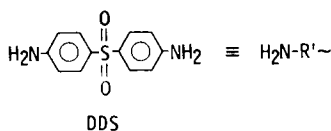
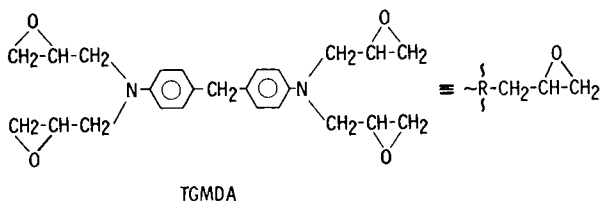
A Waters Associates Prep LC System/500 was used for preparative SEC. Samples were injected using a 12 mL loop valve and the column set consisted of two 2.5-in diameter x 4-ft length columns with 80-100 $\text{\AA}$  and 700/2000 $\text{\AA}$  Styragel packing. Operating conditions are shown below:

Sample Concentration: 20g/100mL  
Mobile Phase: THF (UV grade, Burdick & Jackson Labs)  
Flow Rate: 40mL/min  
Detector: differential refractive index (RI)  
Run Time: 94 min

### Cure Mechanism

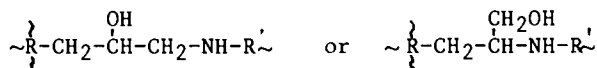
Epoxy-amine curing reactions are known to be exceedingly complex. More than one reaction can occur and the temperature dependence of each reaction may be quite different. For the TGMDA-DDS system, moisture and resin impurities can not only behave as catalysts but also may affect the network structure and properties of the cured resin (2). Because of the tetra-functional nature of the monomers, steric effects may lead to alternative reactions and highly cross-linked network structures may occur relatively early in the curing reaction. Indeed as polymerization proceeds, viscosity increases and the glass transition temperature of the reaction mixture gradually approaches and may exceed the curing temperature. As a result, reactive species become diffusion limited and eventually may either seek other reaction pathways or stop reacting entirely.

Denoting the structures

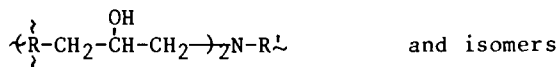


the most likely reactions and reaction product structures are shown below -

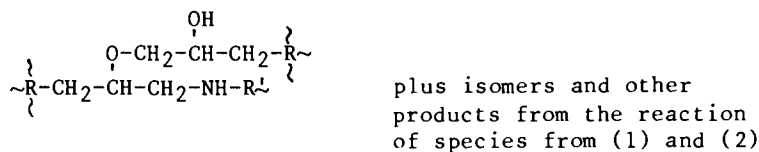
- (1) epoxy-primary amine addition



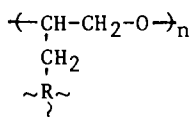
- (2) epoxy-secondary amine addition



- (3) epoxy-hydroxyl addition



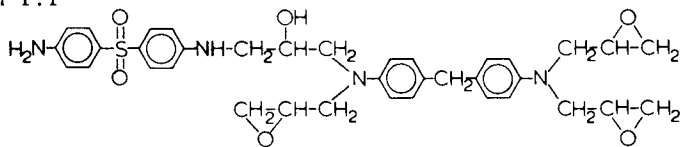
- (4) epoxy-epoxy homopolymerization



Preparative SEC

Samples for preparative SEC were prepared by partially polymerizing about 10g of a TGMDA/DDS mixture. To optimize the formation of the initial, relatively simple reaction products, a TGMDA resin formulation consisting of 25% by weight DDS was cured for 23 minutes at 145°C in vacuo. The RI detector trace from the preparative SEC of this reaction mixture is illustrated in Figure 1. Four injections were made successively at 60 minute intervals and fractions 1:1 and 2:1 were collected as indicated. Following the application of a vacuum to remove solvent, approximately 0.3g fraction 1:1 and 0.1g fraction 2:1 were realized. Analytical SEC and reverse phase high performance liquid chromatography (HPLC) showed that fraction 1:1 was 97% pure. Using Fourier transform infrared (FTIR) and  $H^1/C^{13}$  NMR spectroscopy, fraction 1:1 was identified as the TGMDA-DDS epoxy-primary amine addition product shown below.

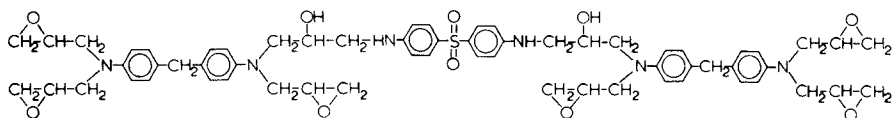
## Fraction 1:1



1-1 PRODUCT

Although a single peak was observed using SEC, fraction 2:1 was found to contain three components by HPLC analysis. The SEC analysis indicates that the components of fraction 2:1 have quite similar molar volumes. To ascertain the ratio of monomers in each component and obtain more information about the reaction mechanism, FTIR spectra of the 2:1 components were run and compared with the spectra of TGMDA, DDS, and the 1-1 product. Absorbance bands for hydroxy ( $3500\text{ cm}^{-1}$ ) and secondary amine ( $3410\text{ cm}^{-1}$ ) groups were apparent in the spectra of all three components. There was no evidence suggesting the presence of aliphatic ether linkages of the type  $-\text{CH}_2-\text{O}-\text{CH}_2-$  or  $>\text{CH}-\text{O}-\text{CH}_2-$ . From the results of the chromatographic and FTIR analyses, the following structures are postulated for the components found in fraction 2:1.

## Fraction 2:1



2-1 PRODUCT

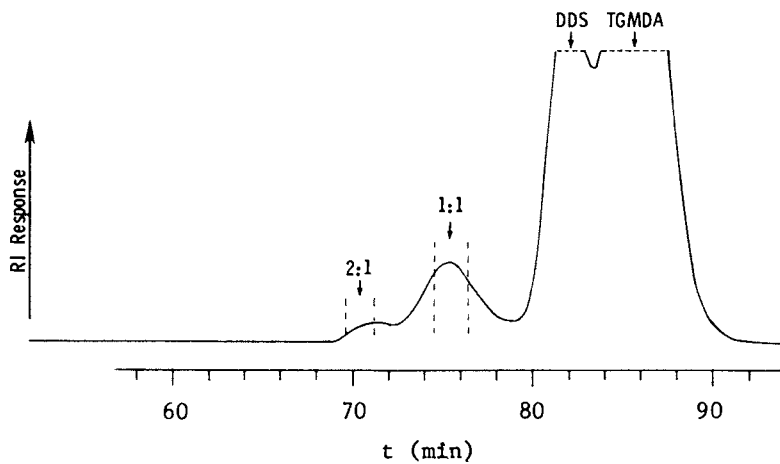
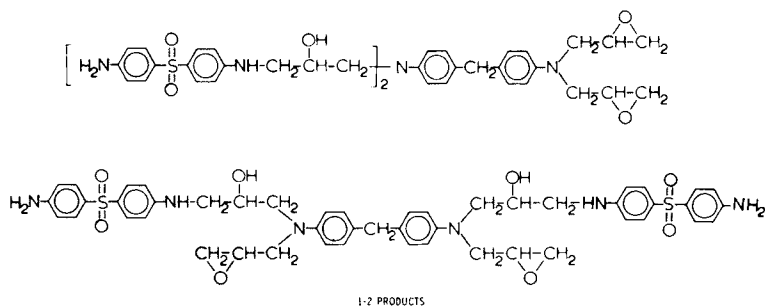


Figure 1. Preparative SEC of TGMDA/DDS (25%) resin reacted 23 min at 145 °C.



Fractions of the higher molecular weight, more complex reaction products were obtained by the preparative SEC of further advanced TGMDA/DDS reaction mixtures. For example, the proposed components of the next highest oligomer fraction are the 3-1, 2-2, and 1-3 TGMDA-DDS products. The relative ratio of the products depends upon the initial composition of the TGMDA/DDS resin formulation.

### Analytical SEC

With standards for calibration, SEC may be applied to determine monomer and reaction product concentrations, molecular weight (MW) averages, and gel content in TGMDA/DDS reaction mixtures. Typical SEC chromatograms are shown in Figure 2. The chromatograms are displaced along the ordinate to illustrate changes in composition accompanying the cure of the TGMDA/DDS(25%) resin at 177°C. Reaction products elute with retention times between 28 and 32 minutes. Areas under the SEC peaks and peak segments are directly proportional to the concentrations of the components. The initial reaction products are TGMDA-DDS oligomers. As the reaction proceeds, higher MW, soluble products are formed. The onset of gelation is indicated by the formation of insoluble products. At the onset of gelation (30 min in Figure 2), substantial amounts of the monomers remain unreacted. As gelation continues, areas of peaks representative of high MW products rapidly diminish and eventually the concentrations of extractable monomers approach zero.

The weight percentage of each component or set of components designated  $C_i$  may be calculated from their respective peak areas  $A_i$

$$\%W_i = \frac{A_i K_i}{C_0 V} \cdot 100\% \quad (1)$$

where  $K_i = C_{i,s} \cdot V_s / A_{i,s}$  is the calibration constant,  $C_0$  is the concentration ( $\mu\text{g}/\mu\text{L}$ ) of the sample assuming complete solubility,  $V$  is the injection volume ( $\mu\text{L}$ ), and subscript "s" denotes the respective parameters for the calibration standards. Using a 254nm



UV absorbance detector, it is noted that the calibration constants for TGMMA and DDS are quite similar and that the 1-1 product has a different constant which is essentially identical to those of the higher MW products. For components having retention times less than 30 min, their total weight percentage may be calculated from the sum of area segments  $A_j$  between 28 and 32 min taken at 0.1 min intervals; i.e.,

$$\%W_i = \frac{K \sum A_j}{C_0 \cdot V} \cdot 100\% \quad (2)$$

where  $K$  is a constant. The gel content is calculated using the equation

$$\%gel = 100\% - \sum \%W_i \quad (3)$$

The MW calibration curve is shown in Figure 3. Discrete MW values obtained by averaging the MW's of components eluting at the same retention times are indicated as data points. Even though DDS has the lowest MW, its retention time is less than that of TGMMA. This apparent anomaly is attributed to differences in the extent of solvation of the two molecules. DDS has amino-groups which are highly polar and may hydrogen bond with THF to form a solvated species having a larger molar volume than that of TGMMA in THF. Data points for the intermediate MW reaction products fit on the same line as DDS and may be extrapolated (dashed line) to account for higher MW components.

Standard equations are applied to calculate number-, weight-, and z-average MWs

$$M_n = \sum W_i (\sum W_i / M_i) \quad (4)$$

$$M_w = \sum (W_i M_i) / \sum W_i \quad (5)$$

$$M_z = \sum (W_i M_i^2) / \sum W_i M_i \quad (6)$$

where  $W_i$  is the weight fraction of component(s)  $C_i$  of average molecular weight  $M_i$ . For components eluting in the extrapolated region at time  $t_i$ ,  $M_i$  is defined by

$$\log_{10} M_i = 6.697 - 0.1172 \cdot t_i \quad (7)$$

### Results and Discussion

The isothermal cure kinetics of a series of TGMMA/DDS resin formulations were investigated over the temperature range 121°-187°C. Figure 4 illustrates data obtained for the resin TGMMA/DDS(25%) at 177°C. During the early stage of cure prior to the onset of

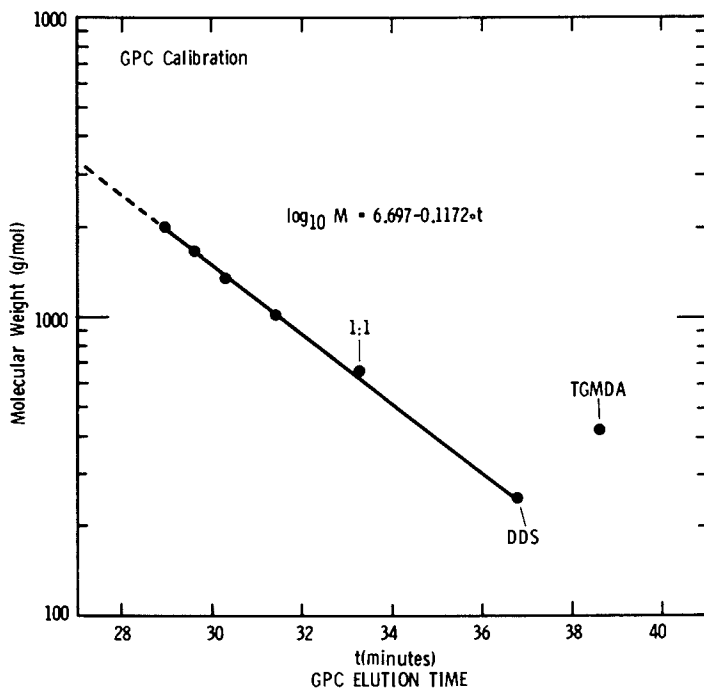


Figure 3. SEC calibration plot for TGMDA-DDS reaction products.



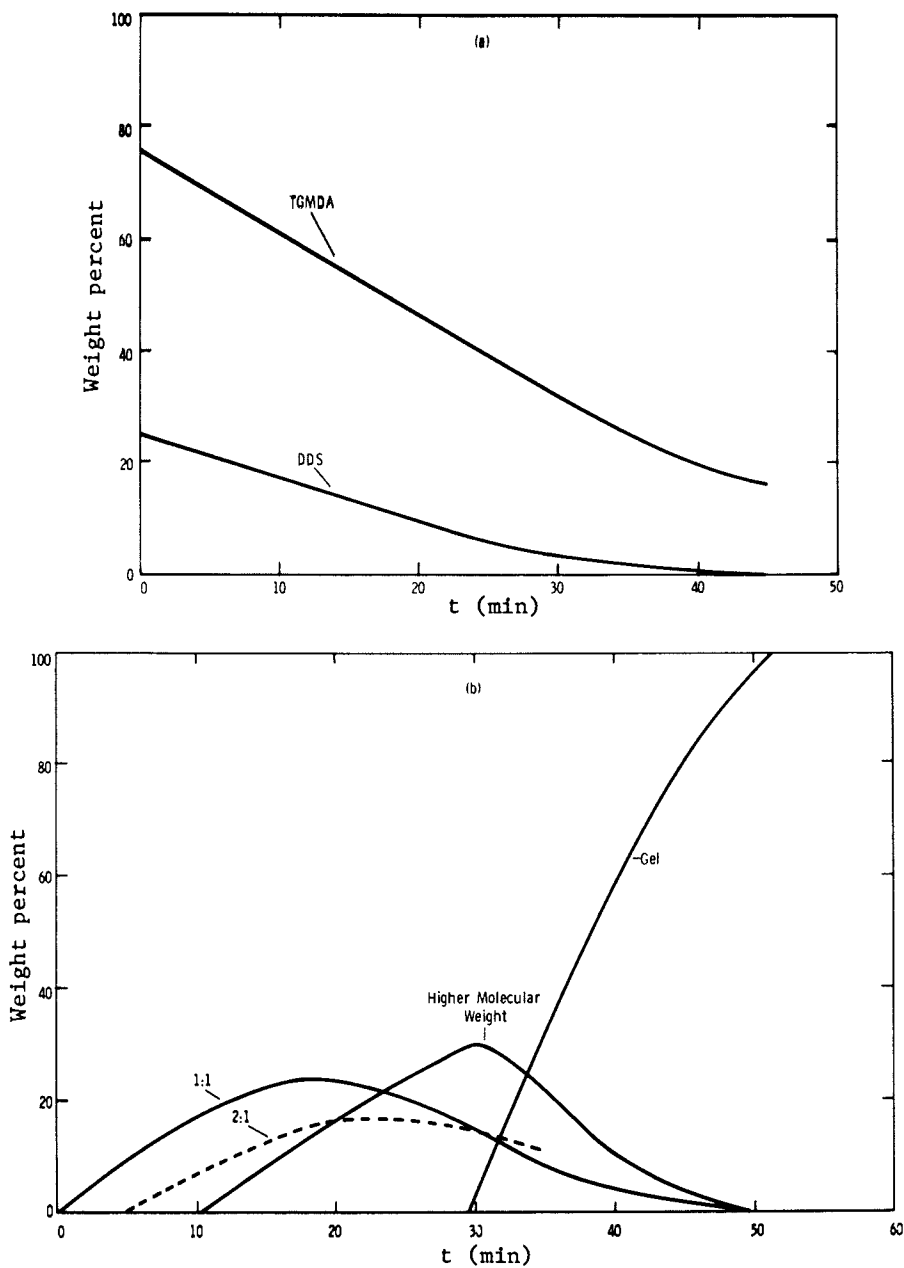


Figure 4. Weight percentages (a) of TGMDA and DDS and (b) of TGMDA/DDS reaction products vs. reaction time for TGMDA/DDS (25%) cured at 177 °C.

gelation, simple epoxy-primary amine addition is the predominant reaction. The 1-1 product forms first and increases steadily in concentration until its rate of reaction exceeds its rate of formation. The total concentration of higher MW products approaches a maximum at the onset of gelation and then decreases sharply as gelation proceeds.

A plot of experimental data (Figure 5) shows that the concentrations  $C$  (mol/kg) of TGMDA and DDS decrease in parallel as the reaction time increases; i.e.,

$$-d[\text{TGMDA}]/dt = -d[\text{DDS}]/dt \quad (8)$$

Equation 8 holds over nearly 20% of the total theoretical extent of reaction and adequately describes the early stages of reaction of the TGMDA/DDS(25%) resin over the entire temperature range investigated (Figure 6). Indeed FTIR spectroscopic analysis of the reaction mixture at various cure times supports the conclusion that there is a one-to-one correlation between epoxide concentration and TGMDA concentration and that no major side reactions occur during the early stages of cure.

Stoichiometric studies show that the reaction is first-order with respect to the concentration of TGMDA and second-order with respect to DDS in the early stages of reaction.

$$-d[\text{TGMDA}]/dt = k_3[\text{TGMDA}] [\text{DDS}]^2 \quad (9)$$

Results from rate studies at 161° and 177°C are shown in Table I. Third-order rate constants  $k_3$  calculated from data obtained at 161°C are in excellent agreement over a broad range of TGMDA/DDS resin compositions. The slight increase in the 177°C  $k_3$  values with increasing DDS concentration is attributed to problems in sampling with the DSC heating stage; i.e., at higher temperatures and higher DDS concentrations, the initial rate of reaction is sufficiently large that the sample heat-up time becomes a significant factor in rate determinations (Table I).

The third-order rate expression (Equation 9) is applicable over the temperature range 121° to 187°C. The Arrhenius relationship describing the temperature dependence of the rate constant  $k_3$  (Figure 7) is

$$k_3 [\text{kg}^2\text{mol}^{-2}\text{min}^{-1}] = 2.15 \times 10^6 \cdot \exp(-16600/RT) \quad (10)$$

where  $R = 1.9872 \text{ cal} \cdot \text{mol}^{-1}\text{K}^{-1}$ ,  $T$  is temperature (°K), and the activation energy is  $16,600 \text{ cal} \cdot \text{mol}^{-1}$ .

An activation energy may also be determined from the gelation data (Figure 8). For example, the relationship

$$t_{\text{gel}}^{-1} [\text{min}^{-1}] = 2.22 \times 10^6 \cdot \exp(-16100/RT) \quad (11)$$

was determined from the temperature dependence of the reaction time

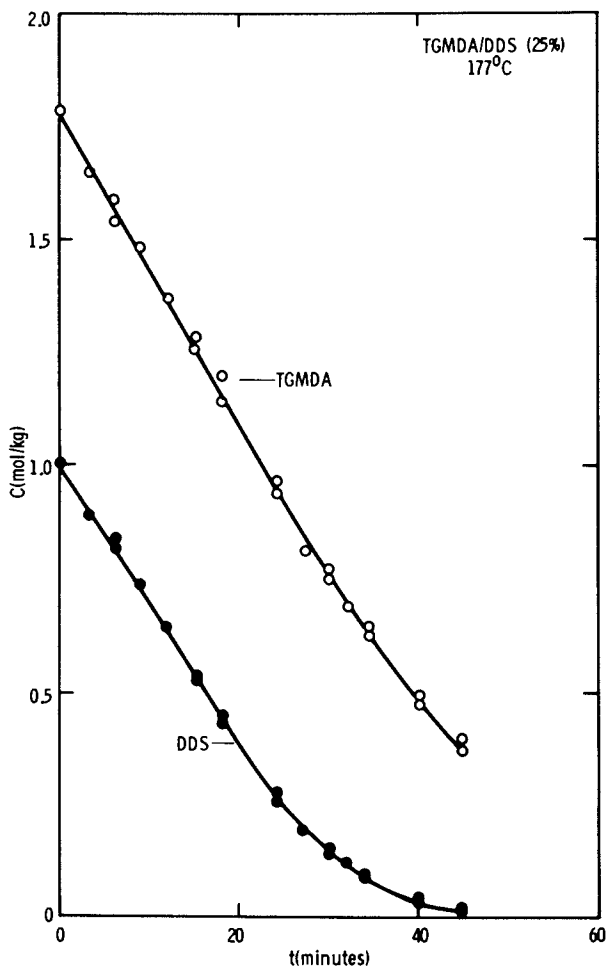


Figure 5. TGMDA and DDS concentrations vs. reaction time for TGMDA/DDS (25%) cured at 177 °C.

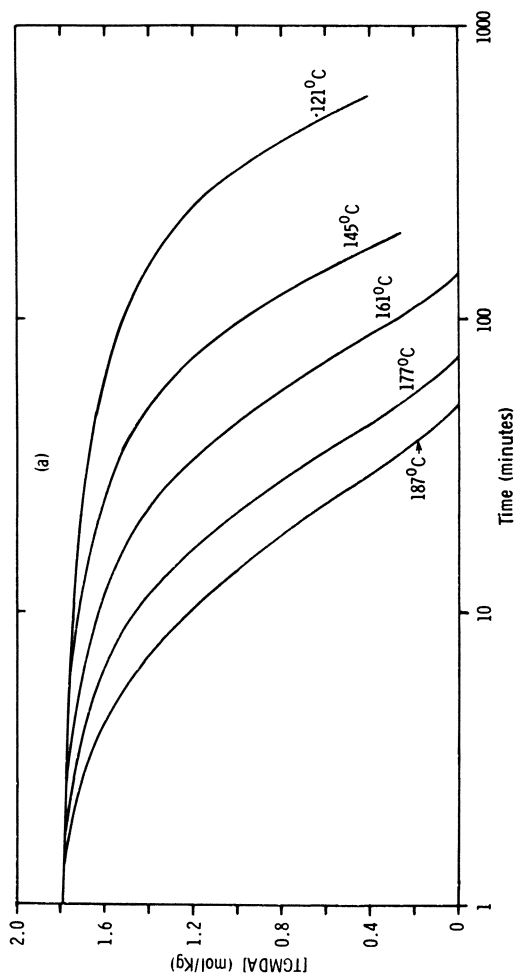


Figure 6. Semilogarithm plots of (a) TGMDA and (b) DDS monomer concentrations vs. reaction time for TGMDA/DDS (25%) cured at different temperatures.

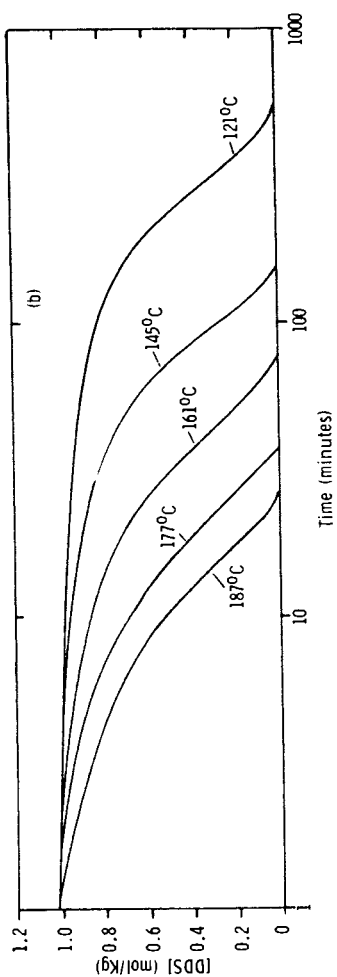


Figure 6. Continued

American Chemical  
Society Library  
1155 16th St. N. W.

Washington, D. C. 20038

In Size Exclusion Chromatography; Provdor, T.;

ACS Symposium Series; American Chemical Society: Washington, DC, 1984.

Table I  
TGMDA/DDS Rate Study

Temperature °C	DDS (weight-%)	[DDS] <sub>0</sub>	(mol·kg <sup>-1</sup> ) [TGMDA] <sub>0</sub>	(mol·kg <sup>-1</sup> min <sup>-1</sup> ) -d[TGMDA]/dt	(kg <sup>2</sup> mol <sup>-2</sup> min <sup>-1</sup> ) k <sub>3</sub>
161	15	0.605	2.014	0.0078	0.0106
	25	1.008	1.778	0.0195	0.0108
	37	1.49	1.493	0.0355	0.0107
	50	2.02	1.185	0.0526	0.0109
177	15	0.605	2.014	0.0132	0.0179
	25	1.008	1.778	0.0332	0.0184
	37	1.49	1.493	0.0741	0.0224

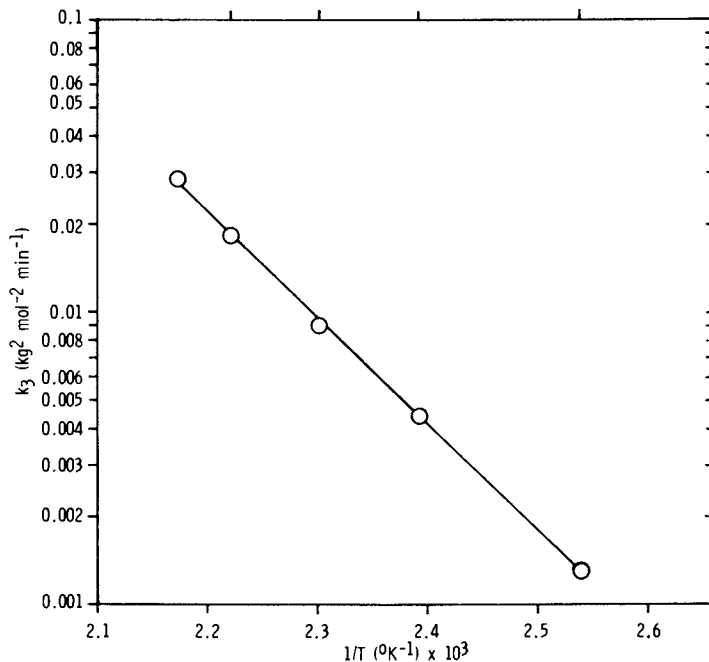


Figure 7. Arrhenius plot of the TGMDA/DDS third-order rate constant  $k_3$ .

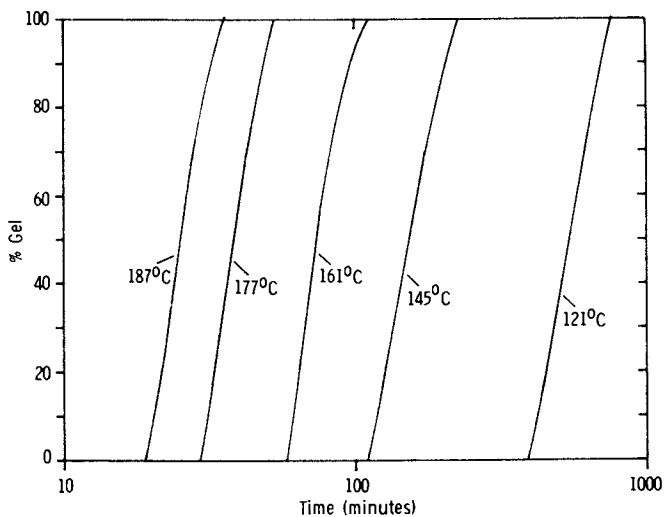


Figure 8. Semilogarithm plot of weight percentage gel vs. reaction time for TGMDA/DDS (25%) cured at different temperatures.

to the onset of gelation  $t_{gel}$  for the TGMDA/DDS(25%) resin formulation (Figure 9). It is noted that the activation energy  $16,100 \text{ cal}\cdot\text{mol}^{-1}$  is quite similar to the value derived from kinetics data for the initial epoxy-primary amine addition reaction.

The rate of change and values of the MW parameters provide information relating to the formation of the gel network. MW parameters for the TGMDA/DDS(25%) resin are plotted versus reaction time at  $177^\circ\text{C}$  (Figure 10).  $M_w$  and  $M_z$  are most sensitive to the formation of high MW products and approach infinity (indicated by dashed lines) as the reaction nears the onset of gelation. The finite values of the parameters beyond the onset of gelation and the downward curvature of the plots (solid lines) are a consequence of the fact that only soluble components can be analyzed by SEC and that the highest MW products tend to be incorporated into the gel network first. Also, the  $M_z$  plot tends to curve downward earlier because the SEC calibration is no longer applicable in the high MW region when the reaction reaches the stage where a variety of highly branched products are formed. Only  $M_n$  can be interpreted beyond the onset of gelation by including the weight fraction of insoluble gel in the numerator of Equation 4.

The MW parameters and gel formation are dependent upon stoichiometry. Plots of the number-average MW ratio  $(M_n)_t/(M_n)_0$  and gel fraction  $f_{gel}$  versus the fraction of TGMDA reacted at time  $t$  (Figure 11) show that, as the weight % DDS is decreased, less TGMDA is required to react for the mixture to attain specific degree of polymerization and gel fraction values. The data suggests that the effective functionality of DDS is less than 4. Although not prevalent in the early stage of cure, the epoxy-hydroxyl addition reaction would effectively increase the functionality of TGMDA and produce a similar result. The plots would overlap only if the functional groups of each monomer were equally reactive. Consequently, a more highly crosslinked network is formed as the % DDS is decreased, at least down to concentrations of 15% DDS. At lower DDS concentrations or higher extents of reaction, the trend may be reversed as other, perhaps more complex, reactions occur.

Recently, FTIR spectroscopy studies have been reported which support the above observations. Moacanin et al (3) concluded that two reactions dominate the TGMDA/DDS cure: epoxy-primary amine addition is the principal reaction occurring during the early stage of cure followed by the epoxy-hydroxyl addition reaction. Indeed they find that the rate of epoxy-hydroxyl addition is at least an order of magnitude slower than for the epoxy-primary amine reaction at  $177^\circ\text{C}$ . Furthermore, Morgan et al (4) report that the epoxy-secondary amine addition and epoxy-epoxy homopolymerization reactions also occur at  $177^\circ\text{C}$  but at rates that are approximately 10 and 200 times slower, respectively, than the epoxy-primary amine reaction.



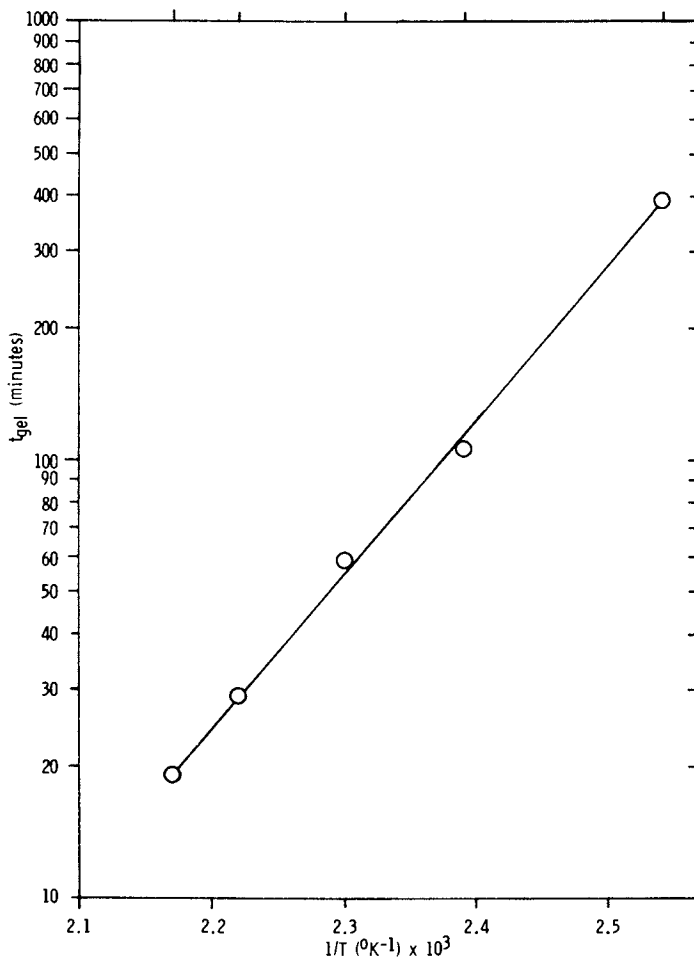


Figure 9. Arrhenius plot of the reaction time to the onset of gelation  $t_{gel}$  for the TGMDA/DDS (25%) resin.

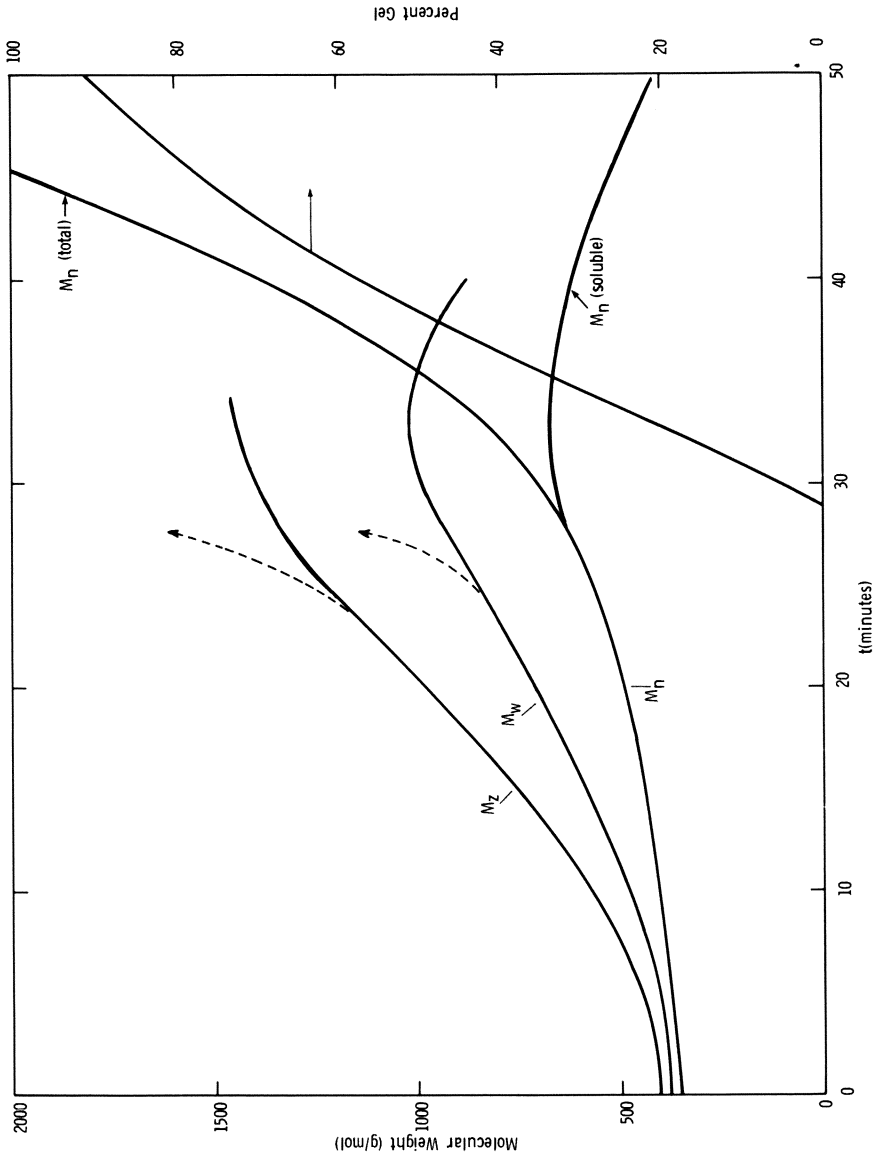


Figure 10. Plot of the MW parameters and the weight percentage gel vs. reaction time for TGMDA/DDS (25%) cured at 25 °C.

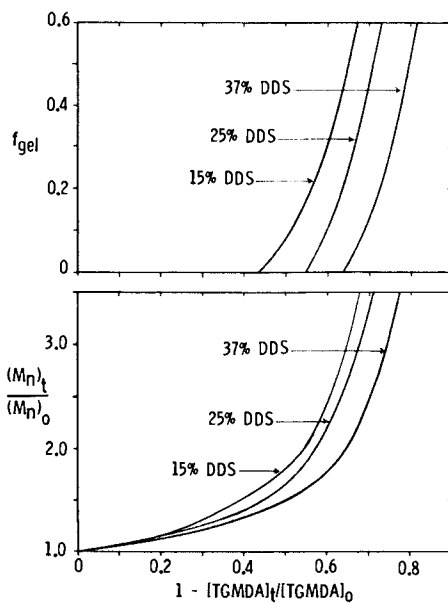


Figure 11. Gel fraction  $f_{\text{gel}}$  and number-average MW ratio (degree of polymerization) vs. fraction TGMDA reacted at time  $t$  for TGMDA/DDS mixtures cured at  $177^\circ\text{C}$ .

### Conclusions

1. Preparative and analytical SEC are powerful techniques for investigating the curing behavior of epoxy resins.
2. Epoxy-primary amine addition is the only reaction detectable in the earliest stage of the TGMDA/DDS cure and is the predominant reaction at least up to the onset of gelation.
3. TGMDA/DDS cure kinetics is adequately described by a third-order rate expression (Equation 9) during the early stage of cure.
4. The same rate expression and cure mechanism for the early stage of cure apply over the temperature range 121° to 187°C. Arrhenius relationships for the temperature dependence of the rate constant and onset of gelation have been determined.
5. Variations in the degree of polymerization and gel fraction data with changes in stoichiometry suggest the DDS secondary amine is not as reactive as the primary amine and beyond the early stages of reaction indicate the presence of alternative reaction mechanisms. Consequently, it is expected that variations in stoichiometry of TGMDA/DDS resins should have a predictable effect on network structure and properties of the cured resin.

### Acknowledgment

The authors are grateful to Ms. Judith Brodtkin for her assistance in running the SEC experiments.

### Literature Cited

1. Hagnauer, G. L. and Pearce, P. J. Org. Coat. Appl. Polym. Sci. Proc., Am. Chem. Soc., 1982, 46, 580.
2. Hagnauer, G. L.; Pearce, P. J.; LaLiberte, B. R. and Roylance, M. E. Org. Coat. Appl. Polym. Sci. Proc., Am. Chem. Soc., 1982, 47, 429.
3. Moacanin, J.; Cizmecioglu, M.; Tsay, F. and Gupta, A. Org. Coat. Appl. Polym. Sci. Proc., Am. Chem. Soc., 1982, 47, 587.
4. Morgan, R. J., Happe, J. A. and Mones, E. T., Lawrence Livermore National Laboratory. Preprint UCRL-88513, presented at the 28th National SAMPE Symposium, Anaheim, CA, April 1983.

RECEIVED October 13, 1983

## Sulfonated Poly(styrene-Divinylbenzene) Networks Scission Study Using Aqueous Size Exclusion Chromatography

DAVID H. FREEMAN and XUN LIANG<sup>1</sup>

Department of Chemistry, University of Maryland, College Park, MD 20742

Several reports have been made on the degradation by hydrogen peroxide (Fenton's reagent) of ion exchange resins (sulfonated PSDVB). The reaction causes weight loss, swelling and eventual dissolution (1). Diffusion and secondary chemical reactions are possible; the scission rates vary oppositely with the amount of crosslinking (2). The rate differs among the DVB isomers, meta or para, used in the original PSDVB copolymerization (3).

Few structural tools are available to assess the structure of crosslinked networks directly. A frequent approach is to derive such information from kinetic study of unreacted monomer during the polymerization process (4). The possibilities for deriving structural information by characterizing network fragments has not been fully explored.

The groundwork for the present study has been developed in previous studies. For example, scission through peroxide oxidation or ultrasonic treatment of polystyrene chains has been found by size exclusion chromatography to involve preferential attack at the mid-chain position (5). Given this evidence it is expected that branched polymers should give a correspondingly skewed molecular weight distribution. This reasoning suggests one of the pathways by which a scission experiment may convey topological information.

PSDVB copolymers and their ion exchange derivatives consist of a three dimensional four-connected network structure. Such networks may have a statistically isotropic structure that includes tetrahedral cells, such as the "X" unit structure described by Flory (6). The four-connectedness results from the expected pairwise chain connecting function of

<sup>1</sup>On leave from Department of Chemistry, Nankai University, Tianjin, People's Republic of China

the DVB units. However, a more complete topological model for such networks should, at least in principle, provide for the 34 configurations described by Ziabecki (7). Although it is important to consider the theoretical perspectives, experiments that probe polymer molecular topology are rare indeed.

If one assumes that a network consists only of Flory tetrahedral cells, or X-units, the average mass of the unit cell can be estimated from the monomers used in the reaction mixture. Consider a reaction mixture that incorporates  $f$  moles of a sum,  $D$ , of meta and para DVB isomers plus an assumed equal portion  $E$ , of the usual meta and para isomers of the EVD (ethylvinylbenzene) contaminants, plus  $1-f$  moles of styrene. The estimated X-unit contains an average of  $(1-f)/f$  moles of styrene per mole of DVB. The mass of the average X-unit,  $MX$ , can be calculated from the following expression:

$$MX = ((1-f)/f)MS + ME + MD \quad (1)$$

where  $M$  refers to mass and  $S$ ,  $E$ , and  $D$  refer to the incorporated moieties from styrene, plus the assumed equal mole fractions,  $f$ , of DVB and EVB monomers, respectively. The mass of the sulfonated X-unit in the cation exchange derivative, is obtained by modifying the values of  $MS$ ,  $ME$  and  $MD$  by adding the appropriate sulfonate and counterion masses.

The average mass of a single chain between crosslinks,  $MC$  is estimated from:

$$MC = (MX - MD)/2 \quad (2)$$

The division by two denotes the topological requirement (6) of two inter-crosslink chains per DVB, in the present model of a closed X-type network structure. (Consider two X units with their chain ends joined together. There are four chain lines and two vertices.)

An example of the possibility that network scission experiments may be subject to topological interpretation is suggested by the results reported by Hookway and Shelton (2). Of particular interest is the degelation point where the network dissolves. (Degelation implies transition through a gel point that may or may not be related structurally to the usual non-gel to gel transition observed in the corresponding network synthesis. The data (ref. 2, Fig. 3) show that hydrogen peroxide causes the release of about 0.5 mole

of carbon dioxide per crosslink to reach the degelation point. Since there are two lengths of chains per DVB vertex, this corresponds to about one mole of carbon dioxide released for each intercrosslink chain in the original network. This suggests the possibility that the scission reaction may be topologically selective and it may be of value for investigating the topology of fragment formation, and for studying the chemistry of scission degradation.

The goal of the present work is to examine the feasibility of obtaining topologically significant results from scission experiments, and to determine whether the topology of branched structures can be studied using topologically selective scission processes. (It has not yet been proved that any reaction offers such selectivity.) The first step, as will be described, is to examine the high points of the molecular weight distribution of the scission fragments.

The present experimental approach is based on the chromatographic advantages provided by the diol or glycerol derivatives of porous silica stationary phases available for use in HPLC. These have recently become available for estimating the molecular size of polyelectrolytes using aqueous size exclusion chromatography. The conditions for reproducible polyelectrolyte size measurements, and their possible perturbations have been summarized by Barth (8).

## EXPERIMENTAL

Bio-Rad AG50W resins (sulfonated PSDVB), 50-100 mesh, were treated with NaOH and distilled water washes. The weighing state was obtained after 12 hours of drying in air at 75-80 C. Reagent grade chemicals were used throughout.

The scission reaction was carried out with a fixed addition of 1.50g of the dry resin, 10 mg of ferrous sulfate heptahydrate and 50 ml of 3% w/v hydrogen peroxide in a round Pyrex flask. The evolved carbon dioxide was vented to the atmosphere through serial traps containing sulfuric acid followed by a soda lime sorption tube. The magnetically stirred reaction flask was submerged in an oil bath heated with an immersed electrical coil and a magnetic stirrer positioned below the bath. The temperature was maintained at 50 +/- 1 C. After varied times 1.0 ml samples of liquid were withdrawn. There were fewer than six withdrawals in a given reaction sequence.

The liquid chromatographic analysis was carried out using serial 4x300mm u-Bondagel E-125 and E-500 columns obtained from Waters Associates, Inc. The carrier was prepared to contain (A) 0.25M sodium perchlorate, 0.1% sodium lauryl sulfate that was dissolved and brought to pH 7.2 using ammonium phosphate and (B) tetrahydrofuran. An A/B ratio of 9:1 was mixed and filtered through a 0.2um membrane.

It is noted that these analytical conditions were not problem-free. Period column washing with water and frequent pump disassembly and cleaning were necessary to compensate for column and apparatus fouling that may have been caused by higher molecular weight homologs in the sodium lauryl sulfate additive.

The calibration standards included sodium form polystyrene sulfonates obtained from Pressure Chemical Co., Pittsburgh, Pa., and sodium toluene sulfonate. Measurements were taken at 0.5 to 1.0ml/min flow rates. The logarithm of the molecular weight of the standards was linear it suggests a framework for approaching an interpretation of the structure of the scission products. This application of size exclusion chromatography measurements must be viewed as a first approximation because of the unmeasured differences between the chromatographic behavior of the linear standards and the expected branched structure of the scission products.

## RESULTS

Scission reactions were carried out with nominal 4, 8 and 12 mole %DVB where  $f = 0.04, 0.08$  and  $0.12$ , respectively. The corresponding times required to reach degelation were estimated as 4, 7.5 and 10 hours. The time uncertainty of the degelation "point" is estimated as 0.2 to 0.5 hr.

The treatment with hydrogen peroxide caused the residual resin weight to decrease with time. The weight of the 12 %DVB resin measured after drying was observed to undergo a linear descent starting at 1.5g and falling to zero at 10 hrs where degelation occurred. The results are shown in Figure 1. This shows that the intermediate scission pathway is a macroscopically continuous process unmarked by abrupt change in the chemical pathway. Fragmentation starts at the beginning of the degradation and an accompanying weight loss occurs until dissolution is complete.



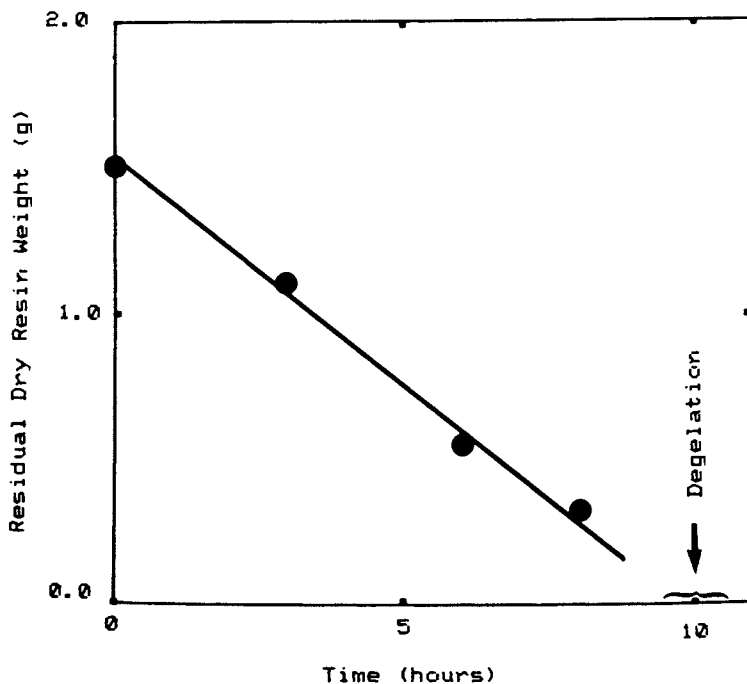


Figure 1. The measured dry weight after hydrogen peroxide scission of sulfonated PSDVB (12% DVB cation exchange resin) is seen to decrease linearly with reaction time. The time obtained by extrapolating to zero weight corresponds to visual observation degelation indicated by the disappearance of the resin particles.

The aqueous size exclusion chromatograms obtained for the three resins throughout their scission were marked by an early appearance of a dominant peak at molecular weight 200 Daltons. Similarly, all analyses in the vicinity of the time of degelation were marked by a major prominence with an estimated molecular weight of 2000 Daltons or slightly larger. With X8 and X12 we also observed a small peak of intermediate molecular weight in the range between 400 and 900 Daltons.

The variation of the SEC analyses with time was examined in detail with the X12 resin. The results are shown in Figure 2. The early and sustained presence of the molecular weight 200 peak indicates formation of fragments whose molecular weight corresponds to the pendant sulfonated aromatic rings (or a possibly related degradation product) as an initially prominent and subsequently continuing feature of the scission process. Close inspection of the chromatograms showed the appearance of an unresolved satellite peak of variable apparent area corresponding to still smaller size molecules.

Following the emergence of the preceding low molecular weight peak, the degradation moved into dominance by larger size fragments indicated by one peak of 500-750 molecular weight accompanied by a lesser peak with molecular weight in the range of 2000-2500. As the degradation moved into the half way point and beyond, the relative amounts of material represented by these two peaks were reversed, the larger molecular weight being clearly dominant at the time of degelation.

The molecular weight of these two peaks can be compared to the reference values of  $MC = 873.2$  and  $MX = 1987.6$  calculated from Equations 2 and 1, respectively, for  $f = 0.12$ .

The close correspondence between the fragments molecular weights, 500-750 observed ( $873.2$  calculated) and 2000-2500 observed ( $1987.6$  calculated), leads to the conclusion that linear chain fragments and X-units are apparently both formed after the scission process begins.

The early formation of relatively small soluble fragments of molecular weight 200 is followed by an increasing amount of fragment of molecular weight 750 but the absence of the 2000-2500 molecular weights. At the mid-point of the degradation the 2000-2500 molecular weight peak arises and then dominates the degradation product mixture.

The formation of small fragments with molecular weight near 200 suggests that pendant group scission

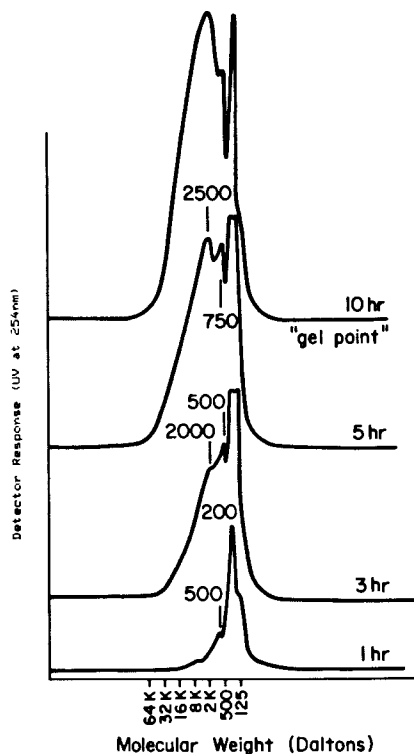


Figure 2. Size exclusion chromatograms of samples taken during hydrogen peroxide degradation of the 12% DVB sample whose mass depletion is shown in Figure 1. The potential for formation of topologically significant scission fragments is indicated. The apparent molecular weight at 200 Daltons is close to that of the sulfonated pendant aromatic rings. Peaks in the range 2000–2500 are near the calculated mass (1978.6) of the average X-unit cell defined by Flory (6). Peaks of approximate molecular weight 500–750 are comparable to expected average intercross-link chain mass (873).

accompanies and probably precedes chain scission. Unit scission is required to remove a pendant group fragment. The delayed appearance of the 500-750 peak and still later appearance of the 2000-2500 peak are consistent with topological requirements that release of a linear chain as a scission product requires two cuts on the same chain while at least four cuts on four contiguous chains are required to remove an X-unit.

It is worth noting that evidence is not apparent for the formation of still larger molecular weight fragments, referring to fragments whose molecular weights would imply two or more X-units connected by a single unbroken chain. A possible explanation for this is that the formation of such larger fragments is statistically less unlikely. Moreover, even if such larger fragments were formed, it is possible that they would be trapped within the network. Their eventual release would be eclipsed by a diffusion impediment that could enhance their remaining as stationary targets for scission, for example, of a single connecting chain that would form two sub-fragment X-units. Once the latter cut were made, the possible diffusional barrier would be lowered.

To summarize, the following hierarchy in the formation of scission fragments is consistent with the experimental results:

SCISSION FRAGMENT -----	NO. OF CUTS -----	ORDER OF APPEARANCE -----
pendant group	1	Initial
chains	2	Second
X-units (+)	4	Third
Higher (+-, etc.)	6(etc)	Not observed

The present experiments may be subject to some uncertainty in terms of molecular weight estimates and diffusion effects that could affect the exactness of these interpretations. The conclusion is reached that the experiments strongly suggest evidence for discontinuous topological quantification. In other words, the order and rate of fragment release is consistent with expectations based on fragment topology.

Further study of network fragments will eventually require coping with the possibility of a larger range of scission fragments than have been identified here. The reason for expecting the added complexity stems from the fact that size exclusion chromatography is non-interactive and therefore has an obvious tendency to mask chemical differences between molecules of different composition but similar size. Even so, the potential for using the characterization of network fragments to probe the topological aspects of branched or crosslinked polymer structure emerges as an area that invites further study.

## LITERATURE CITED

1. Wood, W., *J. Phys. Chem.* 61, 832 (1957).
2. Hookway, H.T., and Selton, B., *J. Phys. Chem.* 62, 493-4 (1958).
3. Wiley, R., and Reich, E., *J. Polym. Sci. A-1*, 6, 3174-6 (1968).
4. Dusek, K., and Prins, W., *Adv. Polym. Sci.* 6, 1-102 (1969).
5. Smith, W.B., and Temple, H.W., *J. Phys. Chem.* 72, 4613-9 (1968).
6. Ziabicki, A., *Polymer* 20, 1373-1381 (1979).
7. Flory, P.J., *J. Phys. Chem.* 11, 512 (1943).

RECEIVED October 31, 1983

# Fractionation and Characterization of Commercial Cellulose Triacetate by Gel Permeation Chromatography

F. MAHMUD and E. CATTERALL<sup>1</sup>

Department of Applied Chemistry, Faculty of Applied Science, Coventry (Lanchester) Polytechnic, Coventry, England

Commercial cellulose triacetate samples were fractionated by both fractional precipitation and preparative gel permeation chromatography (GPC). The triacetate fractions were characterized by viscometry, high speed membrane osmometry (HSMO) and GPC. A fair agreement has been found between the molecular weights of various triacetate fractions determined by the three procedures.

All unfractionated cellulose triacetate samples and high molecular weight fractions showed a shoulder on the high molecular weight side of the GPC distribution. Material isolated from this region was found to be highly enriched in mannose and xylose, attributed to the presence of a hemicellulose derivative. Cellulose triacetate from cotton linters did not show this behavior.

The universal calibration approach ( $[\eta].M$  vs elution volume) for polystyrene standards and narrow molecular triacetate fractions show slight deviation from linearity. This departure from linearity has been attributed to differences in both hydrodynamic behavior and the Mark-Houwink exponent 'a' for the two polymers in question.

A literature survey (1 - 11) on the fractionation of cellulose triacetate by precipitation indicates that in most cases it has been unsuccessful due to the possibility of hydrogen bonding between polymer and solvent in solutions (10, 12). GPC has been applied to the fractionation of cellulose derivatives by many workers. Segal (13), Meyerhoff (14 - 16), Muller and Alexander (17) have reported the fractionation of cellulose nitrate by GPC. Muller and Alexander (17), Brewer, Tanghe, Bailly and Burr

<sup>1</sup>Current address: Petroleum and Gas Technology Division, Research Institute, University of Petroleum and Minerals, Dhahran, Saudi Arabia

(18) have also used GPC for the fractionation of cellulose acetate and carbanilate respectively. Maley (19) and Cazes (20) reported some work on GPC fractionation of cellulose esters, but gave no data. It is worth mentioning here that the successful fractionation of cellulose triacetate has not been reported so far in the literature.

The prime object of the present study was to determine the compositional polydispersity of commercial cellulose triacetate and to examine the effect of molecular weight and molecular weight distribution on the mechanical properties of the fibres.

### Experimental

Materials. Cellulose triacetate samples with 61.7 - 62% acetyl value, were all commercial grade and were supplied by Courtauld's Ltd., Coventry England. The chemicals and the solvents used in this work were all analytical grade materials.

Fractionation Procedures. 1. Fractional precipitation. A 10% (m/V) solution of a commercial grade triacetate sample was dissolved in 300 ml N-methylpyrrolidone and 700 ml of acetone (30:70 V/V) and was thermostated for 2 hours at 25°C prior to the addition of 460 ml of petroleum ether (60-80°C) as precipitant. The solution with the precipitant was gently warmed to 45°C to redissolve the precipitate and gradually cooled in the thermostat. Phase separation took place after a while, and the phases were isolated from each other by filtration. The gel like phase thus isolated was the first primary fraction. The subsequent fractions were isolated in the same way by the further successive additions of precipitant to the solution. The last fraction was isolated by the addition of a large volume of the precipitant and allowing the solution to stand for 72 hours before the phase separation is affected by filtration as stated above.

Seven primary cellulose triacetate fractions were isolated by this method. The first primary fraction rich in hemicellulose was redissolved and reprecipitated into three subfractions in the same way as described above. The refractionation of the first fraction was necessary to isolate the hemicellulose material for subsequent analysis and characterisation.

2. Gel Permeation Chromatography (GPC). Waters Associate Model 200 GPC was used with 4' x 3/8" 'styragel' columns with an internal diameter of 0.311" and refractometer detector. The basic characteristics and operation of the instrument have been previously described in detail (19-20). Some of the operating conditions used in this study are outlined below.

Column exclusion limits :  $7 \times 10^5$  -  $5 \times 10^6$ ,  $5 \times 10^6$ ,  $5 \times 10^3$  &  $2 - 5 \times 10^3 \text{ \AA}$

Mobile phase : Dichloromethane

Flow rate : 1 ml/min.  
Sample concentration : 0.5% m/V  
Sample solution preparation: Allowed to stand overnight and then filtered through glass sinter No. 1 porosity.  
Operating temperature : Ambient  
Injection volume : 2 ml  
Refractive index attenuator: X8(1/16" null glass)  
Syphon size : 5 ml

Choice of Solvent. N-Methylpyrrolidone (NMP) was initially used as the mobile phase but proved to be unsatisfactory because of (i) high solution viscosities, (ii) exceedingly small differences in refractive index between NMP and cellulose triacetate solutions, (iii) erratic base line. In view of this dichloromethane was employed. Some additional benefits derived from this mobile phase are: (i) a decrease in elution volume due to low solution viscosities, (ii) fast solvent recovery due to low boiling point of dichloromethane and (iii) ease of obtaining preparative GPC cuts of cellulose triacetate.

Preparative GPC of Cellulose Triacetate Sample. A 1% (m/V) solution of cellulose triacetate (medium) prefiltered through porosity 3 glass sinter was fractionated by repeated injection through the column set described above. Seven cuts covering the entire elution curve were collected. The flow rate, injection time and the experimental conditions were identical to those stated above.

A total of 50 injections were made. Fractions were recovered by removing dichloromethane under vacuum at low temperature. The cuts were characterized in the same way as described previously for cellulose triacetate fractions.

Calibration of Gel Permeation Chromatograph. The chromatographic system was calibrated using:

- (1) Polystyrene standars
- (2) Narrow molecular weight cellulose triacetate fractions
- (3) A 'universal' calibration approach

Polystyrene standards. Solutions of the monodisperse polystyrenes (Waters, Mass., USA) in N-methylpyrrolidone (0.5% m/V) and dichloromethane (0.125% m/V) were used as calibrants. Figure 1 shows a plot of  $\log(\eta)$  vs.  $\log M_n$  for cellulose triacetate fractions in dichloromethane at 21 °C.



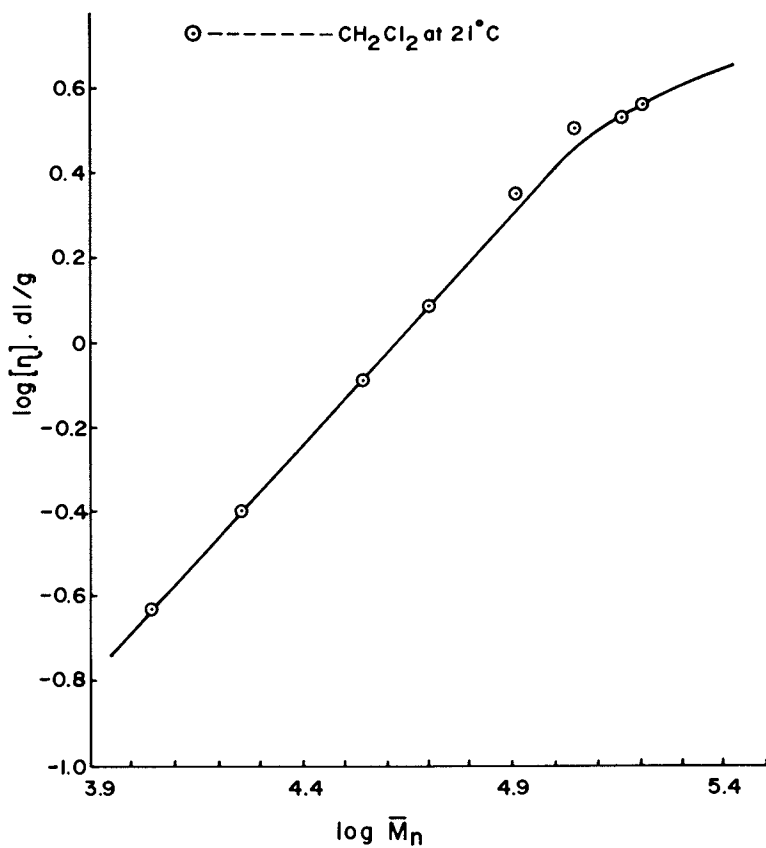


Figure 1. Log  $[\eta]$  versus log  $\bar{M}_n$  relationship for cellulose triacetate fractions.

Narrow Molecular Weight Triacetate Fractions. Narrow molecular weight cellulose triacetate fractions were obtained by both fractional precipitation and preparative GPC as described above. The number average molecular weight ( $M_n$ ) of the various fractions and cuts was determined by high speed membrane osmometry. A linear dependence of GPC elution volume on log molecular weight for all cellulose triacetate fractions was found in both N-methylpyrrolidone and dichloromethane.

Universal Calibration. A function of the hydrodynamic volume  $[\eta] \cdot M$  was plotted against the elution volumes of cellulose triacetate fractions and polystyrene standards run in dichloromethane have all indicated slight deviation from linearity as shown in Figure 2.

### Discussion

Fractional Precipitation of Cellulose Triacetate. The reported partial or non-fractionation of cellulose triacetate from chlorinated hydrocarbons or acetic acid may be explained in terms of the polymer-solvent interaction parameter  $\chi$  (1-11). The  $\chi$ -values for cellulose triacetate-tetrachloroethane and cellulose triacetate-chloroform systems are reported (10,21) as 0.29 and 0.34 respectively. The lower values of  $\chi$  for such systems will result in a smaller or negative heat of mixing ( $\Delta H_m$ ) and therefore partial or non-fractionation of the polymer in question results.

The poor fractionation from acetic acid has been attributed to the intermolecular hydrogen bonding between solvent molecules and thus a lesser polymer-solvent interaction. This means the total heat evolved due to hydrogen bonding between polymer and solvent molecules will be smaller than in the case of chloroform and tetrachloroethane and hence  $\Delta H_m$  (22) will be larger or more positive.

The structural homogeneity of the various cellulose triacetate fractions obtained by fractional precipitation was established by both infrared and nuclear magnetic resonance spectroscopy.

Calibration of Gel Permeation Chromatograph Polystyrene Calibration. A plot of molecular size in ( $\text{\AA}$ ) versus elution volume for polystyrene standards in dichloromethane showed deviation from linearity at about 2,200  $\text{\AA}$  which may be attributed to imperfect column resolution, peak broadening, axial dispersion and skewing. The extensive tailing of the chromatograms of high molecular weight polystyrene standards observed in dichloromethane has also been reported in the literature (23-26).

Narrow Molecular Weight Triacetate Calibration. A linear relationship was found when  $\log M_n$  against the elution volumes of various cellulose triacetate fractions was plotted. For narrow molecular weight distribution triacetate fractions, the GPC experimental average molecular weight, termed  $M_{\text{peak}}$  can be expected to conform to the following equation

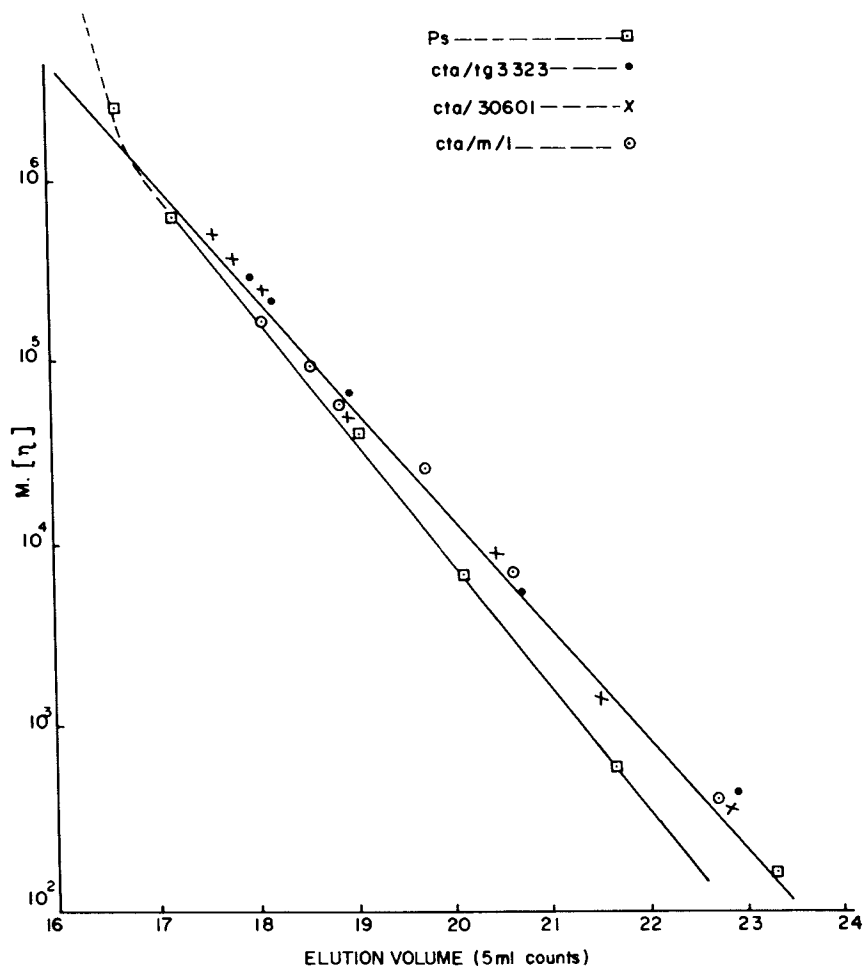


Figure 2. Universal calibration ( $M \cdot [\eta]$  vs elution volume) in dichloromethane at 21 C.

$$\bar{M}_{\text{peak}} \approx \bar{M}_w \approx \bar{M}_v \approx \bar{M}_n$$

However, for unfractionated triacetate samples and for fractions of broader molecular weight distribution, this equation will not hold and therefore taking  $\bar{M}_n$  or  $\bar{M}_v$  as  $\bar{M}_{\text{peak}}$  will lead to serious errors. This fact is evident from the results shown in Table I.

The apparent difference between viscosity average ( $\bar{M}_v$ ) and number average molecular weight ( $\bar{M}_n$ ) for unfractionated triacetate samples and high molecular weight fractions may be attributed to the presence of hemicellulose and polydispersity effect in these materials as shown in the table in question and in Figure 3.

Universal Calibration. Plots of  $[\eta] \cdot M$  against elution volumes indicate that polystyrene and cellulose triacetate follow different calibrations as shown in Figure 2. This deviation from linearity may be due to the following reasons.

1. Linear polymers, polystyrene and cellulose triacetate exhibit differences in hydrodynamic behavior in solution. Cellulose and its derivatives are known to have highly extended and stiff chain molecules below a  $\bar{D}_p$  of about 300, but as the  $\bar{D}_p$  increases above 300 the chain tends to assume the character of a random coil (27,28). The assumption that hydrodynamic volume control fractionation in GPC may not be true for polystyrene and cellulose triacetate, though it has been found satisfactory for non-polar polymers in good solvents (29).

2. The Mark-Houwink exponent 'a' for cellulose triacetate in dichloromethane was found 1.10-1.14 compared to polystyrene with 'a' = 0.71. These values were obtained experimentally in the present work.

Parikh (12) has found higher values for the exponent 'a' using the following polymer-solvent systems:

- (i) Cellulose triacetate-chloroform at 25°C : 'a' = 1.33
- (ii) Cellulose triacetate-tetrachloroethane at 25°C : 'a' = 1.24
- (iii) Cellulose triacetate-Acetic acid at 25°C: 'a' = 1.18.

Though the 'a' values for cellulose triacetate-dichloromethane system appear high in the present study, it is still not surprising when compared to the above stated 'a' values reported by Parikh (12). The difference in the values of 'a' for polystyrene and cellulose triacetate may account partly for the deviation in slopes as shown in Figure 2.

Ethyl cellulose and cellulose triacetate have been shown to form hydrogen bonded associates with dichloromethane (10,30). If this is so, then cellulose triacetate-dichloromethane interaction will be favored over polystyrene-cellulose triacetate interaction and thus no adsorption should be expected.

The partial blocking of the GPC column with  $5 \times 10^5 \text{ \AA}$  exclusion limit in both dichloromethane and N-methylpyrrolidone may be attributed to the presence of hemicellulose in both unfractionated triacetate samples and high molecular weight fractions used in this work. The blocking of the column in question was indicated

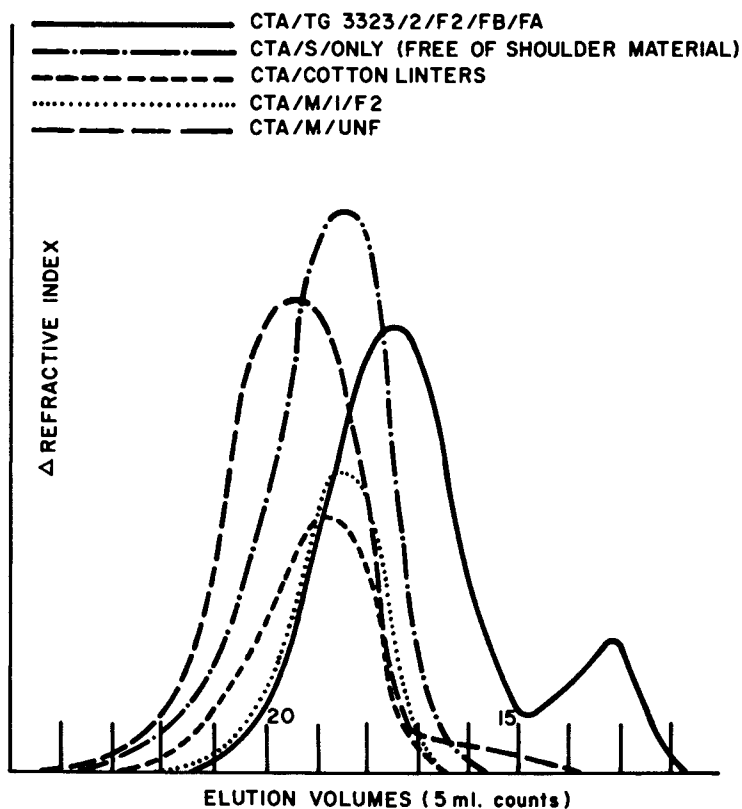


Figure 3. Gel permeation chromatograms of various triacetate samples and fractions.

Table 1. Analytical Data of Various Cellulose Triacetate Samples and Fractions

Sample	21°C [ $\eta$ ] CH <sub>2</sub> Cl <sub>2</sub>	$\bar{M}_n$	$\bar{M}_v$	E. V. (5ml) (DCM)	$\bar{D}_p$	$\bar{M}_n$ (GPC) (DCM)	$\bar{M}_w$ (GPC) (DCM)	$\bar{M}_w/\bar{M}_n$ (DCM)
CTA/M/1/UNF	2.04	72000	105680	18.60	250	46000	121334	2.63
CTA/M/1/F1	2.88	114200	115880	18.22	396	97420	165639	1.70
CTA/M/1/F1/FA	3.20	228375	151360	17.80	793	1110474	217469	1.96
CTA/M/1/F1/FB	2.72	188720	137090	18.10	655	108525	186029	1.71
CTA/M/1/F1/FC	1.68	82210	83946	18.64	285	91907	109982	1.19
CTA/M/1/F2	1.95	111090	113760	18.22	385	91000	124957	1.37
CTA/M/1/F3	1.58	93916	85310	18.64	326	70362	99050	1.40
CTA/M/1/F4	1.38	87000	77804	19.00	302	60000	88982	1.48
CTA/M/1/F5	1.18	66300	67143	19.64	230	46620	55926	1.19
CTA/M/1/F6	0.60	35658	36658	20.60	123	19800	36158	1.80
CTA/M/1/F7	0.236	14170	16136	23.00	49	18600	19196	1.03

by a rapid rise in the system pressure which necessitated the removal of this column in order to overcome the problem stated above.

Meyerhoff (14-16) has also observed similar blocking of the gel column using cellulose trinitrate fractions with molecular weight above  $1.4 \times 10^6$ , while fractions with molecular weight  $4.2 \times 10^5$  could not be separated. It is obvious from these results that he did not, however, realize the presence of the hemicellulose derivatives in the wood-pulp based cellulose nitrate and its role in blocking of the high porosity column as shown in this study.

#### Acknowledgments

Many people and organisation have contributed to this work, notably Courtauld's Ltd., Coventry, England.

#### Nomenclature of Cellulose Triacetate Samples and Fractions

Samples: In CTA/S/UNF, CTA/M/UNF, CTA/3060/UNF and CTA/TG 3323/UNF CTA stands for cellulose triacetate. The designation of S, M, 3060 and TG 3323 are batch numbers given to these samples by Courtauld's Ltd. UNF is the symbol for unfractionated sample.

Fractions: Each triacetate fraction, like the respective sample, starts with the symbol CTA (first column from left to right) and is then followed by the batch number (2nd column), fractionation number (3rd column), fraction number (4th column) and sub-fraction number (5th column respectively).

### Literature Cited

1. Elod, E. and Schmidt-Bielenberg, J. Physik. Chem. **B25**, 38, 1934.
2. Lachs, H.J., Kolloid, **J.**, 79, 91, 1937.
3. Levi, G. R., Gazz. Chim. Ital., **68**, 589, 1938.
4. Bezzi, S., Atti Ist. Veneto Sci., **99**, 905, 1939-40; Chemical Abstracts, **38**, 1356, 1944.
5. Munster, A., J. Polym. Sci., **5**, 58, 1950.
6. Cumberbirch, R. J. E., Shirley Institute Memoirs, **31**, 1958.
7. Thinius, K., Plaste Kautschuk, **6**, 547, 1959.
8. Okunev, P.P. and Tarakanov, O. G., Vysokomol. Soed., **4**, 5, 688, 1962.
9. Dymarchuk, N.P., Zhurnal Prikladnoi Khimi, **37**, No. 10, pp 2263-2268, English Translation, October 1964.
10. Howard, P., and Parikh, R. S., J. Polym. Sci., **A-1**, **4**, 407-418, 1966.
11. Geller, B. E., Khimicheski Volokna, **11**, No. 5, pp 1-6, English Translation, 1969.
12. Parikh, R.S., Ph.D. Thesis, University of Surrey, 1965.
13. Segal, L., J. Polym. Sci., **B4**, 1011, 1966.
14. Meyerhoff, G., Makromolek. Chem., **89**, 282, 1965.
15. Meyerhoff, G. and Jovanovic, S., J. Polym. Sci., **B5**, 495, 1967.
16. Meyerhoff, G., Makromolek. Chem., **134**, 129, 1970.
17. Muller, T. E., and Alexnader W. J., in "Analytical Gel Permeation Chromatography" (J. Polym. Sci. C, **21**), Johnson, J. F. and Porter, R.S., Eds., Interscience, New York, p. 283, 1968.
18. Brewer, R. J., Tanghe, L. J., Bailey, S. and Burr, J. T., J. Polym. Sci., **A-1**, **6**, 1697, 1968.
19. Maley, L. E., Analysis and Fractionation of Polymers, J. Polym. Sci., **C-8**, 253-268, 1965.
20. Cazes, J., J. Chem. Educ., **43**, A567, 1966.
21. Hager, O. and Vander Wyk, A. J. A., Helv. Chim. Acta, 1940 **23**, 484.
22. Hildebrand, J. and Scott, R., "The Solubility of Non-Electrolytes," 3rd Ed., Reinhold, 1949.
23. Harmon, D. J., in "Analysis and Fractionation of Polymers," J. Polym. Sci., **C-8**, Mitchell, J., Jr. and Billmeyer, F.W., Jr., Eds., Interscience, New York, p. 243, 1965.
24. Tung, L. J., J. Polym. Sci. **10**, 375, 1261, 1274, 1966.
25. Hess, M. and Kratz, R. F., J. Polym. Sci. **A-2**, **4**, 73, 1966.
26. Smith, W. N., J. Appl. Polym. Sci., **11**, 639, 1967.

27. Flory, P. J., "Principles of Polymer Chemistry," Cornell Univ. Press, Ithaca, New York, Chap. 13, 1953.
28. Stamm, A. J., "Wood and Cellulose Science," Ronald, New York, pp 96, 108, 1966.
29. Dawkins, J. V., Br. Polym. J., 4, 87-101, 1972.
30. Brookshaw, A. P., Br. Polym. J., 5, 229-239, 1973.

RECEIVED December 12, 1983



## Author Index

- Adesanya, B. A., 113  
Albaugh, E. W., 47  
Alden, Peter G., 145  
Alfredson, Thomas V., 73  
Anthony, Rayford G., 257  
Ayorinde, A. J., 321  
Barth, Howard G., 207  
Bidlingmeyer, Brian A., 171  
Bo, Shu-Qin, 125  
Borst, D., 47  
Browning, Horace L., Jr., 219  
Catterall, E., 365  
Cheng, Rong-Shi, 125  
Dumoulin, M. M., 97  
Ekmanis, Juris L., 145,171  
Francis, D. C., 3  
Freeman, David H., 355  
Grinshpun, V., 273  
Hagnauer, Gary L., 333  
Humphrey, W. D., 321  
Johnson, A. F., 25  
Jordan, R. C., 295  
Kah, A. F., 57,281  
Kerber, Jack D., 189  
Kim, Dong Hyun, 25  
Koehler, M. E., 57,281  
Krishen, A., 241  
Kuo, C., 57,281  
Lee, C. H., 321  
Liang, Xun, 355  
MacArthur, A., 227  
Mahmud, F., 365  
Malihi, F. B., 281  
McHugh, A. J., 3  
McIntyre, D., 227  
Miller, Ronald L., 189  
Mori, Sadao, 135  
Niemann, T. F., 57  
O'Driscoll, K. F., 273  
Overton, James R., 219  
Pearce, Peter J., 333  
Perry, William J., 73  
Philip, C. V., 257  
Plass, N. C., 113  
Provdor, T., 57,281  
Regnier, Fred E., 207  
Richardson, Harold, 171  
Rivard, R. J., 295  
Rudin, A., 273  
Savoca, J., 227  
Schultz, Herman S., 145  
Seeger, R., 227  
Sehon, R. D., 295  
Shih, A. L., 227  
Silver, S. F., 295  
Talarico, P., 47  
Tallman, Lori, 73  
Timm, D. C., 113,321  
Utracki, L. A., 97  
Warren, F. Vincent, Jr., 171  
Yen, H. C., 113

## Subject Index

### A

- Addition, epoxy and primary and secondary amine, 336,350,354  
Aggregate elimination in polyethylene solutions, 276-79  
n-Alcohols, molecular weight vs. retention volume, 246f  
n-Alkane analysis  
  columns, 242-43  
  molecular weight vs. retention volume, 246f  
Amine-epoxy curing reactions,  
  mechanism, 335-36  
Anhydride, epoxy resin  
  formulation, 329t  
Anthracene, supercritical fluid  
  chromatograph, 51-56  
Antioxidant in polyethylene and  
  molecular weight averages vs.  
  residence time, 101-8  
Approximation method, Q-factor,  
  calibration curve, 76,84-87,93  
Aqueous SEC of narrow molecular weight  
  distribution standards, calibration  
  curves, 78-79,87-93  
Aromatic compounds, supercritical  
  fluid chromatograph, 51-56  
Aromatic gel, effect on size  
  separation of aromatic  
  species, 261-69  
Arrhenius relationships,  
  N,N'-tetraglycidyl methylene  
  dianiline, reaction with  
  4,4'-diaminodiphenyl  
  sulfone, 344-54  
Asphalt, 265,268f

## Author Index

- Adesanya, B. A., 113  
Albaugh, E. W., 47  
Alden, Peter G., 145  
Alfredson, Thomas V., 73  
Anthony, Rayford G., 257  
Ayorinde, A. J., 321  
Barth, Howard G., 207  
Bidlingmeyer, Brian A., 171  
Bo, Shu-Qin, 125  
Borst, D., 47  
Browning, Horace L., Jr., 219  
Catterall, E., 365  
Cheng, Rong-Shi, 125  
Dumoulin, M. M., 97  
Ekmanis, Juris L., 145,171  
Francis, D. C., 3  
Freeman, David H., 355  
Grinshpun, V., 273  
Hagnauer, Gary L., 333  
Humphrey, W. D., 321  
Johnson, A. F., 25  
Jordan, R. C., 295  
Kah, A. F., 57,281  
Kerber, Jack D., 189  
Kim, Dong Hyun, 25  
Koehler, M. E., 57,281  
Krishen, A., 241  
Kuo, C., 57,281  
Lee, C. H., 321  
Liang, Xun, 355  
MacArthur, A., 227  
Mahmud, F., 365  
Malihi, F. B., 281  
McHugh, A. J., 3  
McIntyre, D., 227  
Miller, Ronald L., 189  
Mori, Sadao, 135  
Niemann, T. F., 57  
O'Driscoll, K. F., 273  
Overton, James R., 219  
Pearce, Peter J., 333  
Perry, William J., 73  
Phillip, C. V., 257  
Plass, N. C., 113  
Provdor, T., 57,281  
Regnier, Fred E., 207  
Richardson, Harold, 171  
Rivard, R. J., 295  
Rudin, A., 273  
Savoca, J., 227  
Schultz, Herman S., 145  
Seeger, R., 227  
Sehon, R. D., 295  
Shih, A. L., 227  
Silver, S. F., 295  
Talarico, P., 47  
Tallman, Lori, 73  
Timm, D. C., 113,321  
Utracki, L. A., 97  
Warren, F. Vincent, Jr., 171  
Yen, H. C., 113

## Subject Index

### A

- Addition, epoxy and primary and secondary amine, 336,350,354  
Aggregate elimination in polyethylene solutions, 276-79  
n-Alcohols, molecular weight vs. retention volume, 246f  
n-Alkane analysis  
  columns, 242-43  
  molecular weight vs. retention volume, 246f  
Amine-epoxy curing reactions,  
  mechanism, 335-36  
Anhydride, epoxy resin  
  formulation, 329t  
Anthracene, supercritical fluid  
  chromatograph, 51-56  
Antioxidant in polyethylene and  
  molecular weight averages vs.  
  residence time, 101-8  
Approximation method, Q-factor,  
  calibration curve, 76,84-87,93  
Aqueous SEC of narrow molecular weight  
  distribution standards, calibration  
  curves, 78-79,87-93  
Aromatic compounds, supercritical  
  fluid chromatograph, 51-56  
Aromatic gel, effect on size  
  separation of aromatic  
  species, 261-69  
Arrhenius relationships,  
  N,N'-tetraglycidyl methylene  
  dianiline, reaction with  
  4,4'-diaminodiphenyl  
  sulfone, 344-54  
Asphalt, 265,268f

- Automated data analysis system
  - for dilute solution light scattering of branched copolymers, 300-304
  - for Waters Associates model 150C ALC/GPC system with multiple detectors, 57-71
- Average molecular weight
  - flow rate errors, 204t
  - monomeric contamination in polystyrene epoxy, 121-22
- Axial dispersion in polymer fractionation modeling, 33
- Azobisisobutylnitrile, initiator for polystyrene, frequency distributions, 113,115-17

## B

- Backmixing in polymer fractionation model, 27-31
- Bandwidth
  - in high-speed GPC
    - column efficiency, 191,193
    - Ultrastryragel columns, 147
- Benz(a)pyrene, supercritical fluid chromatograph, 51-56
- Benzene
  - solvent system and viscosities of high molecular weight polymers, 232t
  - supercritical fluid chromatograph, 51-56
  - for Ultrastryragel columns, plates vs. pores, 156-62
- Benzoic acid and pressure programming in supercritical fluid chromatography, 53-56
- Benzyl alcohol from a steroid cream, 177,179f
- Block copolymers, linear and branched
  - divinyl benzene coupling, 295-318
  - low-angle laser light scattering detection, 295-318
- Boiling point, methylene chloride/hexafluoroisopropanol, 220
- Bond strengths, effect on polymer degradation, 231
- Boundary conditions, Dankwert's, in polymer fractionation modeling, 28-29
- Branching functionality, styrene-isoprene and styrene-butadiene copolymers, 306,311-13
- Branching parameter, SEC/LALLS theory, 300-302
- Broad molecular weight distribution
  - standards of polymers, 73-94
  - 1,2-polybutadiene fractions, 125-34
  - polyvinyl chloride, linear calibration, 78,85-86

- Broadening
  - instrumental, 195,198t
  - polymer fractionation modeling, 35-43
- Butadiene, dilute solution light scattering detection, 304
- n*-Butyl lithium, initiator for polystyrene, frequency distributions, 113,115-17
- Butylated hydroxyanisole and butylated hydroxytoluene separation on Ultrastryragel column, 176-78
- Butylated *p*-cresol/dicyclopentadiene product, 247,249,250f
- tert-Butylstyrene cross-linked with 1,2-polybutadiene, 321-26

## C

- Calibration
  - for cellulose triacetate fraction analysis, 367-68,369,371-73
  - using deuterium oxide, 207-17
  - of GPC/viscometer system, 285
  - linear, 74-76,79-84,88-91,93
  - using narrow and broad molecular weight distribution standards for polymers, 73-94
  - using polyethylene, GPC/LC, 98
  - using polystyrene, 35,36f
  - narrow molecular weight distribution, 125-34
  - subject to Poisson constraints, 113-24
- Q-factor approximation method, 76,84-87,93
- for small molecule separation, 173-75,177-85
- for *N,N'*-tetraglycidyl methylene dianiline reaction with 4,4'-diaminodiphenyl sulfone, 339-41
- of Ultrastryragel columns, 145-55
- universal, 300,301
- universal, and hydrodynamic volume of polymers, 76-77,84-88,93
- Calibration function of column, definition, 125-26
- Capillary-cylindrical pore model for porous-partitioning hydrodynamic chromatography, 8-12
- Capillary hydrodynamic chromatography, comparison of model calculations with experimental data, 6-7
- Capillary viscosity detector for high-performance GPC, 281-94
- Cellulose triacetate, fractionation and characterization, 365-75
- Chain degradation, loop entanglement model rationalization, 237-40

- Chain flexibility effect, degradation of high molecular weight polymers in cyclohexane, 230,233-35
- Chain growth  
 polymerization, 1,2-polybutadiene polymer cross-linked with tert-butylstyrene, 321-26
- Chain length calibration curve, coefficients, 58,61f
- Chain length determination, small molecules and oligomers, 244-47
- Charcoal lighter, 265,267f
- Chloroform solvent system for linear and branched copolymers, dilute solution light scattering detection, 304
- $\alpha$ -Chloronaphthalene solvent systems for polyethylene, 274
- Chromatographic curves, symmetrical and skewed peaks, 29-30,35-43
- Chrysenes, supercritical fluid chromatograph, 51-56
- Column oven, supercritical fluid chromatography, 48-51
- Columns, 191  
 efficiency  
 in high-speed GPC, 191,193  
 bandwidth  
 plates, 191,192f  
 Ultrastyrigel, 177  
 glass with glyceryl silane, 209-17  
 linear, monodisperse and polydisperse calibration relation, 126  
 molecular weight calibration function, 125-26  
 for oligomer analysis, 242-43  
 organic polymer-based high efficiency, 145-68  
 plate count, for resins of narrow molecular weight distribution, 115-17  
 silica bead packed, dispersion of polystyrene and 1,2-polybutadiene, 128t  
 silica and SynChropak, column calibration using deuterium oxide, 207-17  
 for small molecule analysis, 242-43
- Styrigel  
 calibration curve, 98-100  
 degradation of high molecular weight polymers in cyclohexane, 230-40  
 styrene/divinylbenzene copolymer bead, dispersion of polystyrene and 1,2-polybutadiene, 128t
- SynChropak, 209-17
- Ultrastyrigel, 175  
 calibration  
 curves, 148-53,177,179-85
- Columns--Continued  
 pore size distribution, 180-85  
 probe mixture definition, 153-56  
 small molecule separation, 156-60
- Computer model of polymer fractionation, 25-43
- Concentration detector and viscosity detector, interface, 281-86
- Continuous capillary viscosity detector for high-performance GPC, 281-94
- Controlled-flow pressure-programmed supercritical fluid chromatograph, 47-56
- m-Cresol in methylene chloride/hexafluoroisopropanol solvent system, 221-25
- p-Cresol-dicyclopentadiene product, butylated, 247,249,250f
- Cross-link structure  
 polybutadiene and tert-butylstyrene thermoset resin, 321-30  
 sulfonated styrene/divinylbenzene copolymer degradation, 355-57
- Cure kinetics  
 1,2-polybutadiene polymer cross-linked with tert-butylstyrene, 321-26
- N,N'-tetraglycidyl methylene dianiline epoxy resin, reaction with 4,4'-diaminodiphenyl sulfone, 333-54
- Curing schedules for epoxy resin formulation, 329t
- D
- Dankwert's boundary conditions, polymer fractionation modeling, 28-29
- Data acquisition for high-speed GPC, 199,201-2
- Data processing, 302  
 for dilute solution light scattering of branched copolymers, 300-304  
 for GPC/viscometer system, 282,284f,285  
 for high-speed GPC, 199,201-2  
 for Waters Associates model 150C ALC/GPC system with multiple detectors, 57-71
- Data reliability in polyethylene analysis, 97-109
- Dead volume between differential refractometer and viscometer detectors, 289,290f
- Degradation  
 hydrogen peroxide, of sulfonated styrene/divinylbenzene copolymers, 355-63

- Degradation--Continued  
 loop entanglement model  
 rationalization, 237-40  
 of polystyrene, 121-22  
 shear  
 and molecular parameter data of  
 polyethylene resins, 103-9  
 of very high molecular weight  
 polymers, 227-40  
 thermal, and molecular parameter  
 data of polyethylene  
 resins, 103-9
- Degradation kinetics constant,  
 polyethylene resins, 101-3
- Degree of polymerization of  
 1,2-polybutadiene polymer cross-  
 linked with tert-  
 butylstyrene, 323-26
- Detectors  
 concentration, interface with vis-  
 cosity detector, 281-86  
 differential refractometer and  
 viscometer, dead  
 volume, 289,290f  
 for high-speed GPC flowcell  
 effect, 196-99  
 response time effect, 199,200f  
 low-angle laser light  
 scattering, 295-318  
 multiple, for Waters Associates  
 model 150C ALC/GPC system, 57-71  
 viscosity, interface with concentra-  
 tion detector, 281-86
- Deuterium oxide  
 for column calibration, 207-17  
 on controlled-pore glass and  
 SynChropak columns  
 elution volume and flow  
 rate, 210,213  
 injection concentration, effect on  
 peak height and retention  
 volume, 213t
- Dextrans, linear calibration, 79,88-93
- Diameter--See Radius
- 4,4-Diaminodiphenyl sulfone, reaction  
 with N,N'-tetraglycidyl methylene  
 dianiline, 333-54
- Dibutyladipate, molecular weight vs.  
 retention volume, 246f
- 2,6-Di-tert-butyl-p-cresol, molecular  
 weight vs. retention  
 volume, 246f
- o-Dichlorobenzene solvent systems for  
 polyethylene, 274
- Dichloromethane solvent system for  
 cellulose triacetate fraction  
 analysis, 367
- Dicumyl peroxide, hydrocarbon resin  
 formulation, 327t
- Dicyclopentadiene-p-cresol product,  
 butylated, 247,249,250f
- n-Didecyl, didodecyl, and diethyl  
 phthalate, molecular weight vs.  
 retention volume, 246f
- Differential refractometer and vis-  
 cosity detector interface, 281-86
- Differential refractometer and vis-  
 cosity detector interface, dead  
 volume, 289,290f
- Diffusion of solute within gel  
 structure, model, 27-31
- Diffusivity, effective, polymer frac-  
 tionation modeling, 31-33
- Dilaurylthiodipropionate in  
 polyethylene, molecular weight  
 averages vs. residence  
 time, 100-109
- Dilute solution light scattering of  
 homopolymers and copolymers,  
 theory, 297-300
- Dimensionless parameter in polymer  
 fractionation modeling, 35-43
- Diocetylquinone, 252
- Dispersion  
 axial, polymer fractionation  
 modeling, 33  
 model development of polymer  
 fractionation, 27-31  
 spreading factor, molecular weight  
 calibration, 125-34
- Distributions, population density, of  
 1,2-polybutadiene polymer cross-  
 linked with t-butylstyrene, 321-26
- Divinyl benzene  
 coupling, linear and branched block  
 copolymers, 295-318  
 isomers, and sulfonated  
 styrene/divinylbenzene copolymer  
 degradation, 355-57
- E
- Effective diffusivity, polymer  
 fractionation modeling, 31-33
- Efficiency of columns  
See also Plates  
 in high-speed GPC  
 bandwidth 191,193  
 plates, 191,192f
- Elution time, mean dimensionless,  
 equations for first, second, and  
 third moments, 30
- Elution volume deviation and size  
 factors for small molecules and  
 oligomers, 245-47
- Elution volumes  
 of deuterium oxide and glucose on  
 controlled-pore glass and  
 SynChropak columns, 210,213  
 of n-hydrocarbons, 245  
 and molecular weight  
 calibration, 125-34

## Elution volumes--Continued

- of polystyrene, 173
- of styrene-isoprene and styrene-butadiene copolymers, 306,311-18
- and temperature effect, 214-16
- Epon 828 and nadic methyl anhydride, 326-30
- Epoxy-amine curing reactions, mechanism, 335-36,350,354
- Epoxy cresol Novalac oligomer separation, 191,192f
- Epoxy-epoxy homopolymerization, 336,350,354
- Epoxy resin, 121-22
  - 1,2-polybutadiene polymer and *tert*-butylstyrene, curing and cross-link structure, 321-26
  - N,N'*-tetraglycidyl methylene dianiline and 4,4'-diaminodiphenyl sulfone, cure kinetics, 333-54
- Exclusion, plate reduction in high-speed GPC, 196t

## F

- Fenton's reagent degradation of sulfonated styrene/divinylbenzene copolymers, 355-63
- Filters, hydraulic, effect on baseline noise of viscometer trace, 287,287f
- Flory tetrahedral cells, sulfonated styrene/divinylbenzene copolymer degradation, 355-57
- Flow rate
  - and baseline noise effect of viscometer trace, 286,287f
  - and elution volume effect, deuterium oxide and glucose, 213
  - and separation speed, 193,194f
- Flow rate errors, effect on high-speed GPC, 203-4
- Flowcell of detector, effect on high-speed GPC, 196-99
- Fluid chromatograph, supercritical, with pressure programming and controlled flow, 47-56
- Fractional precipitation of cellulose triacetate, 366,369
- Fractionation models, 25-43
  - cellulose triacetate characterization, 365-75
  - Dankwert's boundary conditions, 28-29
  - dimensionless parameter, 35-43
  - mass transfer coefficient and axial dispersion, 33
  - mobile and stationary phase material balance equation, 27-28
  - tortuosity, 32-33

- Fractionation of styrene/divinylbenzene networks by hydrogen peroxide, 355-63
- Fritted discs, effect on degradation of high molecular weight polymers in cyclohexane, 230-32
- Functionality of 1,2-polybutadiene polymer cross-linked with *tert*-butylstyrene, 325-30
- Fuzes statistical methods for molecular weight distributions, 135-42

## G

- Gasoline, 265,266f
- Gaussian pore size distribution, 173,185
- Gel content
  - and degradation of high molecular weight polymers, 235-36
  - and mobile-phase mass transfer, 27-31
  - and reaction time of *N,N'*-tetraglycidyl methylene dianiline and 4,4'-diaminodiphenyl sulfone, 339-41
- Glass with glyceryl silane and Synchropak column packing material, 209-17
- Glucose and deuterium oxide on controlled-pore glass and SynChropak columns, elution volume, 210,213
- Grain bait, determination of warfarin, 177,178f

## H

- Hamaker constant, 13-17
- Heat exchanger in supercritical fluid chromatograph, 48-51
- Heavy water
  - for column calibration, 207-17
  - on controlled-pore glass and SynChropak columns elution volume and flow rate, 210,213
  - injection concentration, effect on peak height and retention volume, 213t
- High-density polyethylene, 97-98,274-79
- High-density polyethylene, molecular weight averages with antioxidant, 101-5,107-9
- High molecular weight polymethyl methacrylate, differential refractometer and viscosity chromatogram, 289,290f

- High-performance GPC with continuous capillary viscosity detector, 281-94
- High-pressure, low-density, polyethylenes, 274-79
- High-speed GPC, 189-206  
bandwidth, column efficiency, 191,193  
data acquisition and processing, 199,201-2  
detector  
effect of flowcell, 196-99  
effect of response time, 199,200f  
flow rate errors, 203-4  
instrumental band broadening, 195,198t  
plates,  
column efficiency, 191,192f  
reduction at exclusion and at permeation, 196t  
polystyrene, speed of separation, 193,194f  
pumps, 205  
sampling rate, 201t  
solvent delivery, 203-6  
temperature control, 202-3  
tubing diameter, 196
- High-speed membrane osmometry, triacetate characterization, 365
- High-temperature SEC of polyethylene, 273-79
- Homopolymerization, epoxy-epoxy, 336,350,354
- Hydraulic filters, effect on baseline noise of viscometer trace, 286,287f
- Hydrocarbon resin formulation, dicumyl peroxide, 327t
- Hydrodynamic behavior, cellulose triacetate fractions, 371
- Hydrodynamic chromatography, mechanisms, 4-8
- Hydrodynamic volume of polymers, universal calibration method, 76-77,84-88,93
- Hydrogen peroxide degradation of sulfonated styrene/divinylbenzene copolymer, 355-63
- Hydroquinones, 252
- I
- Inhomogeneity index equations and uncertainty of spreading factor with polystyrene and polybutadiene, 130,132f
- Injection concentration, effect on peak height and retention volume of deuterium oxide, 213t
- Injection volume effect, 195-96
- Instrumental band broadening in high-speed GPC, 195,198t
- Integral methods for calibration, 73-74
- Ion exchange resins, 355-63
- Ionic marker species, velocity equations, 5
- Isomers of divinyl benzene and sulfonated styrene/divinylbenzene copolymer degradation, 355-57
- Isoprene, dilute solution light scattering detection, 304
- Isothermal cure kinetics of *N,N'*-tetraglycidyl methylene dianiline reaction with 4,4'-diaminodiphenyl sulfone, 333-54
- K
- Kinetic distributions of nadic methyl anhydride and phenyl glycidyl ether, 113
- Kinetics, cure  
of 1,2-polybutadiene polymer cross-linked with *tert*-butylstyrene, 321-26  
of *N,N'*-tetraglycidyl methylene dianiline, reaction with 4,4'-diaminodiphenyl sulfone, 333-54
- L
- Laplace domain solution of initial and boundary conditions, 29-30
- Laser light scattering detection, low-angle  
for aggregation detection, 273-79  
of dilute solutions, theory, 297-300  
of linear and branched block copolymers, 300-18
- Linear calibration methods, 74-76,79-84,88-91,93
- Linear column, monodisperse and polydisperse calibration relation, 126
- Linear low-density polyethylenes, 274-79  
molecular weight averages with antioxidants, 100
- Linear molecular sizes from valence-bond structures, 258-59,261
- Log-normal distribution function, MWD of high-density polyethylene, 107
- Loop entanglement model rationalization of GPC chain degradation, 237-40
- Low-angle laser light scattering detection, 295-318

- Low-angle laser light scattering  
 detection--Continued  
 for aggregation detection, 273-79  
 of dilute solutions, theory, 297-300  
 of linear and branched block  
 copolymers, 300-18
- Low-density linear  
 polyethylenes, 274-79
- Low-density polyethylenes, molecular  
 weight averages with  
 antioxidant, 101,104-7
- M
- Mark-Houwink exponent for cellulose  
 triacetate in dichloromethane, 371
- Mark-Houwink parameters for polystyrene  
 in GPC/viscometer system, 289,292-93
- Mark-Houwink relationships for  
 poly(ethylene terephthalate) and  
 polystyrene in methylene  
 chloride/hexafluoroisopropanol, 220
- Marker velocities, equations, 5
- Mass transfer between gel and mobile  
 phase, model development of  
 polymer fractionation, 27-31,33
- Mathematical modeling of separation  
 mechanisms, 3-22
- Matrix  
 nonporous, 4-5  
 porous, 5-6
- Mean dimensionless elution time,  
 equations for first, second, and  
 third moments, 30
- Mechanisms  
 high molecular weight polymer  
 degradation, 237  
 hydrodynamic chromatography, 4-8  
 separation, mathematical  
 modeling, 3-22
- N,N'-tetraglycidyl methylene  
 dianiline reaction with  
 4,4'-diaminodiphenyl  
 sulfone, 335-36,341-54
- Medium density polyethylene, molecular  
 weight averages with  
 antioxidant, 101,104-7
- Melt-phase poly(ethylene phthalate) in  
 methylene chloride/hexafluoro-  
 isopropanol solvent system, 221-25
- Membrane osmometry, high speed, for  
 triacetate characterization, 365
- Mercury porosimetry, physical charac-  
 teristics of SEC packings, 212t
- Methylene chloride/hexafluoroiso-  
 propanol properties, 220  
 as solvent system for poly(ethylene  
 terephthalate), 219-25
- Methylpyrrolidone solvent system for  
 cellulose triacetate fraction  
 analysis, 367
- Mobile phase  
 mass transfer to and from gel  
 phase, 27-31  
 material balance equation, 27  
 in supercritical fluid  
 chromatograph, 48-51  
 for urea, 214
- Modeling of fractionation, 25-43  
 Dankwert's boundary  
 conditions, 28-29  
 dimensionless parameter, 35-43  
 mass transfer coefficient and axial  
 dispersion, 33  
 mobile and stationary phase material  
 balance equation, 27-28  
 tortuosity, 32-33
- Molar volume determination for small  
 molecules and oligomers, 244-47
- Molecular distribution, precision for  
 resins of narrow molecular  
 distributions, 113-24
- Molecular size calculation  
 linear, from valence-bond  
 structures, 258-59,261  
 small molecules and  
 oligomers, 244-47
- Molecular weight  
 of oligomeric species, 245  
 of poly(methyl methacrylate), dif-  
 ferential refractometer and vis-  
 cometer chromatogram, 289,290f  
 precision for resins of narrow  
 molecular distributions, 113-24  
 of styrene/divinylbenzene copolymer  
 fragments after degradation with  
 hydrogen peroxide, 358-63  
 of triacetate fractions, 365
- Molecular weight averages  
 with antioxidant, 101,104-7  
 flow rate error effect, 204t  
 of polyethylene in various  
 solvents, 276,277t  
 of polystyrene epoxy, due to  
 monomeric contamination, 121-22  
 of polystyrene standard, empirical  
 equation, 173  
 temperature effect, 203t  
 of N,N'-tetraglycidyl methylene  
 dianiline reacted with  
 4,4'-diaminodiphenyl  
 sulfone, 339-54
- Molecular weight calibration curve,  
 coefficients, 58,61f
- Molecular weight calibration function,  
 of column, definition, 125-26



- Molecular weight determination and aggregation elimination in polyethylene, 273-79  
dilute solution light scattering of branched copolymers, 298-302
- Molecular weight distribution  
Fuzes statistical methods, 135-42  
of 1,2-polybutadiene fractions, broad, 125-34  
of polyethylene, high density, log-normal distribution function, 107  
of poly(ethylene terephthalate), 225  
of polystyrene  
  GPC/viscometer system, 289,292-93  
  narrow, simultaneous calibration of molecular weight separation and column dispersion, 125-34  
  using Simpson's rule, averages in time-volume space, 62  
  standard calibration techniques for narrow and broad 73-94  
  of triacetate fractions, narrow, for cellulose triacetate fraction analysis, 379-71
- Molecular weight/elution volume, styrene-isoprene and styrene-butadiene copolymers, 306,311-18
- Monomeric contamination in polystyrene epoxy, error in average molecular weights, 121-22
- Motor oils, 265,268f
- N
- Nadic methyl anhydride and Epon 828, 326-30
- Nadic methyl anhydride epoxy, 113
- Naphtha, 265,266f
- Naphthalene, supercritical fluid chromatograph, 51-56
- Narrow molecular weight distribution polymer standards, 73-94
- Narrow molecular weight distribution polystyrene standards  
  calibration of molecular weight separation and column dispersion, 125-34  
  identification by Fuzes statistical methods, 137  
  viscometer chromatogram, 286,288f
- Narrow molecular weight distribution triacetate of cellulose triacetate fraction analysis, 379-71
- Noise, baseline, in GPC/viscometer system, 286,287f
- Nonox dilaurylthiodipropionate in polyethylene, molecular weight averages vs. residence time, 100-109
- Nonporous matrix, 4-5
- Nonylphenol-formaldehyde adducts, molecular weight vs. retention volume, 246f
- Number average degree of polymerization and calibration for improved resolution, 115,118
- Number average molecular weight of polydisperse polymer, definition, 125-27
- Number average molecular weight of polyethylene in various solvents, 276,277t
- O
- Octyl hydroquinone, 252
- Oils, motor and transmission, 265,267f,268f
- Optical considerations, dilute solution light scattering of branched copolymers, 297-98
- Organic polymer-based high-efficiency columns, 145-68
- Osmometry, high-speed membrane, for triacetate characterization, 365
- Oxidation of styrene/divinylbenzene copolymers by hydrogen peroxide, 355-63
- P
- Packing diameter in the pore-partitioning model and separation factor-particle diameter behavior, 5-7,13-17
- Packing of styrene/divinylbenzene copolymer for petroleum crude analysis, 257
- Packing systems, porous, separation mechanisms and deviation from models, 3-22
- Particle diameter-separation factor behavior in pore-partitioning model, 13-17
- Particle velocities, equations, 5
- Peak height and retention volume of deuterium oxide, effect of injection concentration, 213t
- Permeation and plate reduction in high-speed GPC, 196t
- Petroleum crude and distillate analysis, 257-69
- Phenol, effect of pressure programming in supercritical fluid chromatograph, 53-56
- Phenol-formaldehyde resins, 247,248f
- Phenol-tetrahydrofuran complex, 260f
- Phenyl glycidyl ether epoxy, 113

- Phenyl group, interaction with aromatic structures, 261,263
- Phthalate ester, separation, 191,192f
- Plasticizers, 249-52
- Plate count  
 in high-speed GPC  
 column efficiency, 191,192f  
 reduction at exclusion and permeation, 196t  
 for resins of narrow molecular weight distribution, 115-17  
 for small molecule and oligomer analysis, 242-43  
 in Ultrastryagel  
 columns, 148,153,156-62
- Pneumatic pressure transmitter for supercritical fluid chromatograph, 48-51
- Poisson distribution and calibration for improved resolution, polystyrene, 113-24
- 1,2-Polybutadiene  
 broad molecular weight distribution fractions, 125-34  
 cross-linked with *tert*-butylstyrene, 321-26
- Polychlorinated biphenyls, 252
- Polydimethylsiloxane, high molecular weight, shear degradation, 227-40
- Polydisperse polystyrene, nonaqueous separations, calibration curves, 77-78,80-87
- Polydispersity ratios of polyethylene resins, 101-3
- Polyethylene  
 high-temperature SEC, 273-79  
 polydispersity ratios of resins, 101-3  
 refractive index increments in various solvent systems, 274,275t  
 reliability of molecular parameter data, 97-109  
 solution chemistry, aggregation, 273-79
- Polyethylene glycol, narrow MWD standards, calibration curves, 78-79,87-93
- Polyethylene oxide, narrow MWD standards, calibration curves, 78-79,87-93
- Poly(ethylene terephthalate) in methylene chloride/hexafluoroisopropanol solvent system, 219-25
- Polyhexylisocyanate, high molecular weight, shear degradation, 227-40
- Polyisoprene, high molecular weight, shear degradation, 227-40
- Polymer diffusivity, 32
- Poly(methyl methacrylate), high molecular weight, differential refractometer and viscometer chromatogram, 289,290f
- Polynuclear aromatic compounds, effect of pressure on separation, 53t
- Polystyrene  
 azobisisobutylnitrile initiation, frequency distributions, 113,115-17  
*n*-butyl lithium initiation, frequency distributions, 113,115-17  
 calibration standard, 35,36f  
 flow rate effect on separation, 193,194f  
 molecular weight separation and column dispersion, narrow MWD, 125-34  
 nonaqueous separations, 77-78,80-87  
 Ultrastryagel columns, 148-68  
 weight average molecular weight, empirical equation, 173  
 decomposition, 121-22  
 elution volume, 173  
 Fuzes statistical methods for identification, 137  
 GPC/viscometer system, molecular weight distribution statistics, 289,292-93  
 Mark-Houwink relationships, in methylene chloride/hexafluoroisopropanol, 220  
 narrow MWD standard, viscometer chromatogram, 286,288f  
 oligomer mix, plates vs. pores in Ultrastryagel columns, 156-62  
 polydisperse, nonaqueous separations, calibration curves, 77-78,80-87  
 pressure programming in supercritical fluid chromatograph, 53-56  
 shear degradation, high molecular weight, 227-40
- Polystyrene/divinylbenzene copolymer packing for petroleum crude analysis, 257  
 sulfonated, scission study, 355-57
- Poly(vinyl chloride), broad MWD standard, linear calibration, 78,85-86
- Population density distribution and calibration for improved resolution, 113-24  
 for nadic methyl anhydride and Epon 828, 326  
 for 1,2-polybutadiene polymer cross-linked with *tert*-butylstyrene, 321-26

- Pore partitioning hydrodynamic chromatography, mathematical modeling, 8-22
- Pore radius, 6
- Pore radius for the pore-partitioning model and separation factor-particle diameter behavior, 13-17
- Pore size distribution  
for small molecule separation, 172-73,185  
Ultrastryragel column, 180-85
- Pore size effect, degradation of high molecular weight polymers in cyclohexane, 230,235
- Pore size, Ultrastryragel columns, 148, 149f
- Pore sizes, GPC/LC of polyethylene, 98
- Pore volume characterization, deuterium oxide, 207-17
- Pore volume fraction, 6
- Pore volume fraction  
accessible, polymer fractionation modeling, 31  
polymer fractionation modeling, 31
- Pores vs. plates in Ultrastryragel columns, 156-62
- Porosil C, supercritical fluid chromatograph, 51-56
- Porosimetry, mercury, physical characteristics of SEC packings, 212t
- Porous packing systems, separation mechanisms and deviation from models, 3-22
- Precipitation, fractional, of cellulose triacetate, 366,369
- Pressure-programmed controlled-flow supercritical fluid chromatograph, 47-56
- Probe mixtures for Ultrastryragel columns, 145-47,153,156-68
- Propagation rate and calibration for improved resolution, 113-24
- Pump pulsations in GPC/viscometer system, 286,287f
- Pumps for high-speed GPC, 205
- Q
- Q-factor approximation method, calibration curve, 76,84-87,93
- Quinones, 252
- R
- Radius of pore--See Pore radius
- Rate constant for  $N,N'$ -tetraglycidyl methylene dianiline reaction with 4,4'-diaminodiphenyl sulfone, 344-54
- Reaction rates of 1,2-polybutadiene polymer cross-linking with tert-butylstyrene, 321-26
- Refractive index increments, polyethylene in various solvent systems, 274,275t
- Refractometer, 57-71  
interface with viscosity detector, 281-86
- Reliability of data, polyethylenes, 97-109
- Reproducibility of data, 98
- Reproducibility of data in high-speed GPC, 205-6
- Resin  
high-density polyethylene, 101-5,107-9  
low-density polyethylene, 101,104-7  
medium-density polyethylene, 101,104-5  
phenol-formaldehyde, 247,248f  
thermoset, cross-link structure, 321-30
- Resin cure kinetics of  $N,N'$ -tetraglycidyl methylene dianiline reaction with 4,4'-diaminodiphenyl sulfone, 333-54
- Resolution  
polymer fractionation modeling, 35-43  
specific, definition, 172
- Resolution optimization for resins of narrow molecular distributions, 113-24  
for small molecules, 171-86
- Resorcinol, pressure programming in supercritical fluid chromatograph, 53-56
- Retention factor vs. pore partitioning model, 18f
- Retention volume  
of deuterium oxide, effect of injection concentration, 213t  
of styrene-isoprene and styrene-butadiene copolymers, 306,311-18  
in supercritical fluid chromatography, 51-56
- Road asphalt, 265,268f
- S
- Sampling rate effect  
in high-speed GPC, 201t  
on molecular parameter data of polyethylene resins, 103-9
- Santonox-R, in polyethylene, molecular weight averages vs. residence time, 100-109

- Scattering with low-angle laser light, theory, 300
- Scission study of sulfonated styrene/divinylbenzene copolymer, 355-57
- Second virial coefficients, aggregate-free mixtures, 274,276,277t
- Sensitivity of viscometer in GPC/viscometer system, 286-89
- Separation factor-particle size behavior, mathematical modeling, 3-22
- Separation mechanisms, mathematical modeling, 3-22
- Separation of small molecules, optimization of resolution, 171-86
- Separation speed of polystyrene in high-speed GPC, 193,194f
- Separation volume in supercritical fluid chromatography, 51-56
- Sequential U test, molecular weight distribution, 135-42
- Shear degradation and molecular parameter data of polyethylene resins, 103-9 of very high molecular weight polymers, 227-40
- Shear rate, effect on polymer degradation, 231
- Signal-to-noise ratio in GPC/viscometer system, 286-89
- Silica bead packed columns, dispersion of polystyrene and 1,2-polybutadiene, 128t
- Simpson's rule for molecular weight distribution averages in time-volume space, 62
- Size factors and elution volume deviation for small molecules and oligomers, 245-47
- Size separation of aromatic species, effect from aromatic gel, 261-69
- Size separation mechanism in hydrodynamic chromatography, 4-8
- Size of Styragel bead, effect on degradation of high molecular weight polymers, 236-37
- Skewed peaks, 37
- Small molecule separation columns, 242-43 optimization of resolution, 171-86 pore size distributions, 172-73,185 Ultrastryragel 156-60
- Solid-phase prepared poly(ethylene terephthalate) in methylene chloride/hexafluoroisopropanol solvent system, 221-25
- Solute diffusion within gel structure, model development of polymer fractionation, 27-31
- Solution chemistry of polyethylene, aggregation, 273-79
- Solution preparation polyethylene GPC/LC, 98 polyethylene resins, effect on molecular parameter data, 103-9
- Solutions, effective linear molecular size, 259
- Solvent delivery in high-speed GPC, 203-6
- Solvent effects degradation of high molecular weight polymers in cyclohexane, 230,232-33 effective linear sizes of molecules in solution, 259-62 in small molecule separation, 176-77
- Solvent systems benzene, relative and reduced viscosities of high molecular weight polymers, 232t for cellulose triacetate fraction analysis, 367 for dilute solution light scattering detection, linear and branched copolymers, 304 methylene chloride/hexafluoroisopropanol for poly(ethylene terephthalate), 219-25 for polyethylene refractive index increments, 274,275t 1,2,4-trichlorobenzene, 98-100
- Solvent temperature and flow in supercritical fluid chromatography, 48-51
- Specific resolution, definition, 172
- Speed of separation of polystyrene in high-speed GPC, 193,194f
- Spreading factor See also--Dispersion molecular weight calibration, 125-34
- Stabilizers, effect on molecular parameter data of polyethylene resins, 103-9
- Stationary phase material balance equation, polymer fractionation modeling, 27
- Stationary phase in supercritical fluid chromatography, 51-56
- Statistical methods, Fuzes, for molecular weight distributions, 135-42
- Step-growth polymerization of nadic methyl anhydride and Epon 828, 326
- Steroid cream, 177,179f
- Stoichiometry of  $N,N'$ -tetraglycidyl methylene dianiline reaction with 4,4'-diaminodiphenyl sulfone, 344-54

- Structure  
 cured *N,N'*-tetraglycidyl methylene dianiline reacted with 4,4'-diaminodiphenyl sulfone, 335-56,341-54  
 sulfonated styrene/divinylbenzene copolymers, 355-57  
 thermoset resin cross-link, 321-30
- Styragel bead size, effect on degradation of high molecular weight polymers, 236-37
- Styragel column  
 calibration curve, 98-100  
 degradation of high molecular weight polymers in cyclohexane, 230-40
- Styrene, dilute solution light scattering detection, 304
- Styrene-based columns, 145-68
- Styrene/butadiene copolymers, 306,311-18
- Styrene/divinylbenzene copolymer  
 bead columns, dispersion of polystyrene and 1,2-polybutadiene, 128t  
 packing for petroleum crude analysis, 257  
 sulfonated, scission study, 355-57
- Styrene/isoprene copolymers, 295-318
- Sulfonated styrene/divinylbenzene copolymer, scission study, 355-57
- Supercritical fluid chromatography, pressure-programmed controlled-flow, 47-56
- Swellant, gel, effect on degradation of high molecular weight polymers, 235-36
- Symmetrical chromatograms, polymer fractionation, 29-30,35-37
- SynChropak columns, 209-17
- T
- Temperature control in high-speed GPC, 202-3
- Temperature dependence of *N,N'*-tetraglycidyl methylene dianiline and 4,4'-diaminodiphenyl sulfone reaction, 344-54
- Temperature effect on elution volume, 214-16
- Temperature treatment of polyethylene solutions, 276-79
- N,N'*-Tetraglycidyl methylene dianiline, reaction with 4,4'-diaminodiphenyl sulfone, 333-54
- Tetrahedral cells, Flory, sulfonated styrene/divinylbenzene copolymer degradation, 355-57
- Theoretical plates, polymer fractionation modeling, 41-42
- Thermal degradation, effect on molecular parameter data of polyethylene resins, 103-9
- Thermal, temperature treatment of polyethylene solutions, 276-79
- Thermoset resin cross-link, structure, 321-30
- 4,4'-Thiobis(6-*tert*-butyl-*m*-cresol), in polyethylene, molecular weight averages vs. residence time, 100-109
- Time-volume space, molecular weight distribution averages using Simpson's rule, 62
- Toluene  
 molecular weight vs. retention volume, 246f  
 solvent system, dilute solution light scattering detection, linear and branched copolymers, 304
- Topanol in polyethylene, molecular weight averages vs. residence time, 100-109
- Tortuosity, polymer fractionation modeling, 32-33
- Total exclusion, 35, 38f
- Transmission oil, 265,267f
- Transmitter, pneumatic pressure, supercritical fluid chromatography, 48-51
- Triamcinolone acetone from steroid cream, 177,179f
- 1,1,3-Tri(*tert*-butylhydroxymethylphenyl)butane in polyethylene, molecular weight averages vs. residence time, 100-109
- 1,2,4-Trichlorobenzene solvent, 98-100,274
- 2,2,3-Trimethyl-1,2-dihydroquinoline, 247,248f
- Tubing diameter effect in high-speed GPC, 196
- U
- U test, sequential, molecular weight distribution, 135-42
- Ultrastryragel columns, 175  
 calibration  
 curves, 145-55,177,179-85  
 efficiency, 177  
 pore size distribution, 180-85  
 probe mixtures, 145-47,153,156-68  
 for small molecule separation, 156-60
- Universal calibration, 300,301  
 for cellulose triacetate fraction analysis, 369,371-73  
 hydrodynamic volume of polymers, 76-77,84-88,93

Urea as mobile phase, 214  
 UV detector, supercritical fluid chromatograph, 51-56

## V

Valence-bond structures, linear molecular sizes, 258-59,261  
 Velocities, particle and marker, equations, 5  
 Virial coefficients, second, aggregate-free mixtures, 274,276,277t  
 Viscometer  
   and differential refractometer, interface and dead volume, 289,290f  
   sensitivity in GPC/viscometer system, 286-89  
 Viscometry, triacetate characterization, 365  
 Viscosity detector, continuous capillary, 281-94  
 Viscosity measurements, degradation of high molecular weight polymers in cyclohexane, 230-32  
 Viscosity ratio, for styrene-isoprene and styrene-butadiene copolymers, 306,311-18  
 Volume, dead, between differential refractometer and viscometer interface, 289,290f  
 Volume, elution, molecular weight calibration, 125-34  
 Volume, pore, 6,31

## W

Warfarin from grain bait, determination, 177,178f

Water, heavy  
   for column calibration, 207-17  
   on controlled-pore glass and SynChropak columns  
     elution volume and flow rate, 210,213  
     injection concentration, effect on peak height and retention volume, 213t  
 Water-insoluble polymers, nonaqueous separations, calibration curves, 77-78,80-87  
 Water-soluble polymers, narrow MWD standards, calibration curves, 78-79,87-93  
 Weight average degrees of polymerization and calibration for improved resolution, 115,118  
 Weight average molecular weight dilute solution light scattering of branched copolymers, 299-302  
   polydisperse polymer, definition, 125-27  
   polyethylene in various solvents, 276,277t  
   polystyrene standard, empirical equation, 173  
   temperature effect, 203t  
 Weight distribution and calibration for improved resolution, 118

## X

o-Xylene, plates vs. pores in Ultrastragel columns, 156-62  
p-Xylene, molecular weight vs. retention volume

*Production by Paula Bérard  
 Indexing by Florence Edwards  
 Jacket design by Anne G. Bigler  
 based on an idea by Ann Kah*

*Elements typeset by Hot Type Ltd., Washington, D.C.  
 Printed and bound by Maple Press Co., York, Pa.*